REPORT DOCUMENTATION PAGE	Form Approved OMB No. 0704-0188

1. AGENCY USE ONLY *(Leave blank)*	2. REPORT DATE	3. REPORT TYPE AND DATES COVERED
	2.Jul.99	DISSERTATION

4. TITLE AND SUBTITLE
MESOSCALE
~~NUMERICAL~~ SIMULATIONS OF DYNAMICAL FACTORIS DISCRIMINATING BETWEEN A TORNADO OUTBREAK AND NON-EVENT OVER THE SOUTHEAST US

5. FUNDING NUMBERS

6. AUTHOR(S)
MAJ EGENTOWICH JOHN M

7. PERFORMING ORGANIZATION NAME(S) AND ADDRESS(ES)
NORTH CAROLINA STATE UNIVERSITY

8. PERFORMING ORGANIZATION REPORT NUMBER

9. SPONSORING/MONITORING AGENCY NAME(S) AND ADDRESS(ES)
THE DEPARTMENT OF THE AIR FORCE
AFIT/CIA, BLDG 125
2950 P STREET
WPAFB OH 45433

10. SPONSORING/MONITORING AGENCY REPORT NUMBER
FY99-140

11. SUPPLEMENTARY NOTES

12a. DISTRIBUTION AVAILABILITY STATEMENT
Unlimited distribution
In Accordance With AFI 35-205/AFIT Sup 1

12b. DISTRIBUTION CODE

13. ABSTRACT *(Maximum 200 words)*

DISTRIBUTION STATEMENT A
Approved for Public Release
Distribution Unlimited

14. SUBJECT TERMS

15. NUMBER OF PAGES
268

16. PRICE CODE

17. SECURITY CLASSIFICATION OF REPORT	18. SECURITY CLASSIFICATION OF THIS PAGE	19. SECURITY CLASSIFICATION OF ABSTRACT	20. LIMITATION OF ABSTRACT

ABSTRACT

EGENTOWICH, JOHN MARK. Mesoscale Simulations of Dynamical Factors Discriminating Between a Tornado Outbreak and Non-Event Over the Southeast US. (Under the direction of Yuh-Lang Lin and Allen J. Riordan)

We found a self-maintaining, low-level instability originated in the lee of the Sierra Madre Mountains, propagated eastward along the Gulf Coast states and over the Carolina Piedmont at the time of the 1988 Raleigh tornado outbreak. This instability was characterized by a surface trough, low-level potential vorticity (PV) maximum, mid-level jet and a warm airmass located to its southeast. These features created an environment favorable to deep convection and the release of latent heat that helped maintain the low-level trough and PV as it propagated across the Gulf Coast.

The STJ was crucial to this 3-day process. It transported stratospheric PV-rich air to the south then downward to the mid-levels over the Mexican plateau. Its associated ageostrophic circulation created upper-level divergence (mass removal from the air column) that helped to maintain deep convection and the surface trough. It phased with the PJ creating upper-level divergence and ascent over the Piedmont.

We developed a predictive tornado index based on: upper-level divergence, airmass buoyancy and the low-level tilting effects associated with shear and thermal gradients. We found values greater then 15 corresponded to tornadic activity early in the period (over TX, AR, LA and MS) and over central NC.

Additionally, the event case was compared to a synoptically similar case where severe weather was forecasted but did not develop over the Piedmont. In the non-event case there was no STJ, mid-level jet, low-level PV or surface instability over the southeast US.

MESOSCALE SIMULATIONS OF DYNAMICAL FACTORS DISCRIMINATING BETWEEN A TORNADO OUTBREAK AND NON-EVENT OVER THE SOUTHEAST US

by

MAJOR JOHN M. EGENTOWICH
UNITED STATES AIR FORCE

1999

268 PAGES

DOCTOR OF PHILOSOPHY
FROM
DEPARTMENT OF MARINE, EARTH, AND ATMOSPHERIC SCIENCES
NORTH CAROLINA STATE UNIVERSTIY

References

Bluestein, H. B., 1993: Synoptic-Dynamic Meteorology in Midlatitudes, Volume II Observations and Theory of Weather Systems, Oxford University Press, 594 pp.

Bolin , B., 1956: An improved barotropic model and some aspects of using the balance equation for three dimensional flow. *Tellus*, **8**, 67-75.

Charney, J. G., 1955: The use of the primitive equation of motion in numerical weather prediction. *Tellus*, **7**, 22-26.

Daley, R., 1991: *Atmospheric Data Analysis*, Cambridge University Press, 457 pp.

Danielsen, E., 1968: Stratospheric-tropospheric exchange based on radioactivity, ozone, and potential vorticity. *J. Atmos. Sci.*, **25**, 502-518.

Davies-Jones, R., D. Burgess, and M. Foster, 1990: Test of helicity as a forecast parameter. *Preprints*, 16th Conf. Severe Local Storms, Kananaskis, Alberta, Amer. Meteor. Soc., 588-592.

Egentowich, J. M., M. L. Kaplan, Y.-L. Lin and A. J. Riordan, 1999a: Mesoscale simulations of dynamical factors discriminating between a tornado outbreak and non-event over the southeast US part I: 84 - 48 hour precursors. Submitted to *Weather and Forecasting*.

Egentowich, J. M., M. L. Kaplan, Y.-L. Lin and A. J. Riordan, 1999b: Mesoscale simulations of dynamical factors discriminating between a tornado outbreak and non-event over the southeast US part II: 48 - 6 hour precursors. Submitted to *Weather and Forecasting*.

Fawbush, E. J. and R. C. Miller, 1954: The types of airmasses in which North American tornadoes form. *Bull. Amer. Meteor. Soc.*, **35**, 154-165.

Gidel L. T., and M. A. Shapiro, 1979: The role of clear air turbulence in the production of potential vorticity in the vicinity of upper tropospheric jet stream-frontal systems. *J. Atmos. Sci.*, **36**, 2125-2138.

Gonski R. F., B. P. Woods, and W. D. Korotky, 1989: The Raleigh tornado - 28 November 1988: An operational perspective. Preprints, *12th Conf. on Weather Analysis and Forecasting*, Monterey, CA Amer. Meteor. Soc., 173-178.

Gyakum J. R., Y-H Kuo, Z. Guo, and Y-R Guo, 1995: A case of rapid continental mesoscale cyclogenesis. Part II: Model and observational diagnosis. *Mon. Wea. Rev.*, **123**, 998-1024.

Hamilton, D. W., Y. L. Lin, R. P. Weglarz, and Kaplan, M. L., 1998: Jetlet formation from diabatic forcing with applications to the 1994 Palm Sunday tornado outbreak. *Mon. Wea. Rev.*, **126**, 2061-2089.

Kalnay, E., M. Kanamistu, R. Kistler, W. Collins, D. Deaven, L. Gandin, M. Iredell, S. Saha, G. White, J. Woollen, Y. Zhu, M. Chelliah, W. Ebisuzaki, W. Higgins, J. Janowiak, K. C. Mo, C. Ropelewski, J. Wang, A. Leetmaa, R. Reynolds, R. Jenne, and D. Joseph, 1996; The NMC/NCAR 40-year reanalysis project. *Bull. Amer. Meteor. Soc.*, **77**, No. 3, 437-471.

Kaplan, M. L., and D. A. Paine, 1977: The observed divergence of the horizontal velocity field and pressure gradient force at the mesoscale. It's implications for the parameterization of three-dimensional momentum transport in synoptic-scale numerical models. *Beitr. Phy. Atmos.*, **50**, 321-330.

Kaplan, M. L., V. M. Karyampudi, 1992: Meso-beta numerical simulation of terrain drag-induced along stream circulations. Part I: Midtropospheric frontogenesis. *Meteor. Atmos. Phys.*, **49**, 133-156.

Kaplan, M. L., V. M. Karyampudi, 1992: Meso-beta numerical simulation of terrain drag-induced along stream circulations. Part II: Concentration of potential vorticity within dryline bulges. *Meteor. Atmos. Phys.*, **49**, 157-185.

Kaplan, M. L., J. W. Zack, V. C. Wong, and J. J. Tuccillo, 1982a: Initial results from a mesoscale atmospheric simulation system and comparisons with the AVE-SESAME I data set. *Mon. Wea. Rev.*, **110**, 1564-1590.

Kaplan, M. L., Y-L. Lin, D. W. Hamilton, and Rozumalski, R. A., 1997: The numerical simulation of an unbalanced jetlet and its role in the Palm Sunday 1994 tornado outbreak in Alabama and Georgia. *Mon. Wea. Rev.*, **126**, 2133-2165.

Kaplan, M. L., R. A. Rozumalski, R. P. Weglarz, Y. L. Lin, S Businger, and R. F. Gonski, 1995: Numerical simulation studies of the mesoscale environment conductive to the Raleigh tornado. *NOAA Tech. Memo ER-90*, 1-101.

Karyampudi, V. M., M. L. Kaplan, S. E. Koch, and R. J. Zamora, 1995. The influence of the Rocky Mountains on the 13-14 April 1986 severe weather outbreak. Part 1: Mesoscale lee cyclogenesis and its relationship to severe weather and dust storms. *Mon. Wea. Rev.*, **123**, 1394-1422.

Keyser, D., and M. A. Shapiro, 1986: A review of the structure and dynamics of upper-level frontal zones. *Mon. Wea. Rev.*, **114**, 452-499.

Kocin, P. J., L. W. Uccellini, J. W. Zack, and M. L. Kaplan, 1985: A mesoscale numerical forecast of an intense convective snowburst along the East Coast. *Bull. Amer. Meteor. Soc.*, **66**, 1412-1424.

Lanicci, J. M. and T. T. Warner, 1991a: A synoptic climatology of the elevated mixed-layer inversion over the southern Great Plains in Spring. Part 1: Structure, dynamics, and seasonal evolution. *Wea. & Forecasting*, **6**, 181-197.

Lanicci, J. M. and T. T. Warner, 1991b: A synoptic climatology of the elevated mixed-layer inversion over the southern Great Plains in Spring. Part 2: the life cycle of the lid. *Wea. & Forecasting*, **6**, 198-213.

Lanicci, J. M. and T. T. Warner, 1991c: A synoptic climatology of the elevated mixed-layer inversion over the southern Great Plains in Spring. Part 3: Relationship to severe-storms climatology. *Wea. & Forecasting*, **6**, 214-226.

Lin, Y.-L., and T.-A. Wang, 1996: Flow regimes and transient dynamics of two-dimensional stratified flow over an isolated mountain ridge. *J. Atmos. Sci.*, **53**, 139-158.

Lin, Y.-L., R. D. Farley, and H. D. Orville, 1983: Bulk parameterization of the snow field in a cloud model, *J. Clim. Appl. Meteorol.*, **22**, 1065-1092.

Mahrt, L., and H. Pan, 1984: A two-layer model of soil hydrology. *Bound.-Layer Meteor.*, **29**, 1-20.

MESO, 1995: MASS Version 5.8 Reference Manual, MESO, Inc., Troy, NY, 119 pp.

Miles, J. W., 1961: On the stability of heterogeneous shear flows. *J. Fluid Mech.*, **10**, 496-508.

Murry, R. and S. M. Daniels, 1953: Transverse flow at entrance and exit to jet streams. *Quart. J. Roy. Meteor. Soc.*, **79**, 236-241.

Newton, C. W., 1958: Variations in frontal structure of upper level troughs. *Geophysica*, **6**, 357-375.

NOAA, 1990: Storm data, **32, 01**, 66 pp.

NOAA, 1988: Storm data, **30, 11,** 72 pp.

Noilhan, J., and S. Planton, 1989: A simple parameterization of land surface processes for meteorological models. *Mon. Wea. Rev.*, **117**, 536-549.

Reed, R. J., 1955: A study of a characteristic type of upper-level frontogenesis. *J. Meteor.*, **12**, 226-237.

Reiter, E. R., 1967: *Jet Streams*, Doubleday & Company, Inc., 189 pp.

Riehl, H and coauthers, 1952: Forecasting in the Middle Latitudes. Meteor. Monogr., No 5, Amer. Meteor. Soc., 80 pp.

Rozumalski, R. A., 1997: The role of jet streak regeneration forced by a deepening continental planetary boundary layer in the explosive surface cyclogenesis of 28 March 1984. Ph. D. Thesis., North Carolina State University, 360 pp. (Available from the corresponding author).

Tripoli G. J. and W. R. Cotton 1989:Numerical Study of an Observed Orogenic Mesoscale Convective System. Part 1: Simulated Genesis and Comparison with Observations. *Mon. Wea. Rev.*, **117**, 273-304.

Tripoli G. J. and W. R. Cotton 1989:Numerical Study of an Observed Orogenic Mesoscale Convective System. Part 2: Analysis of Governing Dynamics. *Mon. Wea. Rev.*, **117**, 305-328.

Uccellini L. W. and D. Johnson 1979: The coupling of upper and lower tropospheric jet streaks and implication for the development of severe convective storms. *Mon. Wea. Rev.*, **107**, 682-703.

Uccellini L. W, and S. E. Koch 1987: The synoptic setting and possible energy sources for mesoscale wave disturbances. *Mon. Wea. Rev.*, **115**, 721-729.

Uccellini L. W., and P. J. Kocin, 1987: The interaction of jet streak circulations during heavy snow events along the East Coast of the United States. *Wea. & Forecasting*, **1**, 289-308.

Uccellini L. W., P. J. Kocin, R. A. Petersen, C. H. Wash and K. F. Brill, 1984: The President's day cyclone of 18-19 February 1979: Synoptic overview and analysis of the subtropical jet streak influencing the pre-cyclogenetic period. *Mon. Wea. Rev.*, **112**, 31-55.

Van Tuyl A. H., J. A. Young, Numerical Simulation of Nonlinear Jet streak Adjustment,. *Mon. Wea. Rev.*, **110**, 2038-2054.

Whitaker, J. S., L. W. Uccellini, and K. F. Brill, 1988: A model-based diagnostic study of the rapid development phase of the Presidents' Day cyclone. *Mon. Wea. Rev.*, **116**, 2337-2365.

Zack, J. W., and M. L. Kaplan 1987: Numerical simulations of the subsynoptic features associated with the AVE-SESAME I case. Part I: The preconvective environment. *Mon. Wea. Rev.*, **115**, 2367-2393.

Zang, D. L., and R. A. Anthes, 1982: A high resolution model of the plantary boundary layer-sensitivity tests and comparisons with SESAME-79 data. *J. Appl. Meteor.*, **21**, 1594-1609.

Zehnder, J. A., and D. Keyser, 1991: The influence or interior gradients of potential vorticity on rapid cyclogenesis. *Tellus*, **43A**, 198-212.

ABSTRACT

EGENTOWICH, JOHN MARK. Mesoscale Simulations of Dynamical Factors Discriminating Between a Tornado Outbreak and Non-Event Over the Southeast US. (Under the direction of Yuh-Lang Lin and Allen J. Riordan)

We compared the 1988 Raleigh tornado outbreak (event) to a synoptically similar case (non-event) where severe weather was forecasted but did not develop over the Piedmont. We compared the development of the synoptic situations over a 3 day period before the event/non-event time.

In the event case, a self-maintaining, low-level circulation originated in the lee of the Sierra Madre Mountains, propagated eastward along the Gulf Coast states and over the Piedmont at the time of the tornado outbreak. This circulation was characterized by a surface trough, low-level potential vorticity (PV), mid-level jet and a warm airmass located to its southeast. The low-level PV originated over the Mexican plateau, transported to the mid-levels by the ageostrophic circulation associated with the subtropical jet (STJ) and to the low-levels by a hydrostatic mountain wave. The low-level PV was primarily maintained by tilting effects associated with diabatic heating. The warm airmass originated over the Mexican plateau, moved over the Gulf Coast states, and in conjunction with cold air advection to the northwest created an intense northwestward-directed pressure gradient force and a mid-level jet. The mid-level jet entrance region with its thermally direct ageostrophic circulation enhanced ascent over the surface trough. These features

created an environment favorable to deep convection and the release of latent heat that helped maintain the low-level trough and PV as it propagated across the Gulf Coast.

The STJ was crucial to this 3-day process. It transported stratospheric PV-rich air to the south then downward to the mid-levels over the Mexican plateau. Its associated ageostrophic circulation created upper-level divergence (mass removal from the air column) that helped to maintain deep convection and the surface trough. It phased with the PJ creating upper-level divergence and ascent over the Piedmont.

We developed a predictive tornado index based on: upper-level divergence, airmass buoyancy and the low-level tilting effects associated with shear and thermal gradients.

In the non-event case the STJ, mid-level jet, low-level PV and the low-level circulation were absent over the southeast US.

MESOSCALE SIMULATIONS OF DYNAMICAL FACTORS DISCRIMINATING BETWEEN A TORNADO OUTBREAK AND NON-EVENT OVER THE SOUTHEAST US

by

JOHN M. EGENTOWICH

A dissertation submitted to the Graduate Faculty of
North Carolina State University
in partial fulfillment of the
requirements for the Degree of
Doctor of Philosophy

DEPARTMENT OF MARINE, EARTH, AND ATMOSPHERIC SCIENCES

Raleigh

1999

APPROVED BY:

Gerald F. Watson

Michael L. Kaplan

Allen J. Riordan
Co-chair of Advisory Committee

Yuh-Lang Lin
Co-chair of Advisory Committee

PERSONAL BIOGRAPHY

Major John M. Egentowich is an Officer in the United States Air Force. He was born in Hinsdale, Illinois on March 27, 1960. He received a Bachelor of Science degree in Chemistry from University of Illinois in 1983. Upon graduation, he was commissioned a Second Lieutenant through the Officer Training School in San Antonio, Texas. His active military career began at 21st Headquarters Weather Support Unit, McGuire Air Force Base, New Jersey. He was promoted to the rank of First Lieutenant in May 1986.

He entered North Carolina State University in 1987 through the Air Force Institute of Technology program earning a Master of Science in Meteorology. His thesis topic dealt with the processes associated with "Coastal Frontogenesis". He was promoted to the rank of Captain in May 1988.

In 1989, he was assigned to Offutt AFB, Nebraska. He was assigned as Chief, Combat Weather Displays and Applications and was responsible for the development of automated meteorological applications.

In 1993, he was assigned to Headquarters European Command, Stuttgart Germany. He was responsible for plans and policies of meteorological and oceanographic support to operations in the European theater. He was also the senior meteorological and oceanographic officer for the Special Operations Command, Europe.

In 1996, he was selected by the Air Force Institute of Technology program to attend North Carolina State University to work towards his Ph.D. He was promoted to the rank of Major in March 1996.

Major Egentowich has earned the Senior Meteorologist Badge and the Basic Parachutist Badge. His military decorations include the: Defense Meritorious Service Medal, Joint Service Commendation Medal, Air Force Commendation Medal, Air Force Achievement Medal, Combat Readiness Medal, Armed Forced Expeditionary Medal, Armed Forced Service Medal, National Defense Medal, and NATO Medal.

He is married to the former Krista Kim Zolkowski and has two daughters, Alexandra Day, and Alyson Taylor.

DEDICATION

This work is dedicated to the ladies in my life; my wife Krista and my two daughters, Alexandra and Alyson.

ACKNOWLEDGMENTS

I wish to thank Professors Yuh-Lang Lin, Michael L. Kaplan, Allen Riordan and Gerald F. Watson for their guidance throughout my research and the preparation of this dissertation.

I also would like to thank Drs. Robert Rozumalski and Kenneth Waight III for their help with the MASS model and MASS trajectory software.

I wish to thank the other graduate students who have helped me in my work.

Finally, I want to thank AFIT for the opportunity to pursue my graduate studies.

TABLE OF CONTENTS

LIST OF TABLES

Chapter 4

LIST OF FIGURES

Page

Chapter 1

Chapter 2

Chapter 3

Chapter 4

CHAPTER 1

INTRODUCTION

1.1 Literature review

The Raleigh, NC tornado of 28 November 1988 was an extraordinary event that stimulated a great deal of interest from the weather forecasting and research communities. This tornado violated climatology as it occurred in the middle of the night in late November with an unusual F4 intensity for NC and was part of a larger outbreak across NC and VA. This devastating tornado was on the ground for 83 miles resulting in 4 deaths, 154 injuries, and an estimated 77.2 million dollars in property damage (NOAA 1988; see Fig. 1). It occurred in the vicinity of the polar jet (PJ) entrance region, not the exit region, counter to jet streak dynamical paradigms (e. g., Kaplan and Paine 1977; Uccellini and Johnson 1979; Kocin et al. 1985, Zack and Kaplan 1987; Uccellini and Koch 1987). These studies among others, assume that the vertical differential advection of temperature and moisture within the transverse circulation associated with the jet streak exit region controls the development of deep conditional instability; through adiabatic expansion, cold advection aloft, and warm advection within the low-level return branch. Furthermore, significant vertical shear is established within the exit region as the low-level return branch and its cross-stream isallobaric wind component accelerates under the rightward-directed inertially-forced mid-upper tropospheric decelerating ageostrophic wind component. Additionally, the shear and instability are juxtaposed with

vertically-increasing quasi-geostrophic positive vorticity advection as well as low-level warm advection thus rendering the same region to be predisposed to substantial rising motion and moistening conditions (Uccellini and Johnson 1979). The combination of a climatologically rare event and its development within the *entrance* region of a PJ streak may have proved sufficient to deter the National Weather Service from issuing any severe thunderstorm or tornado watches prior to the initiation of the severe weather in Raleigh (Gonski 1989). *This is because much, if not most, of our severe weather prediction paradigms are implicitly based on the PJ streak exit regional model.* The violent episode of severe weather at Raleigh was not isolated, being also part of a larger outbreak, which produced numerous other tornadoes.

From a scientific perspective, the development of a devastating tornado in the PJ entrance region indicates that our understanding of forcing mechanisms for severe weather are limited at best if not far too simplistic. Severe weather predictive indices based upon typical jet exit region dynamics, i. e., convective instability/buoyancy, vertical wind shear, and storm relative helicity were all sufficiently unremarkable. Also, the severe weather occurred within a region of negative vorticity advection at 500 mb and weak low-level warm advection thus minimizing typical quasi-geostrophic indicators of severe weather potential (Gonski 1989). The inability of standard indices/dynamical paradigms to indicate at least modest tornadic potential for such an *extreme* climatologically anomalous event clearly raises the possibility that our scientific understanding of the mechanism of tornadic development is flawed. Therefore, the

ambiguity accompanying the Raleigh tornado case study indicates that considerable research is yet to be done to truly determine the mechanisms that produce severe weather in the southeast US.

Upper level jet streaks are often the driving force for surface weather (Keyser and Shapiro, 1986). Therefore, its extremely important to understand the circulation in the vicinity of jet streaks in addition to the transverse ageostrophic circulation around the jet. Many authors (e.g. Holton, 1979) have shown the relationship between the geostrophic and the ageostrophic modes using the geostrophic momentum approximation:

$$\frac{D\vec{V}}{Dt} \approx \frac{D\vec{V}_g}{Dt} = -f\mathbf{k} \times \vec{V}_{ag} \tag{1}$$

For a straight-line jet streak, a thermally direct circulation characterizes the entrance region, while a thermally indirect circulation is found in the exit region (Riehl, 1952; Murry and Daniels 1953; Newton 1958; Reiter 1967; Uccellini and Johnson 1979). In the typical straight jet streak, the vertical motions are characterized by a four-cell pattern around the jet streak. Areas of upward motion will be in the right entrance region and the left exit region and downward motion will be in the left entrance region and the right exit region. These secondary transverse circulations develop so the atmosphere maintains a balance between the mass and momentum fields in an effort to maintain a quasi-geostrophic state. Furthermore, when there is significant thermal advection and/or curvature, the ageostrophic circulation will be displaced from the axis of the jet streak. For example, with cold air advection in the northwest quadrant, the ageostrophic

circulation will be displaced to the south in the entrance region and to the north in the exit region (Keyser and Shapiro, 1986).

The upper-level jet streak and its associated transverse ageostrophic circulation are coupled to the lower level circulation. In this case, the low-level circulation is critical to the transport of warm, moist air to the northeast, which is one of the key ingredients for severe weather. Uccellini and Johnson (1979) studied the coupling and interaction of the low-level and upper-level jet streaks. At the upper-level, within the jet exit region, and assuming quasi-geostrophic and frictionless flow, the inertial-advective component of the ageostrophic wind dominates the transverse circulation. In the low levels, the isallobaric component of the ageostrophic wind dominates the transverse circulation, defined as:

$$U_{ag} = f^{-1}\left[\underbrace{k \times \frac{\partial U_g}{\partial t}}_{1} + \underbrace{U \bullet \nabla_\theta (k \times U_g)}_{2}\right]. \qquad (2)$$

On the right hand side of the above equation, term one is the isallobaric component and term two is the inertial advective component. In order to maintain quasi-geostrophic (QG) or semi-geostrophic (SG) balance, mass adjustments occur which are dominated by the cross-stream wind component (term 1). In highly ageostrophic fluids the along-stream wind component (term 2) can be very important. This is because there is not enough time for the Coriolis force to dominate the adjustment. As the air parcels move into the exit region of a straight jet streak, they move into an area of weaker winds (i.e. they decelerate). These parcels have higher kinetic energy than the environment can support so they are deflected to the right of the flow by the Coriolis force into an area of

higher pressure and hence, the parcels decelerate. The environment returns to a balance between the mass and momentum fields. Thus, the flow in the exit region is supergeostrophic. As the parcels are deflected to the right there is an area of convergence in the right exit region of the jet streak and an area of divergence in the left exit region of the jet streak. By Dines compensation there must be sinking below the area of convergence in the right exit region and ascent below the area of divergence in the left exit region. At the lower levels the sinking will create an area of mass convergence below the right exit region and ascent will create an area of mass divergence below the left exit region. Consistent with the above sentence, the area below the right exit region will experience pressure rises and below the left exit region there will be pressure falls. A leftward-directed pressure gradient will develop creating a low-level ageostrophic return branch component (an isallobaric response). Also, the sinking will result in an area of adiabatic warming in the column of air and ascent will result in adiabatic cooling in the column of air. Thus the thermal wind balance will be maintained by producing cross-stream temperature gradients supporting quasi-geostrophic flow. The indirect circulation around the exit region of a jet streak increases the horizontal temperature gradient and returns the mass and momentum fields to a state of balance. The circulation about the entrance region of the jet streak is just the opposite -- a direct circulation converting potential energy into kinetic energy. The isallobaric response will be for the winds to shift to the area of low-level convergence. So, if the isallobaric wind component develops, one can expect the development of a low-level jet (LLJ). The isallobaric wind

component is perpendicular to the upper-level jet streak and is primarily responsible for the LLJ being at a significant angle to the jet axis within the exit region (Uccellini and Johnson 1979). So, the development of the LLJ is essential to transport the warmer air, moisture northeastward and it produces strong vertical wind shear creating the instability for severe weather. Since, we are investigating a severe weather event and non-event we will investigate the upper-level jet development, upper-level divergence, and the development of the LLJ. We will also investigate the adjustments in both the event and non-event case studies to see if they conform to the above quasi-geostrophic paradigm.

A potential major complicating issue to the Uccellini and Johnson (1979) circulation has been proposed by Uccellini and Kocin (1987) and applied in Kaplan et al. (1998) is the juxtapositioning of the PJ streak and subtropical jet (STJ) streak (Fig. 2). The two transverse ageostrophic circulations associated with the jet streaks phase in a manner which produces an area of intense and very deep vertical motion; the direct circulation associated with the PJ entrance region phases with the indirect circulation accompanying the STJ exit region. These circulations maximize themselves at different vertical levels. Between the two upper-level jet streaks there is confluence in the low levels, ascent through the column, and difluence in the upper levels. With both jet streaks producing divergence aloft over the same area one would intuitively expect a substantial amount of mass removed from the column of air.

Kaplan et al. (1998) proposed a new paradigm, with three primary concepts, for severe weather occurring over the southeast US. The first is the role of proximal

transverse secondary circulations and their deep quasi-geostrophic vertical motions accompanying both the PJ entrance region and the STJ exit region. Second, geostrophic adjustment of the mass field to the wind field in proximity to the continental air and polar air interface, i.e., low-level fronts accompanying the return branch of the STJ streak and return branch of the PJ streak, result in an unbalanced midtropospheric mesoscale jet streak or jetlet. This adjustment is necessitated by the ever-increasing cross-stream height gradient accompanying the low-level ageostrophically driven frontogenesis. Third, parcels experience intense stretching and tilting as they are caught up in the thermally direct unbalanced circulation in the right front quadrant of the geostrophically adjusting jetlet. We will apply this new paradigm to both the event and non-event cases.

The secondary circulations associated with the PJ and STJ transport air from very different source regions, producing a strong cross-stream frontal zone, and a mid-level unbalanced jetlet. The jetlet is unbalanced because it is constantly accelerating (developing) over an area where normally it would be decelerating. The exit region of the developing jetlet is a region of extreme thermal wind imbalance since vertical motions are no longer balanced, i.e., accelerations occur where the Uccellini and Johnson (1979) paradigm proposes decelerating flow! The unbalanced jetlet can enhance destabilization of the environment over the warm tropical airmass in a manner that is much more efficient than can a balanced jet streak. If the ascent extends farther into the tropical air this facilitates a more intense and prolonged destabilization and the formation of severe weather to the right of the quasi-geostrophic balanced jet. That is because air

parcels converging into the unbalanced region can be more rapidly destabilized as they have larger amounts of Convective Available Potential Energy.

When the Lagrangian Rossby number is much greater than 0.5 the four-cell vertical motion pattern around the jet streak is significantly altered (Van Tuyl and Young, 1982). The transverse balanced ageostrophic circulations are assumed to break down (Uccellini and Koch, 1987) and the motions around the jet will be altered to a two or three cell pattern as the jet accelerates in an attempt to balance itself. This is also apparent when there is strong curvature or unbalanced flow. The effect of curvature is to reinforce the downward motion in the entrance region and increase the upward motion in the exit region. The three-dimensional parcel trajectories facilitate the calculation of the Rossby number. The traditional Lagrangian Rossby number (Ro_L) is defined as

$$Ro_L = \frac{\left|D\vec{V}/Dt\right|_{Total}}{f\left|\vec{V}\right|}. \tag{4}$$

If the environment is unbalanced (manifested in the development of a jetlet) there are accelerations occurring in the unbalanced region; these accelerations favor areas of divergence. So, an analysis of the divergence fields (via the divergence equation) will help us understand the mass adjustments in the atmosphere. Horizontal divergence is defined as the spreading out of the winds. The opposite of divergence is convergence; thus, the coming together of the winds. Surface convergence plays a strong role in convection, as does upper-level divergence because it maintains an environment where the potential instability can be realized.

From the horizontal equations of motion in pressure coordinates, the divergence equation can be obtained. Starting with the u-component:

$$\frac{\partial u}{\partial t}+u\frac{\partial u}{\partial x}+v\frac{\partial u}{\partial y}+\omega\frac{\partial u}{\partial p}-fv=-\frac{\partial \Phi}{\partial x}+F_u \tag{5}$$

and then the v-component:

$$\frac{\partial v}{\partial t}+u\frac{\partial v}{\partial x}+v\frac{\partial v}{\partial y}+\omega\frac{\partial v}{\partial p}+fu=-\frac{\partial \Phi}{\partial y}+F_v \tag{6}$$

Where u and v are the horizontal wind components in the west-east and south-north directions respectively, ω is the vertical velocity in pressure coordinates, f the Coriolis parameter, Φ the geopotential, and F_u and F_v represent frictional and other subgrid-scale effects. Differentiating (5) with respect to x and (6) with respect to y, yields:

$$\frac{\partial(8)}{\partial x}=\frac{\partial^2 u}{\partial x\partial t}+\frac{\partial^2 u}{\partial x^2}+u\frac{\partial^2 u}{\partial x^2}+\frac{\partial v}{\partial x}\frac{\partial u}{\partial y}+v\frac{\partial^2 u}{\partial x\partial y}+\frac{\partial \omega}{\partial x}\frac{\partial u}{\partial p}+\omega\frac{\partial^2 u}{\partial x\partial p}-\frac{\partial f}{\partial x}v-f\frac{\partial v}{\partial x}$$
$$=-\frac{\partial^2 \Phi}{\partial x^2}+\frac{\partial F_u}{\partial x}$$
$$\frac{\partial(9)}{\partial y}=\frac{\partial^2 v}{\partial y\partial t}+\frac{\partial u}{\partial y}\frac{\partial v}{\partial x}+u\frac{\partial^2 v}{\partial x\partial y}+\frac{\partial^2 v}{\partial y^2}+v\frac{\partial^2 v}{\partial y^2}+\frac{\partial \omega}{\partial y}\frac{\partial v}{\partial p}+\omega\frac{\partial^2 v}{\partial y\partial p}+\frac{\partial f}{\partial y}u+f\frac{\partial u}{\partial y}$$
$$=-\frac{\partial^2 \Phi}{\partial y^2}+\frac{\partial F_v}{\partial y}$$

When the two equations above are combined vectorially, the divergence equation is obtained.

Let $D\equiv\nabla\cdot\mathbf{V}$, $\zeta=\frac{\partial v}{\partial x}-\frac{\partial u}{\partial y}$, $\gamma=\frac{\partial f}{\partial x}$, and $\beta=\frac{\partial f}{\partial y}$, the equation can be reduced to :

$$\underbrace{\frac{\partial D}{\partial t}}_{1}+\underbrace{\mathbf{V}\cdot\nabla D}_{2}+\underbrace{D^2}_{3}+\underbrace{\frac{\partial \omega}{\partial p}D}_{4}+\underbrace{\omega\frac{\partial D}{\partial p}}_{5}+\underbrace{J(u,v)}_{6}-\underbrace{\gamma v}_{7}+\underbrace{\beta u}_{8}-\underbrace{f\zeta}_{9}=-\underbrace{\nabla^2\Phi}_{10}+\underbrace{\frac{\partial F_u}{\partial x}+\frac{\partial F_v}{\partial y}}_{11} \tag{7}$$

where $\nabla \equiv \frac{\partial}{\partial x} + \frac{\partial}{\partial y}$ and $J(u,v) \equiv \frac{\partial u}{\partial x}\frac{\partial v}{\partial y} - \frac{\partial v}{\partial x}\frac{\partial u}{\partial y}$

Terms 1 and 2 in (7) collectively are the inertial terms where Term 1 is the local time tendency of the divergence and Term 2 is the horizontal advection of the divergence. Term 3 is the divergence squared term. Term 5 is the vertical advection of the divergence. Term 11 is the divergence of the frictional stresses. Terms 6 through 10 collectively are called the balance equation. In the absence of large divergence tendencies, terms 6 through 10 alone resolve the divergence (Charney, 1955; Bolin, 1956; Zack and Kaplan, 1987). Term 6 is the Jacobian of the horizontal velocity. Term 7 (8) is the East-West (North-South) Coriolis force change times the North-South (East-West) velocity. Term 9 is the Coriolis force times the vertical vorticity of the horizontal velocity $\left(\hat{k} \bullet \nabla \times \vec{V}\right)$. Finally term 10 is the Laplacian of the geopotential height, or the mass term.

Surface forcing and upper-level jets result in the divergence usually being largest in the lower and upper troposphere. The largest contributors in the equation are usually the terms in the balance equation, especially the Laplacian of the geopotential height, during times of small divergence tendency (e.g., a high pressure region). In other situations (e.g., a jet, a front, or convection) the full divergence equation must be used since $\nabla \bullet \vec{V}$ is significant in magnitude. As the flow becomes unbalanced the midlevel $\nabla \bullet \vec{V}$ is more significant. The advection, tendency, and again the Laplacian of the geopotential height terms are often the main terms involved here (Kaplan and Paine,

1977). Once the divergence terms are known, areas of convergence following a parcel and hence, a mesoscale divergence field can be evaluated. Thus, the divergence fields can corroborate the existence of the unbalanced jet development and the thermally direct circulation associated with the unbalanced flow in its exit region. These areas can be related to the vertical motions in the atmosphere. Also, the upper-level divergence should accompany the frontogenesis forcing (tilting and confluence) and ascent over the hot, moist air. The divergence fields in the event case can be compared to the non-event case highlighting divergence field differences (and vertical velocities) between the cases. For the non-event case, we expect the upper-level divergence to be weaker or be displaced from the forecasted area of severe weather development -- either one would inhibit the development of severe weather. Most importantly, deep vertical divergence is necessary to remove the mass from the column producing vertical stretching and surface mesolows.

It is assumed that a favorable large-scale hydrostatic environment, which is rich in rotational energy (cyclonic vorticity), is necessary for convective storms to produce focused vortices such as tornadoes. There are four ways in which the environment can contribute rotational energy to intensifying convection. First, environmental vorticity can be converged into a supercell through the convergence term in the vorticity equation. Second, vertical wind shears can enhance the tilting of horizontal vorticity into the vertical in proximity to a supercell. Third, strong thermal boundaries, which represent solenoidal maxima, can be a source of baroclinically-generated vorticity. Fourth, frictional stresses can increase in an environment with intense rotation near the earth's

surface thus enhancing frictionally generated vorticity. A hydrostatic environment which is rich in potential vorticity (PV), i.e., the product of the vertical vorticity and static stability, is likely to be an environment which favors the intensification of supercell convection into rotating convection because of all four of these forcing mechanisms. First, by definition, a significant magnitude of environmental PV cannot be separated from the magnitude of the vertical component of vorticity. Second, strong horizontal wind shears accompanying vertical vorticity maxima imply vertical shears as they often occur near thermal boundaries or highly confluent circulations. Therefore, high vorticity implies high vertical shear. Third, thermal boundaries, fronts, and highly confluent circulations are typically baroclinic/solenoidal in structure. Strong vertical potential temperature gradients are typically associated with large horizontal gradients of potential temperature near fronts and, hence near solenoids. Fourth, inflow variations into a larger scale circulation facilitate frictional convergence and this inflow is facilitated when confluent flows rich in vorticity exist near the earth's surface. Therefore, PV is an excellent tracer for the potential rotational energy if it can be combined with a favorable environment for the generation and maintenance of convection.

The diabatic production of PV has been related to rapid surface cyclogenesis (Gyakum, et al. 1995). They found horizontal gradients of grid-scale latent heating produced a mid-tropospheric PV anomaly was related to rapid surface frontogenesis. Also, they concluded surface sensible heating created a boundary layer anomaly, which interacted with the mid- and upper-level PV maxima resulting in rapid surface

cyclogenesis. Finally, they concluded surface frontogenesis produced a vertical wind shear enhancing the diabatic generation of PV through tilting.

Potential vorticity in the midlevels is defined (in isobaric coordinates) as

$$\mathrm{PV} = -\frac{\partial\theta}{\partial p}\left(\zeta_{\mathrm{p}} + f\right) - k \bullet \frac{\partial \vec{\mathrm{V}}_{\mathrm{h}}}{\partial p} \times \nabla_p \theta. \tag{8}$$

The first term on the right side represents the contribution due to absolute vorticity on pressure surface in a statically stable environment. The second term represents the contribution due to the tilting of isentropic surfaces and thus may be expected to be important in an area of a tropopause fold. Term 1 is typically associated with a balanced QG fold as in the non-event case while term 2 is associated with unbalanced tilting and is more important in the event case.

The generation of mesoscale PV may be examined using the Lagrangian PV equation (Gidel and Shapiro, 1979). It is defined as

$$\frac{\mathrm{d}}{\mathrm{dt}}\left[-(\zeta_\theta + f)\frac{\partial\theta}{\partial p}\right] = -(\zeta_\theta + f)\frac{\partial}{\partial p}\left[\frac{\mathrm{d}\theta}{\mathrm{dt}}\right] - \left(\frac{\partial\theta}{\partial p}\right)\hat{k}\nabla_\theta \times \mathrm{F} + \left(\frac{\partial\theta}{\partial p}\right)\hat{k} \bullet \nabla_\theta\left[\frac{\mathrm{d}\theta}{\mathrm{dt}}\right] \times \frac{\partial\vec{\mathrm{V}}}{\partial\theta}. \tag{9}$$

The first term on the right side of the equation relates to the production or destruction of PV to vertical gradients of diabatic heating with isentropic absolute vorticity. This term is often called the stability change term since it is related to the changes in static stability $\left(\frac{\partial\theta}{\partial p}\right)$ due to heating. The second term represents the change in PV resulting from frictional stresses (F). Term three on the right side of the equation represents the change in PV resulting from the tilting of the horizontal component of vorticity into the vertical

through horizontal diabatic heating. Regions of strong static stability enhance the production of PV. PV will be generated when a vertical potential temperature gradient is tilted as is it brought down the mountains and there is an existing vertical wind shear near the surface in the lee of the mountains. Consequently, diabatic heating along frontal zones is an excellent environment for the production of PV due to the strong static stabilities and vertical wind shears.

In the remainder of this chapter we will: compare the synoptic situations of the event and non-event cases and discuss the accuracy of the simulations. In Chapter 2 (Paper I) we will explore the early environment 84-48 hours before the event and non-event. Their relationships between the existence of the STJ, its effects on the lower environment (associated mass and momentum adjustments, development of a LLJ, and low-level PV). In all the papers, we will compare the synoptic environment of the RDU tornado event to a synoptically similar event with severe weather forecasted but none developed over central NC. In the two companion papers our investigation of the pre-tornadic environment will contract in both temporal and spatial resolution. In Chapter 3 (Paper II) we will explore the middle time period environment 48-6 hours before the event and non-event. In Chapter 4 (Paper III) we will explore the environment over the last 6 hours before the event and non-event. Finally, in Chapter 5 we will summarize and present our conclusions.

1.2 Synoptic comparison of event to non-event

One unique aspect of this research is that we are comparing a tornadic weather event of 28 November 1988 at 0600 UTC (referred to as event) to a non-event starting at 1800 UTC 25 and ending 0000 UTC 26 January 1990 (referred to as non-event). Since the synoptic situations were so similar and yet the outcomes were dramatically different there must be some crucial and subtle difference(s) that greatly enhance the potential for severe weather. A direct comparison between the cases should highlight these differences. In the event case, no severe weather was forecasted in NC and an F4 tornado ripped through the Piedmont area, originating near Raleigh, NC and traveling northeast. In the non-event case, severe weather was forecasted by the local NWS office and from the National Severe Storm Prediction center located in Kansas City but didn't materialize over NC. Considerable research followed trying to determine why the severe weather failed to materialize but all the research focused on the event case. We are not aware of any research that has included a detailed comparison between two synoptically similar situations with such dramatically different results!

In addition, we talked to the forecaster on duty before both the event and the non-event. He explained his reasoning behind both forecasts. In 1988 severe weather was not forecasted because it did not fit the "normal" synoptic situation for a severe weather event. In fact, it was deemed a non-significant severe weather event and the forecaster worked other weather forecasting priorities. The outcome is now well known. For

comparison, the time of the event is 0600 UTC 28 November 88. This time is based on the time the tornado touched down in Raleigh, NC.

The 1990 case was significantly different from the 1988 case in both forecasts and outcome. Prior to the 1990 non-event, several forecasting agencies outside the Raleigh Office called to discuss the potential for severe weather so the Raleigh forecasters were already "expecting" severe weather. On-duty forecasters expected severe weather at RDU at 1800 UTC 25 January 1990 (non-event time). The reasoning for the time of the non-event follows. The sub-synoptic scale indicated a meso-trough associated with a convective complex over GA/SC would advance into the Piedmont around 1800 UTC. The 1235 UTC radar depiction had a solid line of heavy thunderstorms (stretching from western SC to central GA) with maximum tops to 8100 m moving northeast at 26 ms^{-1}. Six hours before the expected event the strong convection extended from western SC to western FL (just as in the event case). So, the severe convection would move over central NC near 1800 UTC. In addition, the expected severe weather coincided with the maximum heating of the day. The forecasters also had model data leading them to believe 1800 UTC would be the time of severe weather over the Piedmont. Significant features noted were: RH values ahead of trough increasing; a dry-air slot moving above the moist air; boundary-level accelerating flow and confluence ahead of the surface front; general stability indexes. AFOS hourly update program showed strong theta (thermal) advection near the surface and strong moisture convergence over the Piedmont. Also, the radar echoes had similar patterns upstream (SC and GA). These factors led the

forecasters to believe the storms would move over central NC around 1800 UTC. In addition, our hand analysis of surface data indicated a small-scale trough of low pressure moved over central NC between 1800 and 2000 UTC on 25 January 1990. For this study, we're using a synoptic-scale perspective with a characteristic time scale of 6 to 12 hours. Here we take synoptic-scale as the time required for the atmosphere to be effected by the Coriolis force (6-12 hours). This is the time scale most forecasters deal with on a daily basis. We will refer to 1800 as the onset of the non-event time and will end the non-event when the front moves over RDU (approximately 0000 UTC 26 January 1990).

a. Important similarities 6 hours before event and non-event

First, we will show the striking similarities between the two different cases. The forecasters did not have any detailed checklist to follow; they mainly relied on subjective analysis and experience. In fact, the forecaster on duty for the 1988 case was also on duty for the 1990 case. First, comparing the NWS analysis six hours before each event: 0000 UTC, 28 November 1988 to 1200 UTC, 25 January 1990.

In both cases, the 200 mb analysis (Fig. 3a and b) had a deep trough of low pressure running north-south from MN to El Paso, TX. The orientation of the troughs was the same in both cases. The PJ core stretched from eastern TX over the Appalachian Mountains and up to Quebec. The direction and speeds were also similar with a maximum speed of 33 to 36 ms^{-1} over the Appalachian Mountains. Over the southeastern states, the winds were turning to the right of the isobars implying supergeostrophic

speeds. The temperature pattern was also similar with a warm pool (- 45 ° C) over the plains states. In addition, the thermal advection was similar between the two cases.

The 300 mb analysis (Fig. 4a and b) indicates a deep trough of low pressure running north-south from MN to western TX and a ridge of high pressure was over the Rocky Mountains. The trough axis is oriented the same between the two cases. The 56 ms^{-1} isotach extended from central TX to Canada. An 87 ms^{-1} jet core was located over TN and KY (event) and over AR/TN (non-event). Also, the isotachs had the same pattern and the winds were deflecting to the right over the southeastern states implying supergeostrophic speeds. The temperature pattern was also similar with warm air advection over the southeastern coastal states and GSO temperatures of - 40/39 ° C (event/non-event).

The 500 mb analysis (Fig. 5a and b) had a deep trough of low pressure over the mid-part of the continent with a cut-off low over MI and WI. The orientation of the trough of low pressure extended back over the Big Bend region of TX. The jet core extended from GGG over Charleston, WV (CRW) and up into Canada. The general flow (both speed and direction) over the southeastern states was the same for both cases. Also, the temperature pattern was very similar in both cases with a cold pool (- 35 °C) over the Midwest US and -11 °C over HAT.

The 700 mb analysis (Fig. 6a and b) had a deep trough of low pressure stretching from WI to Del Rio, TX (DRT). There was a cut-off low over IL in the 1990 case and nearing a cut-off low over Green Bay, WI (GRB) in the 1988 case. This creates a similar

flow pattern over the southeastern states. The maximum band of wind runs from TX northeastwards. The temperature advections were similar for both cases with cold air advection over the MS and TN valley.

The 850 mb analysis (Fig. 7a and b) had a low pressure center over the northern Midwest with a trough extending over the TN valley and down to New Orleans, LA (SLI). In the 1988 case, a low pressure system was beginning to cut off over GRB with a minimum height of 128 dm. In the 1990 case, the low had cut off over northern IL with a minimum height of 128 dm. The gradient was slightly tighter in the 1990 case. The band of maximum winds (generally 20 to 25 ms^{-1}) was located from southwest to northeast, over the southeastern U.S. The temperature field was very similar between the cases -- unseasonably warm over the southeast US with the temperatures 2 to 4 °C warmer for the 1988 case. Cold air advection was occurring over the TN valley.

The surface analysis (Fig. 8a and b) had a frontal system over the TN valley and approaching the Piedmont. Also, a stationary boundary (Piedmont front) was located over the Carolina area. Over the NC coast southerly winds were transporting warm temperatures over the area. The coastal regions were in the low to mid 20s °C and inland temperatures were unseasonable warm.

The radar Summaries had many similarities (Fig. 9a and b). There was a line of rain and thunderstorms along the Carolina coast and a precipitation free region over the Piedmont. Another line of heavy thunderstorms were over the SC and GA border and they were moving into central NC at 26 to 31 ms^{-1}.

b. Important differences, 6 hours before the event and non-event

The 200 mb analysis had a few noticeable differences. First, there was slightly more ridging over Nova Scotia and into the Atlantic in the 1988 case. Second, the winds were stronger over GSO in the 1988 case (64 ms^{-1} versus 46 ms^{-1}) and throughout the southeastern states. For example, Charleston, SC had 50 ms^{-1} in the event case and only 36 ms^{-1} in the non-event and Savannah, GA SC had 50 ms^{-1} in the event case and only 38 ms^{-1} in the non-event. The higher speeds across the southeastern states are a direct reflection that *the STJ exit region is present over the Piedmont in the 1988 case.*

The 300 mb level had a stronger ridge off the northeastern states in the 1988 case. The trough of low pressure over the central US wasn't as deep in the 1988 case. For example, the 881 dm line was over Minneapolis (MSP) in the 1988 case and in 1990 the 873 dm line was over MSP. Also, there was stronger cold air advection over the Midwest and the TN valley in 1988 than in 1990.

The 500 mb level also had a stronger ridge off the northeastern states in the 1988 case. Also, the pressure gradient was slightly weaker over MI to OH in the 1990 case. This translated to a weaker jet from Pittsburgh, PA (PIT) into Canada in the 1990 case. Over Buffalo, NY (BUF) the wind was 64 ms^{-1} in 1988 and only 28 ms^{-1} in the 1990 case. *There was stronger cold air advection over the Tennessee valley in the 1988 case and there was stronger cold air advection over Arkansas in the 1990 case.*

The 700 mb analysis had slight differences in the height contours. With the cut-off low in the 1990 case a weak ridge develops over Lake Ontario. This creates stronger winds over the northeastern states in the 1988 case. There is a significant difference in the temperatures over the southeastern states. In the 1988 case the temperatures are 3 to 6 ° C warmer over the southeast US.

The 850 mb analysis had differences between the two cases. First, a weak ridge developed over Lake Erie in the non-event case. Second, the temperatures were considerably warmer in the 1988 case (2 to 4 °C) over the southeast US.

The surface analysis has several mesoscale differences. The first apparent difference is the temperature fields. *In the 1988 case, the temperatures over the Carolina Piedmont were 5 °C warmer than in the 1990 case.* The second major difference was the mesoscale pressure pattern. The event case has the main trough over the Appalachian Mountains with a clearly defined mesolow over Augusta, GA (AGS). The non-event case has the main trough running north/south from IN to AL. Also, there is not a clearly defined mesolow over NC, SC, or GA. The 1012 mb isobar does bulge into central SC; this could be the onset of a meso-trough or mesolow development. In addition, surface streamlines derived from hourly data reveal dramatic differences between the cases. The event case has strong surface confluence associated with the mesolow over SC and along the trough on the east side of the Appalachian Mountains. The non-event case has very uniform flow over the coastal states -- no confluence over SC. The only confluence area is associated with the trough located west of the Appalachians.

Comparing the 0035 UTC 28 November 1988 and 1235 UTC 25 January 1990 radar summaries revealed several striking differences. In both cases, a line of heavy thunderstorms were over the SC and GA border however the maximum tops on the thunderstorms were considerably higher in the 1988 case. The thunderstorm tops were about 14 km in the 1988 case and only 8.1 km in the1990 case. In addition, the event case had more clusters of cumulonimbus clouds indicating better convective instability and organization.

c. Synoptic examination 24 hours before event and non-events

A brief synoptic comparison 18 hours preceding the tornado event and non-event is essential to show continuity. We will compare the 200, 500 and the 850 mb NWS analysis valid 1200 UTC, 27 November 1988 and 0000 UTC, 25 January 1990.

First, comparing the 200 mb levels (Fig. 10a and b), there is a trough of low pressure over the Midwestern states. The trough is slightly deeper in the event case and the non-event case has slightly more tilt. The PJ core stretched from northeast TX over the TN valley and up over Canada. In both cases, the area of maximum wind was over western KY at approximately 70 ms^{-1}. The southern part of the jet core in the non-event dips over TX giving the appearance of a STJ. At the same time, the event case has a distinct subtropical finger stretching into MX. Winds over BRO were 50 ms^{-1}, in contrast to 34 ms^{-1} in the non-event. Additionally, winds across the Gulf Coast states were 10-15 ms^{-1} stronger in the event case.

Next, looking at the 500 mb levels (Fig. 11a and b). There is a trough of low pressure from MN down to western TX. In the event case the NWS analysis depicts a closed isobar (528 dm) low over eastern MN. The non-event does not have a closed isobar over MN however the 528 dm trough line does dip into central MN. In both cases, the trough orientation was roughly the same creating similar flow over the southeastern US (the flow over NC originates in southern TX). Winds over the southeastern states were from 240-250 degrees at 30 to 35 ms^{-1}. The temperature pattern is similar between both cases, over the southeastern US they are between -9 and -13 °C.

Finally, comparing the 850 mb levels (Fig. 12a and b). In the event case, there is a trough of low pressure from WI down to eastern TX. In the non-event case, there is a trough of low pressure in the same area however a cut off low is forming over MO. In both cases, the flow over the southeastern states is from the southwest at 10 to 20 ms^{-1}. The non-event case appears to have some cold air damming along the eastern side of the Appalachian Mountains so the temperatures are slightly lower over that area. For example, temperatures over HAT are 11/10 °C (event/non-event) and CHS are 13/12 °C (event/non-event) while inland temperatures over GSO are 13/5 °C (event/non-event) and AHN are 12/7 (event/non-event).

d. Synoptic examination 24 to 48 hours before Event to Non Event

The synoptic situation 42 hours preceding the tornado event and non-event were still very similar between the event and non-event. There was a deep trough of low

pressure over the Midwestern states and a ridge over the East Coast. The wind fields and thermal fields were also comparable.

e. Synoptic examination 72 before event and non-event

Moving back in time 72 hours from the event and non-event places the base times for the model simulations at 06 UTC, 25 November 1988 and 18 UTC, 22 January 1990, respectively. So, comparing the simulation to NWS analysis at 66 hours before each event has the base times at 12 UTC, 25 November 1988 to 00 UTC, 23 January 1990, respectively. The two cases were synoptically very different across the central US and MX.

The event case 200 mb NWS analysis (Figs. 13a and b) had a deep trough running north-south over the Rocky Mountains and a weak ridge over the Appalachian Mountains. The non-event case had a ridge spanning the Rocky Mountains and MX and a weak trough over the Appalachian Mountains. In the event case, the PJ core extends down the west coast to Huatabampo, MX then northeastward to MSP. The most significant difference between the two cases was the presence of the STJ streak across central MX in the event case. Wind speeds over central MX were between 35 to 50 ms^{-1}. The non-event case had a more zonal flow with a wide PJ streak over the central US. The upper-level ridge dominated over MX so the winds were from the west at ~ 15 ms^{-1}. Also, the 300 mb NWS analyses were synoptically similar to the 200 mb analysis.

The event case 500 mb NWS analyses (Figs. 14a and b) depict a deep trough extending north-south over the Rocky Mountains and a ridge over the Appalachian Mountains. The event case flow was from central MX up and over the central US. The non-event case had a weak trough over the Rocky Mountains and over the Appalachian Mountains with a weak ridge between. The flow in the non-event case is much more zonal than in the event case.

The 850 mb NWS analyses (Figs. 15a and b) have significant differences between the cases. Both show a trough over the eastern side of the Rocky Mountains. The Geopotential heights are much lower in the event case. The temperature pattern was similar around the trough with cold air advection over NM and warm air advection over TX and into MO. One noticeable difference is that the temperatures are 6 to 8 °C warmer in the event case. In the event case there is high pressure just offshore of GA while the non-event has weak high pressure over the central Gulf of Mexico. So, the flow in the event case is much more zonal.

1.3 Numerical Model

Due to the lack of high-resolution observational data, numerical simulations must be employed to understand the environments prior to the event and non-event. The MASS model version 5.8 (MESO, 1995) was used to produce the simulations for this study. This MASS model is a modified version of the model originally developed by Kaplan *et al.* (1982). The numerical experiments completed are summarized in Table 1.

The large scale simulation, with a grid resolution of 72 km, was employed primarily to understand the synoptic situation, verify the model, and produce a data base used for trajectory analysis (tracing origins of airmasses, back 72 hours). The 24 km simulations were used to locate potentially important mesoscale features, produce a more accurate data base for trajectory analysis, and produce hourly data sets to be used as boundary conditions for the finer mesh runs. The finest mesh (12 km) simulations were produced to examine: 1) the potentially important mesoscale features as determined in the 24 km simulations, 2) the mesoscale adjustments important to the mesoscale features, and 3) trajectory analysis preformed on the 12 km grids. The grid coverage is depicted in Figs. 16a and b.

The NMC/NCAR Reanalysis Project (Kalnay et al. 1996) provided the first guess fields used to produce the database which will initialize the numerical model. The dataset was reanalyzed using radiosonde balloon data and aviation surface data sets from the hourly observational network using an 3D-Optimal Interpolation (3DOI) scheme (Daley 1991). The incorporation of the observational data sources into the NMC/NCAR analysis

improved the vertical and horizontal resolution of the initial state fields. The grid resolution was 72 km, 24 km, or 12 km at 60 degrees north latitude. The simulations were centered over 36 degrees north latitude so the actual resolution, taking map distortion into account, was much finer (57 km, 19 km, and 9.5 km).

Model Numerics:

1. Hydrostatic primitive equation model (3-D equations for u, v, T, q & p),
2. Vertical resolution is 37 sigma layers for the 72 km run and 40 layers for the 24 & 12 km run,
3. Energy absorbing upper domain sponge layer,
4. Terrain following sigma-p coordinate system,
5. A 30 second short timestep gravity wave mode (forward - backward scheme),
6. A 90 second long timestep slow advection mode (split-explicit time marching integration using the Adams-Bashforth scheme).

Initialization Scheme:

1. A first guess using NMC/NCAR reanalyzed gridded data (2.5 x 2.5 lat/long grid & 17 levels),
2. Reanalysis using 3-D OI scheme (Daley 1991),
3. High resolution average terrain using one pass 9 point smoother,
4. Enhanced moisture analysis through synthetic RH retrieval scheme,
5. Weekly averaged 1 x 1 latitude/longitude sea surface temperature data,
6. Anderson level II land use classification scheme,
7. Climatological subsoil moisture database,
8. Normalized difference vegetation index (NVDI).

Planetary Boundary Layer (PBL):

1. A modified Blackadar high resolution PBL scheme (Zang and Anthes 1982),
2. A surface energy budget based on the Noilhan and Planton scheme (1989),
3. Soil hydrology based on the Mahrt and Pan scheme (1984).

Moisture Physics:

1. Grid scale prognosticatic equations for cloud water & ice, rain, water, and snow (Zang 1989, Lin 83).
2. Sub-grid scale Kuo-MESO convective parameterization scheme.

In addition, three-dimensional parcel trajectories used throughout this paper are derived from a Mesoscale Atmospheric Simulation System Trajectory (MASSTRAJ) software package (Rozumalski, 1997). MASSTRAJ is a three-dimensional trajectory

package utilizing the model-simulated mass and momentum fields to retrace or forecast the path of an air parcel -- producing forward and backward trajectories. Trajectory calculations are performed in the same coordinate system (x, y, and σ) as are the numerical simulations. The parcels are advected by the following time dependent iterative scheme:

$$x^{(n+1)\delta} = x^{n\delta} + \overline{u}_i^{n\delta}\left(m/\Delta x\right)\delta t, \tag{10}$$

$$y^{(n+1)\delta} = y^{n\delta} + \overline{v}_i^{n\delta}\left(m/\Delta y\right)\delta t, \tag{11}$$

$$\sigma^{(n+1)\delta} = \sigma^{n\delta} + \overline{\dot{\sigma}}_i^{n\delta}\,\delta t. \tag{12}$$

M is the map scale factor (accounts for map distortion) on a polar stereographic grid (in meters), Δx and Δy are the model horizontal grid spacing, n is the timestep (ranging from 1 to N where N is an arbitrary user-defined value) and δt is the timestep used between dataset updates for the advection of parcels as determined by $\delta t = \Delta t/N$. Delta t (δt) is the time between the model updates. For the MASSTRAJ simulations, we use Δt = 30 minutes, N = 20, and, therefore, δt = 90 seconds.

The components of the advection velocity (u, v, $\dot{\sigma}$) are determined by the following equations:

$$\overline{u}_i^{\,n\delta} = \overline{u}_i^{t_0} + \left[\frac{\overline{u}_i^{t_0+\Delta t} - \overline{u}_i^{t_0}}{\Delta t}\right] n\delta t, \tag{13}$$

$$\overline{V}_i^{\,n\delta t} = \overline{V}_i^{t_0} + \left[\frac{\overline{V}_i^{t_0+\Delta t} - \overline{V}_i^{t_0}}{\Delta t}\right] n\delta t, \tag{14}$$

$$\overline{\dot{\sigma}}_i^{\,n\delta t} = \overline{\dot{\sigma}}_i^{t_0} + \left[\frac{\overline{\dot{\sigma}}_i^{t_0+\Delta t} - \overline{\dot{\sigma}}_i^{t_0}}{\Delta t}\right] n\delta t. \tag{15}$$

The subscript i denotes the number of iterations completed to determine the final mean advection velocity. The mean velocities between simulated datasets are determined by first temporally interpolating between datasets to obtain an initial velocity at t_0. The parcel is then advected forward or backward by δt to a new location in time and space. Then, the new parcel velocity is determined and the parcel is returned to its original position at the initial time. At this point, the two parcel velocities at t_0 and $t_0+\delta t$ are averaged and the new mean velocity is used to advect the parcel. This iterative process occurs three times before the final mean velocity vector is determined and the final advection of the parcel occurs.

The parcel characteristics are assumed to be the same as the local environment encompassing a representative model grid cube. Any change in the potential temperature is the result of diabatic heating (some interpolation errors may occur). The horizontal gridded data are interpolated to parcel positions using a bi-cubic interpolation method. This method is a mathematical enhancement compared to the bi-linear schemes used in areas where there are large horizontal (nonlinear) gradients of dependant variables (Rozumalski, 1997).

1.4 Verifying simulations

All simulations were verified before the data were used. To do this, charts that included temperature, height and wind analysis were produced from initial model output and subjectively compared to the NWS upper air charts at the standard levels (200, 300, 500, 700, and 850 mb). We compared the synoptic situation, wind direction and speeds, temperatures, and height fields output. The MASS model simulations accurately simulated the environment through model runs. Only discrepancies are noted below.

The initial period model output was verified by subjectively comparing MASS output to NWS upper air charts at 1200 UTC/25, 0000 UTC/26, and 1200 UTC/26 November 1988 and 1200 UTC/22, 0000 UTC/23, and 1200 UTC/23 January 90. The MASS model was able to accurately simulate the event environment through the entire model run with one exception. The surface temperatures over the eastern side of the Appalachian Mountains were 2 - 4 °C too cold. The NWS analysis had a weak surface high just off HAT while the MASS model placed it over eastern NC (200 - 250 km to the west). The difference in the placement of the weak surface high explains the difference in the surface temperatures. The MASS simulation created a weak northwesterly flow allowing cold air damming over VA and the Piedmont. In the NWS analysis the weak surface high was located just offshore creating a weak onshore flow thus bringing warmer air over NC and VA. The only difference between the MASS simulation and the NWS analysis is a low level temperature feature over NC. In this first time period, we're not examining the NC area so we didn't consider this a significant problem.

The last 36 hour event case simulation did remarkably well reproducing small-scale features found on the NWS analysis. The only exception occurred at 0000 UTC, 28 November 1988, the heights were slightly lower (10-20 dm at the 850, 700 and 500 mb levels) in the simulation but the gradient across the East Coast was consistent between the MASS output and NWS charts. Since the wind speeds (< 5 ms^{-1}) and direction and temperatures were very accurate (< 2 °C) the height differences were considered insignificant. In the non-event case, the simulation was accurately reproducing the environment until 1200 UTC, 25 January 90. The surface low pressure over the Great Lakes region was slightly deeper (~ 4 mb) than the NWS analysis and the surface temperatures over the Carolina Piedmont were slightly warmer (2-3 °C) in the simulation (not completely reflecting the cold air damming).

For the event and non-event case, 24 hour, 24 km simulations were completed and the output grids were used for boundary conditions on nested 12 km simulations. For the 24 km simulations, Manually Digitized Radar (MDR) data was used to nudge the simulations for the first 13 hours. For this verification, NWS surface and upper-level maps and the radar composite were used. The model accurately simulated the environment.

The event case nested run began at 1600 UTC, 27 November 1988 and ran for 18 hours, to 1000 UTC, 28 November 88. The 12 km simulation was not nudged with MDR data because the MDR resolution was 40 km. With that large difference between resolutions we felt the MDR data would induce errors into the 12 km nested simulation.

The MASS model accurately simulated the environment through the entire model run. The non-event case nested run began at 0400 UTC, 25 January 90 and ran for 18 hours, to 2200 UTC, 25 January 90. We conclude that the MASS simulation accurately reproduced the environment through the entire model run.

1.5. References

Bolin , B., 1956: An improved barotropic model and some aspects of using the balance equation for three dimensional flow. *Tellus*, **8**, 67-75.

Charney, J. G., 1955: The use of the primitive equation of motion in numerical weather prediction. *Tellus*, **7**, 22-26.

Daley, R., 1991: *Atmospheric Data Analysis*, Cambridge University Press, 457 pp.

Gidel L. T., and M. A. Shapiro, 1979: The role of clear air turbulence in the production of potential vorticity in the vicinity of upper tropospheric jet stream-frontal systems. *J. Atmos. Sci.*, **36**, 2125-2138.

Gonski R. F., B. P. Woods, and W. D. Korotky, 1989: The Raleigh tornado - 28 November 1988: An operational perspective. Preprints, *12th Conf. on Weather Analysis and Forecasting*, Monterey, CA Amer. Meteor. Soc., 173-178.

Gyakum J. R., Y-H Kuo, Z. Guo, and Y-R Guo, 1995: A case of rapid continental mesoscale cyclogenesis. Part II: Model and observational diagnosis. *Mon. Wea. Rev.*, **123**, 998-1024.

Holton, J. R., 1979: *An Introduction to Dynamic Meteorology,* Academic Press, 391 pp.

Kalnay, E., M. Kanamistu, R. Kistler, W. Collins, D. Deaven, L. Gandin, M. Iredell, S. Saha, G. White, J. Woollen, Y. Zhu, M. Chelliah, W. Ebisuzaki, W. Higgins, J. Janowiak, K. C. Mo, C. Ropelewski, J. Wang, A. Leetmaa, R. Reynolds, R. Jenne, and D. Joseph, 1996; The NMC/NCAR 40-year reanalysis project. *Bull. Amer. Meteor. Soc.*, **77**, No. 3, 437-471.

Kaplan, M. L., and D. A. Paine, 1977: The observed divergence of the horizontal velocity field and pressure gradient force at the mesoscale. It's implications for the parameterization of three-dimensional momentum transport in synoptic-scale numerical models. *Beitr. Phy. Atmos.*, **50**, 321-330.

Kaplan, M. L., J. W. Zack, V. C. Wong, and J. J. Tuccillo, 1982a: Initial results from a mesoscale atmospheric simulation system and comparisons with the AVE-SESAME I data set. *Mon. Wea. Rev.*, **110**, 1564-1590.

Kaplan, M. L., Y-L. Lin, D. W. Hamilton, and Rozumalski, R. A., 1997: The numerical simulation of an unbalanced jetlet and its role in the Palm Sunday 1994 tornado outbreak in Alabama and Georgia. *Mon. Wea. Rev.*, **126**, 2133-2165.

Kaplan, M. L., R. A. Rozumalski, R. P. Weglarz, Y. L. Lin, S Businger, and R. F. Gonski, 1995: Numerical simulation studies of the mesoscale environment conductive to the Raleigh tornado. *NOAA Tech. Memo ER-90*, 1-101.

Keyser, D., and M. A. Shapiro, 1986: A review of the structure and dynamics of upper-level frontal zones. *Mon. Wea. Rev.*, **114**, 452-499.

Kocin, P. J., L. W. Uccellini, J. W. Zack, and M. L. Kaplan, 1985: A mesoscale numerical forecast of an intense convective snowburst along the East Coast. *Bull. Amer. Meteor. Soc.*, **66**, 1412-1424.

Lin, Y.-L., R. D. Farley, and H. D. Orville, 1983: Bulk parameterization of the snow field in a cloud model, *J. Clim. Appl. Meteorol.*, **22**, 1065-1092.

Mahrt, L., and H. Pan, 1984: A two-layer model of soil hydrology. *Bound.-Layer Meteor.*, **29**, 1-20.

MESO, 1995: MASS Version 5.8 Reference Manual, MESO, Inc., Troy, NY, 119 pp.

Murry, R. and S. M. Daniels, 1953: Transverse flow at entrance and exit to jet streams. *Quart. J. Roy. Meteor. Soc.*, **79**, 236-241.

Newton, C. W., 1958: Variations in frontal structure of upper level troughs. *Geophysica*, **6**, 357-375.

NOAA, 1988: Storm data, **30, 11,** 72 pp.

Noilhan, J., and S. Planton, 1989: A simple parameterization of land surface processes for meteorological models. *Mon. Wea. Rev.*, **117**, 536-549.

Reiter, E. R., 1967: *Jet Streams*, Doubleday & Company, Inc., 189 pp.

Riehl, H and coauthers, 1952: Forecasting in the Middle Latitudes. Meteor. Monogr., No 5, Amer. Meteor. Soc., 80 pp.

Rozumalski, R. A., 1997: The role of jet streak regeneration forced by a deepening continental planetary boundary layer in the explosive surface cyclogenesis of 28 March 1984. Ph. D. Thesis., North Carolina State University, 360 pp. (Available from the corresponding author).

Uccellini L. W. and D. Johnson 1979: The coupling of upper and lower tropospheric jet streaks and implication for the development of severe convective storms. *Mon. Wea. Rev.*, **107**, 682-703.

Uccellini L. W, and S. E. Koch 1987: The synoptic setting and possible energy sources for mesoscale wave disturbances. *Mon. Wea. Rev.*, **115**, 721-729.

Uccellini L. W., and P. J. Kocin, 1987: The interaction of jet streak circulations during heavy snow events along the East Coast of the United States. *Wea. & Forecasting*, **1**, 289-308.

Van Tuyl A. H., J. A. Young, Numerical Simulation of Nonlinear Jet streak Adjustment,. *Mon. Wea. Rev.*, **110**, 2038-2054.

Zack, J. W., and M. L. Kaplan 1987: Numerical simulations of the subsynoptic features associated with the AVE-SESAME I case. Part I: The preconvective environment. *Mon. Wea. Rev.*, **115**, 2367-2393.

Zang, D. L., and R. A. Anthes, 1982: A high resolution model of the plantary boundary layer-sensitivity tests and comparisons with SESAME-79 data. *J. Appl. Meteor.*, **21**, 1594-1609.

Table 1. The MASS modeling simulations performed in the study.

Initialization (UTC)	Duration (hours)	Resolution (km)	Matrix size (x, y, z)	Modifications
1200 UTC 24 Nov 88	24	24	170, 130, 40	None
0000 UTC 25 Nov 88	72	72	130, 110, 37	None
0000 UTC 22 Jan 90	24	24	170, 130, 40	None
1200 UTC 22 Jan 90	72	72	130, 110, 37	None
0000 UTC 25 Nov 88	36	24	170, 130, 40	None
1200 UTC 23 Jan 90	36	24	170, 130, 40	No latent heating
1200 UTC 23 Jan 90	36	24	170, 130, 40	None
0000 UTC 26 Nov 88	36	24	170, 130, 40	No latent heating
0000 UTC 26 Nov 88	36	24	170, 130, 40	None
1200 UTC 24 Jan 90	36	24	170, 130, 40	No latent heating
1200 UTC 24 Jan 90	36	24	170, 130, 40	None
0000 UTC 27 Nov 88	36	24	205, 155, 40	No latent heating
0000 UTC 27 Nov 88	36	24	205, 155, 40	None
1200 UTC 27 Nov 88	24	24	205, 155, 40	Yes, MDR data
1200 UTC 27 Nov 88	24	12	205, 155, 40	None
1200 UTC 24Jan 90	36	24	205, 155, 40	None
1200 UTC 24Jan 90	36	24	205, 155, 40	No latent heating
0000 UTC 25 Jan 90	24	24	205, 155, 40	Yes, MDR data
0000 UTC 25 Jan 90	24	12	205, 155, 40	None

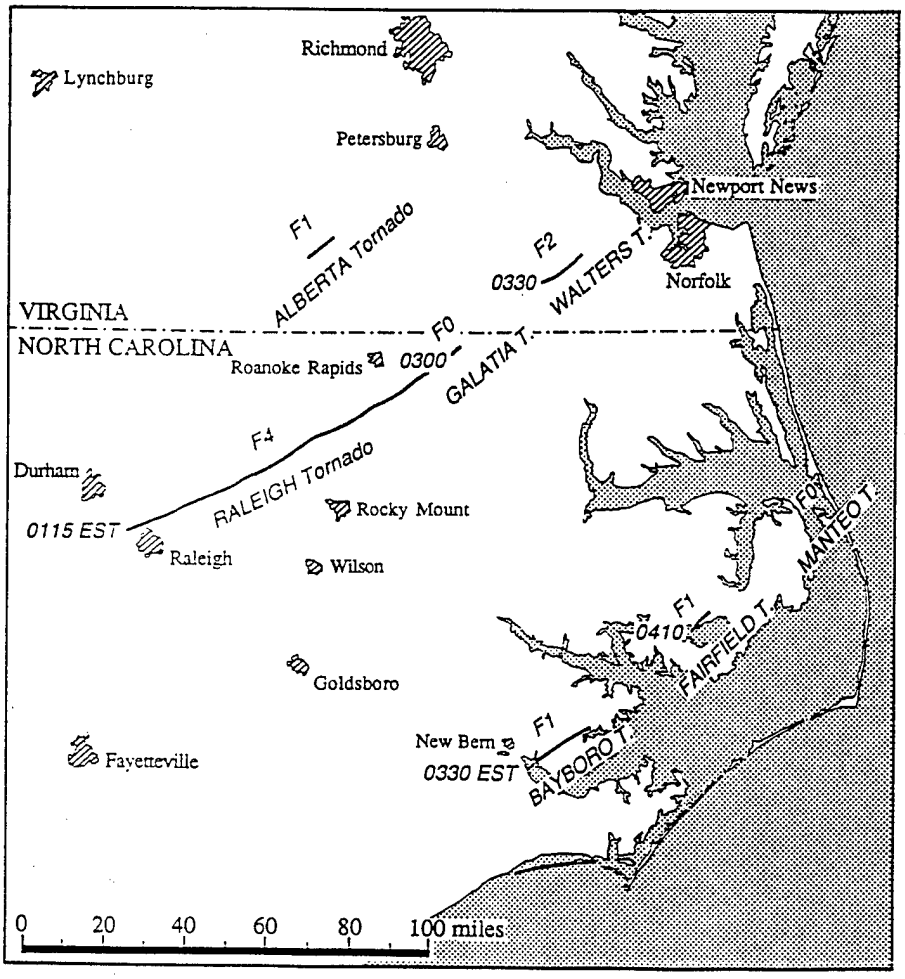

FIG. 1. Tornado paths and estimated F-scale intensity observed on 28 November 1988 (Adapted from STORM DATA 1998).

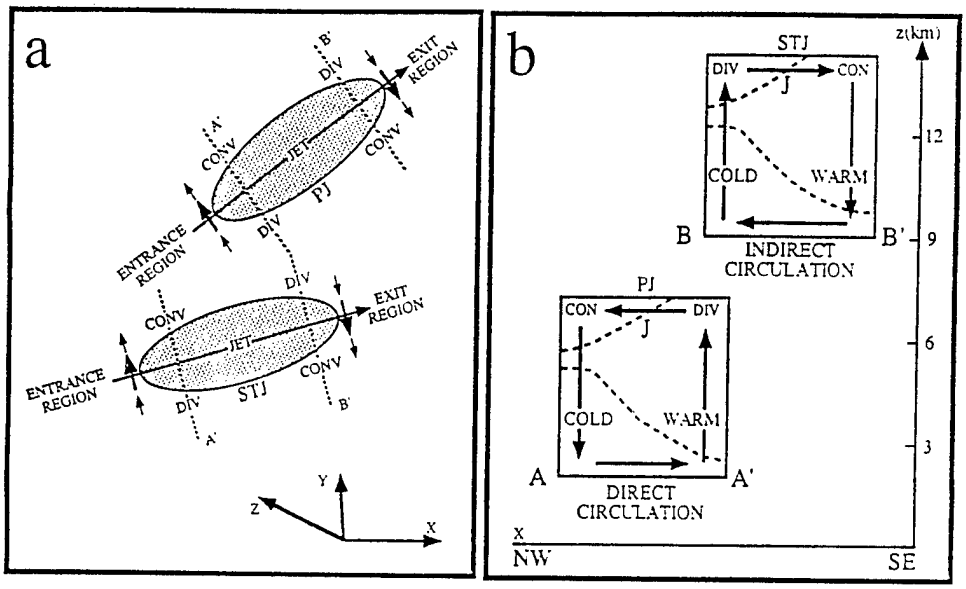

FIG. 2. Schematics depicting (a) horizontal and (b) vertical structures of the transverse ageostrophic circulations about the polar and subtropical jet streaks from Kaplan et al. (1988).

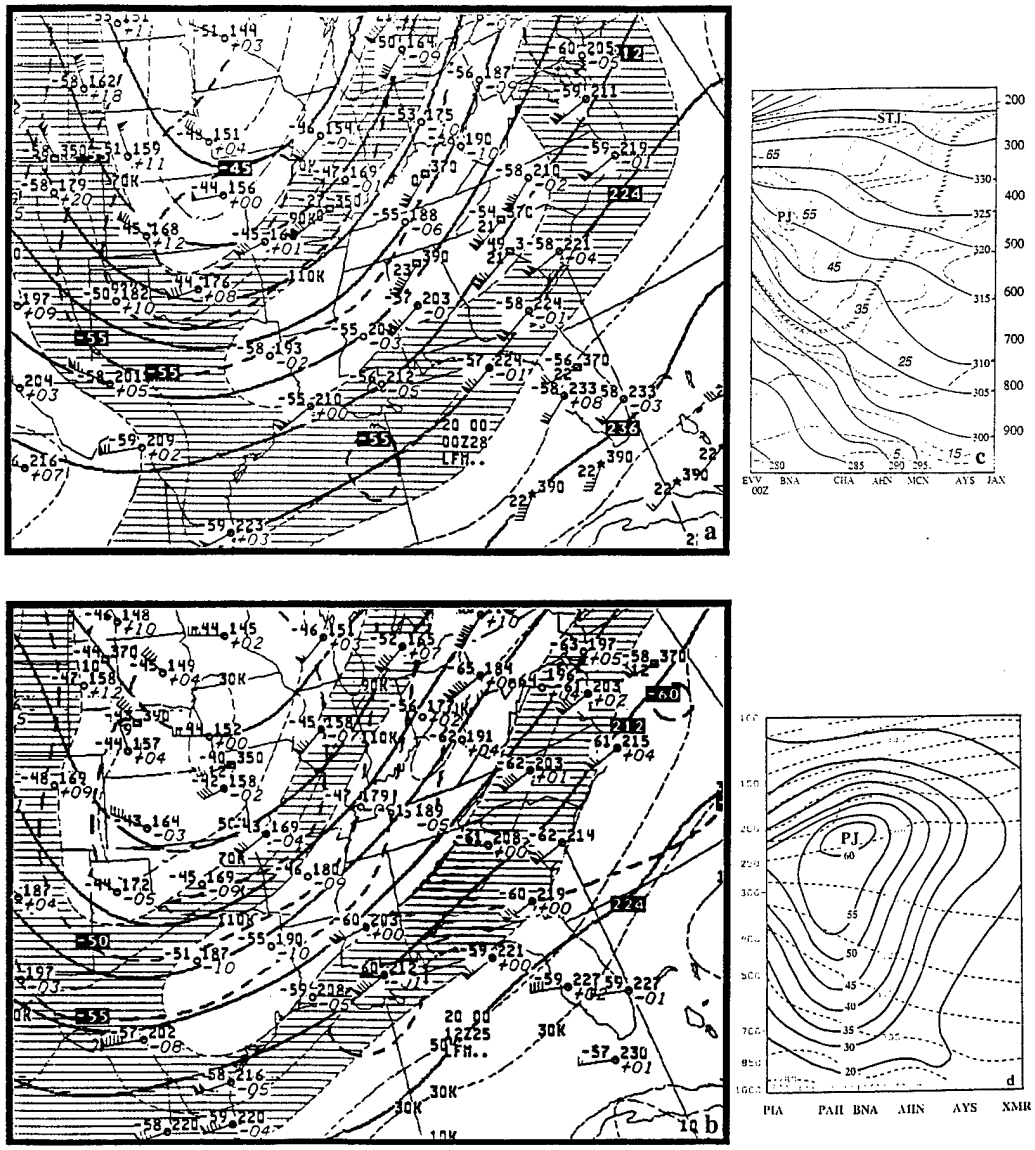

FIG. 3. (a) NWS 200 mb analysis of isotachs (knots) and vectors, temperature (C) and height (dm) and (c) observationally derived cross section from Evansville, IN (EVV) to Jacksonville, FL (JAX), isotachs (dashed line, ms^{-1}) and θ (solid line, K) valid at 0000 UTC 28 November 1988. (b) NWS 200 mb analysis of isotachs and vectors (knots), temperature (C) and height (dm) and (d) observationally derived cross section from Peoria, IL (PIA) to Cape Kennedy, FL (XMR) isotachs (solid line, ms^{-1}) and θ (dashed line, K) valid at 1200 UTC 25 January 1990.

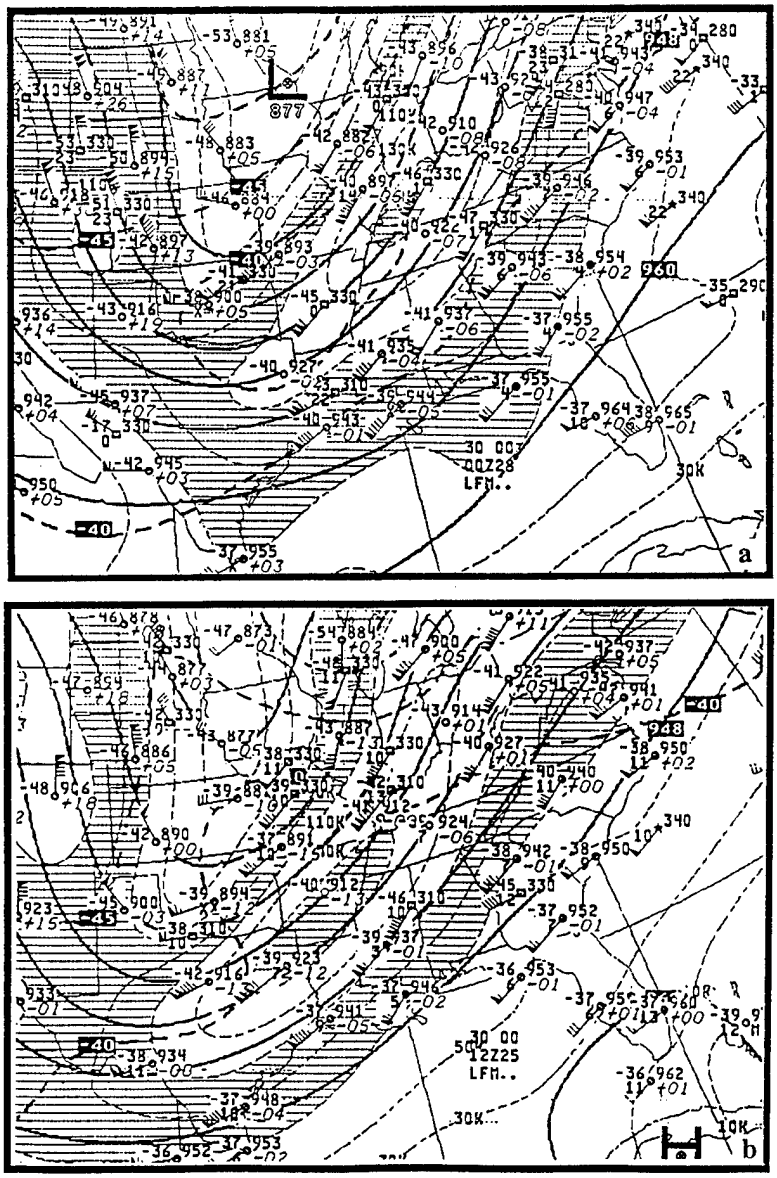

FIG. 4. NWS 300 mb analysis of wind vectors (knots), temperature (C), and height (dm) valid at (a) 0000 UTC 28 November 1988 and (b) 1200 UTC 25 January 1990.

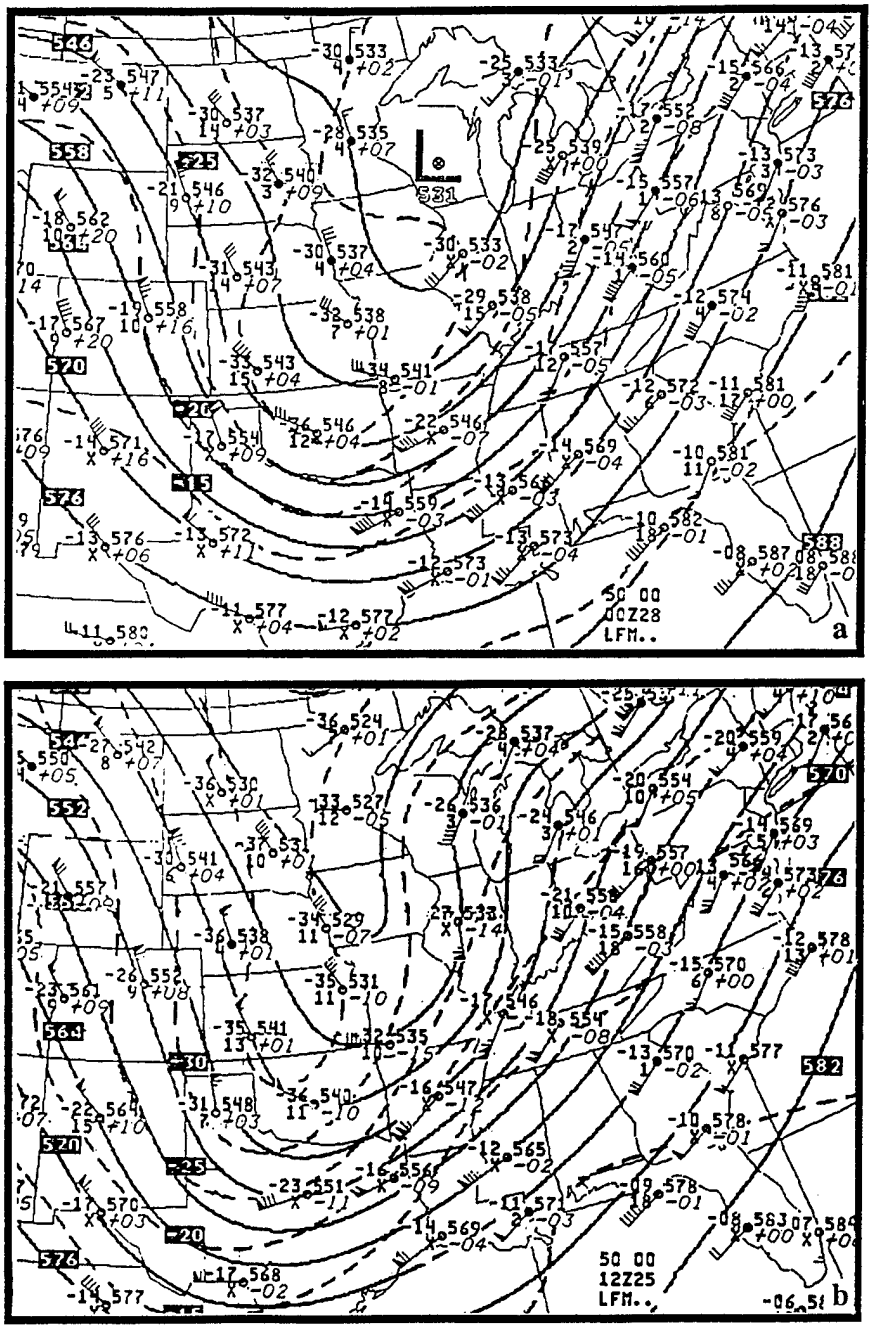

FIG. 5. NWS 500 mb analysis of wind vectors (knots), temperature (C), and height (dm) valid at (a) 0000 UTC 28 November 1988 and (b) 1200 UTC 25 January 1990.

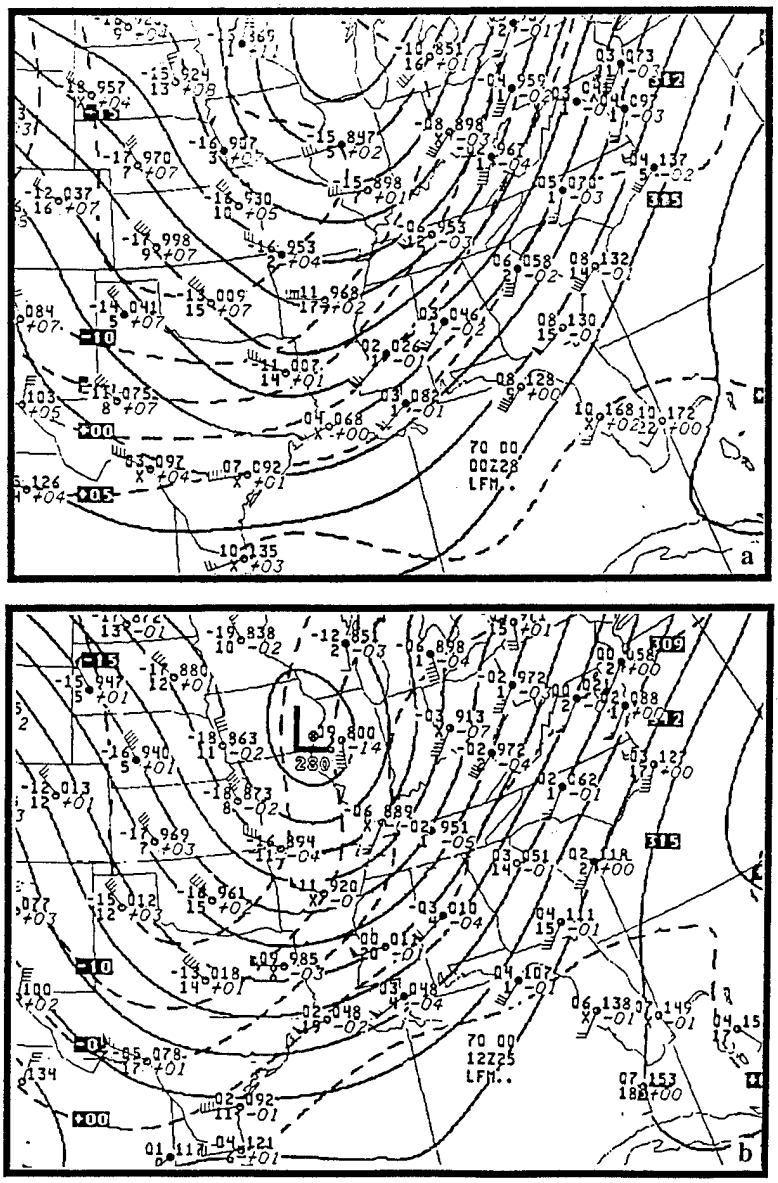

FIG. 6. NWS 700 mb analysis of wind vectors (knots), temperature (C), and height (dm) valid at (a) 0000 UTC 28 November 1988 and (b) 1200 UTC 25 January 1990.

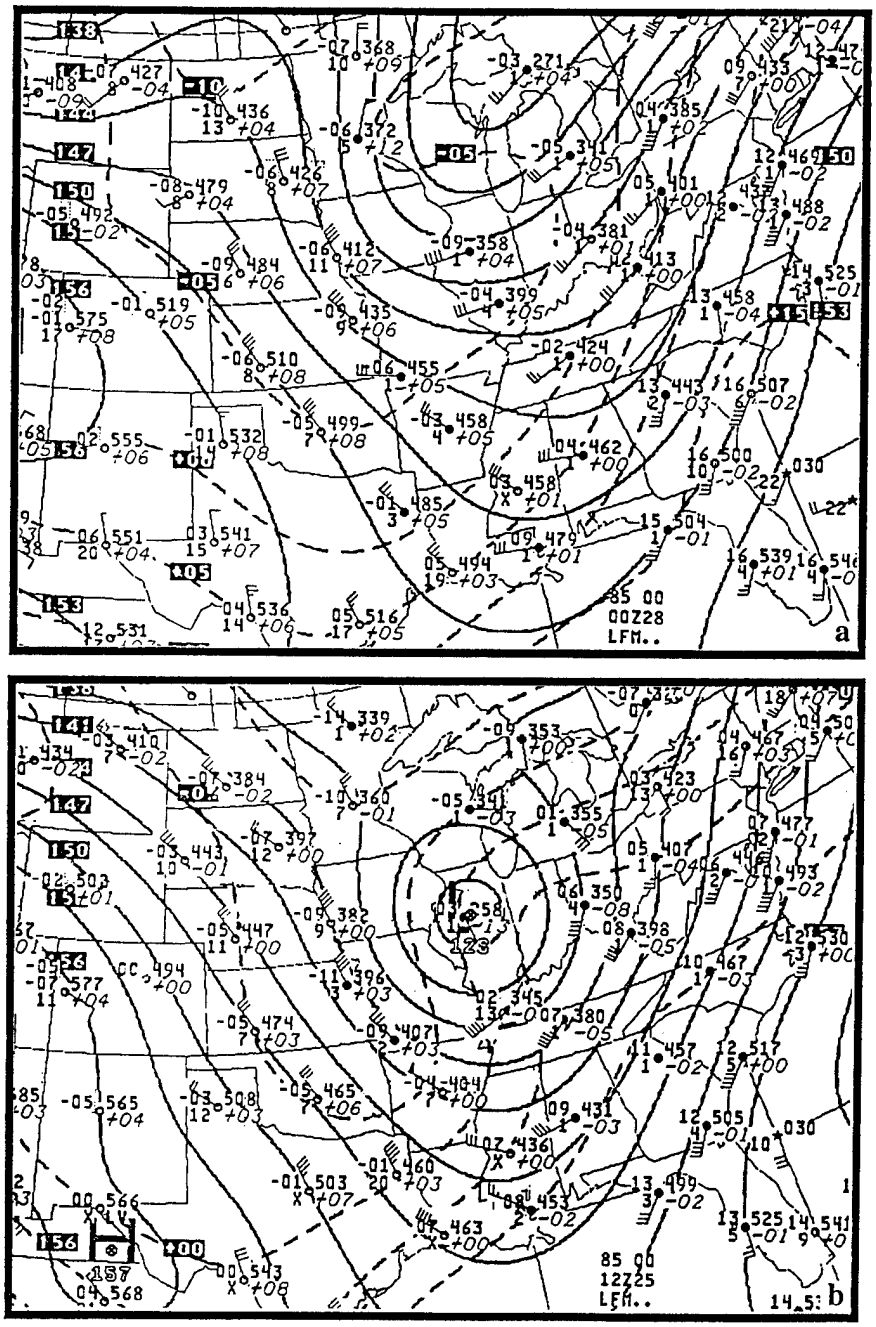

FIG. 7. NWS 850 mb analysis of wind vectors (knots), temperature (C), and height (dm) valid at (a) 0000 UTC 28 November 1988 and (b) 1200 UTC 25 January 1990.

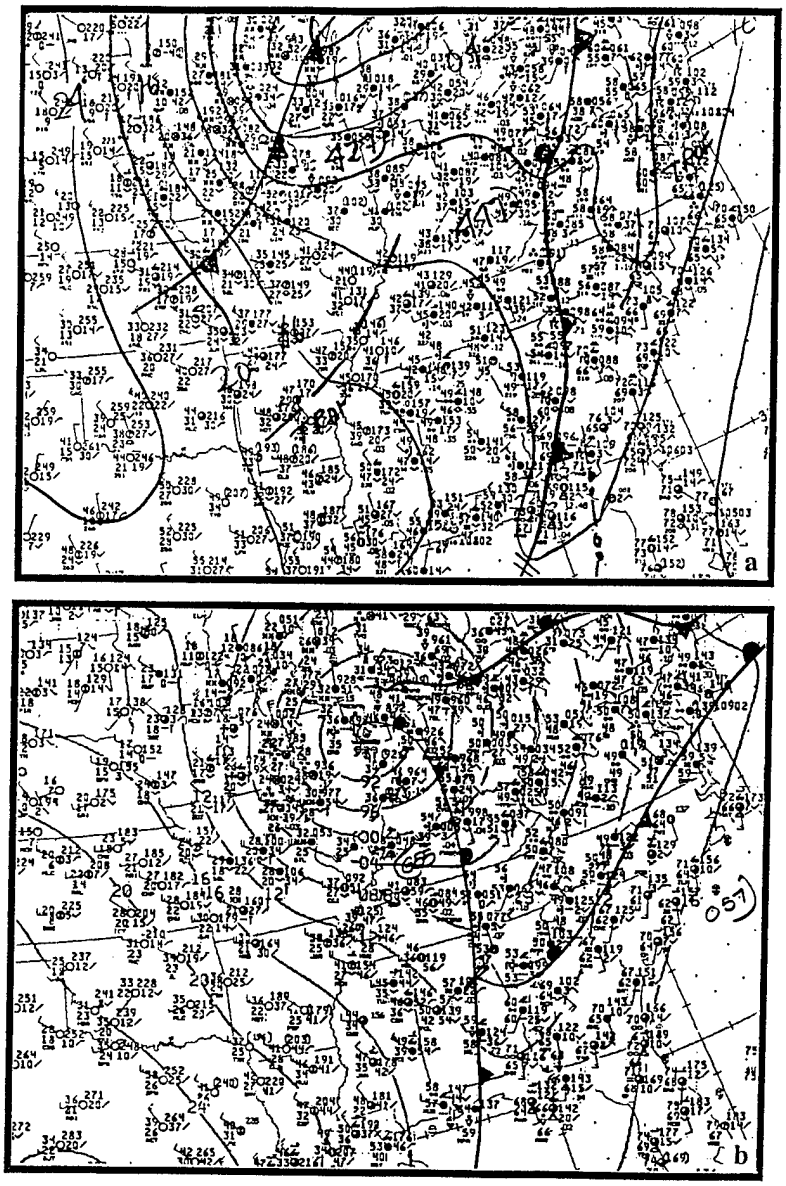

FIG. 8. NWS Surface plots valid at (a) 0000 UTC 28 November 1988 and (b) 1200 UTC 25 January 1990.

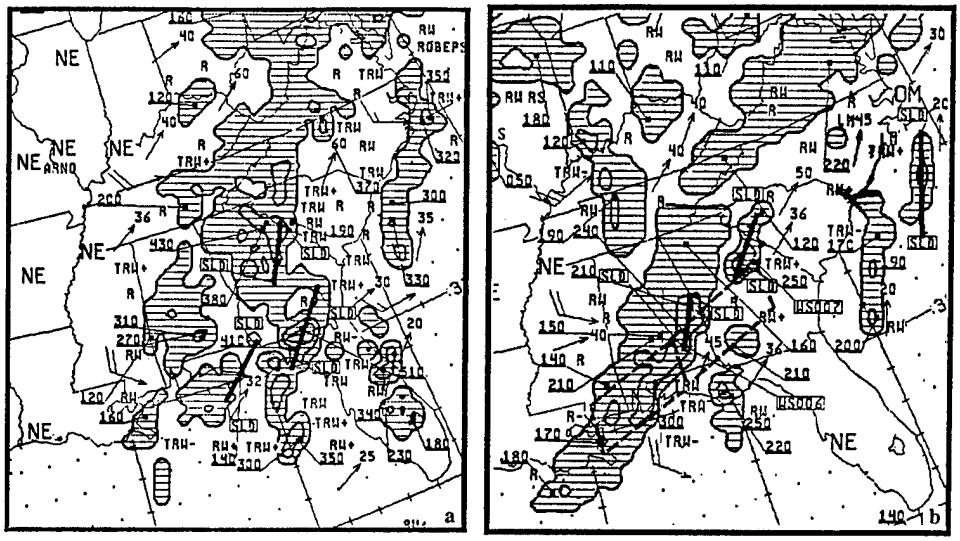

FIG. 9. NWS radar summaries valid at (a) 0035 UTC 28 November 1988 and (b) 1235 UTC 25 January 1990.

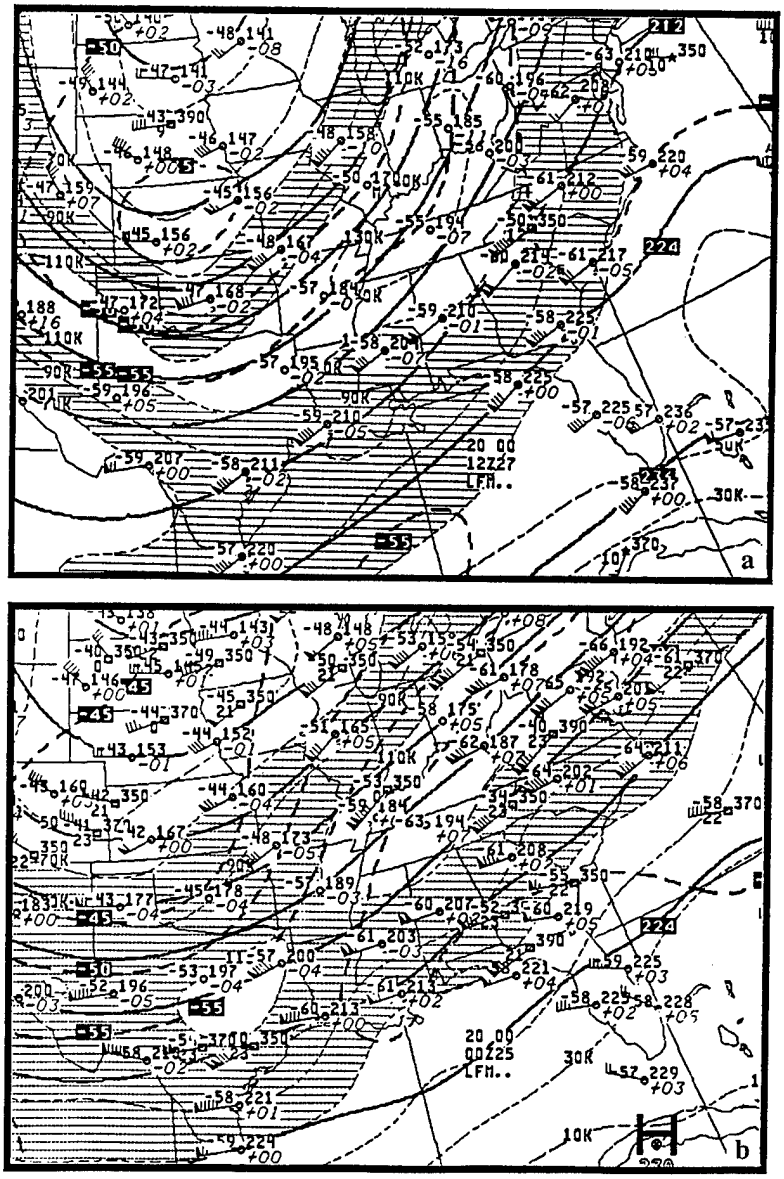

FIG. 10. NWS 200 mb analysis of wind vectors (knots), temperature (C), and height (dm) valid at (a) 1200 UTC 27 November 1988 and (b) 0000 UTC 25 January 1990.

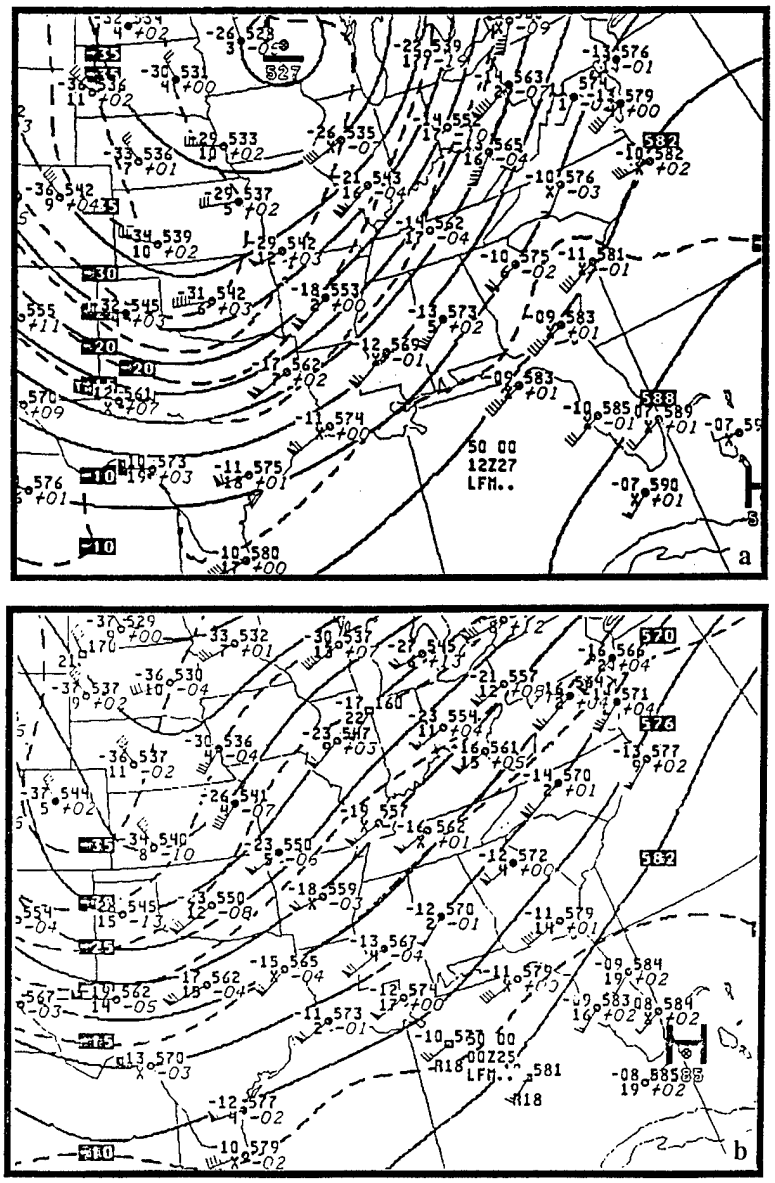

FIG. 11. NWS 500 mb analysis of wind vectors (knots), temperature (C), and height (dm) valid at (a) 1200 UTC 27 November 1988 and (b) 0000 UTC 25 January 1990.

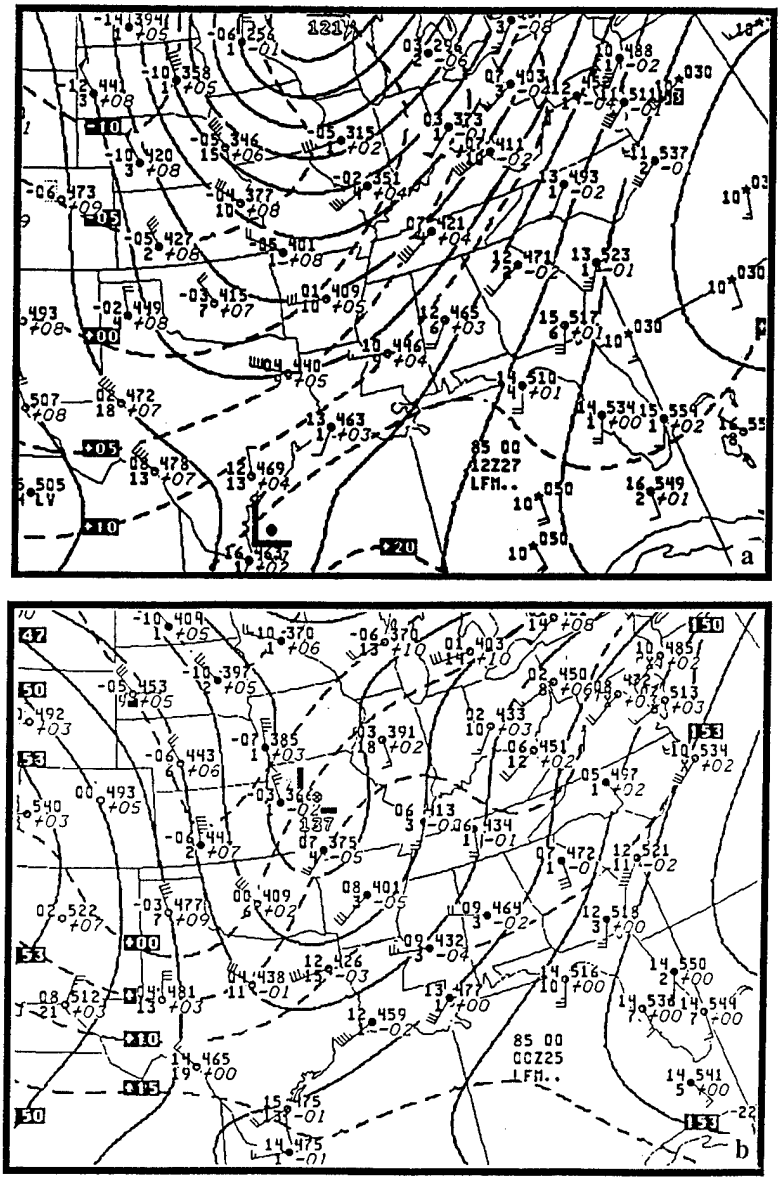

FIG. 12. NWS 850 mb analysis of wind vectors (knots), temperature (C), and height (dm) valid at (a) 1200 UTC 27 November 1988 and (b) 0000 UTC 25 January 1990.

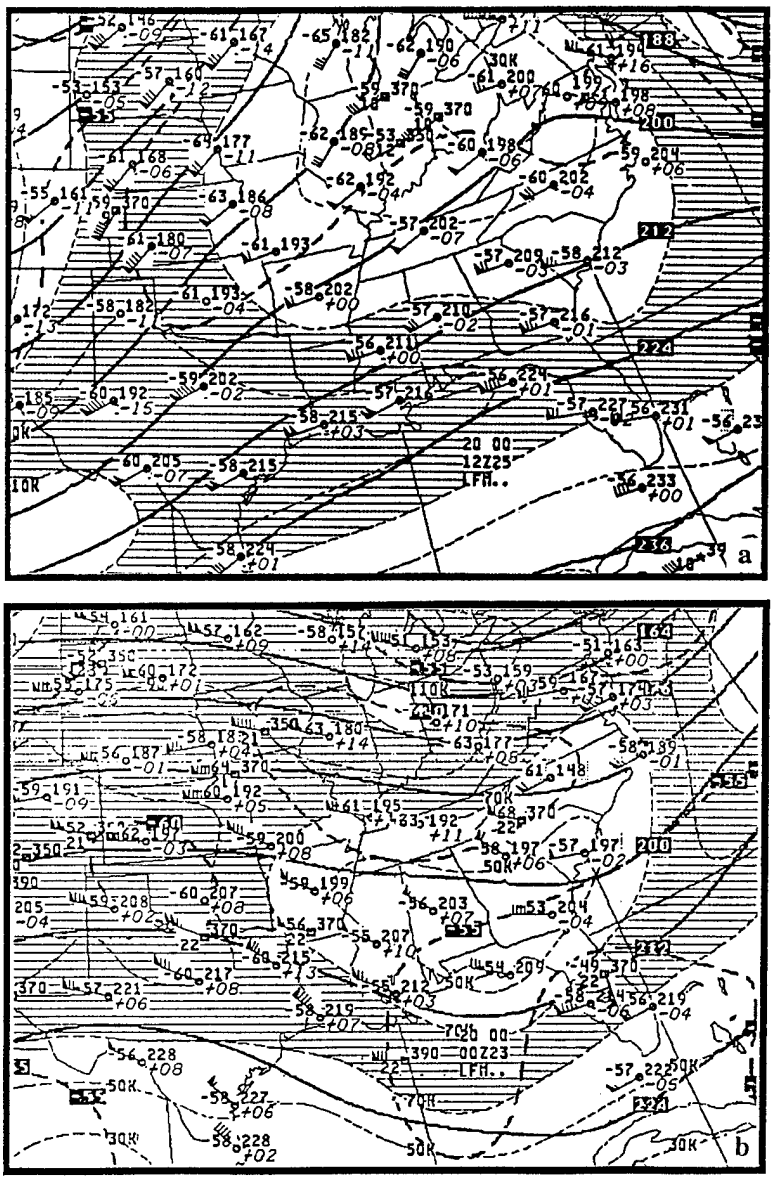

FIG. 13. NWS 200 mb analysis of wind vectors (knots), temperature (C), and height (dm) valid at (a) 1200 UTC 25 November 1988 and (b) 0000 UTC 23 January 1990.

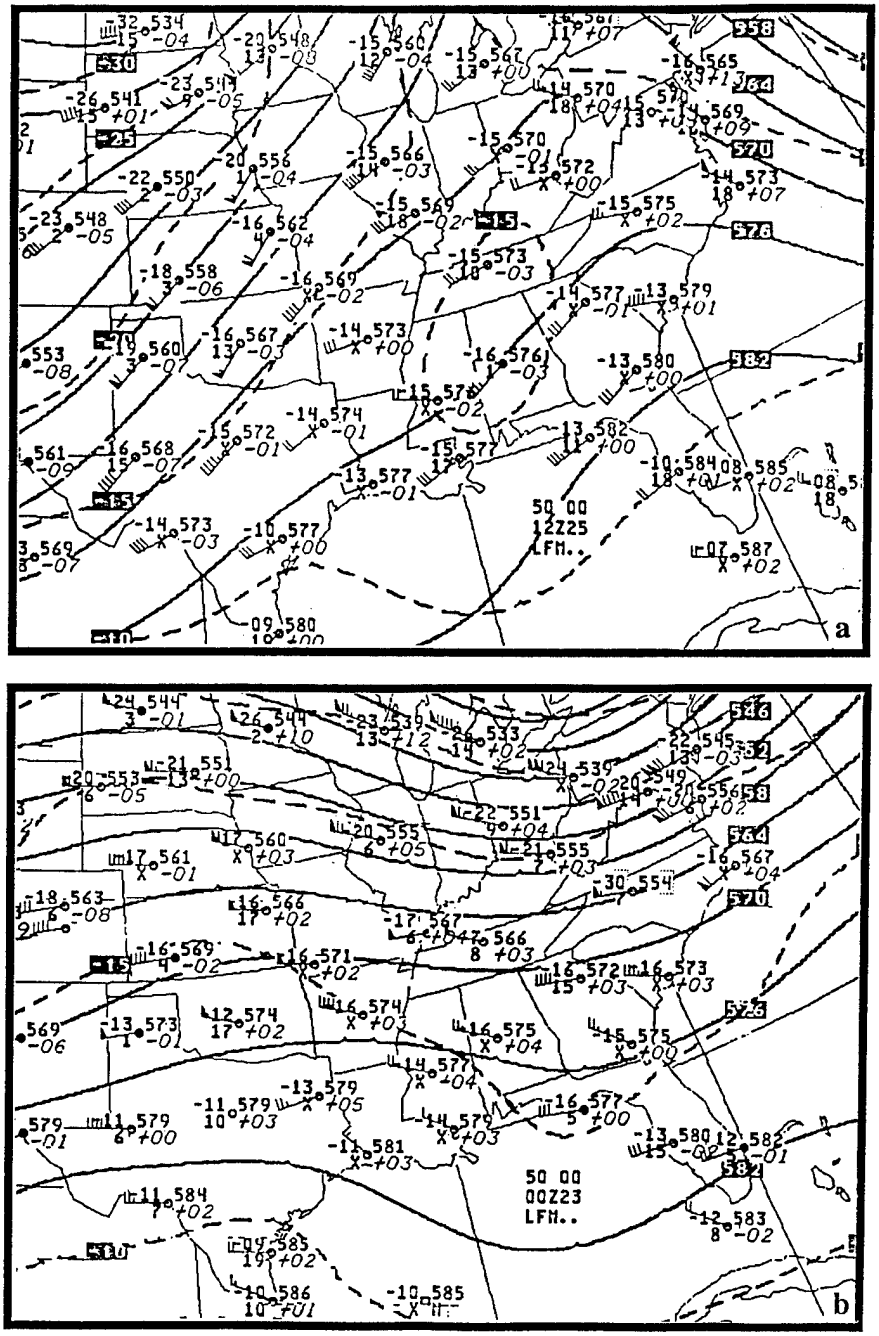

FIG. 14. NWS 500 mb analysis of wind vectors (knots), temperature (C), and height (dm) valid (a) 1200 UTC 25 November 1988 and (b) 0000 UTC 23 January 1990.

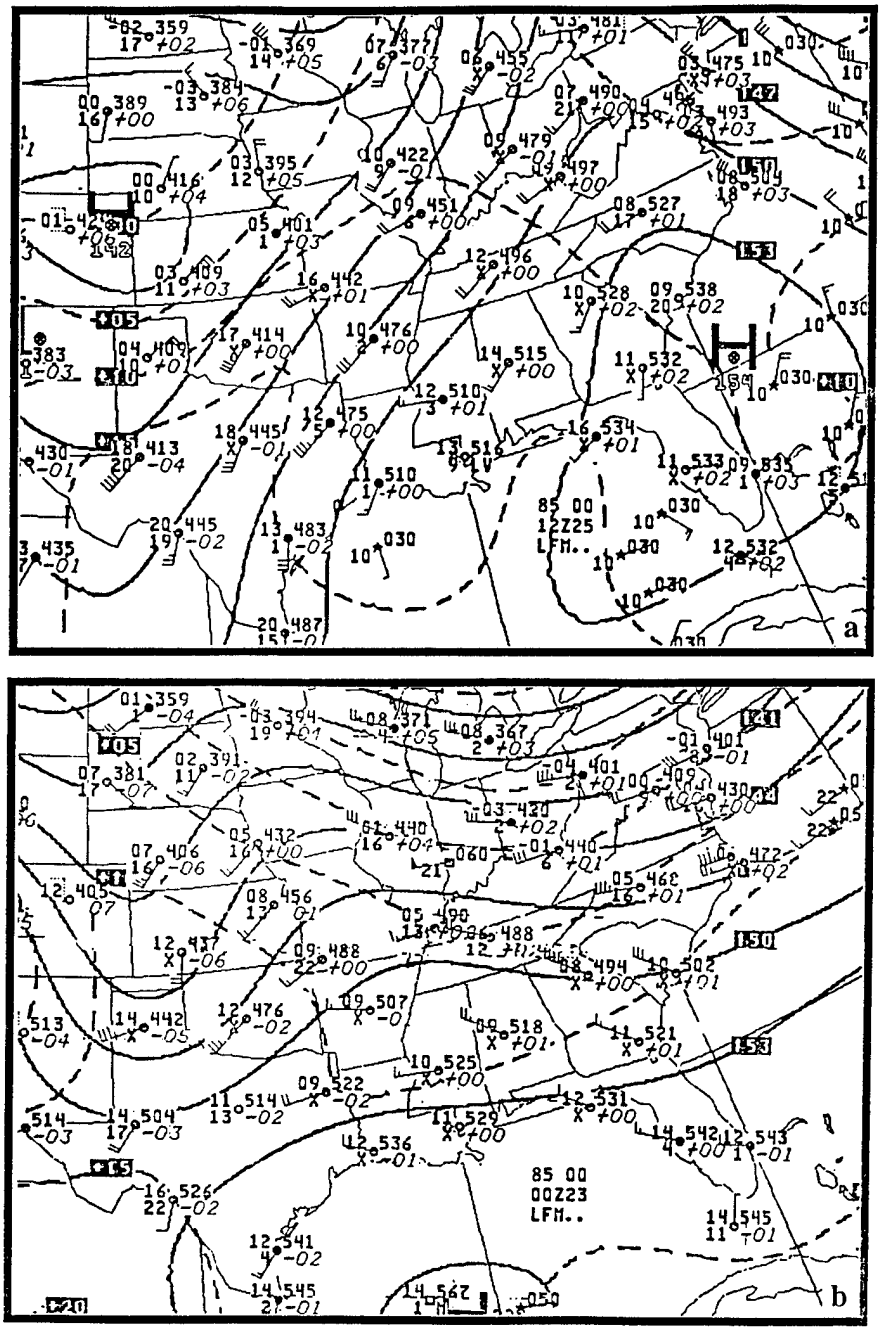

FIG. 15. NWS 850 mb analysis of wind vectors (knots), temperature (C), and height (dm) valid at (a) 1200 UTC 25 November 1988 and (b) 0000 UTC 23 January 1990.

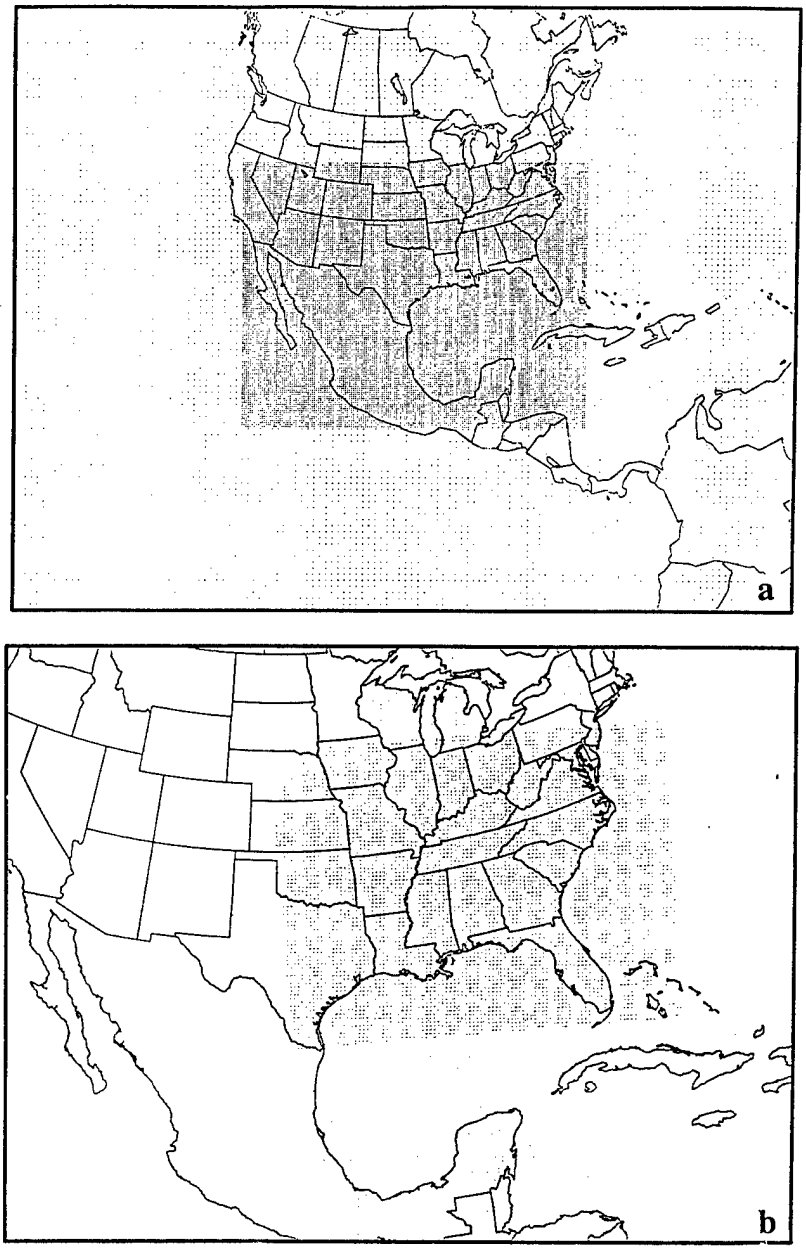

FIG. 16. Area of integration for simulations used in this study (a) depicts area of 72 km (130 x 110) and 24 km (170 x 130) simulations and (b) depicts area of 24 km (205 x 155) and 12 km (205 x 155) simulations.

CHAPTER 2

MESOSCALE SIMULATIONS OF DYNAMICAL FACTORS DISCRIMINATING BETWEEN A TORNADO OUTBREAK AND NON-EVENT OVER THE SOUTHEAST US

PART I: 84 - 48 HOUR PRECURSORS

John M. Egentowich, Michael L. Kaplan, Yuh-Lang Lin* and Allen J. Riordan

(Submitted to Weather and Forecasting for publication)

**Corresponding author address*: Dr. Yuh-Lang Lin, Department of Marine, Earth and Atmospheric Sciences, North Carolina State University, Raleigh, NC 27695-8208.

E-mail: yl_lin@ncsu.edu

Abstract

Observational analysis and mesoscale numerical simulations are in agreement concerning key dynamical processes which occurred over Mexico and the Gulf of Mexico 84 hours prior to the 1988 Raleigh (RDU), NC tornado outbreak. The subtropical jet (STJ) over northern Mexico and its associated transverse ageostrophic circulation forced air down the eastern side of the Sierra Madre Mountains creating adiabatic warming due to compressional heating. Along with this warm air, a low-level trough of low pressure formed and a low-level jet (LLJ) developed over the western Gulf of Mexico. This LLJ began the process that transported very warm and potential vorticity (PV) rich air from the Mexican plateau to the Carolina Piedmont.

The low-level PV maximum over central NC at the time of the tornado was a coherent entity traceable back 84 hours to the Mexican plateau. Over the Mexican plateau, the STJ transported the PV rich air southward then down to the midlevels. There was substantial heating over the plateau producing a deep well-mixed layer and a mountain-plains solenoid. An area of strong vertical convergence developed in the 500-600 mb layer, which increased the thermal gradient and maintained the PV. This midlevel PV was transported to the low-levels by a hydrostatic mountain wave. As the PV maxima moved down the lee of the mountains it increased due to strong static stability, tilting and frictional effects. Finally, the PV maxima moved along the Gulf Coast and up the East Coast to Raleigh, NC.

1. Introduction

The Raleigh, NC tornado of 28 November 1988 was an extraordinary event, which has stimulated a great deal of interest from the weather forecasting and research communities. This tornado violated climatology as it occurred in the middle of the night in late November with an unusual F4 (for NC) intensity. This devastating tornado was on the ground for 83 miles resulting in 4 deaths, 154 injuries, and an estimated 77.2 million dollars in property damage (NOAA 1988). It occurred in the vicinity of the polar jet (PJ) entrance region, not the exit region, where previous jet dynamical paradigms have focused (e. g., Kaplan and Paine 1977; Uccellini and Johnson 1979; Kocin et al. 1985, 1986; Zack and Kaplan 1987; Uccellini and Koch 1987). The violent episode of severe weather at Raleigh was not isolated, being also part of a larger outbreak near the PJ entrance region, which produced numerous tornadoes over NC and VA. Severe weather predictive indices based upon typical jet exit region dynamics, i. e., convective instability/buoyancy, vertical wind shear, and storm relative helicity were all sufficiently unremarkable to prevent the National Weather Service from issuing *any* severe weather watch or warning boxes prior to observations of severe weather (Gonski 1989). Furthermore, the severe weather occurred within a region of negative 500 mb vorticity advection and weak low-level warm advection thus minimizing typical quasi-geostrophic (QG) indicators of severe weather potential (Gonski 1989). The inability of standard indices/dynamical paradigms to indicate at least modest tornadic potential for such an *extreme* climatologically anomalous event clearly raises the possibility that our scientific

understanding of the mechanism of the mesoscale environment conducive to tornadic development is limited. *This is reasonable because most of our severe weather prediction paradigms were implicitly based on the PJ streak exit region model.* Therefore, the ambiguity accompanying the Raleigh tornado case study indicates that considerable research is yet to be done to truly determine the mechanisms that produce severe weather in the southeast US.

Upper level jet streaks and their associated transverse ageostrophic circulations are often the driving force for surface weather. The transverse circulations with upward (downward) motion exist at the left (right) exit region of the jet streak develop so that the atmosphere maintains a balance between the mass and momentum fields in an effort to maintain a QG state. The upper-level jet streak and its associated transverse ageostrophic circulation are coupled to the low-level circulation (Uccellini and Johnson, 1979).

A potential complicating issue to the Uccellini and Johnson paradigm (1979) proposed by Uccellini and Kocin (1987) and applied in Kaplan et al. (1998) is the juxtapositioning of the PJ streak and subtropical jet (STJ) streak (Fig. 1). The two transverse ageostrophic circulations, associated with the jet streaks, phase in a manner which produces an area of intense and very deep vertical motion; the direct circulation, associated with the PJ entrance region, phases with the indirect circulation accompanying the STJ exit region. Between the two upper-level jet streaks there is confluence in the low levels, ascent through the column, and difluence in the upper levels. With both jet

streaks producing divergence aloft over the same area one would intuitively expect a substantial amount of mass removed from the column of air.

Kaplan et al. (1998) proposed a new paradigm for severe weather development over the southeast US with three primary concepts. First, the juxtapositioning of the PJ entrance region and the STJ exit region and their transverse secondary circulations create deep QG vertical motions. Second, geostrophic adjustment of the mass field to the wind field occurs near the continental air and polar air interface, i.e., low-level fronts accompany the return branch of the STJ streak and return branch of the PJ streak resulting in an unbalanced mid-tropospheric mesoscale jet streak or jetlet. Third, a parcel undergoes stretching and tilting as it is caught up in the thermally direct unbalanced circulation in the right front quadrant of the geostrophically adjusting jetlet.

The secondary circulations associated with the PJ and STJ transport air from very different source regions, producing a strong cross-stream frontal zone, and an unbalanced, mid-level jetlet. The jetlet is unbalanced because it is constantly accelerating under the STJ exit region where it normally would be decelerating. The exit region of the developing jetlet is a region of extreme thermal wind imbalance since vertical motions are no longer balanced, i.e., accelerations occur where the Uccellini and Johnson (1979) paradigm proposes decelerating flow. The unbalanced jetlet, and ascent, extends over the tropical air creating a longer and more intense destabilization and the formation of severe weather to the right of the QG-balanced PJ. That is because air parcels converging into

the unbalanced region can be more rapidly destabilized as they have larger Convective Available Potential Energy.

It is assumed that a favorable large-scale hydrostatic environment, which is rich in rotational energy (cyclonic vorticity), is necessary for convective storms to produce focused vortices such as tornadoes. There are four ways in which the environment can contribute rotational energy to intensifying convection: (1) through the convergence of vorticity, (2) vertical wind shears that enhance the tilting of horizontal vorticity into the vertical, (3) baroclinically-generated vorticity (solenoidal maxima), and (4) frictionally generated vorticity. A hydrostatic environment which is rich in potential vorticity (PV), i.e., the product of the vertical vorticity and static stability, is likely to be an environment which favors the intensification of supercell convection into rotating convection because of all four of these forcing mechanisms.

First, by definition, a significant magnitude of environmental PV cannot be separated from the magnitude of the vertical component of vorticity. Second, strong horizontal wind shears accompanying vertical vorticity maxima imply vertical shears as they often occur near thermal boundaries or highly confluent circulations. Therefore, high vorticity often implies high vertical shear. Third, thermal boundaries, fronts, and highly confluent circulations are typically baroclinic/solenoidal in structure. Strong vertical potential temperature gradients are typically associated with large horizontal gradients of potential temperature near fronts and, hence near solenoids. Fourth, friction may generate new PV. Therefore, PV is an excellent tracer for the potential rotational

energy if it can be combined with a favorable environment for the generation and maintenance of convection.

Gyakum et al. (1995) related the diabatic production of PV to rapid surface cyclogenesis. This study found that horizontal gradients of grid-scale latent heating produced a mid-tropospheric PV anomaly that was related to rapid surface frontogenesis. Also, surface sensible heating created a boundary layer anomaly, which interacted with the mid- and upper-level PV maxima resulting in rapid surface cyclogenesis. Finally, this study concluded that surface frontogenesis produced a vertical wind shear enhancing the diabatic generation of PV through tilting. Zehnder and Keyser (1991) investigated rapid cyclogenesis in the absence of diabatic effects. They found the interaction between upper- and lower-level disturbances characterized by non-uniform PV results in significant increase in relative vorticity at the surface.

Potential vorticity in the mid-levels (in isobaric coordinates) may be estimated by:

$$\mathrm{PV} = \underbrace{-\frac{\partial\theta}{\partial p}\left(\zeta_{\mathrm{p}} + f\right)}_{1} \underbrace{- k \bullet \frac{\partial \vec{\mathrm{V}}_{\mathrm{h}}}{\partial p} \times \nabla_p \theta}_{2} \qquad (1)$$

Term 1 represents the contribution due to absolute vorticity on a pressure surface in a statically stable environment accompanying a tropopause fold. Term 2 represents the contribution due to the tilting of isentropic surfaces and is expected to be important in an area of an intense baroclinic zone. Typically, PV is estimated using only Term 1; however, in this study Term 2 is essential to understanding the underlying physical processes that separate the event from the non-event. Term 1 is typically associated with

a balanced QG fold as in the non-event case while term 2 is associated with unbalanced tilting and is more important in the event case. The generation of mesoscale PV may be examined in isentropic coordinates using the Lagrangian PV equation (Gidel and Shapiro, 1979):

$$\frac{\mathrm{d}}{\mathrm{dt}}\left[-(\zeta_\theta+f)\frac{\partial\theta}{\partial p}\right]=\underbrace{-(\zeta_\theta+f)\frac{\partial}{\partial p}\left[\frac{\mathrm{d}\theta}{\mathrm{dt}}\right]}_{1}\underbrace{-\left(\frac{\partial\theta}{\partial p}\right)\hat{k}\nabla_\theta\times\mathrm{F}}_{2}+\underbrace{\left(\frac{\partial\theta}{\partial p}\right)\hat{k}\bullet\nabla_\theta\left[\frac{\mathrm{d}\theta}{\mathrm{dt}}\right]\times\frac{\partial\vec{\mathrm{V}}}{\partial\theta}}_{3}. \qquad (2)$$

Term one relates to the production or destruction of PV due to vertical gradients of diabatic heating with isentropic absolute vorticity. This term is often called the stability change term since it is related to the changes in static stability $\left(\frac{\partial\theta}{\partial p}\right)$ due to heating (or cooling) across a layer. Term two represents the change in PV resulting from frictional stresses (F). Term three represents the change in PV resulting from the tilting of the horizontal component of vorticity into the vertical through horizontal diabatic heating. We are examining low-level PV production and maintenance so Term 2 and 3 become large and an essential mechanism for PV production.

In this paper, we will explore the relationship between the existence of the STJ and its effects on the lower environment (associated mass and momentum adjustments, development of a LLJ, and low-level PV) 84-48 hours before the development of severe weather (tornado event over central NC on 28 November 1988). Also, we will compare the synoptic environment of the RDU tornado event to a synoptically similar event where severe weather was forecast but none developed over central NC (25 January 1990). In

the two companion papers our investigation of the pre-tornadic environment will contract in both temporal and spatial resolution. Section 2 will compare the event and non-event cases. Section 3 will briefly describe the mesoscale model used to simulate the early environment. Section 4 deals with the origin of different airmasses at different levels over central NC at the time of the event and non-event. Section 5 examines the numerical simulations of these two cases. In section 6 we will investigate the origins of low-level PV. Finally, in section 7 we will summarize and present our conclusions.

2. Event and non-event comparison

One unique aspect of this paper is that we are comparing the mesoscale environment of a tornadic weather event of 28 November 1988 at 0600 UTC (referred to as event) to that of a non-event of 25 January 1990 (referred to as non-event). In the latter case, the Raleigh NWS (Gonski, personal communication, 1998) expected severe weather to develop over central NC at 1800 UTC (designated as the onset of the non-event). The convective outlook and second day severe outlook were forecasting severe thunderstorms across the Piedmont, with possible isolated tornadoes over GA. In fact, at 1437 UTC, the National Severe Storms Forecast Center (Kansas City) issued a severe thunderstorm watch for central GA, SC and NC valid from 1400 to 2000 UTC. The window of the non-event ends when the front moves over the Piedmont near 0000 UTC 26 January 1990. Since the actual time of the non-event is ambiguous we will examine the non-event over a period of time starting at 1800 UTC 25 and ending 0000 UTC 26 January 1990. Since the synoptic situations were so similar and yet there were dramatic differences in the outcome, there must be some crucial and subtle difference(s) that greatly enhanced the potential for severe weather. A direct comparison between these cases should highlight these differences. In the event case, no severe weather was forecasted in NC and an F4 tornado ripped through the Piedmont area, which originated near RDU and traveled northeast. In the non-event case, severe weather was expected by the local NWS office and from the National Severe Storm Prediction center located in Kansas City but did not materialize over NC.

We perform an in-depth comparison between the event and the expected onset time of the non-event cases. Comparisons back 6, 24 and 48 hours are synoptically similar in many ways but 72 hours prior to event there are striking synoptic differences. For the sake of brevity we will highlight the comparison using the NWS analysis six hours before each event: 0000 UTC, 28 November 1988 to 1200 UTC, 25 January 1990.

In both cases, the 200 mb analysis (Figs. 2a and b) depict a deep trough of low pressure extending north-south from MN to western TX. The orientation of the troughs is the same for the two cases. The PJ core extends from eastern TX over the Appalachian Mountains and northeast to Quebec. Over the southeastern states, the directions of observed winds are displaced to the right of the height contours implying supergeostrophic speeds. The temperature pattern and thermal advection are also very similar between the two cases. The only apparent difference between these cases are stronger winds over the southeastern states (due to the STJ) in the event case. The event case STJ and PJ are clearly depicted in Fig. 2c, a cross section based on observations.

The 500 mb analysis (Figs. 3a and b) depicts a deep trough of low heights over the central part of the continent with a pronounced low over MI and WI. The orientation of the trough of low heights extends back over the Big Bend region of TX. The jet core extends from northeast TX over WV and into Canada. In both cases the flow, in both speed and direction, over the southeastern states are similar. The height gradient is slightly weaker over MI to OH in the 1990 case translating to a slightly weaker midlevel jet in the 1990 case. Also, the temperature pattern is very similar in both cases.

The 850 mb analysis (Figs. 4a and b) depicts a low over the northern Midwest with a trough extending over the TN valley and to central LA. In the 1988 case, a low is beginning to cut off over northern WI with a minimum height of 128 dm. In the 1990 case, the low has cut off over northern IL with a minimum height of 128 dm. The band of maximum winds is located from southwest to northeast over the southeastern US. The temperature field is very similar in both the cases except that temperatures were 2 - 4 °C warmer in the 1988 case over the southeast US.

The 0035 UTC 28 November 1988 and 1235 UTC 25 January 1990 radar summaries (Figs. 5a and b) have many similarities. There is a line of rain and thunderstorms along the Carolina coast and a precipitation free region over the Piedmont. A line of heavy thunderstorms is over the SC and GA border, moving into central NC at 26 to 31 ms^{-1}. However, the height of convective tops is drastically higher in the 1988 case, 14 km versus 8.1 km. In addition, the event case has more clusters of enhanced reflectivity indicating better convective instability and organization.

3. Model summary

Due to the lack of high-resolution observational data, numerical simulations must be employed to understand the environments prior to the event and non-event. The MASS model version 5.8 (MESO 1995) is used to produce the simulations for this study. This MASS model is a modified version of the model originally developed by Kaplan *et al.* (1982). The numerical experiments completed are summarized in Table 1. The grid resolution and coverage are shown in Figs. 6a and b. The model specifics are summarized in the following:

Model numerics:

1. Hydrostatic primitive equation model (3-D equations for u, v, T, q & p),
2. Vertical resolution is 37 sigma layers for the 72 km run and 40 layers for the 24 & 12 km run,
3. Energy absorbing upper sponge layer,
4. Terrain following sigma-p coordinate system,
5. A 30 second short timestep gravity wave mode (forward - backward scheme),
6. A 90 second long timestep slow advection mode (split-explicit time marching integration using the Adams-Bashforth scheme).

Initialization scheme:

1. A first guess using NMC/NCAR reanalyzed gridded data (2.5 x 2.5 lat/long grid & 17 levels),
2. Reanalysis using 3-D OI scheme (Daley 1991),
3. High resolution average terrain using one pass 9 point smoother,
4. Enhanced moisture analysis through synthetic RH retrieval scheme,
5. Weekly averaged 1 x 1 latitude/longitude sea surface temperature data,
6. Anderson level II land use classification scheme,
7. Climatological subsoil moisture database,
8. Normalized difference vegetation index (NVDI).

Plantary Boundary Layer Physics:

1. A modified Blackadar high resolution PBL scheme (Zang and Anthes 1982),
2. A surface energy budget based on the Noilhan and Planton scheme (1989),
3. Soil hydrology based on the Mahrt and Pan scheme (1984).

Moisture physics:

1. Grid scale bulk parameterization of cloud water & ice, rainwater and snow (Zang 1989, Lin et al. 1983),
2. Sub-grid scale Kuo-MESO convective parameterization scheme.

The NMC/NCAR Reanalysis Project (Kalnay et al. 1996) provided the first guess fields for producing the database which is used to initialize the numerical model. The dataset is reanalyzed using radiosonde balloon data and aviation surface data sets from the hourly observational network using a 3D-Optimal Interpolation (3DOI) scheme (Daley 1991). The grid resolutions are 72 km, 24 km, or 12 km, centered at 60 °N. Simulations are centered over 36 °N so the actual resolution, taking map distortion into account, is much finer (57 km, 19 km, or 9.5 km).

In addition, three-dimensional parcel trajectories used throughout this paper are derived from a Mesoscale Atmospheric Simulation System Trajectory (MASSTRAJ) software package (Rozumalski 1997). MASSTRAJ uses model-simulated mass and momentum fields to retrace or forecast the path of an air parcel.

4. Airmass origin: 72 hour back trajectories

Three-dimensional parcel trajectories are constructed from the 72 km and 72 h simulations to identify the airmass origin. Parcels end over central NC at the time of the event and the expected time of the non-event. Trajectories for the 700 mb level are depicted in Fig. 7. In the event case, there are three airstreams flowing into RDU. The upper-level flow (not shown) originates southwest of the Baja of California. The mid-level flow (700 mb) originates off Mexico's west coast near Guadalajara. The low-level flow (not shown) originates south of the Grand Cayman Islands. By comparison, in the non-event case there are two flows into RDU. The upper- and low-level flows (not shown) originate from the western US or over the northern Baja of California. The mid-level flow (700 mb) originates in the Gulf of Mexico.

The mid-level trajectories differ immensely between the event and non-event. The event case 700 mb air parcel originates off Guadalajara at 677 mb and moves over the Sierra Madre Orientals, then descends dramatically (warming by adiabatic compression), moves over the Gulf (moistens), and finally ascends toward RDU (Fig. 7a). When it arrives over central NC it is unseasonably warm (with a temperature of 4 °C). By contrast, the non-event case parcel originates near the Yucatan Peninsula, circles the Gulf and ascends over the southeast US to RDU (Fig. 7b). The air parcel is unseasonably warm; however, it is cooler than the event case.

In summary, the upper- and mid-level airmasses originate over Mexico and the low-level airmass originates over the Gulf of Mexico. In contrast, the high pressure over

Mexico dominates the non-event case flow; thus the upper-level air parcels travel across the southern US. At the low levels the parcels originate over the Gulf of Mexico. It will be shown in the next section that the event case trajectories are dominated by the STJ

5. Simulated jet development

a. Jet development of the event case

The numerical simulations depict strong 200 mb subtropical jetogenesis occurring in northern MX and TX during the 0000 and 1200 UTC 25 November 1988 time period (Figs. 8a, and b). Notice the dramatic jet development increasing in both speed and aerial coverage. The area of jet development is associated with low- to middle-tropospheric cold advection over the Rocky Mountains leading to height falls (north) and height rises (south) above the surface warmed air on the leeside of the Mexican plateau. Hourly thickness advection for the 700-300 mb layer is plotted (Fig. 9) and the explosive jet development is associated with the maximum differential thickness advection. In addition, we examine the ageostrophic circulations about the developing jet (not shown). The ageostrophic flow around the jet streak axis is as expected -- a thermally direct circulation in the entrance region (over western TX) and indirect circulation in the exit region (over the southeast US). Only when the jet entrance region approached the Sierra Madre Mountains is the thermally direct circulation disrupted by large amplitude, lee mountain waves. Parcel trajectories through the jet streak verify the existence of the transverse ageostrophic circulations about the jet (Fig. 10a). Throughout the trajectory period, the jet core is located over TX (Figs. 10b and c). The parcel originates upstream of the developing jet, it accelerates, deflects to the left and ascends when it enters the jet.

The parcel then decelerates, deflects to the right and descends when it exits the jet, consistent with an idealized jet streak (Keyser and Shapiro, 1986).

The STJ's entrance region creates integrated mass flux divergence over eastern MX and the southwestern Gulf of Mexico. In response to the upper-level divergence, the 1470 and 1500 m isoheights (Fig. 11) move southward, which indicates height falls. The 12 to 18 h forecasts show a low-level trough of low pressure developing over eastern MX and the western Gulf. In response to the height falls, the lower tropospheric flow accelerates towards the northeast over the open waters of the Gulf. At 0600 UTC on 25 November 1988 the low-level flow off the TX coast is from the southwest at 5-10 ms^{-1} (Fig. 11a). By 1800 UTC on the 25th (Fig. 11b), the low-level flow becomes more southerly and accelerates to about 15 ms^{-1}. Also, the 16 C isotherm moves farther north. Similarly, the 700 mb level (not shown) offshore low-level flow increases from 5-10 ms^{-1} to 15-20 ms^{-1}. The LLJ is a low-level response to the upper-tropospheric ageostrophic circulation and the low-level trough . The accelerating LLJ transports the hot air from the Mexican plateau region to the eastern Gulf of Mexico coastal states by 1200 UTC 26 November 1988. *It will be shown that this hot air then becomes available to produce a strong midlevel jet and convective instability during periods of geostrophic adjustment ahead of the polar front accompanying the PJ.*

The significance of these dynamics can be best appreciated by depicting a 72-h backward trajectory derived from the 24 km simulation (Fig. 12). The trajectory originates at 700 mb, near RDU at 0000 UTC 28 November 1988. The parcel sinks over

the southern Mexican plateau, moves over the Gulf then takes a northeastward turn (point A) and begins to ascend in response to the increasing northward-directed LLJ (approximately 1800 UTC 25 November 1988). This signals the important role of the STJ in the transport of southern Mexican air towards the southeastern US.

In summary, the STJ is extremely important to low-level dynamics. The transverse ageostrophic circulation associated with the STJ removes mass from the air column, which creates ascent over the western Gulf of Mexico. Thus, a low-level trough and a LLJ develop over the western Gulf. The LLJ transports the hot air from the Mexican plateau to the southeast US.

b. Jet development of the non-event case

In the non-event case there is strong jetogenesis at 300 mb from 1800 UTC 22 to 18 UTC 23 January 1990 (Figs. 13a and b) over CO, KS, OK and MO. Notice the dramatic PJ development with an increase in both speed and coverage. The PJ development also appears on the 200 mb level. Again, the maximum jet development is associated with the maximum height falls and cold air advection. The STJ does not develop over MX during the first 24 h of the simulation; wind speed varies by only 5 ms^{-1}. Throughout the entire period, there is an upper-level ridge over MX so the wind over MX is from the west and turns to the south as it reaches the Gulf of Mexico. The upper-level ridge prevents the STJ from developing near the Gulf of Mexico.

We examine the 850 mb level over the western portion of the Gulf of Mexico for any LLJ development. Figures 14a and b depict the 850 mb level winds valid at 1800 UTC 22 and 1800 UTC 23 January 1990. At 1800 UTC 22 January 1990 the low-level flow is anticyclonic and is centered over the Gulf of Mexico. In the northern half of the Gulf, the flow is from the west at approximately 5 ms^{-1} and in the southern half of the Gulf the flow is from the east at approximately 5 to 10 ms^{-1}. Also, over the southern US the flow is predominantly west to east with the exception of a small area of anticyclonic flow over a weak ridge over MS. By 1800 UTC on the 23rd, an upper-level jet begins to develop over CO, KS, OK, and MO (not shown). The thermally indirect circulation about the jet exit region induces a low-level flow from the south over AL and GA. In addition, the jet entrance region has a corresponding thermally direct circulation creating a low-level northerly flow over CO and NM with the winds accelerating to 10-15 ms^{-1}. However, a LLJ does not develop over the western Gulf to transport the warmer air to the north.

The 0300 UTC 23 January 1990 850 mb ageostrophic wind vectors (not shown) over the western Gulf of Mexico are from the southeast. The southerly ageostrophic flow facilitates the warming of airmass temperatures with time. However, the easterly component of the ageostrophic flow is directed up the Sierra Madre Mountains. Thus, there is adiabatic cooling occurring over the western Gulf and eastern MX as the air ascends. This cooling facilitates the development of a surface anticyclone.

The difference between the cases in the jet development and synoptic situation is apparent when comparing the 850 mb temperatures. Figures 15a and b depicts the 850 mb temperature, pressure, and wind after 24 h of the simulation, valid 1200 UTC 23 January 1990 and 0000 UTC 26 November 1988, respectively. Over the western Gulf, in the event case, the winds are from the southwest and the temperatures are 18 to 20 °C facilitating lee cyclogenesis. In the non-event the winds over the western Gulf coast are from the east and temperatures are 12 to 14 °C.

In summary, the non-event case has a different synoptic pattern, upper-level jet development and thus different low-level responses. At this time (48-72 h before the expected event), the non-event case flow is zonal. A jet streak develops over northern TX stretching into MO (farther to the north than the event case). In the upper-levels, there is a weak ridge over MX. The ridge does not allow the STJ to move anywhere near the Gulf of Mexico inhibiting any LLJ development and the transport of the hot air from over the Mexican plateau towards the US Gulf Coast. Without the hot Mexican air over the southeastern US, the mid-level, cross-stream height gradient is weaker so the midlevel jet doesn't develop above the warm moist tropical air.

6. Potential vorticity

In the event case, the STJ produces large mass and momentum adjustments over the Sierra Madre Mountains and the western Gulf of Mexico, which facilitates the production of PV which can be increased locally either by transport or generation. In this study, we investigate low-level PV production (via Eq. 2), which is largely the product of diabatic processes normally considered small and neglected. We investigate the origins and transport of low-level PV because low-level PV is related to eventual surface mesolow development and severe weather.

a. Origins of low-level potential vorticity 72 hours before event and non-event

For the event case, we examine the origins of the low-level PV maximum ending over central NC at the time of the tornado outbreak. Figure 16 depicts the 72 h path of the low-level PV maximum. The low-level PV is traced using the widely accepted 1 PV unit ($x10^{-6}$ $Kmb^{-1}s^{-1}$) demarcing air of stratospheric origin (Reed 1955; Whitaker et al. 1988). The low-level PV maximum over central NC traces back to an area south of BRO. At the onset of the simulations (0600 UTC 25 November 1988) PV maxima are developing in the lee of the mountains over two areas: near Monterrey, MX (MMTY) and near DRT. The PV maximum near MMTY moves northeastward over Corpus Christi, TX (CRP) where it merges with another PV maximum that formed near DRT. Initially, the DRT PV maximum splits with most of the energy propagating northward, while the PV maximum that moves east is much weaker. Parcel trajectories confirm the relative

strength and movement of the PV maxima. The PV maximum originating near BRO is the most important PV source.

We also examine the origins of the low-level PV maxima for the non-event case. At the non-event time, there is a low-level PV maximum over the Appalachian Mountains, but not over central NC. The PV maximum traces back 21 h into northern MS, then weakens so much that the track is not definable. Also, several PV maxima move east from the lee side of the Rocky Mountains across OK, AR and TN and to the Appalachian Mountains.

There are two significant differences between these cases. First, the event case PV maximum is a coherent and traceable entity over 72 hours, originating south of BRO; while the non-event case PV maximum is not a coherent entity. Second, the non-event case PV maximum appears to originate over the Rocky Mountains in CO. In the event case, the low-level PV maximum originates much farther to the south, over MX.

b. Generation of low-level potential vorticity 72 hours before event and non-event

We investigate the origins of the low-level PV south of BRO. A mountain wave exists after 0600 UTC 25 November 1988 on the east side of the Sierra Madre Mountains (Fig. 17) evident in the low-level folding of the isentropes. Also, the Froude number (Eq. (3)) over the Mexican plateau (upstream) was 1.03, which belongs to a flow regime conducive to producing strong downslope winds (Lin and Wang 1996). The waves generated in the lee of the Sierra Madre mountains (wave breaking region) transport PV

to the low-levels. The 0.5 (PV units) contour extended from the 500-600 mb level over the mountains to the 900 mb level along the coast.

Clearly, the mid-level PV maximum is transported down the mountains but the next question is where does the mid-level PV originate. At 1500 UTC 24 November 1988 (Fig. 18) there is a large upper-level PV maximum (> 4.5 PV units at 200 mb) over TX and northern MX. The 1 PV unit contour extended as far south to the southern tip of the Baja of California. Also, a STJ streak is moving eastward over the west coast of MX, with its exit region and associated thermally indirect ageostrophic circulation indicated by the ageostrophic wind directed to the right of the stream approaching the upper-level PV maximum. Figure 19 (valid 1800 UTC 24 November 1988) is a cross section extending across the STJ exit region and the Mexican plateau depicting the thermally indirect ageostrophic circulation associated with the STJ streak. The thermally indirect ageostrophic circulation creates sinking (A in Fig. 19) in the right exit region of the jet streak (over the Mexican plateau) facilitating the downward transport of PV. Descent in the right exit region of the jet streak core transports a lobe of upper-level PV down to the middle troposphere (500-600 mb). This situation is considerably different from the isolated jet/front system used by Danielsen (1968) to develop his conceptual model of the downward transport of PV in the left entrance region of the jet. He concluded the greatest production of PV is associated with strong static stability found in the left jet entrance region where sinking was also occurring so downward transport of PV would mainly occur in that area. His conceptual model did not include the interaction of several jet

streaks. In the present case, there are two jet streaks within the STJ; the first jet streak (located over TX and the Gulf Coast States) facilitates PV production and transports the PV southward. Then the second STJ streak and its associated thermally indirect circulation transports the PV down to the mid-levels over the Mexican plateau. The downward transport of PV is yet another way the STJ is critical for the future development of severe weather over the southeast US.

The PV is transported to the mid-levels until approximately 2000 UTC 24 November 1988. At the same time, there is substantial heating over the Mexican plateau (Fig. 16). We will refer to the area within the box as the PV generation area. By 0000 UTC 25 November 1988 (Fig. 20), there is a very deep and warm dry adiabatic layer (potential temperature of 310 K up to ~650 mb) over MX, which is being forced by large surface sensible heat fluxes resulting from clear skies, minimal soil moisture and arid conditions. By 2100 UTC, a mountain-plains solenoid (MPS) (Tripoli and Cotton 1989) develops over the PV generation area with strong ascent occurring in the low-levels over the eastern half of the PV generation area. At the same time, the upper-level thermally indirect circulation creates descent to the mid-levels over the eastern half of the PV generation area. At 0100 UTC 25 November 1988 (Fig. 21) these two ageostrophic circulations create an area of vertical convergence in the 500-600 mb layer over the eastern half of the PV generation area (Fig. 16). This convergence perturbs the potential temperature field, increases the thermal gradient (static stability) and generates PV, i.e. the 500-600 mb level PV maximum is increasing. The relative contribution of each term

in the PV (Eq. 2) is evaluated at 0100 UTC about the 625 mb level in the PV generation area in a manor analogous to Kaplan and Karyampudi (1992). Data used in the calculations were taken from parcel trajectory output with the exception of the gradient field, which was derived using a centered finite differencing scheme calculated from trajectories surrounding the center trajectory point. Term one dominates the production of PV (contributing 78%) by the dramatic increase in static stability associated with the intense diabatically-forced thermal gradient (and vertical frontogenesis) above the dry adiabatic layer. The MPS produces a well-mixed, elevated boundary layer. Thus the main contribution to the diabatically-forced thermal layer is the surface sensible heating. This midlevel PV maximum then moves eastward and by 0600 UTC it is over the eastern side of the Sierra Madre Orientals. Later, during the 0600 - 1200 UTC nocturnal period, a hydrostatic mountain wave develops in the lee of the mountains (Fig. 17) facilitating the downward transport of the midlevel PV generated earlier. Model-generated soundings indicate an inversion develops due to radiational cooling over the coastal area in the early morning hours. Thus, the low-level PV moves down the lee of the mountains and increases due to strong static stability in the presence of nocturnal surface cooling.

For the non-event case we again examine the flow on the eastside of the Sierra Madre Mountains near BRO (Fig. 22). In addition to Fig. 22, we examine numerous cross sections at various times. Throughout the simulations there were no low-, mid-, or upper-level PV maxima over the coastal region. *There was a dramatic difference for the non-event case from the event case; the low-level wind field over the Gulf of Mexico was*

from the east thus no mountain waves developed near BRO. Also, there was not a STJ to facilitate the downward transport of mid- or upper-level PV. Additionally, cross sections depict very little daytime heating over the Mexican plateau (Fig. 23). The easterly low-level wind advects moisture rich air over the Mexican plateau producing low-level clouds thus minimizing the solar radiation and surface warming. The advection of relatively warm, moist air off the Gulf reduces the intensity of the nocturnal inversion because of reduced radiational cooling, hence, less PV production occurs as the stability is weaker than in the event case. Throughout the evening, a shallow surface inversion develops over the mountains increasing low-level PV over this region due to the increasing static stability. Additionally, we examine the PV maximum in the non-event case east of the Rocky Mountains over northern TX and OK. Here, the PJ clearly induces waves in the lee of the mountains. Cross sections perpendicular to the PJ indicate downward transport of PV is occurring in the left entrance region of the PJ.

Next, we evaluate the relative contribution of each term in the PV (Eq. 2) as the parcel descends the leeward mountain slope. In the event case, the total PV increased 412 %, from 0.7665 (PV units) to 3.159 (PV units). Term one contributes 30.6% to the production of PV by the change in static stability associated with the developing low-level radiation inversion over the coastal region. Also, vorticity increases due to vortex tube stretching as the air volume advects down the mountains. Term two contributes 31.9% to the change in PV resulting from horizontal gradients of diabatic heating within regions of wind covariances. The 910 mb PV maxima is within the inversion hence it is

affected by friction. Term three contributes 37.5% to the production of PV resulting from the tilting of the horizontal component of vorticity into the vertical through horizontal diabatic heating. In this case, the low-level vertical wind shear and vertical potential temperature gradient advect down the mountains (and is tilted) generating PV. The diabatic forcing mechanisms in the PV equation (Eq. 2) that are typically neglected are very important in the low-level generation of PV.

In the non-event case, the parcel trajectory is drastically different from the event case. It ascends the Sierra Madre Orientals then circles (clockwise) the mountains. Throughout the parcel's ascent up the lee slope of the Sierra Madre Mountains, the total PV decreases from 0.273 PV units at 982 mb to 0.173 PV units at 788 mb. The decrease of low-level PV is due to a production of anticyclonic vorticity. Our calculations from model output indicate that term one produces 69% of the total anticyclonic vorticity. Term one represents the production of anticyclonic PV by vortex tube contracting as the air volume moves up the mountains. Term two contributes 13.8% to the production of anticyclonic PV resulting from horizontal gradients of diabatic heating within regions of wind covariances. The frictional component consists of effects from barotropic surface drag and the baroclinic effect of mixing. Term three represents a smaller amount (17.2%) of anticyclonic PV production as the low-level vertical wind shear and vertical potential temperature gradient are advected up the mountains. Here, the synoptic flow is transporting the parcels in a clockwise direction over the mountains (rightward-directed

KE). We hypothesis that the large scale mixing is bringing down the rightward directed momentum overwhelming the effects of surface drag and producing anticyclonic PV.

c. Maintenance of low-level potential vorticity

We investigate the transport and maintenance of the low-level PV north along the TX coast. First, we examine the possibility that the continuous downward transport of the upper-level PV maintains the low-level PV. We produce numerous cross sections through the low-level PV maximum as it propagates up the TX coast. Throughout this period, there is no downward transport of the upper-level PV. All the cross sections depict a low-level PV maximum but no mid-level or downward transport of upper-level PV. This supports the idea that the PV is generated and maintained in the low-levels.

We examine other potential energy sources (wind shear gradient, potential temperature gradient, and surface convergence) and their relationship to low-level PV. These energy sources all act to produce and/or maintain PV via Term 3 in Eq. (2). The figures valid 1200 UTC on 25 November 1988, depict: 900 mb PV and the gradient of the magnitude of wind shear over the 925 to 850 mb layer (Fig. 24a), 900 mb PV and surface streamlines (Fig. 24b), and 900 mb PV and surface potential temperature (Fig. 24c). Each PV maximum (> 1 PV unit) is associated with a strong vertical and horizontal wind shear gradient, localized areas of strong gradients of potential temperature, and an area of convergence. Throughout the entire simulation there is excellent consistency between these energy sources and the low-level PV maxima. In addition, the strength of the

vertical and horizontal wind shear associated with the LLJ is closely correlated to the low-level PV -- as the shear weakens so does the PV. So, it appears a combination of strong vertical and horizontal wind shear, surface convergence and a thermal gradient are essential ingredients for the production or maintenance of low-level PV. Low-level vertical and horizontal wind shear associated with the LLJ is the most likely transport and maintenance mechanism of PV since the LLJ is tied to the persistent STJ.

Next, we investigate the transport and maintenance of low-level PV for the non-event case. Depictions of the 900 mb PV and the magnitude of wind shear, potential temperature gradient, and surface convergence show a different relationship than the event case. The depictions valid 0000 UTC on 23 January 1990 (Figs. 25a, b, and c) have no significant areas of PV. Over GA, SC and NC there is strong vertical and horizontal wind shear. However, there is no significant convergence and a weak potential temperature gradient thus no low-level PV maximum.

d. Lagrangian investigation of low-level potential vorticity

In the final PV analysis of the event case, we switch to a Lagrangian frame of reference. We locate the PV maximum south of BRO and send a parcel through that area at 0600 UTC 25 November 1988. The parcel originates over the Sierra Madre Mountains at 0300 UTC, descends over the coastal area, then moves northward and merges with another low-level PV maximum (originating from the mountains near DRT) and continues to move northeastward to LA (Fig. 26). When the PV maxima merge near

CRP, there is no increase in the parcel's PV, indicating the PV maxima originating over MX is the dominant feature. In this trajectory, the parcel's motion vector is almost exactly the same as the PV maximum's vector so the parcel's movement and values listed in Table 2 can be considered a volume encompassing the PV maximum. The PV associated with the parcel increased dramatically as it descended to the 910 mb level due to static stability, vortex tube stretching, tilting, and frictional effects. As the PV maximum (parcel) moves northward along the coast it is maintained by convergence, a thermal gradient, and strong low-level wind shear associated with the LLJ. As the LLJ's shear field weakens with time so does the PV maximum. At approximately 0300 UTC 26 November 1988, the parcel enters an area of convective precipitation in eastern TX; consequently, the PV maximum increases from latent heat energy. Figure 26 depicts the parcel trajectory and 900 mb latent heating (Ch^{-1}) at 0400 UTC 26 November 1988. The greatest PV increase (from 0.8989 to 1.705 PV units) occurs when the parcel moves through a latent heating maximum (>40 Ch^{-1}) at 0400 UTC. Sensible heating is also examined, but is negligible (maximum value of 0.11 Ch^{-1}). So, the low-level PV increase is directly related to latent heating.

In summary, south of BRO, the PV is initially transported downward to the mid-levels by the ageostrophic circulation associated with the STJ, maintained by the mountain-plains solenoid, then transported to the low-levels by an ensemble of mountain waves. Also, diabatic effects accompanying increased static stability, vortex tube stretching, tilting and frictional effects generate PV. The PV is transported by the LLJ

and maintained by low-level wind shear and latent heating. The low-level PV maximum originates east of the mountains near BRO, moves northeast, following the coastline along the Gulf States and up to RDU at the time of the tornado.

In the final PV analysis of the non-event case we again examine parcel trajectories. Parcels on the leeward side of the mountains all originate over the low coastal area of northeastern MX, ascend over the Sierra Madre Orientals then move clockwise back over MMTY some 24 hours later (Fig. 27 and Table 4). In this trajectory, the parcel's movement is very different from the PV maximum's movement. The trajectory data depict the parcel's movement through the environment. The synoptic flow and parcel movement is very different from the event cases. In the non-event case, the flow is from the east forcing the air parcels up the mountains. In the lee of the mountains, there is little low-level PV most likely because the east to west flow does not facilitate the development of mountain waves or a surface inversion, which facilitates low-level PV. The parcel ascends the leeward side of the Sierra Madre Mountains then it warms as it descends over the MX plateau. Throughout the parcel's path, there is no convection (latent heating) over the Mexican plateau. As the parcel moves across the Mexican plateau through the evening hours a weak radiation inversion develops, which increases the low-level stability generating small amounts of low-level PV. Weak daytime heating also acts to increase the low-level stability, which maintains the weak, low-level PV. The parcel then begins its slow counterclockwise movement through the Sierra Madre Orientals. The most significant aspect of the parcel trajectory is that the parcel and any

associated PV remains over MX. Without the STJ and its associated LLJ there is no transport of warm, PV rich air to the north.

In summary, very weak, low-level PV is generated over the MX plateau, however, there is not a transport mechanism (a STJ and associated LLJ) to move the PV over the US.

7. Summary

Observational analysis and mesoscale numerical simulations are in agreement concerning key dynamical processes which occurred over MX and the Gulf of Mexico up to 72 hours prior to the 1988 Raleigh, NC, tornado outbreak (event case). Strong cold air advection over NM and northwestern TX intensified the height gradient (PGF) and, in turn, intensified the STJ streak over TX and MX. Initially, the STJ exit region and its associated transverse ageostrophic circulation created sinking over the Mexican plateau. Air was forced down the eastern side of the Sierra Madre Mountains, which warmed due to adiabatic (compressional) heating. Along with this warm air, a low-level trough of low pressure developed over the western Gulf of Mexico. The STJ right entrance region moved over the western Gulf of Mexico, which helped create upper-level divergence, upper-level mass removal and ascent in the air column. The low-level convergence, ascent throughout the levels and velocity divergence aloft helped develop the surface trough and the associated LLJ. This LLJ began the process to transport warm low-level air from the Mexican plateau to the Carolina Piedmont.

The non-event case had a different synoptic pattern. Seventy-two hours before the expected event, the upper-level flow was zonal over the US with a ridge over MX. A PJ developed over northern TX, OK and MO. The upper-level ridge prevented the development of a STJ over Mexico. During the early period, no transport mechanism developed to move the hot, dry air off the Mexican plateau and over the Gulf of Mexico.

There was one very important difference between the cases -- the air over the Gulf was much cooler than the event case (generally 4 to 6 C cooler).

The event case PV was generated in the upper-levels, transported downward in the lee of the mountains to the lower-levels, then advected over central NC arriving 72 hours later at the time of a tornadic outbreak. Initially, there were two jet streaks embedded within the STJ. The first streak (located over TX and the Gulf Coast States) facilitated PV production and transported the PV southward. The second streak and its associated thermally indirect circulation transported the PV down to the mid-levels over the Mexican plateau. At the same time, there was substantial heating over the Mexican plateau producing a very deep and warm dry adiabatic layer over MX, which was forced by large sensible heat fluxes resulting from clear skies, minimal soil moisture and arid conditions. A mountain-plains solenoid circulation developed over the Mexican plateau creating ascent to 550 mb. At the same time, the upper-level transverse ageostrophic circulation created descent down to 500 mb. An area of vertical convergence was created in the 500-600 mb layer increasing the thermal gradient (static stability) and generating PV. The dramatic increase in static stability was primarily responsible for the increase in mid-level PV. This midlevel PV maximum then moved eastward and a hydrostatic mountain wave transported the PV downward near the Mexican coast. As the PV maximum moved downward, it increased due to increasing static stability, tilting of horizontal vorticity into the vertical and frictional effects. The low-level PV then moved along the Gulf Coast and finally north along the East Coast to RDU at the time of the

tornado outbreak. The low-level PV maximum was maintained and increased by a combination of low-level wind shear, latent heating, frictional effects and sensible heating.

There was a dramatic difference in the PV between the event and non-event. The STJ was absent in the non-event case, thus PV was not transported downward to the midlevels. The low-level wind field over the western Gulf of Mexico was from the east advecting clouds over the Mexican plateau minimizing surface heating and inhibiting a deep dry adiabatic layer. The easterly low-level flow prevented the development of mountain waves southwest of BRO inhibiting the downward transport of mid-level PV. In the lee of the mountains and as the parcel ascended the lee slope, anticyclonic PV was generated by all the source terms in Eq. (4) and were roughly the same magnitudes. In addition, the non-event case did not have a LLJ over the western Gulf of Mexico to transport northward any low-level PV. There were two distinct differences between the cases. First, the PV maximum was a coherent and traceable entity over 72 hours in the event case while in the non-event case the PV maximum was not a coherent, long-lasting entity. Second, the event case PV maximum originated much farther to the south (some 1500 km) than that of the non-event case.

Acknowledgements. I would like to thank the Air Force Institute of Technology for the opportunity to pursue my advanced degree. The authors wish to thank Drs Robert Rozumalski and Kenneth Waight III of MESO Inc. for access to and help with the MASS model.

8. References

Daley, R., 1991: *Atmospheric Data Analysis*, Cambridge University Press, 457 pp.

Danielsen, E., 1968: Stratospheric-tropospheric exchange based on radioactivity, ozone, and potential vorticity. *J. Atmos. Sci.*, **25**, 502-518.

Gidel L. T., and M. A. Shapiro, 1979: The role of clear air turbulence in the production of potential vorticity in the vicinity of upper tropospheric jet stream-frontal systems. *J. Atmos. Sci.*, **36**, 2125-2138.

Gonski, R. F., B. P. Woods, and W. D. Korotky, 1989: The Raleigh tornado - 28 November 1988: An operational perspective. Preprints, *12th Conf. on Weather Analysis and Forecasting*, Monterey, CA Amer. Meteor. Soc., 173-178.

Gyakum J. R., Y-H Kuo, Z. Guo, and Y-R Guo, 1995: A case of rapid continental mesoscale cyclogenesis. Part II: Model and observational diagnosis. *Mon. Wea. Rev.*, **123**, 998-1024.

Kalnay, E., M. Kanamistu, R. Kistler, W. Collins, D. Deaven, L. Gandin, M. Iredell, S. Saha, G. White, J. Woollen, Y. Zhu, M. Chelliah, W. EbisuzARi, W. Higgins, J. JanowiAR, K. C. Mo, C. Ropelewski, J. Wang, A. Leetmaa, R. Reynolds, R. Jenne, and D. Joseph, 1996; The NMC/NCAR 40-year reanalysis project. *Bull. Amer. Meteor. Soc.*, **77**, No. 3, 437-471.

Kaplan, M. L., and D. A. Paine, 1977: The observed divergence of the horizontal velocity field and pressure gradient force at the mesoscale. It's implications for the parameterization of three-dimensional momentum transport in synoptic-scale numerical models. *Beitr. Phy. Atmos.*, **50**, 321-330.

Kaplan, M. L., V. M. Karyampudi, 1992: Meso-beta numerical simulation of terrain drag-induced along stream circulations. Part I: Midtropospheric frontogenesis. *Meteor. Atmos. Phys.*, **49**, 133-156.

Kaplan, M. L., V. M. Karyampudi, 1992: Meso-beta numerical simulation of terrain drag-induced along stream circulations. Part II: Concentration of potential vorticity within dryline bulges. *Meteor. Atmos. Phys.*, **49**, 157-185.

Kaplan, M. L., J. W. Zack, V. C. Wong, and J. J. Tuccillo, 1982a: Initial results from a mesoscale atmospheric simulation system and comparisons with the AVE-SESAME I data set. *Mon. Wea. Rev.*, **110**, 1564-1590.

Kaplan, M. L., Y-L. Lin, D. W. Hamilton, and Rozumalski, R. A., 1997: The numerical simulation of an unbalanced jetlet and its role in the Palm Sunday 1994 tornado outbreak in Alabama and Georgia. *Mon. Wea. Rev.*, **126**, 2133-2165.

Keyser, D., and M. A. Shapiro, 1986: A review of the structure and dynamics of upper-level frontal zones. *Mon. Wea. Rev.*, **114**, 452-499.

Kocin, P. J., L. W. Uccellini, J. W. Zack, and M. L. Kaplan, 1985: A mesoscale numerical forecast of an intense convective snowburst along the East Coast. *Bull. Amer. Meteor. Soc.*, **66**, 1412-1424.

Lin, Y.-L., R. D. Farley, and H. D. Orville, 1983: Bulk parameterization of the snow field in a cloud model, *J. Clim. Appl. Meteorol.*, **22**, 1065-1092.

Lin, Y.-L., and T.-A. Wang, 1996: Flow regimes and transient dynamics of two-dimensional stratified flow over an isolated mountain ridge. *J. Atmos. Sci.*, **53**, 139-158.

Mahrt, L., and H. Pan, 1984: A two-layer model of soil hydrology. *Bound.-Layer Meteor.*, **29**, 1-20.

MESO, 1995: MASS Version 5.8 Reference Manual, MESO, Inc., Troy, NY, 119 pp.

Miles, J. W., 1961: On the stability of heterogeneous shear flows. *J. Fluid Mech.*, **10**, 496-508.

Murry, R. and S. M. Daniels, 1953: Transverse flow at entrance and exit to jet streams. *Quart. J. Roy. Meteor. Soc.*, **79**, 236-241.

Newton, C. W., 1958: Variations in frontal structure of upper level troughs. *Geophysica*, **6**, 357-375.

NOAA, 1988: Storm data, **30, 11,** 72 pp.

Noilhan, J., and S. Planton, 1989: A simple parameterization of land surface processes for meteorological models. *Mon. Wea. Rev.*, **117**, 536-549.

Reed, R. J., 1955: A study of a characteristic type of upper-level frontogenesis. *J. Meteor.*, **12**, 226-237.

Reiter, E. R., 1967: *Jet Streams*, Doubleday & Company, Inc., 189 pp.

Rozumalski, R. A., 1997: The role of jet streak regeneration forced by a deepening continental planetary boundary layer in the explosive surface cyclogenesis of 28 March 1984. Ph. D. Thesis., North Carolina State University, 360 pp. (Available from the corresponding author).

Tripoli G. J. and W. R. Cotton 1989:Numerical Study of an Observed Orogenic Mesoscale Convective System. Part 1: Simulated Genesis and Comparison with Observations. *Mon. Wea. Rev.*, **117**, 273-304.

Tripoli G. J. and W. R. Cotton 1989:Numerical Study of an Observed Orogenic Mesoscale Convective System. Part 2: Analysis of Governing Dynamics. *Mon. Wea. Rev.*, **117**, 305-328.

Uccellini L. W. and D. Johnson 1979: The coupling of upper and lower tropospheric jet streaks and implication for the development of severe convective storms. *Mon. Wea. Rev.*, **107**, 682-703.

Uccellini L. W, and S. E. Koch 1987: The synoptic setting and possible energy sources for mesoscale wave disturbances. *Mon. Wea. Rev.*, **115**, 721-729.

Uccellini L. W., and P. J. Kocin, 1987: The interaction of jet streak circulations during heavy snow events along the East Coast of the United States. *Wea. & Forecasting*, **1**, 289-308.

Van Tuyl A. H., J. A. Young, Numerical Simulation of Nonlinear Jet streak Adjustment,. *Mon. Wea. Rev.*, **110**, 2038-2054.

Whitaker, J. S., L. W. Uccellini, and K. F. Brill, 1988: A model-based diagnostic study of the rapid development phase of the Presidents' Day cyclone. *Mon. Wea. Rev.*, **116**, 2337-2365.

Zack, J. W., and M. L. Kaplan 1987: Numerical simulations of the subsynoptic features associated with the AVE-SESAME I case. Part I: The preconvective environment. *Mon. Wea. Rev.*, **115**, 2367-2393.

Zang, D. L., and R. A. Anthes, 1982: A high resolution model of the plantary boundary layer-sensitivity tests and comparisons with SESAME-79 data. *J. Appl. Meteor.*, **21**, 1594-1609.

Zehnder, J. A., and D. Keyser, 1991: The influence or interior gradients of potential vorticity on rapid cyclogenesis. *Tellus*, **43A**, 198-212.

Table 1. The MASS modeling simulations performed in the study.

Initialization (UTC)	Duration (hours)	Resolution (km)	Matrix size (x, y, z)	Modifications
1200 UTC 24 Nov 88	24	24	170, 130, 40	None
0000 UTC 25 Nov 88	72	72	130, 110, 37	None
0000 UTC 22 Jan 90	24	24	170, 130, 40	None
1200 UTC 22 Jan 90	72	72	130, 110, 37	None
0000 UTC 25 Nov 88	36	24	170, 130, 40	None
1200 UTC 23 Jan 90	36	24	170, 130, 40	No latent heating
1200 UTC 23 Jan 90	36	24	170, 130, 40	None
0000 UTC 26 Nov 88	36	24	170, 130, 40	No latent heating
0000 UTC 26 Nov 88	36	24	170, 130, 40	None
1200 UTC 24 Jan 90	36	24	170, 130, 40	No latent heating
1200 UTC 24 Jan 90	36	24	170, 130, 40	None
0000 UTC 27 Nov 88	36	24	205, 155, 40	No latent heating
0000 UTC 27 Nov 88	36	24	205, 155, 40	None
1200 UTC 27 Nov 88	24	24	205, 155, 40	Yes, MDR data
1200 UTC 27 Nov 88	24	12	205, 155, 40	None
1200 UTC 24Jan 90	36	24	205, 155, 40	None
1200 UTC 24Jan 90	36	24	205, 155, 40	No latent heating
0000 UTC 25 Jan 90	24	24	205, 155, 40	Yes, MDR data
0000 UTC 25 Jan 90	24	12	205, 155, 40	None

Table 2. Trajectory initiated at 0300 UTC 25 November 1988, passed through the 910 mb PV maximum (25.7N, 99.8W) at 0600 UTC 25 November 1988 and ended at 0500 UTC 26 November 1988. Trajectory data shown here is every 2 hours and was derived from hourly data of a 24 km MASS simulation. The following abbreviations are defined: Latitude (LAT), Longitude (LON), Pressure (PRS), Temperature (TMP), and Potential Vorticity (PV).

Time (UTC)	LAT (°N)	LON (°W)	PRS (mb)	TMP (°C)	PV (PV units)
25/0400	25.25	100.57	765.3	11.7	.7665
25/0600	25.33	100	910	23.8	3.159
25/0800	25.94	99.52	915.5	22.9	2.408
25/1000	26.09	99.2	914.6	23.3	2.131
25/1200	26.15	98.84	919.4	23.57	1.971
25/1400	26.3	98.48	922.6	23.8	1.695
25/1600	26.6	98.02	908.8	22.53	1.402
25/1800	27.05	97.53	890.6	20.82	1.094
25/2000	27.54	96.99	876.5	19.32	0.959
25/2200	28.09	96.41	866.1	18.1	0.8657
26/0000	28.67	95.82	844.8	16.36	0.8989
26/0200	29.37	95.24	844.6	16.17	1.0932
26/0400	30.16	94.57	837.9	15.27	1.705

Table 3. Same as Table 2 except trajectory initiated at 1800 UTC 22 January 1990 and ended at 1800 UTC 23 January 1990.

Time (UTC)	LAT (°N)	LON (°W)	PRS (mb)	TMP (°C)	PV (PV units)
22/1400	25.6	99.67	982.3	13.2	0.273
22/1600	25.6	99.91	970.8	13.1	0.100
22/1800	25.5	100.2	900.9	14.6	0.060
22/2000	25.5	100.5	811.8	13.1	0.140
22/2200	25.5	100.9	793.0	14.5	0.107
23/0000	25.5	101.2	787.9	14.1	0.173
23/0200	25.8	101.4	797.9	16.0	0.302
23/0400	26.2	101.4	789.6	15.0	0.292
23/0600	26.5	101.4	806.8	16.4	0.489
23/0800	26.86	101.2	819.6	17.6	0.441
23/1000	27.2	100.9	839.6	18.9	0.385
23/1200	27.6	100.7	840.3	18.5	0.461
23/1400	27.9	100.2	821.0	16.5	0.357
23/1600	28.0	99.66	800.9	14.3	0.353

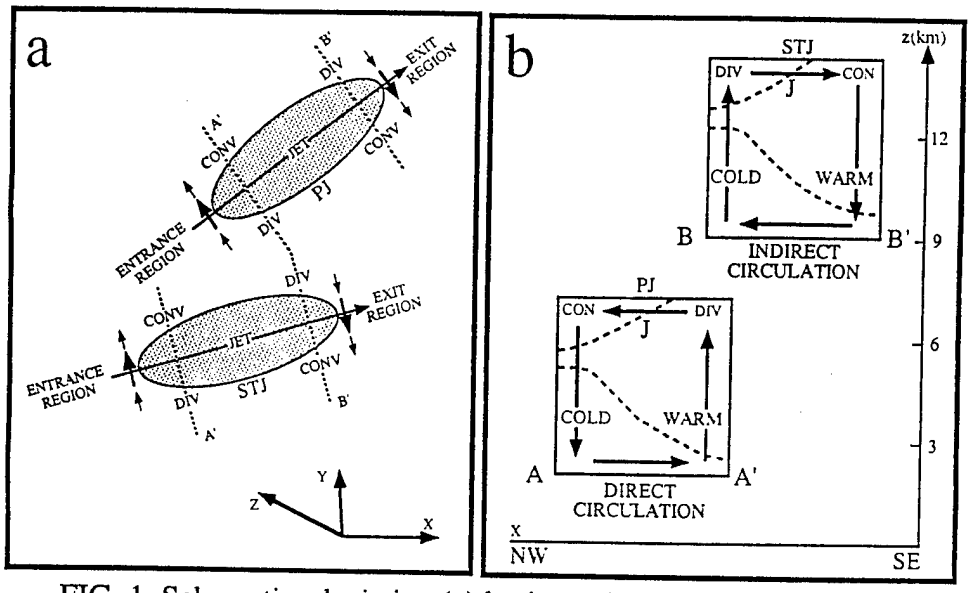

FIG. 1. Schematics depicting (a) horizontal and (b) vertical structures of the transverse ageostrophic circulations about the polar and subtropical jet streaks from Kaplan et al. (1998).

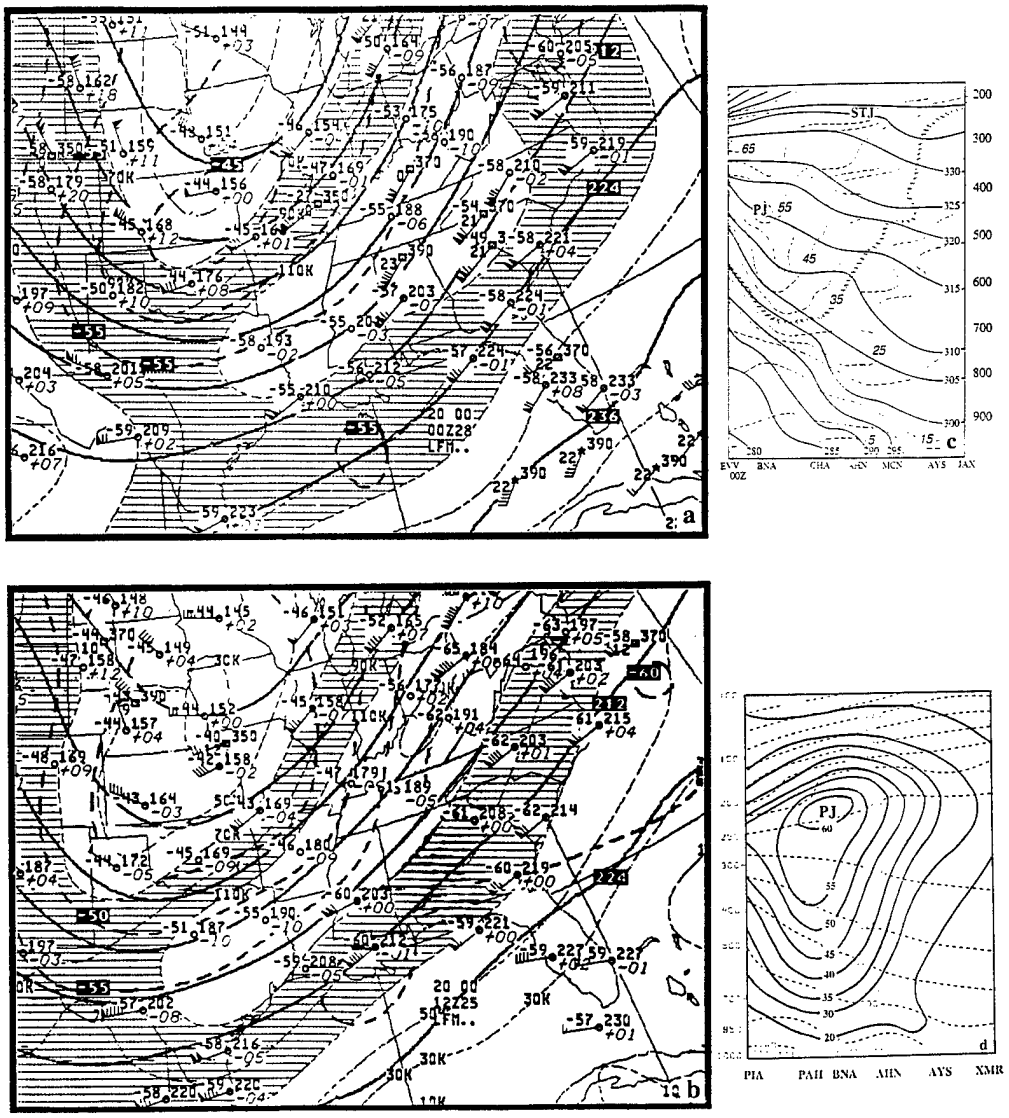

FIG. 2. (a) NWS 200 mb analysis of isotachs (knots) and vectors, temperature (C) and height (dm) and (c) observation derived cross section from Evansville, IN (EVV) to Jacksonville, FL (JAX), isotachs (dashed line, ms^{-1}) and θ (solid line, K) valid at 0000 UTC 28 November 1988. (b) NWS 200 mb analysis of isotachs and vectors (knots), temperature (C) and height (dm) and (d) observationally derived cross section from Peoria, IL (PIA) to Cape Kennedy, FL (XMR) isotachs (solid line, ms^{-1}) and θ (dashed line, K) valid at 1200 UTC 25 January 1990.

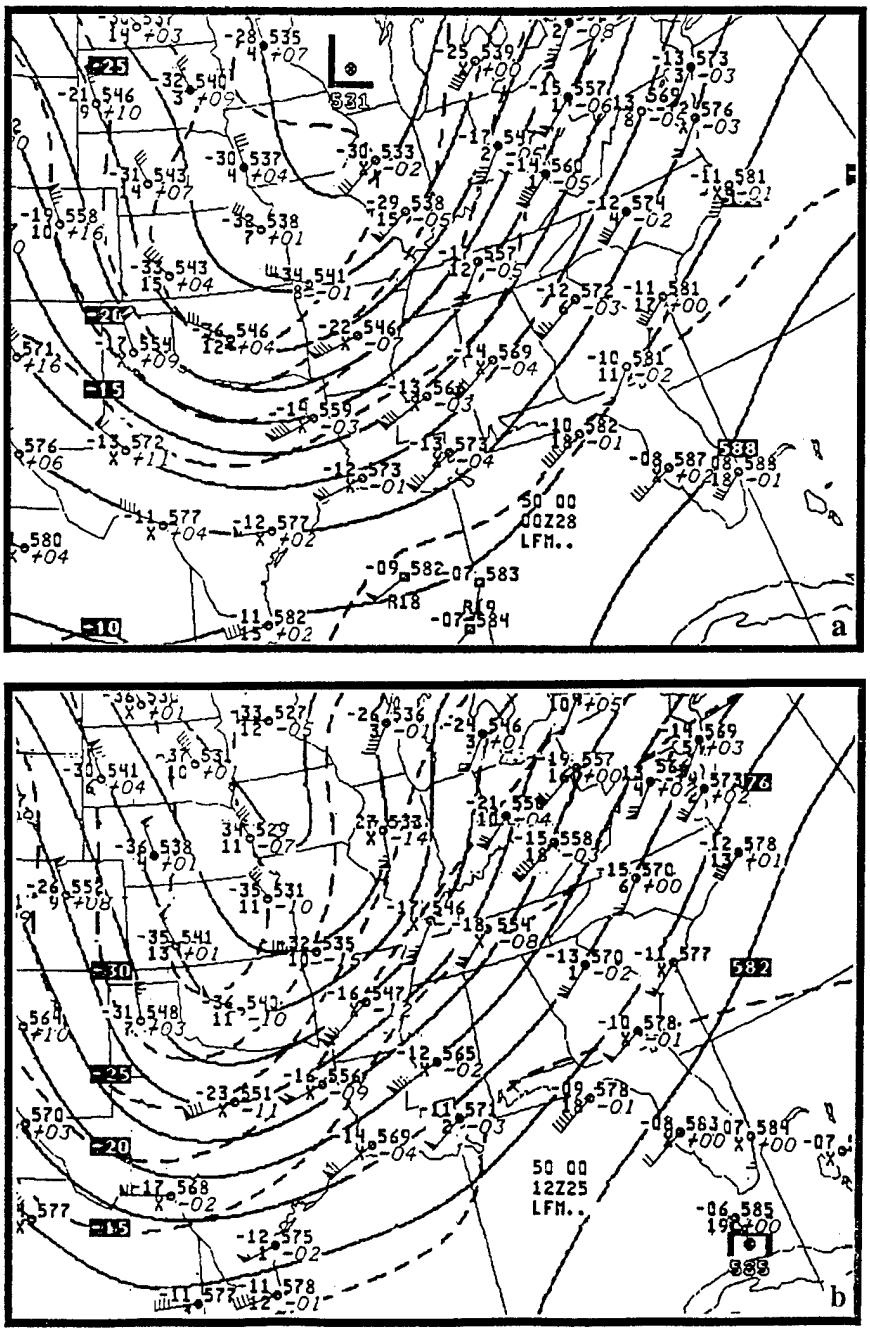

FIG. 3. NWS 500 mb analysis of wind vectors (knots), temperature (C), and height (dm) valid at (a) 0000 UTC 28 November 1988 and (b) 1200 UTC 25 January 1990.

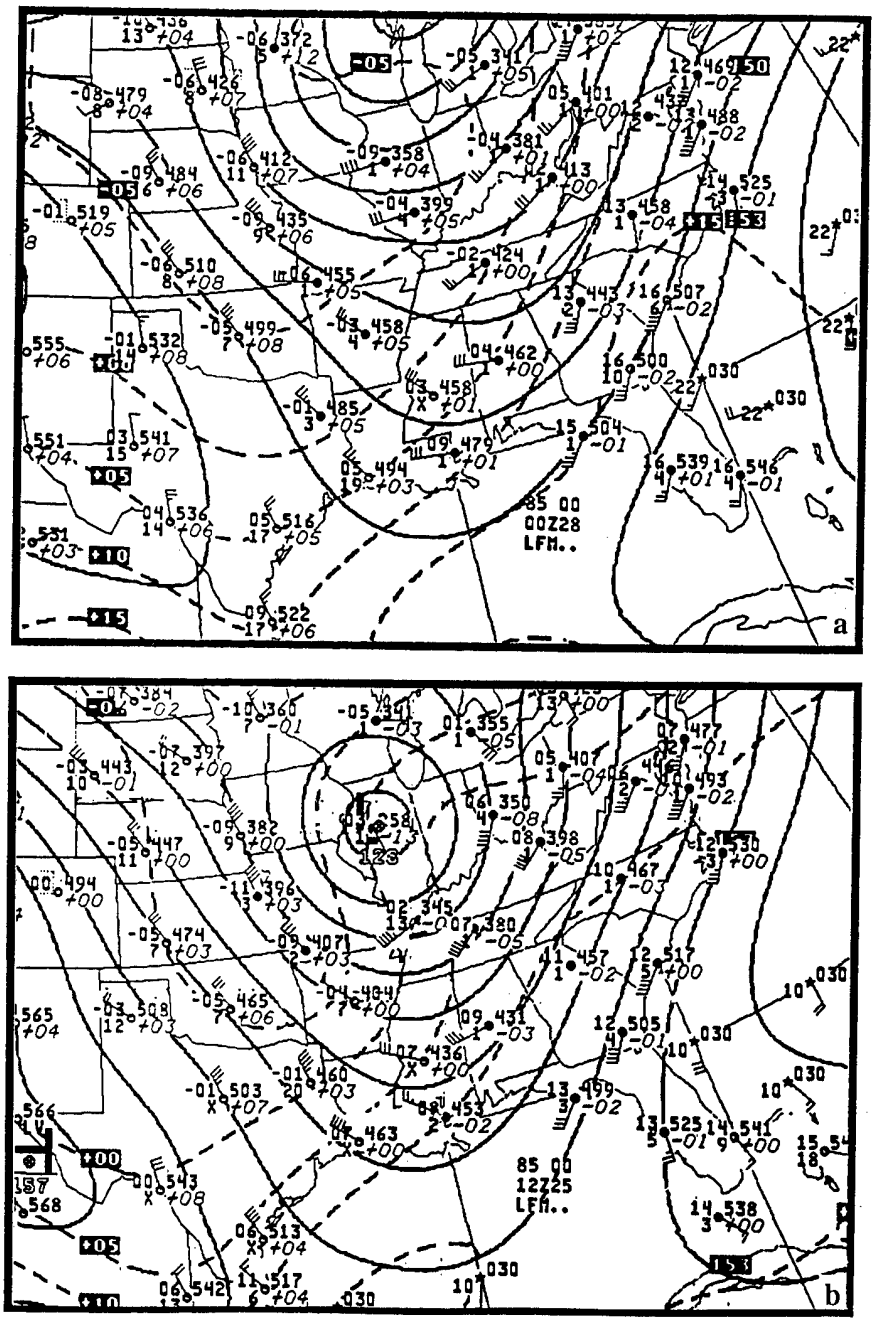

FIG. 4. NWS 850 mb analysis of wind vectors (knots), temperature (C), and height (dm) valid at (a) 0000 UTC 28 November 1988 and (b) 1200 UTC 25 January 1990.

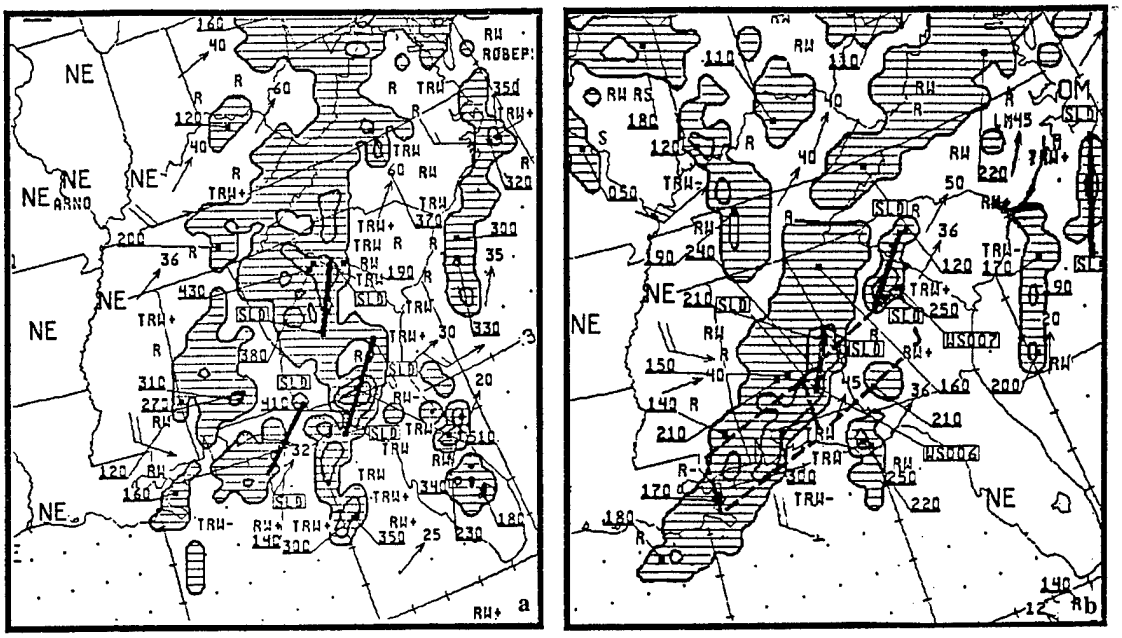

FIG. 5. NWS radar summaries valid at (a) 0035 UTC 28 November 1988 and (b) 1235 UTC 25 January 1990.

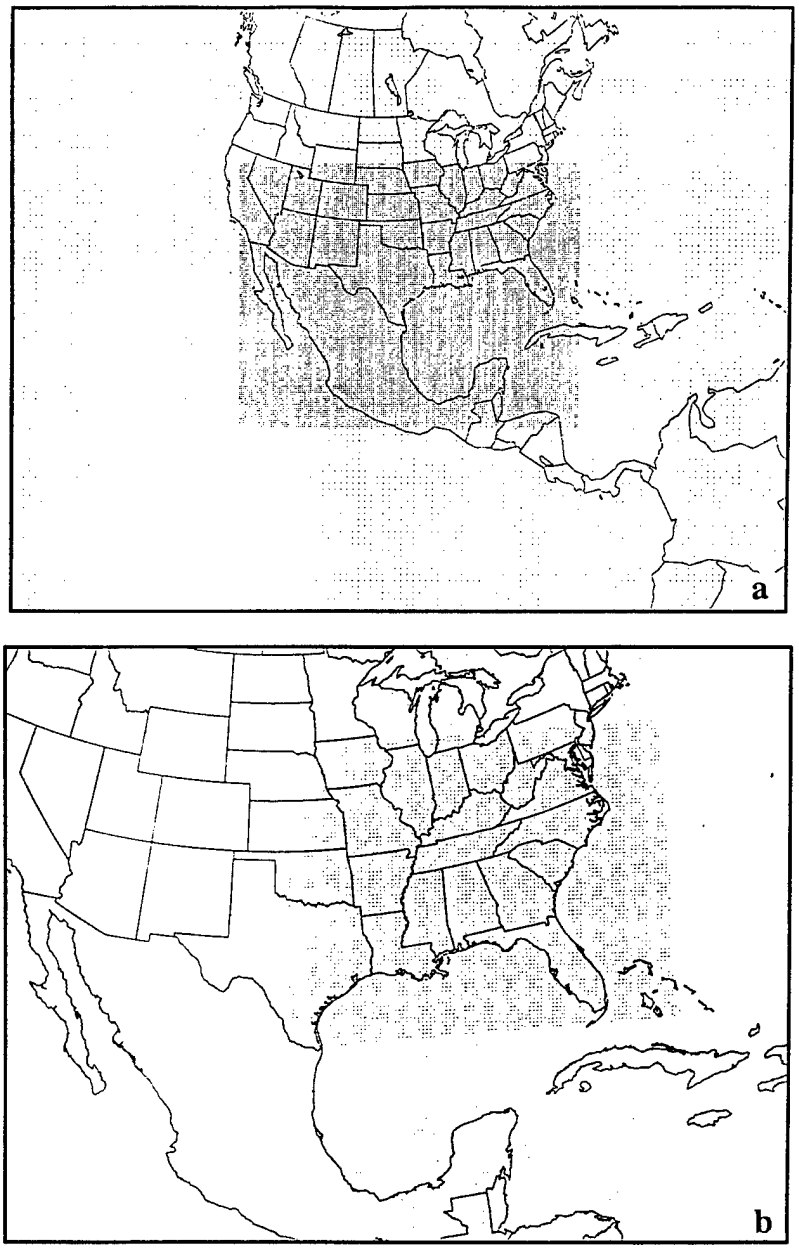

FIG. 6. Area of integration for simulations used in this study (a) depicts area of 72 km (130 x 110) and 24 km (170 x 130) simulations and (b) depicts area 24 km (205 x 155) and 12 km (205 x 155) simulations.

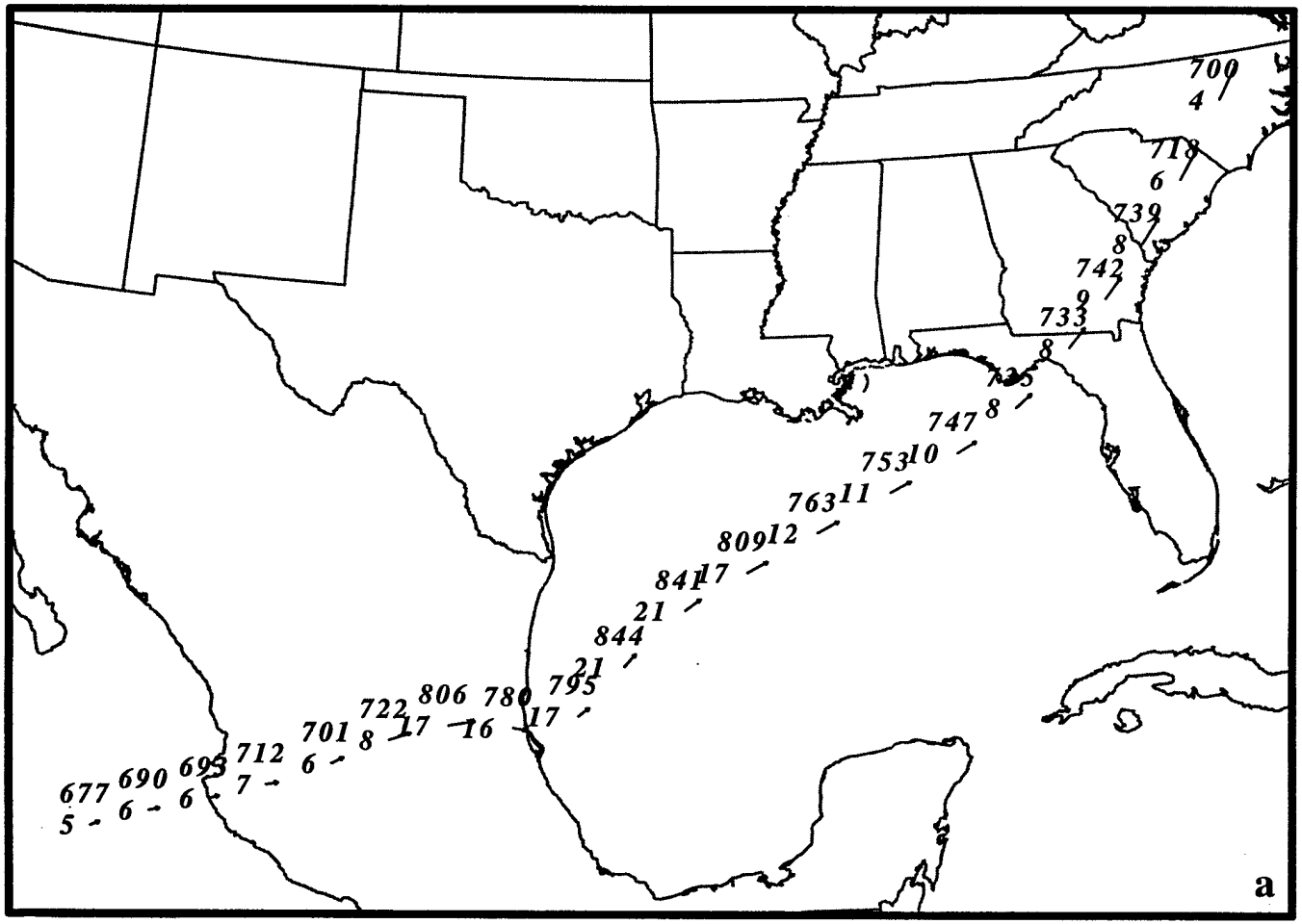

FIG. 7. Trajectories constructed from the 72 km simulations for parcels ending at 700 mb over RDU. Station plots contain pressure (mb) and temperature (C). Displayed wind vectors depict total wind (ms^{-1}). Parcels initialized at (a) 0600 UTC 28 and ended at 0900 UTC 25 November 1988 and (b) 2100 UTC 22 and ended at 1800 UTC 25 January 1990.

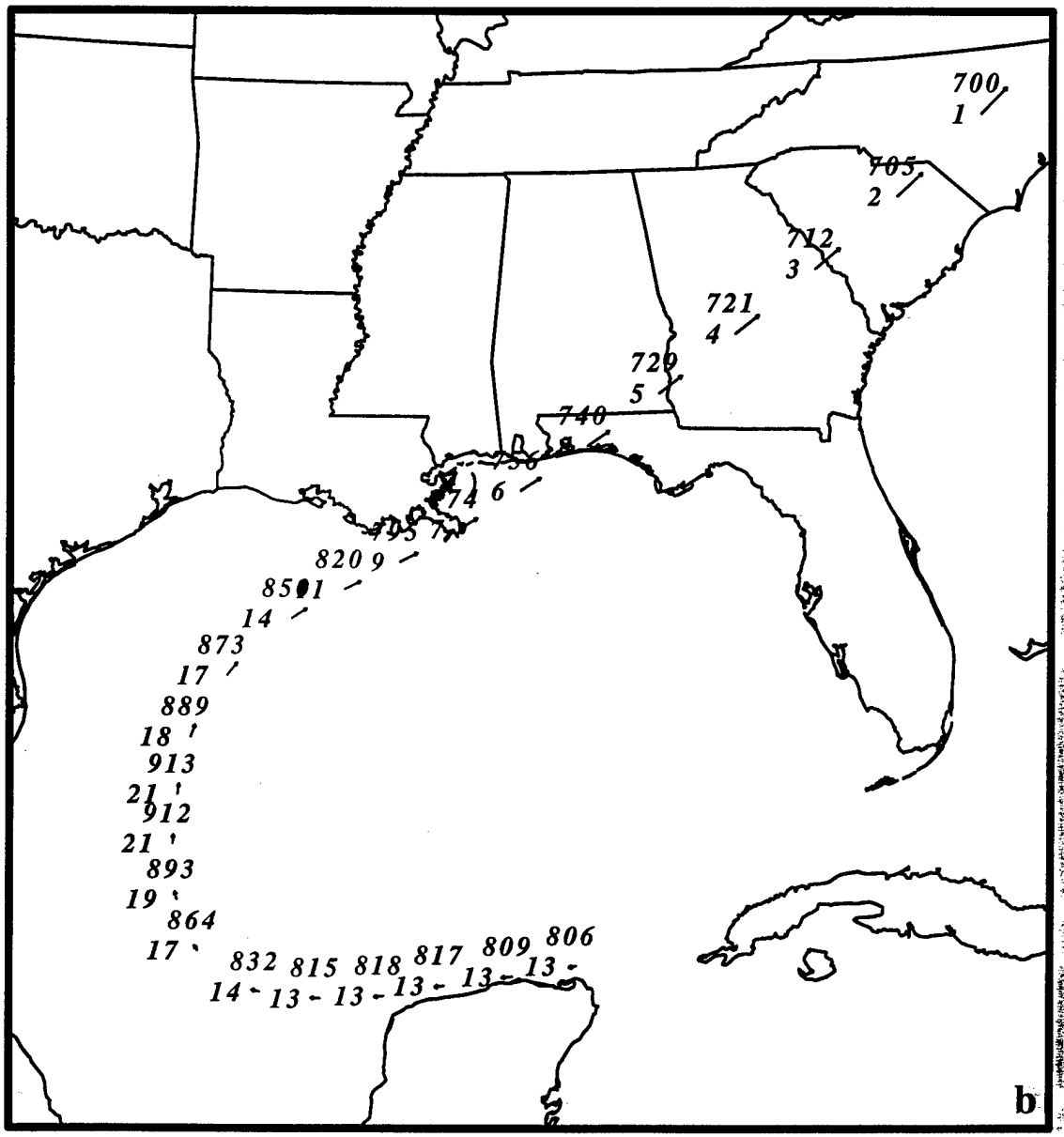

FIG. 7. Continued. Valid at 2100 UTC 22 January 1990 to 1800 UTC 25 January 1990.

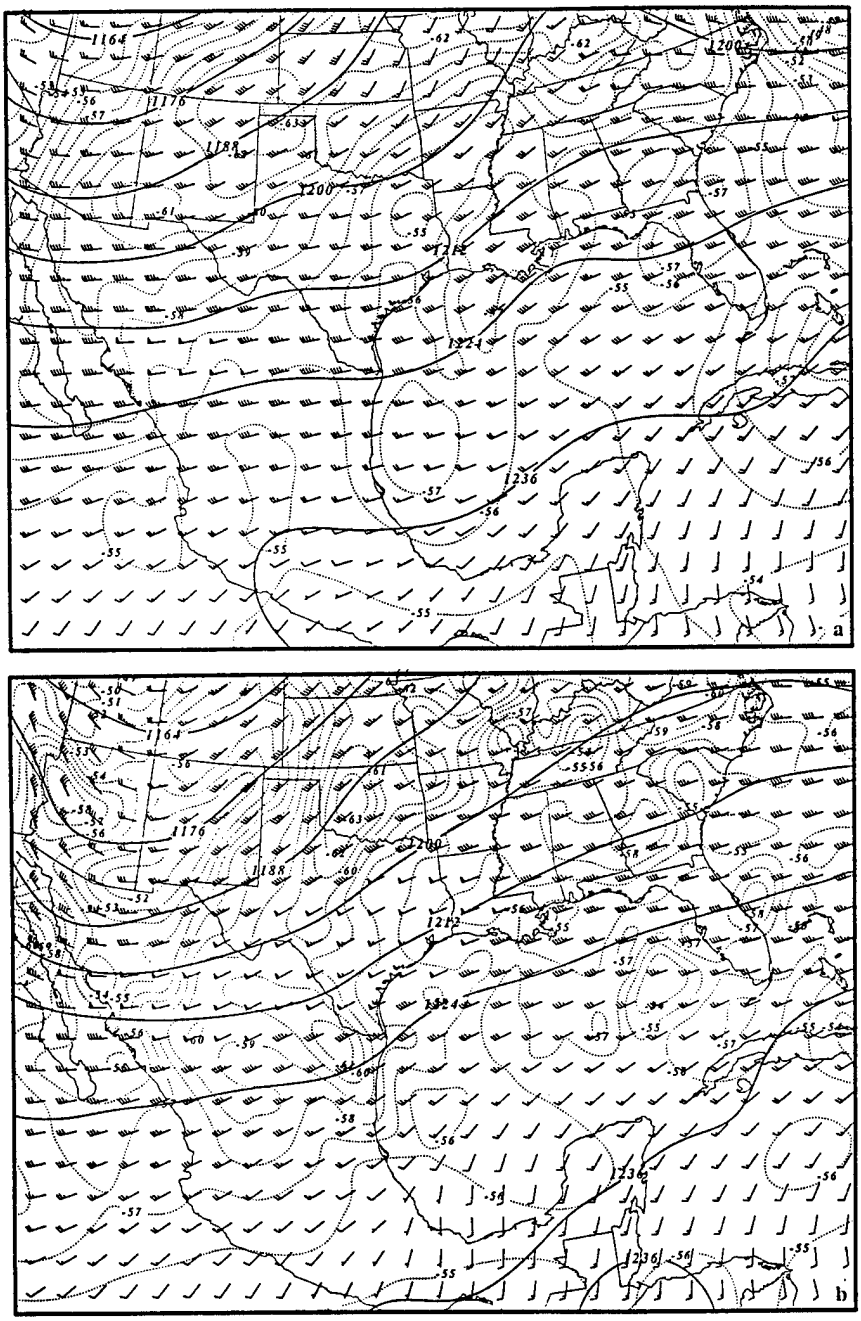

FIG. 8. Rawinsonde-derived analyses of 200 mb wind vectors, temperature (dotted lines, C), and height (solid lines, dm) valid at (a) 0000 UTC 25 and (b) 1200 UTC 25 November 1988.

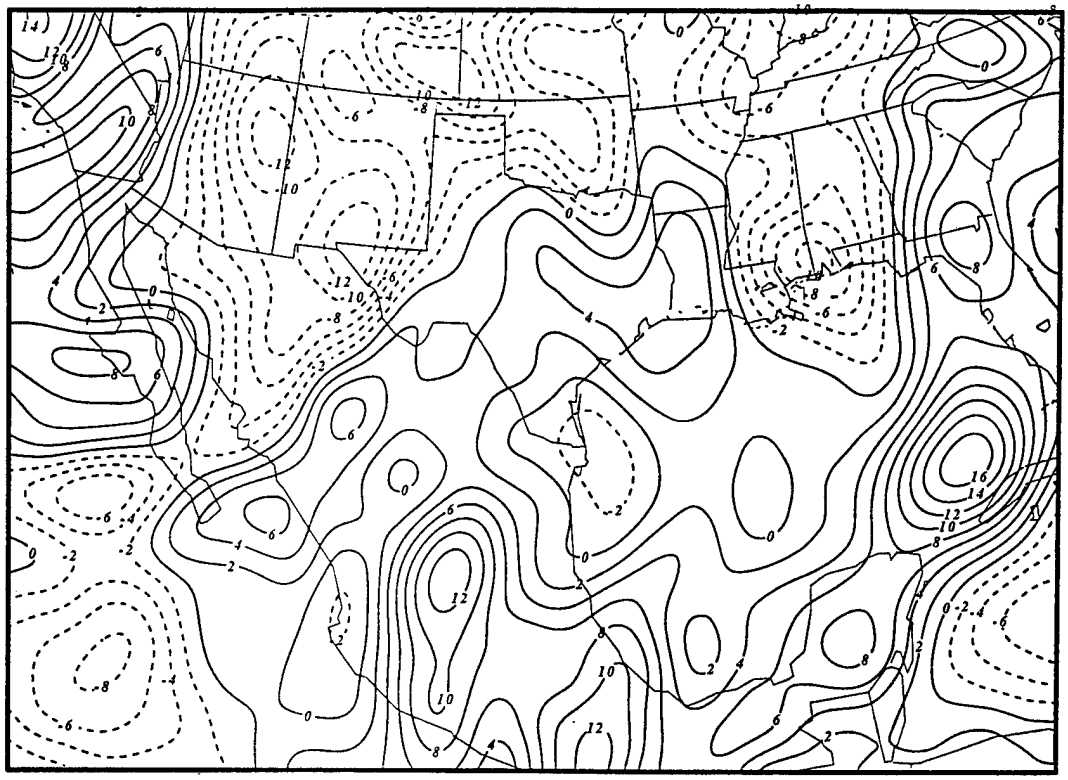

FIG. 9. MASS simulated, 24 km mesh, 700-300 mb, 1 h thickness advection (solid lines denote positive values and dashed lines denote negative values, mh^{-1}) valid at 0600 UTC 25 November 1988.

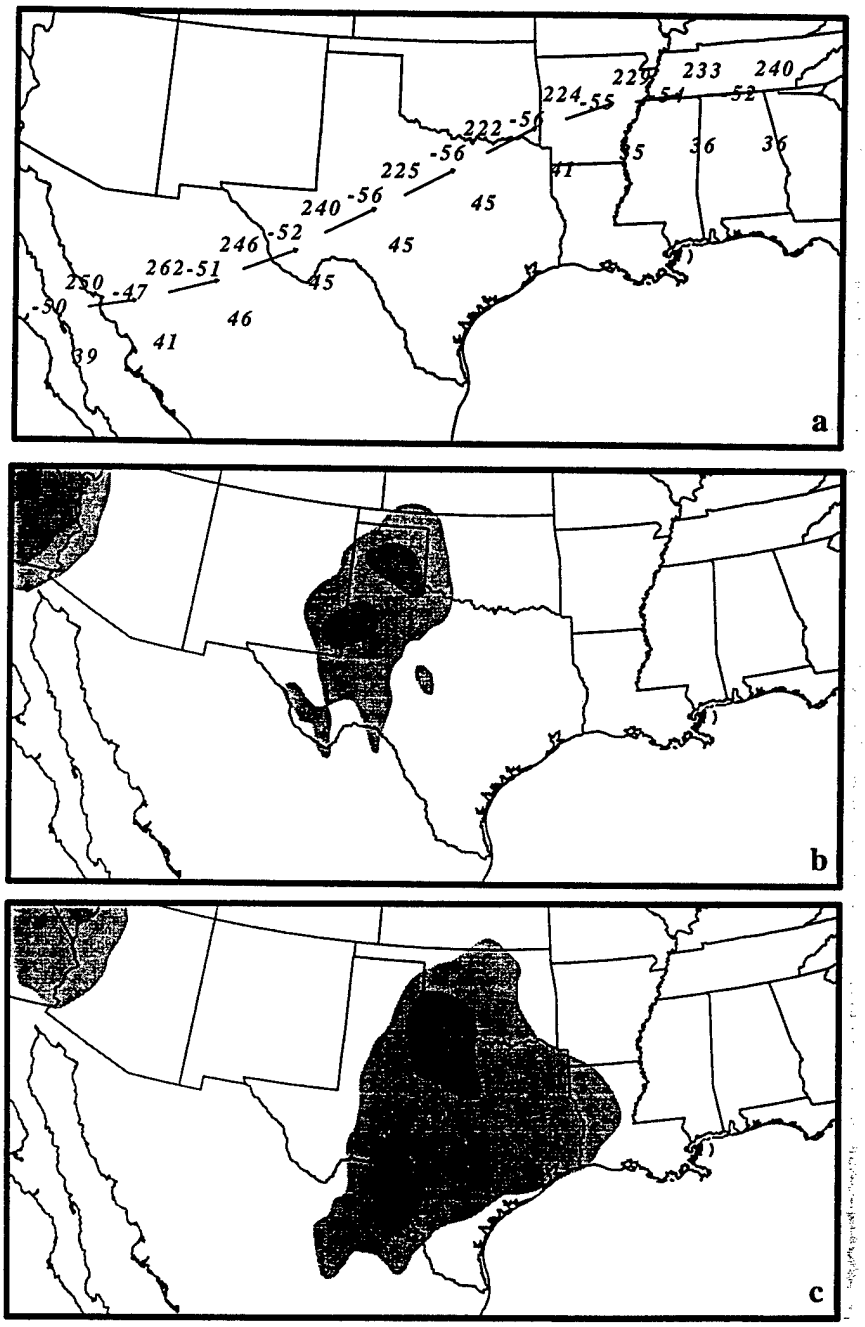

FIG. 10. MASS simulated, 24 km mesh (a) trajectory initialized at 0400 UTC 25 and ended at 0000 UTC 26 November 1988. Station plots contain pressure (mb), temperature (C), and total wind speed (ms^{-1}). Displayed wind vectors depict total wind. (b) 250 mb isotachs (shaded at intervals of 5 for speeds greater than 50 ms^{-1}) valid at 1500 UTC 26 and (c) 250 mb isotachs (shaded at intervals of 5 for speeds greater than 50 ms^{-1}) valid at 2100 UTC 26 November 1988.

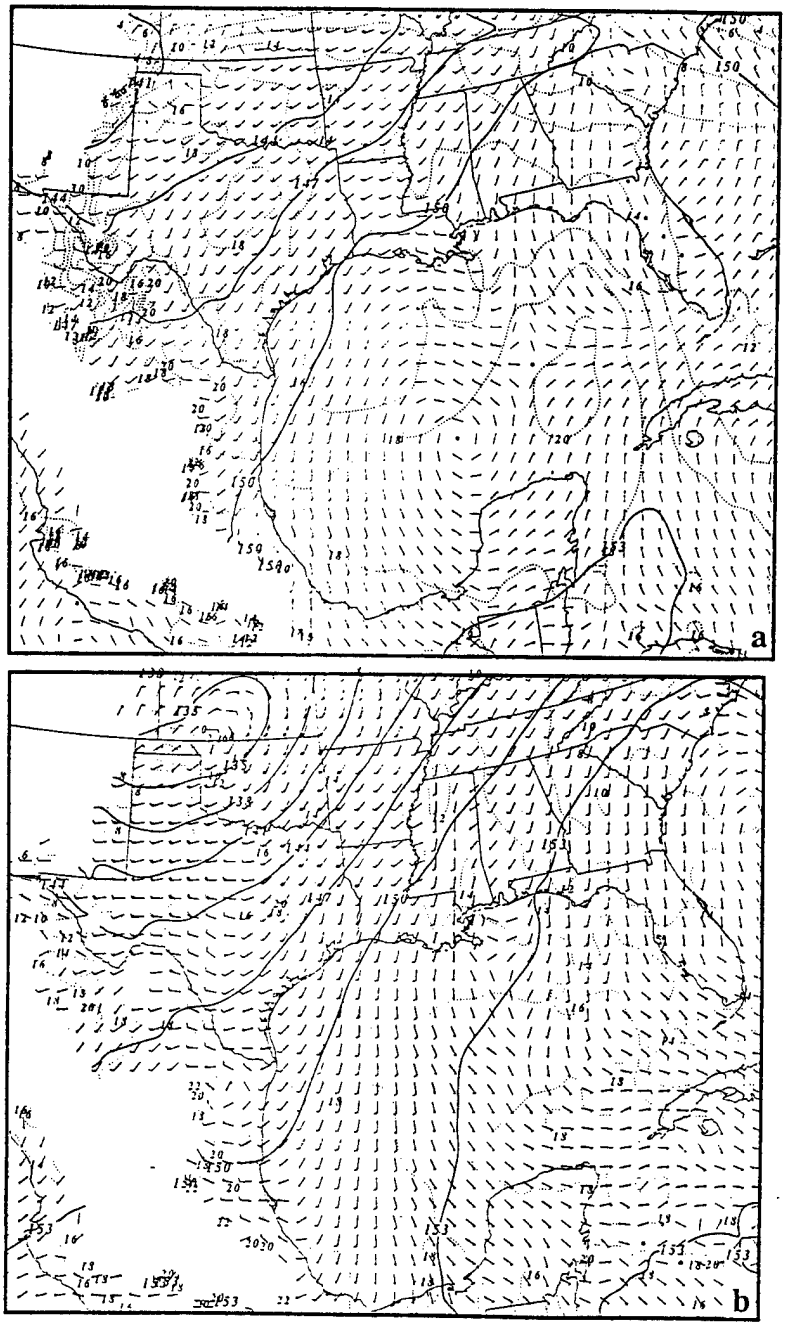

FIG. 11. MASS simulated, 24 km mesh, 850 mb wind vectors, temperature (dotted lines, C), and height (solid lines, dm) valid at (a) 0600 UTC and (b) 1800 UTC 25 November 1988.

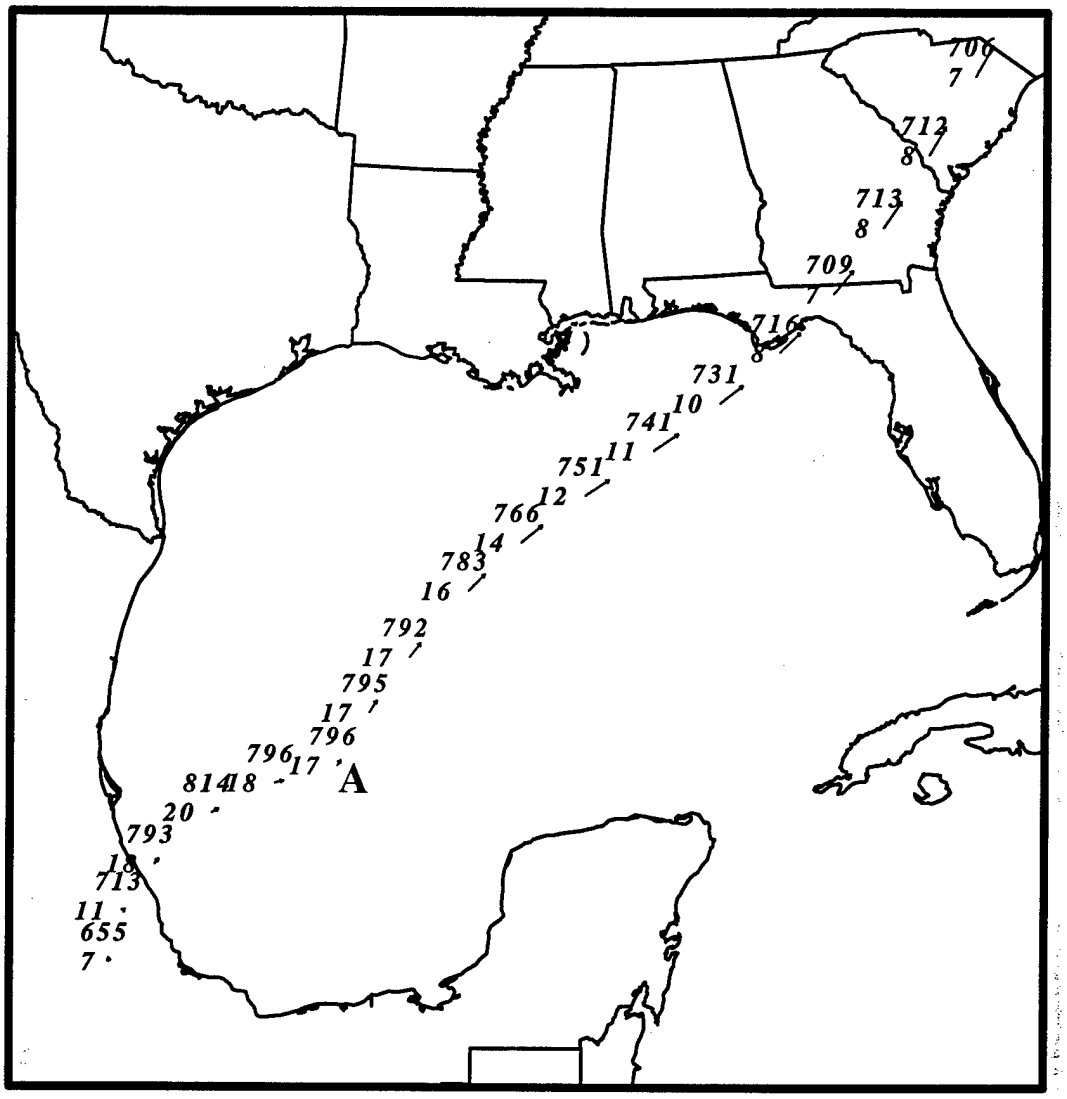

FIG. 12. Trajectory constructed from the 72 km mesh, MASS simulation initialized at 0000 UTC 25 and ended on 0000 UTC 28 November 1988. Station plots contain pressure (mb), temperature (C), and displayed wind vectors depict total wind.

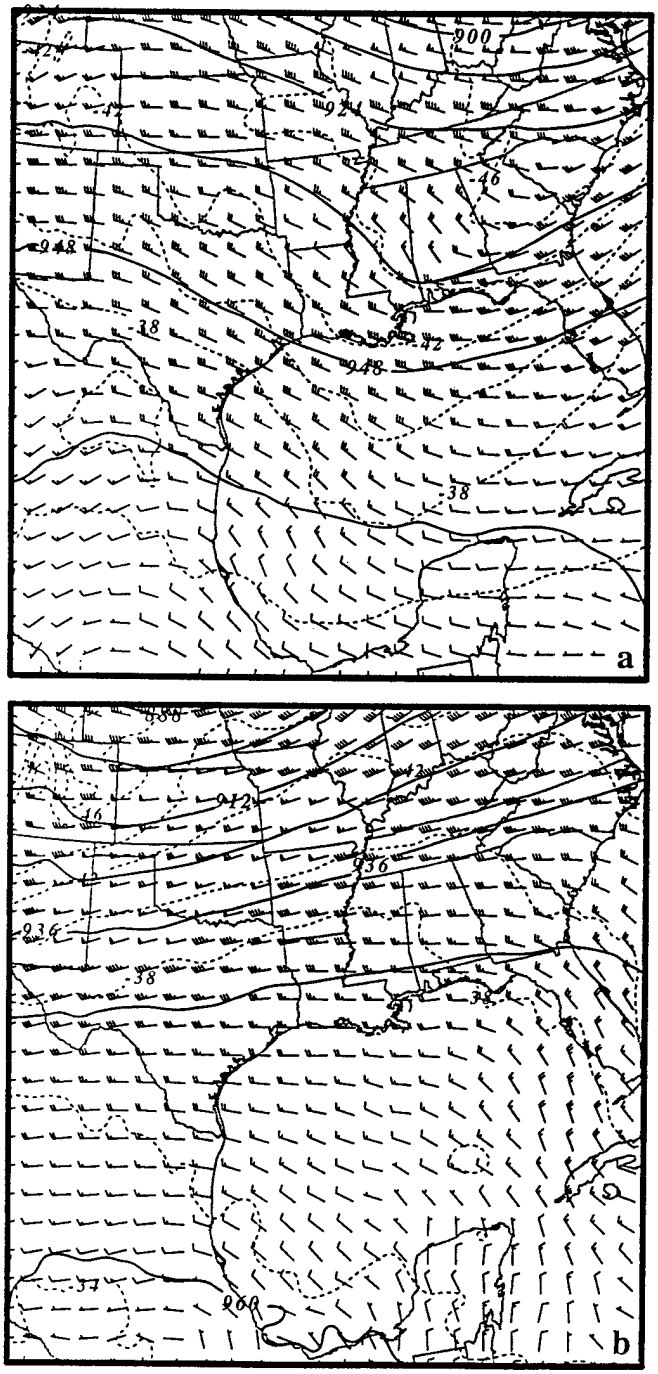

FIG. 13. MASS simulated, 24 km mesh, 300 mb wind vectors, temperature (dashed lines, C), and height (solid lines, dm) valid at (a) 1800 UTC 22 January 1990 and (b) 1800 UTC 23 January 1990.

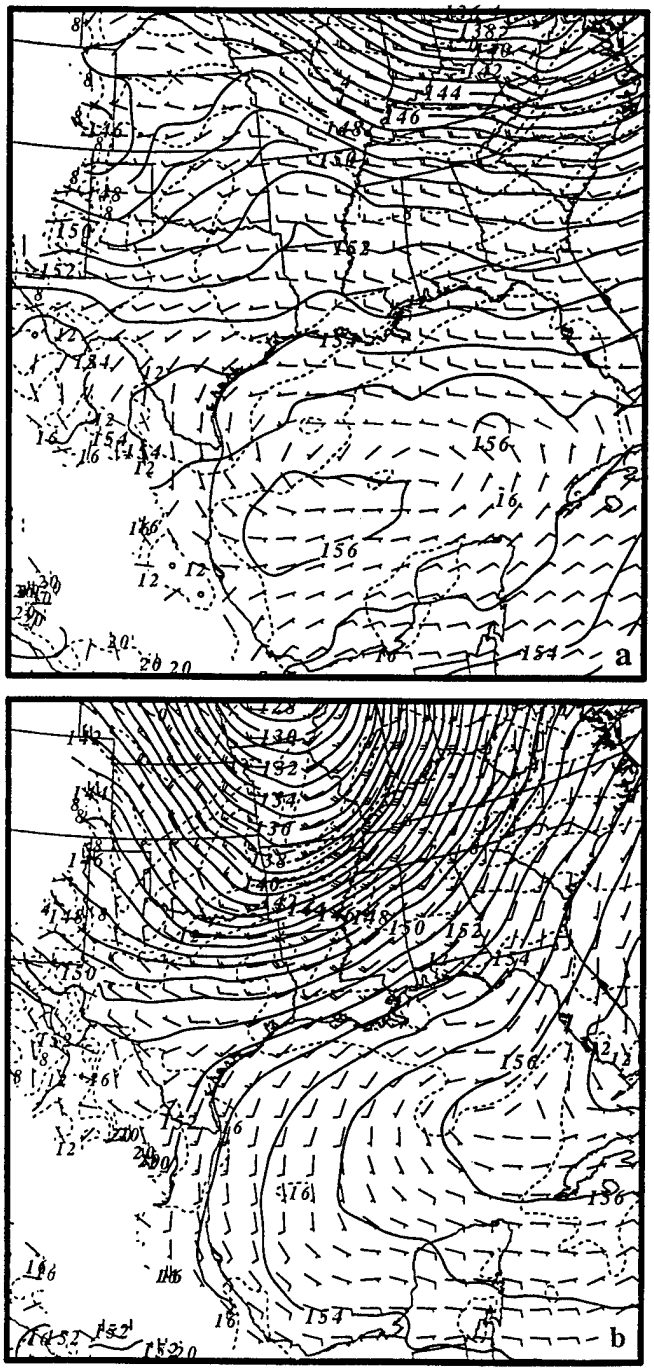

FIG. 14. MASS simulated, 24 km mesh, 850 mb wind vectors, temperature (dashed lines, C), and height (solid lines, dm) valid at (a) 1800 UTC 22 January 1990 and (b) 1800 UTC 23 January 1990.

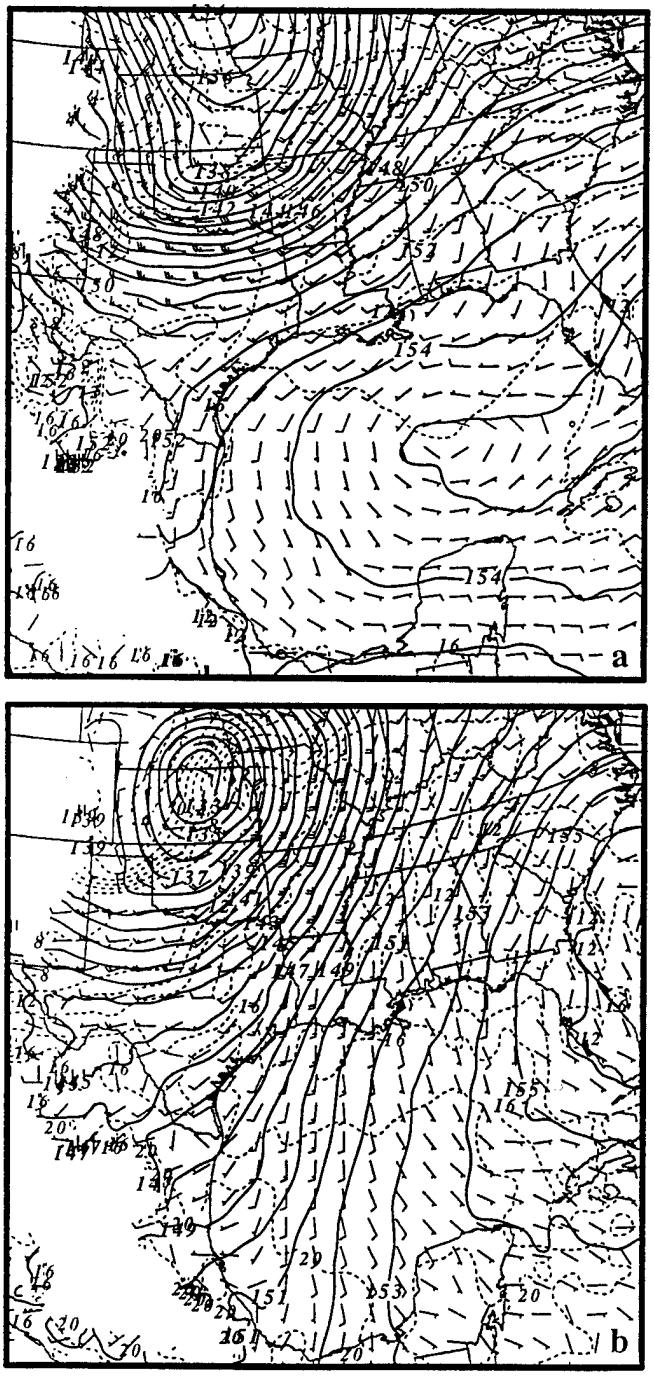

FIG. 15. MASS simulated, 24 km mesh, 850 mb wind vectors, temperature (dashed lines, C), and height (solid lines, dm) valid at (a) 1200 UTC 23 January 1990 and (b) 0000 UTC 26 November 1988.

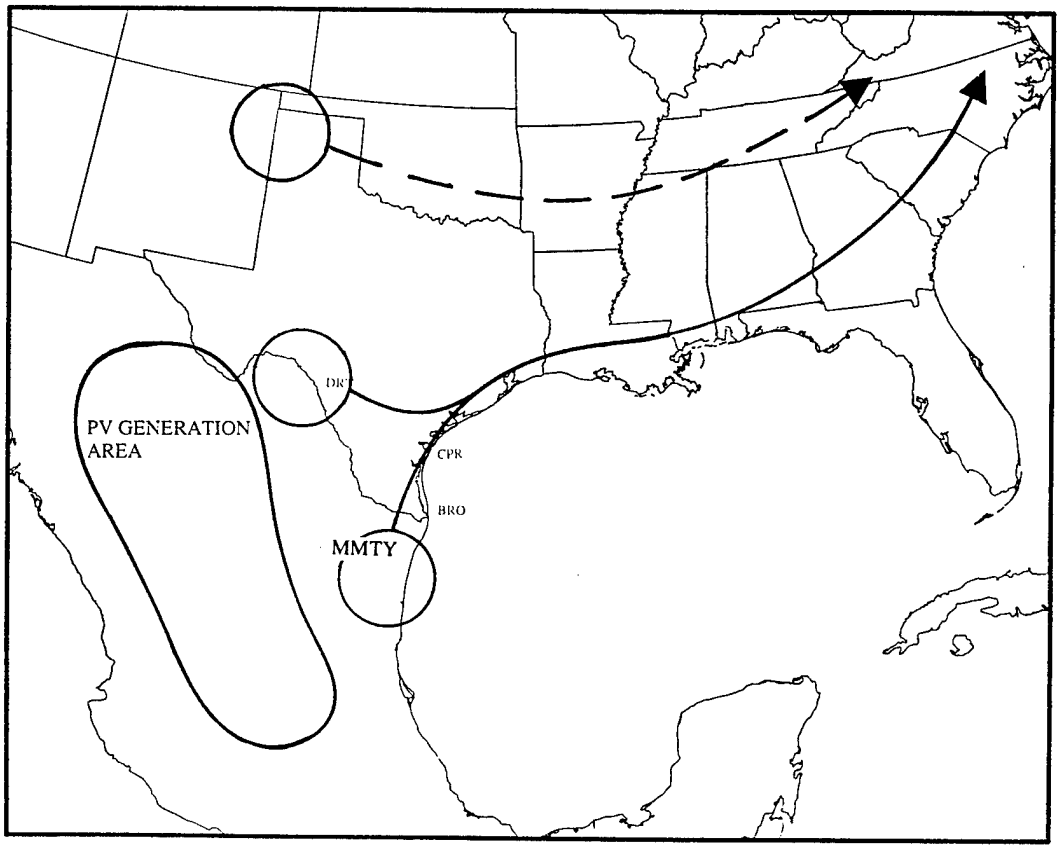

FIG. 16. Depiction of 900 Potential Vorticity maximum track using 24 km mesh MASS simulation data, solid line is event case and dashed line is non-event case.

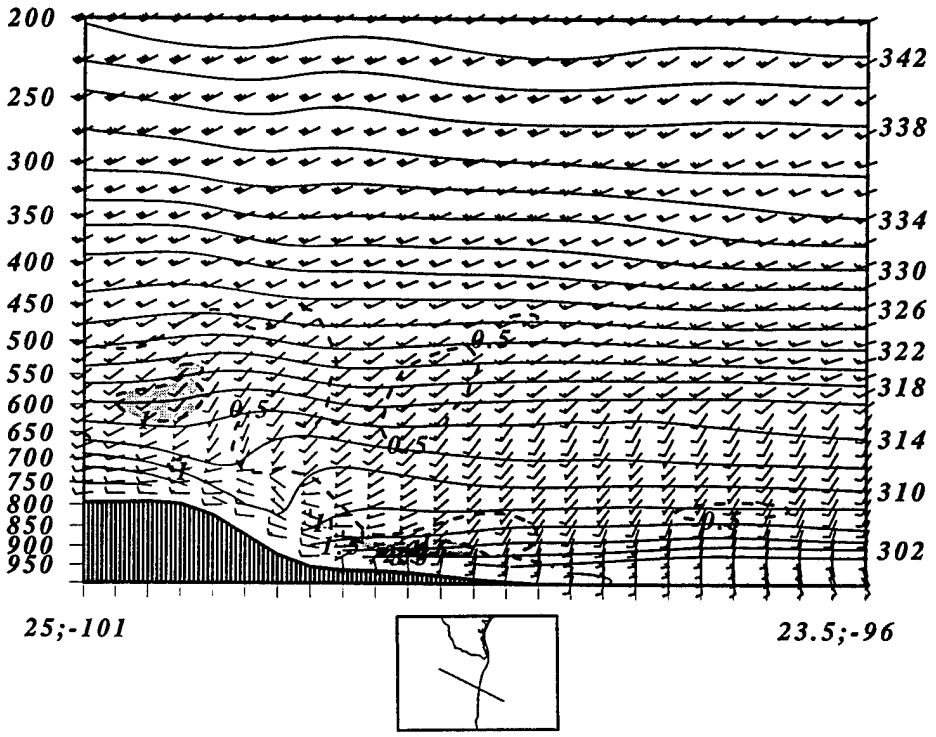

FIG. 17. MASS simulated, 24 km mesh, cross section extending from 25N, 101W to 23.5N, 96W. Including wind vectors, θ (solid lines, K), and PV (dashed lines, contoured by 0.5 and shaded greater than 1 PV unit) valid at 1200 UTC 25 November 1988.

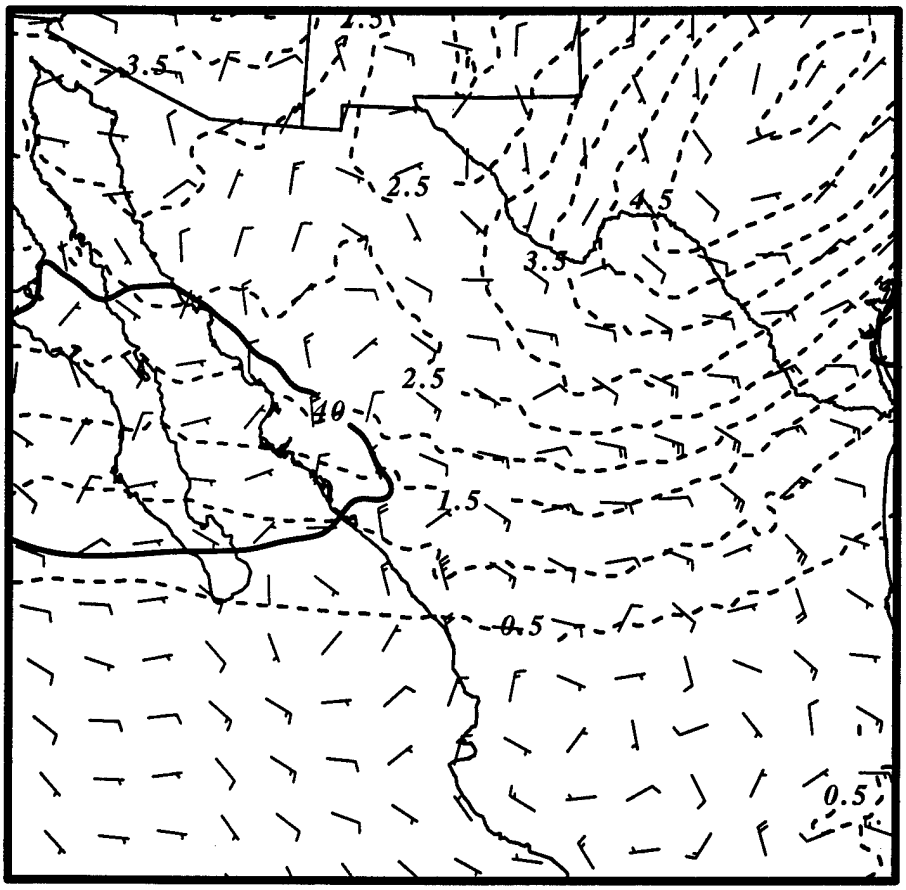

FIG. 18. MASS simulated, 24 km mesh, 200 mb PV (dashed line, contoured by 0.5 PV units), wind speed (solid line, contoured at 40 ms^{-1}) and ageostrophic wind vectors valid at 1500 UTC 24 November 1988.

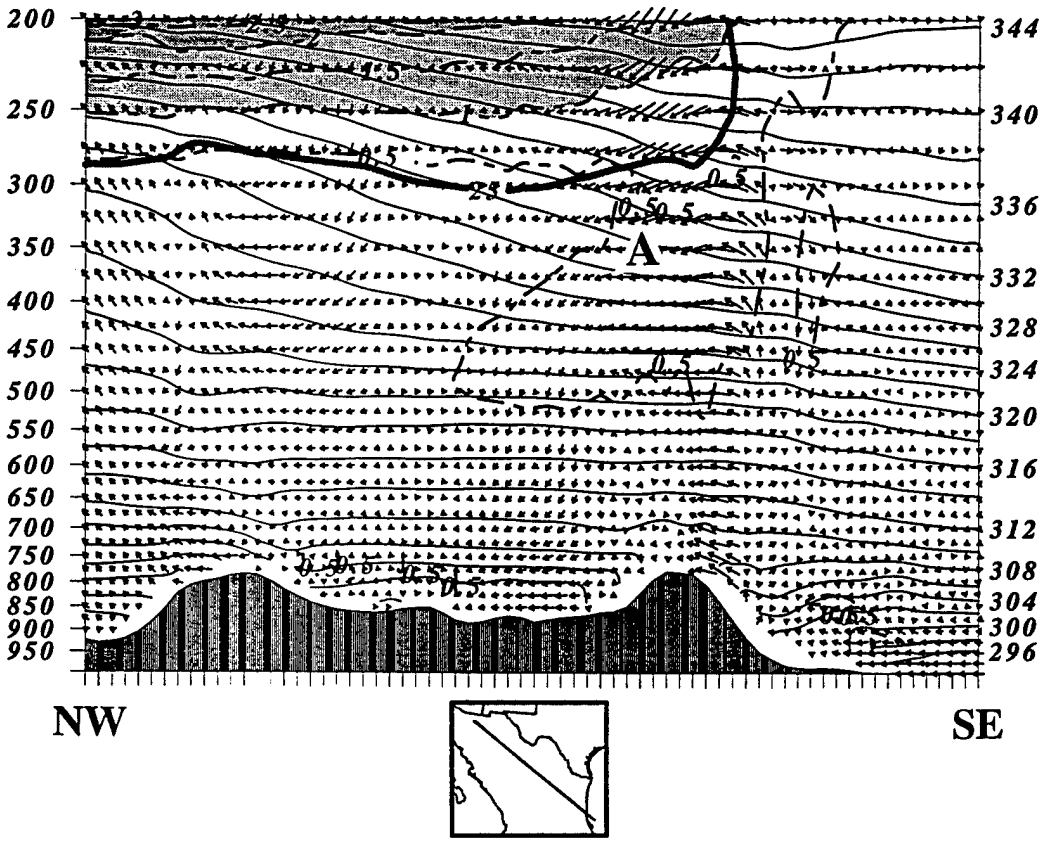

FIG. 19. MASS simulated, 24 km mesh, cross section extending from 30.5N, 110W to 20.5N, 96.5W. Including ageostrophic wind vectors, θ (solid line, K), wind speed (thick solid line, contoured at 25 ms^{-1}) and PV (dashed lines, contoured by 0.5 and shaded greater than 1 PV unit) valid at 1800 UTC 24 November 1988.

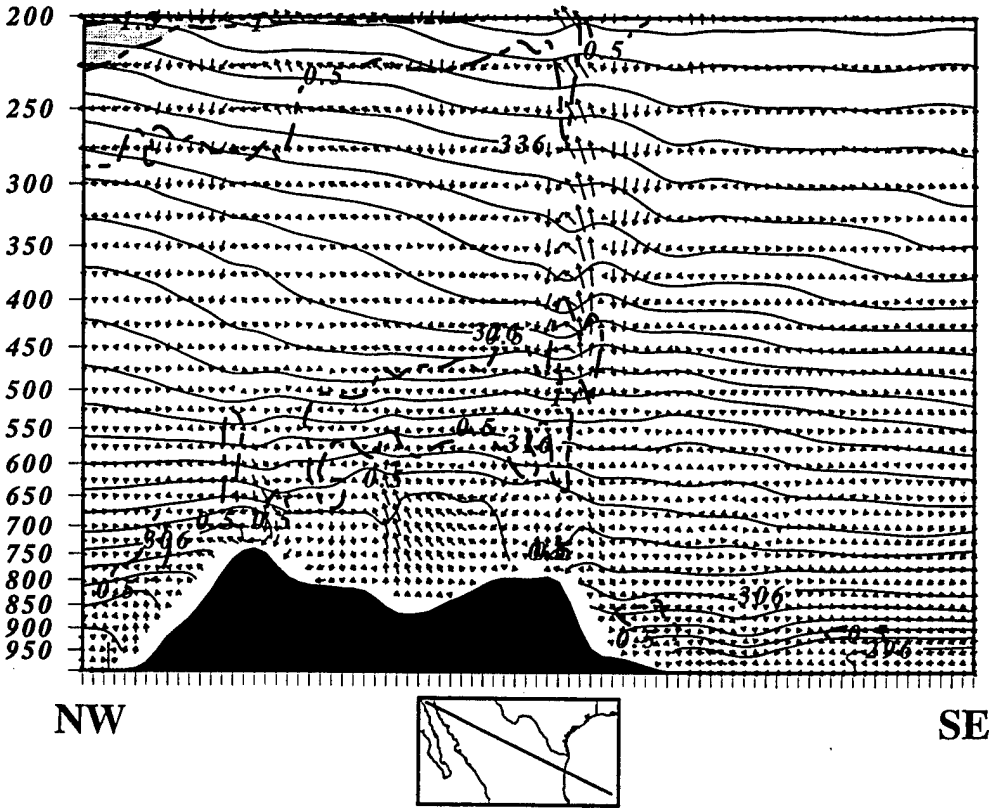

FIG. 20. MASS simulated, 24 km mesh, cross section extending from 26.5N, 110W to 22.2N, 92.5W. Including ageostrophic wind vectors, θ (solid lines, K), and PV (dashed lines, contoured by 0.5 and shaded greater than 1 PV unit) valid at 0000 UTC 25 November 1988.

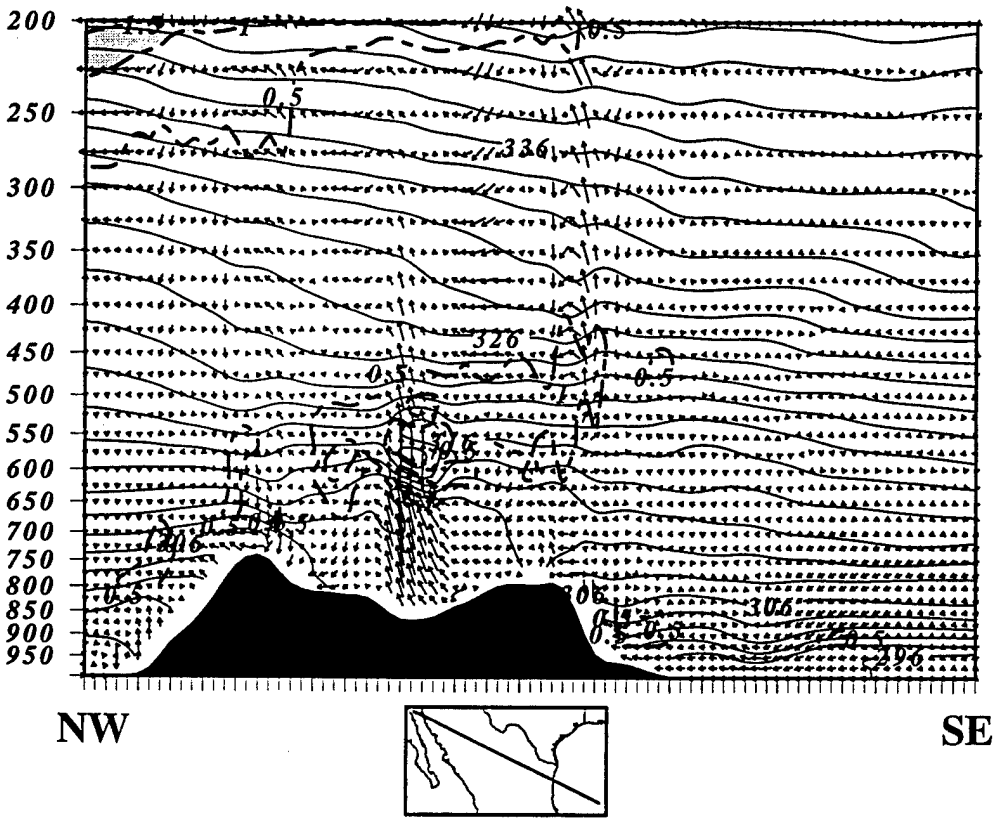

FIG. 21. MASS simulated, 24 km mesh, cross section extending from 26.5N, 110W to 22.2N, 92.5W. Including ageostrophic wind vectors, θ (solid lines, K), and PV (dashed lines, contoured by 0.5 and shaded greater than 1 PV unit) valid at 0100 UTC 25 November 1988.

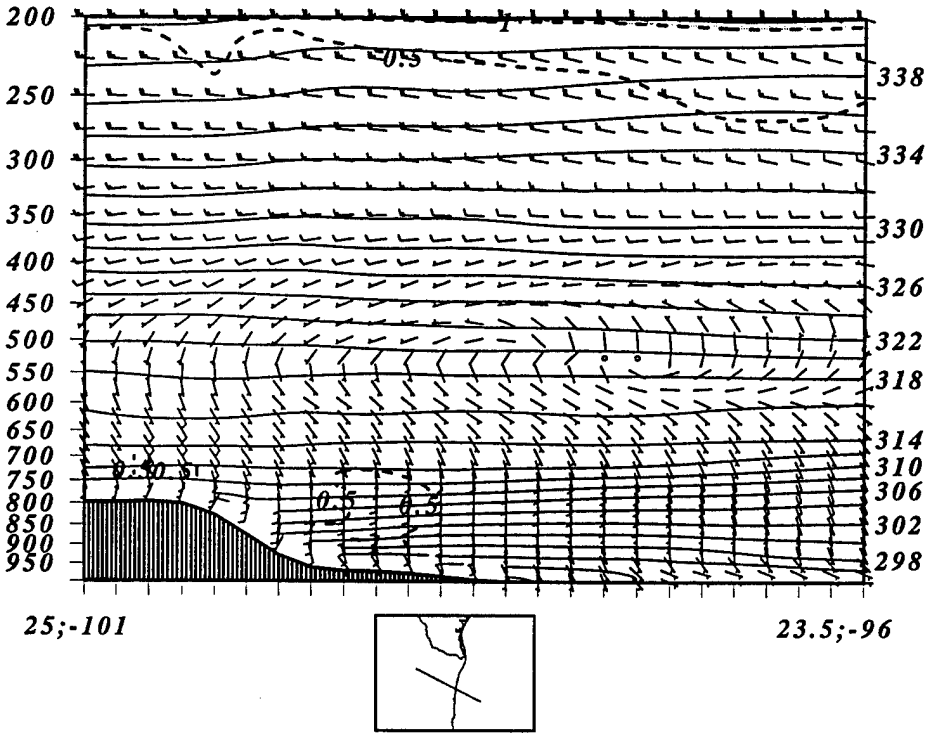

FIG. 22. MASS simulated, 24 km mesh, cross section extending from 25N, 101W to 23.5N, 96W. Including wind vectors, θ (solid lines, K), and PV (dashed lines, contoured by 0.5 and shaded greater than 1 PV unit) valid at 0900 UTC 23 January 1990.

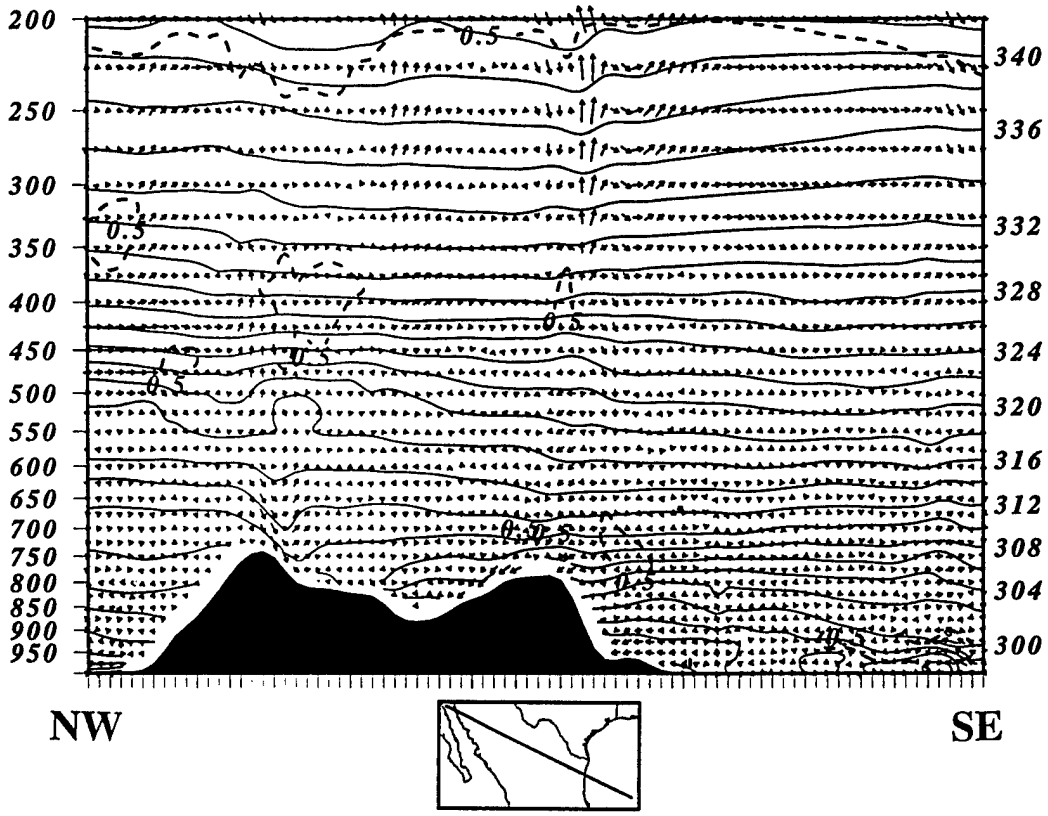

FIG. 23. MASS simulated, 24 km mesh, cross section extending from 26.5N, 110W to 22.2N, 92.5W. Including ageostrophic wind vectors, θ (solid lines, K), and PV (dashed lines, contoured by 0.5 and shaded greater than 1 PV unit) valid at 0000 UTC 23 January 1990.

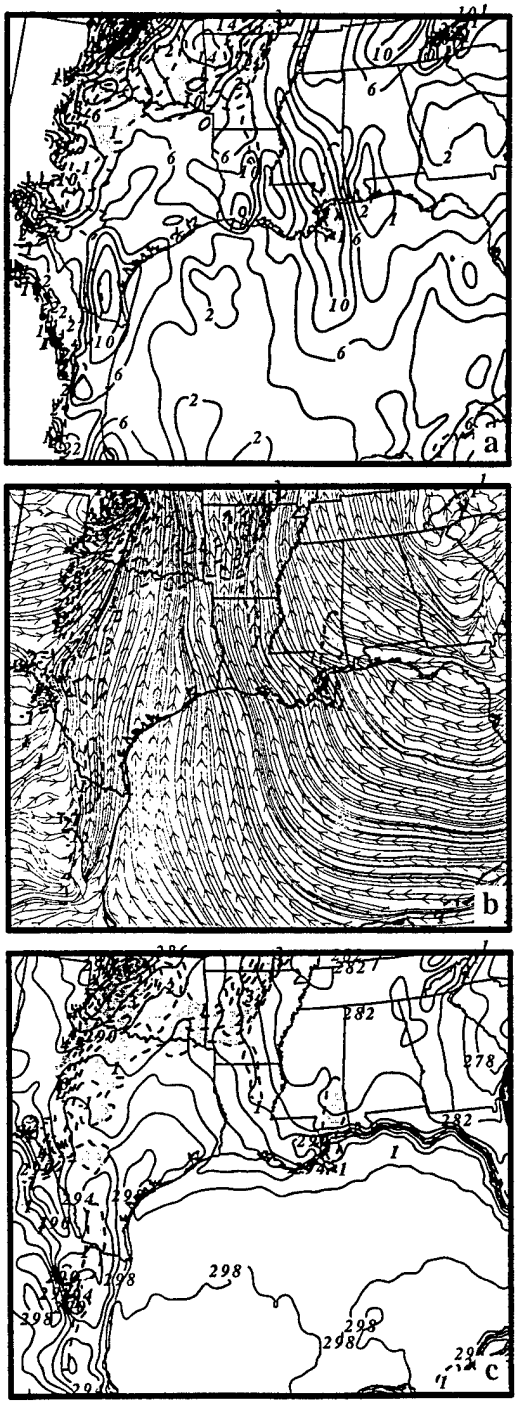

FIG. 24. MASS simulated, 24 km mesh, valid at 1200 UTC 25 November 1988 of PV (contoured (dashed lines) and shaded greater than 1 PV unit) and (a) magnitude of shear (solid lines, ms^{-1}) over the 925 to 850 mb layer, (b) surface streamlines and (c) surface theta (solid lines, K).

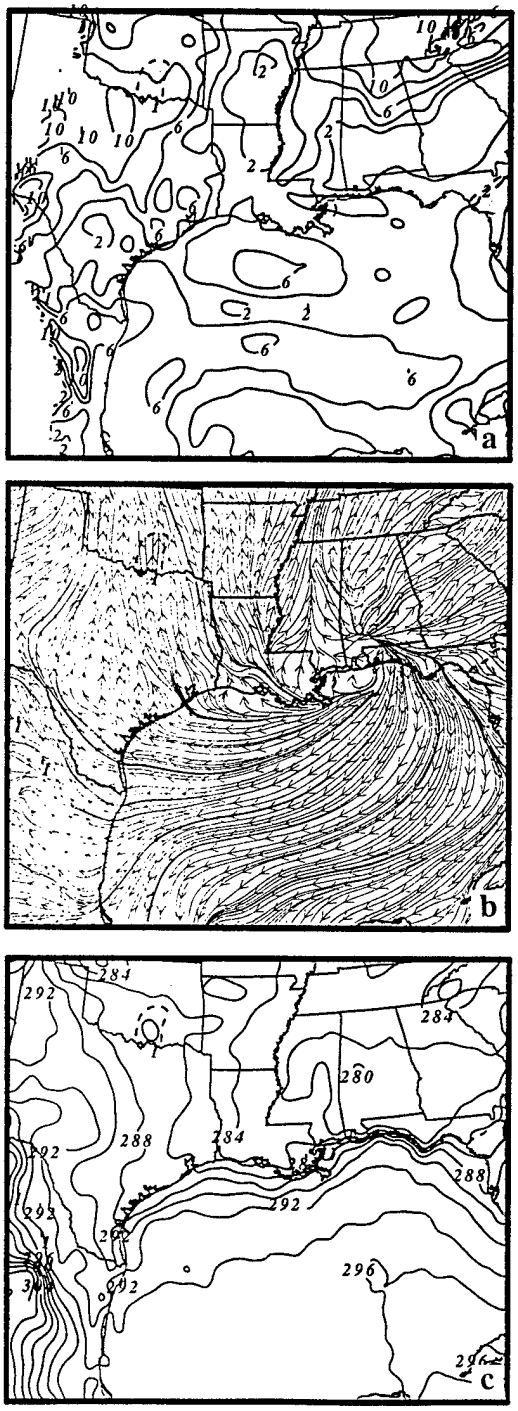

FIG. 25. MASS simulated, 24 km mesh, valid at 0000 UTC 23 January 1990 of 900 mb PV (contoured (dashed line) and shaded greater than 1 PV unit) and (a) magnitude of shear (ms^{-1}) over the 925 to 850 mb layer, (b) surface streamlines and (c) surface theta (K).

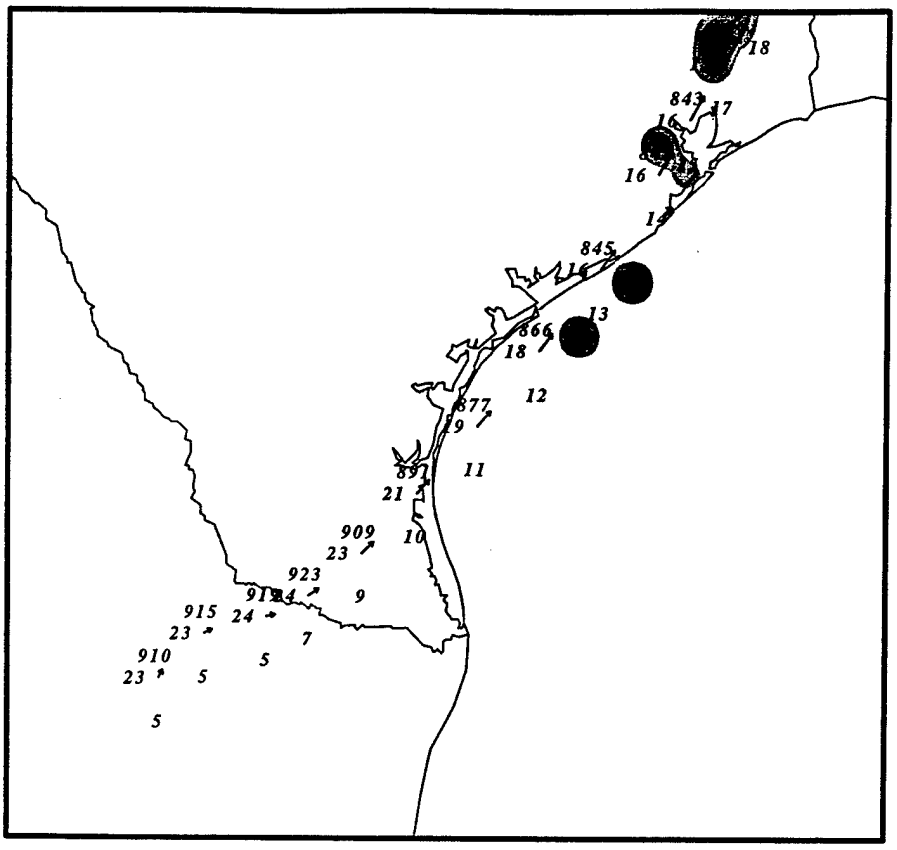

FIG. 26. MASS simulated, 24 km mesh, trajectory initialized at 0600 UTC 25 and ended at 0600 UTC 26 November 1988 plotted over latent heating due to convection (contoured by 10 Chr^{-1}) at 900 mb. Station plots contain pressure (mb), temperature (C), and total wind speed (ms^{-1}). Displayed wind vectors depict total wind.

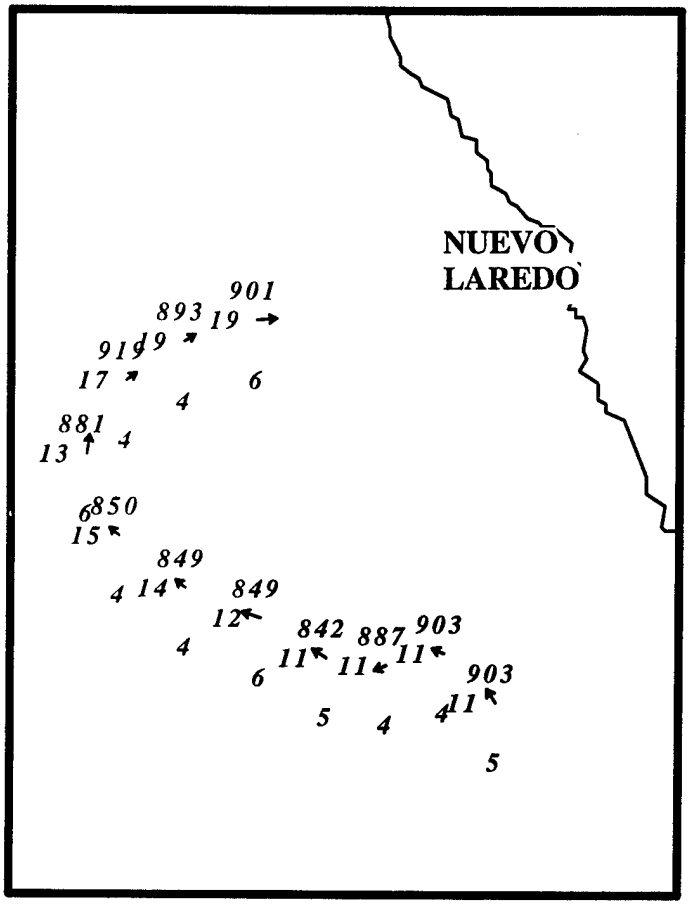

FIG. 27. MASS simulated, 24 km mesh, trajectory initialized at 1800 UTC 22 and ended at 1800 UTC 23 January 1990. Station plots contain pressure (mb), temperature (C), and total wind speed (ms^{-1}). Displayed wind vectors depict total wind.

CHAPTER 3

MESOSCALE SIMULATIONS OF DYNAMICAL FACTORS DISCRIMINATING BETWEEN A TORNADO OUTBREAK AND NON-EVENT OVER THE SOUTHEAST US

PART II: 48 - 6 HOUR PRECURSORS

John M. Egentowich, Michael L. Kaplan, Yuh-Lang Lin* and Allen J. Riordan

(Submitted to Weather and Forecasting for publication)

**Corresponding author address*: Dr. Yuh-Lang Lin, Department of Marine, Earth and Atmospheric Sciences, North Carolina State University, Raleigh, NC 27695-8208.

E-mail: yl_lin@ncsu.edu

Abstract

Using observational analysis and mesoscale numerical simulations we investigate the subtropical jet (STJ) and its effects on the lower environment (associated mass and momentum adjustments, development of a low-level jet (LLJ), and low-level PV) 48 to 6 hours before the Raleigh tornado outbreak (1988). We also compare the environment to a synoptically similar event with severe weather forecasted but did not develop over central NC. In the severe weather case a self-maintaining, low-level circulation originated over Mexico, propagated across the Gulf Coast and moved over the Carolina Piedmont at the time of the tornado. It is characterized by a surface trough, low-level PV maximum, mid-level jet, a warm Mexican airmass and STJ exit region that was co-located and moved across the Gulf Coast States as a coupled system. Initially, an STJ exit region (with thermally indirect ageostrophic circulation) approached the Gulf Coast creating upper-level divergence (mass removal from the air column) and ascent, which helped to maintain a low-level trough. The warm Mexican airmass was located over the Gulf Coast (southeast of the surface trough) creating a northwestward-directed PGF, which created a mid-level jet. The right entrance region of the mid-level jet and its associated thermally direct circulation (ascent) was over the low-level trough. These features created an environment favorable to deep convection and the release of latent heat that generated low-level PV. In the non-event case, these features (low-level warm Mexican airmass, mid-level jet, deep convection, low-level PV and low-level trough) were absent along the Gulf Coast States.

1. Introduction

The Raleigh, North Carolina tornado of 28 November 1988 was an extraordinary event which has stimulated a great deal of interest from the weather forecasting and research communities. This tornado violated climatology as it occurred in the middle of the night in late November with an unusual F4 intensity for NC and was part of a larger outbreak across NC and VA. Previous paradigms based on jet streak dynamics predict severe weather will occur in the vicinity of the polar jet (PJ) exit region not the entrance region. Severe weather predictive indices based upon typical jet exit region dynamics were all sufficiently unremarkable to prevent the National Weather Service from issuing *any* severe weather watch or warning boxes prior to observations of severe weather (Gonski 1989). The inability of standard indices/dynamical paradigms to indicate at least modest tornadic potential for such an *extreme* climatologically anomalous event clearly raises the possibility that our scientific understanding of the mechanism of tornadic development is limited and that more research needs to be done.

Kaplan et al. (1998) proposed a new severe weather paradigm with three primary components. First, the juxtapositioning of the PJ entrance region and the subtropical jet (STJ) exit region and their transverse secondary circulations create deep QG vertical motions. Second, the adjustment of the mass field to the subgeostrophic wind field occurs in proximity to the continental air and polar air interface, i.e., low-level fronts accompany the return branch of the STJ streak and return branch of the PJ streak resulting in midtropospheric mesoscale jet streak. Third, the parcel is subjected to intensifying

stretching and tilting as it is caught up in the thermally direct unbalanced circulation in the right front quadrant of the adjusting jetlet.

The classic "loaded gun" type 1 tornado sounding, (Fawbush and Miller 1954) has a moist unstable layer capped by an elevated mixed layer (EML). The EML creates a large area of instability. Lanici and Warner (1991) performed an in-depth lid study that examines the EML source region of Mexico. They examined the climatology, characteristics, life cycle, and relationship to severe storms. They assume the lid is a feature that facilitates intense convection by greatly increasing the convective instability. *We hypothesize that the warm air off the Mexican plateau (EML) not only creates convective instability but also forces a geostrophic adjustment process that creates a mid-level jet, which maintains a propagating surface trough and facilitates strong convection.*

A hydrostatic environment rich in potential vorticity (PV) is likely to be an environment favoring cyclonic vorticity intensification. Potential vorticity, therefore, is an excellent tracer for the potential rotational energy if it can be combined with an environment favorable for convection. The generation of mesoscale PV may be examined using the Lagrangian PV equation (Gidel and Shapiro 1979); may be estimated by:

$$\frac{\mathrm{d}}{\mathrm{dt}}\left[-(\zeta_\theta+f)\frac{\partial\theta}{\partial p}\right]=\underbrace{-(\zeta_\theta+f)\frac{\partial}{\partial p}\left[\frac{\mathrm{d}\theta}{\mathrm{dt}}\right]}_{1}\underbrace{-\left(\frac{\partial\theta}{\partial p}\right)\hat{k}\nabla_\theta\times\mathrm{F}}_{2}+\underbrace{\left(\frac{\partial\theta}{\partial p}\right)\hat{k}\bullet\nabla_\theta\left[\frac{\mathrm{d}\theta}{\mathrm{dt}}\right]\times\frac{\partial\vec{\mathrm{V}}}{\partial\theta}}_{3}. \qquad (1)$$

Term one defines the mechanism of PV production or destruction due to vertical gradients of diabatic heating with isentropic absolute vorticity. Term two represents the change in PV resulting from frictional stresses. Term three represents the change in PV resulting from the tilting of the horizontal component of vorticity into the vertical through horizontally varying diabatic heating. Gyakum et al. (1995) related the diabatic production of PV to rapid surface cyclogenesis, concluding that surface frontogenesis produced a vertical wind shear enhancing the diabatic generation of PV through tilting. Zehnder and Keyser (1991) investigated rapid cyclogenesis in the absence of diabatic effects. They found the interaction between upper- and lower-level disturbances characterized by non-uniform PV results in significant increase in relative vorticity at the surface.

Egentowich et al. (1999) (hereafter Part 1) compare the event (RDU tornado, 28 November 88) to a non-event (25 January 1990), discuss the early synoptic situation (84-48 hours before the event and non-event), jet development, low-level PV development and warm air transport. In the event case, strong cold air advection over NM and TX tightens the pressure gradient and, in turn, intensifies the STJ streak over TX and MX. The upper-level jetogenesis creates a transverse ageostrophic circulation forcing air down the eastern side of the Sierra Madre Mountains creating adiabatic warming due to compressional heating. Along with this warm air, a low-level trough of low pressure forms over the western Gulf of Mexico. Low-level winds accelerate into this area creating a northward low-level jet (LLJ) off the TX coast, which begins to transport very

warm low-level air from the Mexican plateau to the Gulf Coast. The non-event case has a different synoptic pattern; the upper-level flow is very zonal over the US with a ridge over MX. The PJ develops over northern TX, OK and MO. The ridge prevents the STJ from developing or moving over the Gulf of Mexico. During the early period, no transport mechanism (LLJ) develops to move the hot air off the Mexican plateau over the Gulf.

For the event case, low-level PV is generated in the upper-levels and transported downward in the lee of the Sierra Madre Mountains. The STJ exit region and its associated thermally indirect circulation transports the PV down to the midlevels over the Mexican plateau. At the same time, a mountain-plains solenoid develops due to strong heating over the Mexican plateau creating ascent to 550 mb. An area of strong vertical convergence develops in the 500-600 mb layer increasing the thermal gradient (static stability) and generating PV. This midlevel PV maximum moves eastward and a hydrostatic mountain wave transports the PV downward near the Mexican coast. The low-level PV then moves northeastward along the Gulf Coast. In the non-event, the STJ is absent, thus PV is not transported downward to the midlevels. The low-level wind field over the western Gulf of Mexico is from the east advecting clouds over the Mexican plateau minimizing surface heating and inhibiting the formation of a deep dry adiabatic layer. The easterly low-level flow prevents the development of mountain waves southwest of BRO inhibiting any downward transport of mid-level PV.

So, entering the middle time period, there are significant differences between these cases. This second paper discusses the differences between the cases during this period (48 to 6 hours before the event/non-event). In the event case, a surface trough, low-level PV maximum, mid-level jet, a warm Mexican airmass and STJ exit region are co-located and move across the Gulf Coast States as a coupled circulation system. Initially, an STJ exit region (with thermally indirect ageostrophic circulation) approaches the Gulf Coast. This creates upper-level divergence (mass removal from the air column) ascent in the left exit region, which helps to maintain a low-level trough. The warm Mexican airmass is located over the Gulf Coast (southeast of the surface trough). This warm air facilitates the development of a mid-level, northwestward directed PGF creating a mid-level jet. The mid-level jet entrance region has an associated thermally direct ageostrophic circulation, which enhances ascent over the low-level trough. These features create an environment favorable for deep convection releasing latent heat, generating low-level PV and produce a self-sustaining circulation that moves across the Gulf Coast States and over central NC at the time of the tornado outbreak. In the non-event case, these features (low-level warm Mexican airmass, mid-level jet, deep convection, low-level PV and low-level trough) are absent along the Gulf Coast States. A PJ entrance region and small mid-level jet is over northern MS and AL -- well north of the Gulf Coast.

In this paper, we explore the relationship between the STJ and its effects on the lower environment (associated mass and momentum adjustments, development of a LLJ,

and low-level PV) 48 - 6 hours before the development of severe weather. We also compare the environment to a synoptically similar event when severe weather was forecast but nothing developed near RDU. In section 2 we briefly describe the mesoscale model used for the simulations. Section 3 deals with the development of the jet streaks in both the event and non-event. Section 4 focuses on the development and movement of the surface trough (convergence zone) across the Gulf Coast. In section 5 we investigate the origins of low-level PV. Finally, in section 6 we summarize and present our conclusions.

2. Model summary

Due to the lack of high-resolution observational data, numerical simulations are employed to understand the environments prior to the event and non-event. The MASS model version 5.8 (MESO 1995) produces the simulations for this study. This MASS model is a modified version of the model originally developed by Kaplan *et al.* (1982). The numerical experiments, grid resolution and coverage are summarized in Part 1 (Egentowich et al., 1999). Three-dimensional parcel trajectories used throughout this paper are derived from the Mesoscale Atmospheric Simulation System Trajectory (MASSTRAJ) software package (Rozumalski 1997).

3. Jet development

3.1 Upper-level jet streams

As in Part 1, one of the most significant differences between the two cases is the presence of the STJ in the event case and its absence in the non-event case. In the event case (0000 UTC 26 November 1988 to 0000 UTC 28 November 1988), the jet streams remain in roughly the same locations over North America. The STJ stream extends from the southeastern Pacific across Central Mexico and the southeast US. The PJ stream extends from northwestern Canada southeast over TX (around a trough in the central US) and northward over the Mid-Atlantic States. Individual streaks move through the jet streams changing the convergence/divergence areas, the ageostrophic circulations and vertical motions. The non-event case from 1200 UTC 23 January 1990 until about 1200 UTC 25 January 1990 has an upper-level ridge over Mexico -- preventing the development of the STJ. The PJ develops over northern TX and extends over the northeast US. As the upper-level trough develops over the central US, the PJ dips into central TX and extends over the northeast US. These features are examined and related to the low-level environment.

a. Event case and non-event case observations

Observed data highlight the differences between the event and non-event case and the relationship between the upper-level jets and surface convection. Figure 1 is the 200

mb NWS analyses and cross sections valid 0000 UTC 27 November 1988 and 1200 UTC 24 January 1990. Figure 2 is the radar summary valid 0035 UTC 27 November 1988 and 1235 UTC 24 January 1990. For these time periods, eastern TX, LA and MS is the area of interest. The event case 200 mb NWS analysis (Fig. 1a) depicts an area of strong wind over the Gulf Coast region, which is a reflection of a subtropical jet streak. Also, the observation-derived cross section (Fig. 1b) clearly depicts the PJ and the STJ. There is subgeostrophic wind over the TX, LA and MS coast (wind barbs crossing the isobars toward lower pressure) indicating a jet streak entrance region. Associated with a jet entrance region is a thermally direct ageostrophic circulation, an area of upper-level divergence and ascent over the Gulf Coast. The supergeostrophic wind (wind barbs crossing the isobars toward higher pressure) over the Carolina Coast indicates the presence of a jet streak exit region. The non-event case 200 mb NWS analysis (Fig. 1c) depicts a strong PJ extending from northern TX to the northeast US. The observation-derived cross section (Fig. 1d) depicts only a PJ. There is supergeostrophic wind over the TX coast, LA, MS and AL indicating the wind is decelerating, converging and descending. In the event case, there is divergence in the upper-levels (removal of mass from the air column) facilitating ascent while the non-event case has upper-level convergence and sinking over the western Gulf Coast. This upper-level divergence or convergence directly relates to the strength (depth) of convection. In the event case, the radar summary (Fig. 2a) depicts strong convection with maximum tops near 16 km over LA and MS. In the non-event case, the convection is much less intense with maximum

tops less than 11 km (Fig. 2b). Also, the non-event case radar summary valid 0035 UTC 25 January 1990 is examined (to consider the effect of daytime heating) and the maximum tops were even lower (9.5 km).

b. Event case and non-event case model simulated data

Figure 3 depicts the 200 mb environment valid at 0000 UTC 27 November 1988 and 1200 UTC 24 January 1990 which corresponds with the NWS analysis above. The event case 200 mb analyses (Figs. 3a and c) depict an area of strong wind and subgeostrophy over the Gulf Coast region. Over the TX and LA coast, the ageostrophic wind is directed to the northwest indicating upper-level divergence over the western Gulf Coast. The 200 mb subgeostrophy, northwest directed ageostrophic wind and upper-level divergence area corresponds well with the surface convection; this relationship is consistent over the entire simulation. The non-event case (Fig. 3b) is very different from the event case. There is a strong PJ over central TX and extending northeast. The 200 mb wind over the Gulf Coast is supergeostrophic. Over the LA, MS, AL and FL coast, the ageostrophic wind (Fig. 3d) is directed to the southeast indicating upper-level convergence over the western Gulf Coast area. The 200 mb supergeostrophy, southeast directed ageostrophic wind and upper-level convergence area remains over the Gulf Coast over the entire simulation. The intensity and coverage of upper-level convergence increases with time. So, in the event case there is upper-level divergence, which removes mass from the air column and creates ascent, while the non-event case has upper-level

convergence and sinking over the western Gulf Coast. Also, the ageostrophic wind is much stronger in the event case study.

The event case has significant convection associated with a surface trough over eastern TX and western LA early on 26 November 1988. We investigated the upper-level circulations to determine if they were conducive to deep convection. Figure 4 depicts a cross section near the TX/LA border valid 1500 UTC 26 November 1988. The ageostrophic circulation (wind vectors) depicts a thermally direct circulation associated with the PJ entrance region. Associated with the circulation is an area of strong ascent (Fig. 4a), surface convergence and mid- and upper-level divergence (Fig. 4b). The ascent plume and mid- and upper-level divergence is associated with the surface trough (Fig. 16a) and convection (Fig. 16c). By 0000 UTC 27 November 1988 the STJ is over the Gulf Coastal States. The NWS analysis (Fig. 1a) depicts the STJ exit region, with supergeostrophic wind, over AL, GA and SC while over western TN the wind associated with the PJ is subgeostrophic. Figure 5 depict cross sections over TN and AL bisecting both jet streaks. The cross sections depict both the thermally direct circulation associated with the PJ entrance region and the thermally indirect circulation associated with the STJ exit region. Additionally, there is an area of ascent and upper-level divergence between these jet streaks. Since these features are associated with long lasting jet steaks they are also long lasting and thus facilitate the continuous regeneration of the surface trough and convection. The non-event case analysis (Fig. 1b) depicts supergeostrophic wind over of the Gulf States -- indicating upper-level convergence and descent. Figure 4 depicts cross

sections aligned north/south along the TX/LA border valid (0300 UTC 24 January 1990) as the same relative time as the event case. The atmosphere is very benign -- there is very little upper-level divergence and no organized ascent through these levels. Additionally, the downstream cross sections valid 1200 UTC 24 January 1990 (Fig. 5c and d) are also very benign through the mid- and upper-levels. In summary, the jet streaks and associated ageostrophic circulations create mid- and upper-level ascent and divergence thus assisting in the maintenance of the surface trough and production of deep convection in the event case, while these features are missing in the non-event cases.

We examine how the jet streaks modify the environment by comparing the lifted indices (LI) over the Gulf Coast (Fig. 6). For the event case (Fig. 6a), the LI pattern at 1800 UTC 26 November 1988 depicts large negative LI over LA, AR, MS and AL (east of the surface trough and in the warm Mexican airmass), which indicates great potential for severe weather. The non-event case LI field at 0600 UTC 24 January 1990 (Fig. 6b) depicts large positive LI over the Gulf Coast, which indicates little chance for severe weather. We also examined the LI at 1800 UTC to account for solar heating (not shown). The LI values along the Gulf Coast range from 8 to 20, which again indicates little chance for severe weather.

Three-dimensional parcel trajectories are constructed to illustrate the forced adjustments imposed upon air parcels as they move through the upper-level jet over LA. First, we examine the event case (Fig. 7a and Table 1). As the parcel moves over eastern TX and LA, it moves through an area of strong upper-level divergence and ascent, which

removes mass from the air column and maintains the low-level tough. The trajectory data support the results and conclusion above. The non-event trajectory is depicted in Table 2 and Fig. 7b. The parcel accelerates and ascends slowly along its trajectory. Most notably, the parcel goes through a large area of upper-level convergence, which inhibits any large-scale removal of mass from the air column.

3.2 Mid-level jet development

In this paper, the mid-level jet is defined by winds greater than 35 ms^{-1} and it is centered about the 600 mb level. In the event case, a northeastward directed mid-level jet develops over TX and propagates eastward across the southern states, from TX to GA. In the non-event case, there are two distinct mid-level jets covering two time periods. First, until approximately 2100 UTC 24 January 1990, a thin mid-level jet extends across the southeast US (extending from northern AR to southern TN). Second, after 2100 UTC 24 January 1990 a mid-level jet develops with the low pressure system located to the west of the Appalachian Mountains.

a. Developing thermal and pressure gradients

In the event case, the mid-level jet develops, in large part, due to warm air transported from the Mexican plateau. Figure 8a depicts the warm air moving from the Mexican plateau and over the northwestern Gulf at 1200 UTC 26 November 1988. The 15 °C isotherm (shaded > 15) is over eastern TX and just south of the Gulf Coast. The

airmass over most portions of the Gulf is in excess of 17 °C. Over the next 24 hours, the warm Mexican air moves eastward over the Gulf States. The sensible heating at the 850 mb level is examined but is essentially zero. Figure 8c valid 0600 27 November 1988 depicts the 15 °C isotherm over central MS and AL. The parcel trajectories for this case are located in this warm air mass. The 0000 UTC 28 November 1988 NWS analysis (not shown) depicts the 15 °C isotherm over eastern NC with Charleston, SC reporting 16 °C. The non-event case, depicted in Fig. 8b valid 0000 UTC 24 January 1990, is very different from the event case. The flow is directed upslope or parallel to the Sierra Madre Mountains thus the warm air is not transported down the mountain. The non-event, 850 mb temperature over the Gulf is 3 - 4 °C cooler than the event case. Figure 8d valid 0000 UTC 25 January 1990 depicts the 15 °C air over the western Gulf and the air over the Gulf Coast States, which is about 3 - 4 °C colder than the event case.

The event case jet develops rapidly over central TX between 0900 and 1800 UTC 26 November 1988 (Figs. 9a and b). The jet development corresponds with the increasing 600 mb thermal and height gradient associated with the eastward moving trough. The thermal gradient and the PGF increase dramatically over central LA. At 0900 UTC the magnitude of thermal gradient is about 1 °C/100 km and the PGF per unit mass is 1.9×10^{-3} ms^{-2} and by 1800 UTC the thermal gradient increases to 2.5 °C/100 km and the PGF per unit mass is 3.9×10^{-3} ms^{-2}. Thus, the wind speed increases from 25 ms^{-1} to 41 ms^{-1} during this period.

The 850 and 700 mb level temperature change over the 0900 to 1800 UTC time periods are examined to measure how the warm MX air effects jet development. At the 700 and 850 mb levels (not shown), north of the jetogenesis area (near Wichita Falls) the temperatures decrease by 4 and 6 °C, respectively. South of the jetogenesis area (near Houston) the 700 and 850 mb, the temperatures decrease 1 and 0 °C, respectively. The low-level cooling (near Wichita Falls) decreases the 600 mb heights by approximately 40 m (location A in Fig. 9a and b). The Mexican warm airmass maintains the 600 mb heights over Houston at approximately 4290 m (location B in Fig. 9a and b). So, the warm Mexican plateau airmass over the Gulf Coast sets up an environment favorable for the development of a mid-level jet. The mid-level jet right entrance region is closely associated with the surface trough over TX/LA border and it is well ahead of the NWS surface front location over central TX. In the right entrance region of a thermally direct ageostrophic circulation there is ascent, which helps maintain the surface trough.

For the non-event case, there are two periods in the early development and propagation of the mid-level jet. First, until approximately 0600 UTC 25 January 1990, there is a narrow mid-level jet (winds greater than 35 ms^{-1}) extending over northern LA, MS, AL and TN. The jet is associated with the surface front, a narrow band of cold air advection and a strong height gradient. Over northern MS, at 2100 UTC 23 January 1990 (Fig. 9c) the thermal gradient is about 2 °C/100 km and the PGF per unit mass is 2.17 ms^{-2}. By 0600 UTC 24 January 1990 the thermal gradient is about 4 °C/100 km and the PGF per unit mass is 2.92 ms^{-2}. Thus the wind accelerates from 31 ms^{-1} to 36 ms^{-1}. Later, as

the cold air advection and its associated thermal, height, and pressure gradients weaken, so does the mid-level jet. By 1800 UTC 24 January 1988 (Fig. 9d) the winds over the coastal states decrease by about 5 ms^{-1}. After 0600 UTC 25 January 1990, a strong mid-level jet develops over the TN Valley. The mid-level jet develops with a quasi-geostrophic front/trough system over the Midwest US. Over western TN, at 0300 UTC 25 January 1990, the PGF per unit mass is $1.12x10^{-3}$ ms^{-2} and by 1800 UTC 25 January 1990, the PGF per unit mass is $4.99x10^{-3}$ ms^{-2}, which consequently, forces the wind to increase from 24 ms^{-1} to 53 ms^{-1}.

The low-level mass and momentum adjustments can be related by examining Fig. 10. In the event case, the transport of the warm Mexican airmass increases the PGF and the mid-level jet. Figures 10a and c, valid 1800 UTC 26 and 27 November 1988, depict the equivalent potential temperature (Θ_e) of the Mexican airmass defined here as >330°K. At 1800 UTC 26 November 1988, the warm air originates over the Mexican plateau, extends over the western Gulf and the southeast US. The largest PGF and the mid-level jet is located on the northwest boundary of this airmass, in the 310 to 320 °K (Θ_e) range. By 1800 UTC 27 November 1988 the warm airmass moves over to SC and GA. Figures 10b and d are cross sections through the jet entrance region. Notice how the warm air is to the southeast of the jet. So, in the event case the mid-level jet is associated with the warm Mexican airmass over the Gulf Coast. The right entrance region of the jet with its thermally direct circulation and ascent is associated with the surface trough. In the non-event (Figs. 10e and g), valid 0900 UTC 24 and 25 January 1990, the warm Mexican air

does not move off the plateau. There is a relatively cool pool of air over the western Gulf inhibiting the development of a mid-level jet. The cold air advection over OK, AR and TN increases the PGF and develops a mid-level jet, which is well north of the Gulf Coast.

b. Three-dimensional trajectory analysis

Three-dimensional parcel trajectories are constructed to illustrate the forced adjustments imposed upon the air parcels as they move through or near the mid-level jetogenesis region. The event case parcel trajectory (1200 UTC 26 November 1988 to 1900 UTC 26 November 1988) is depicted in Fig. 11a and Table 3. The parcel originates near the 700 mb level, moves over the surface trough (and the associated convection) near the TX/LA border, ascends rapidly, and ends in the mid-levels over MS. Through 1500 UTC the PGF and the Coriolis force are almost balanced, so the parcel accelerates slightly. The average magnitude difference between the environment PGF and parcel's Coriolis force is 0.19×10^{-3} ms^{-2}. Between 1600 to 1900 UTC the parcel moves over the surface trough and into the convection area and ascends rapidly (from 653 to 595 mb); at this time, the trajectory can be related to Fig. 10a, which depicts the 600 mb jet. Here, the environmental PGF is much stronger than the parcel's associated Coriolis force, which forces the parcel to accelerate greatly. As the parcel ascends, the magnitude difference between the PGF and Coriolis force increases from 0.16×10^{-3} ms^{-2} at 1500 UTC to 1.71×10^{-3} ms^{-2} at 1800 UTC. Thus, as the parcel ascends it encounters a greater PGF/Coriolis force imbalance and must accelerate. Also, the 700 mb level height

contours are more north-south orientated than the 500 mb isobars (the lower-level parcels have more southerly momentum). When the parcel (originating from the 700 mb level) is ejected near the 500 mb level it carries with it more southerly momentum. Thus the parcel at its new higher level crosses the isobars toward lower pressure and accelerates.

The mid-level parcel trajectory of the non-event case (0000 to 0900 UTC 24 January 1990) is depicted in Fig. 11b and Table 4. Table 4 lists the parcel's accelerations as it moves over the Gulf Coast States. Again, the trajectory can be related to Fig. 10c; however, at this time there is no 600 mb jet near the Gulf Coast. Initially, the air parcel accelerates because it is in an area of subgeostrophy. In this case, there is less southerly momentum than the event case. Over the TX coast, trajectories of both the event and non-event case are the same, but once they enter LA, the tracks diverge. In the event case, as the parcels ascend (carrying with them the southerly momentum), the track becomes more northward. The non-event case trajectory remains on a straight path (more easterly than the event case).

c. Mid-level jet development and convection

We examine the relationship between convection and jet development. If convection is an important forcing mechanism for midlevel jet development, suppressing convection will reduce the jet development. As convection develops, the local environment warms due to the release of latent heat increasing the thickness of the air column and the PGF on a pressure surface near the middle of the column, which helps to

accelerate the jet. Also, convection has a predisposition to develop in areas of ascent. We compare the location of convection relative to the mid-level jet. In the event case, the convection area is associated with the mid-level jet right entrance region and in the warm MX airmass. In the non-event case, the only area of significant convection is occurring over the coast near the TX/LA border, which is well away from the mid-level jet.

Another MASS simulation is performed neglecting the release of latent heat (convection) to examine the relationship between jet development and convection. In the event case "no latent heat" simulation, a mid-level jet develops by 1800 UTC 26 November 1988 (Fig. 12) over TX and LA with approximately the same wind speed as in the case with latent heating. This supports the idea that the warm, low-level airmass transported from the Mexican plateau is an important element to maintain the height gradient over the TX/LA border and develop the mid-level jet. The environment is predisposed to produce a mid-level jet. Convection and latent heating does modify the jet over AR. The wind speeds are 5 - 10 ms^{-1} higher for the simulation with convection. For the non-event case, the 600 mb depictions valid 2100 UTC 23 January 1990 (Fig. 13a) and 0600 24 January 1990 (Fig. 13b) highlight the fact that the jet locations and intensity are slightly different between these two cases (with and without latent heating). The 600 mb jet (over LA and MS) is farther to the south in the case with latent heating. The wind speeds are about 5 ms^{-1} faster in the case with latent heating and the area of subgeostrophy is farther to the south. So, the front over MO, IL and KY and its associated precipitation modifies the mid-level winds over the Gulf Coast States.

Parcel trajectories are constructed for the event case without latent heating (Table 5 and Fig. 14). The parcel travels approximately the same path as in the simulation with latent heating supporting the idea that the atmosphere is predisposed to create a mid-level jet with or without the latent heat release. The parcel with latent heating ends at a higher level (550 vs. 583) and slightly faster ($40ms^{-1}$ vs. $38\ ms^{-1}$). Since the parcel with the latent heat exits at a higher level, with more southerly momentum, it remains unbalanced and continues to accelerate (Uccellini et al., 1984). By 2100 UTC (not shown) the size of the jet increases; moving over central MS where the unbalanced parcels with the southerly momentum were located. The parcel without latent heating is more balanced and decelerates at the end of the trajectory. In the non-event case, the parcel trajectories are different between the simulations with or without latent heating (Table 6 and Fig. 15). The parcel with latent heating ends at a higher level (557 vs. 583) and considerably faster ($24ms^{-1}$ vs. $19\ ms^{-1}$). Also, the parcel is directed more northward in the case with latent heating. So, the frontal system and associated latent heat release over MO, IL and KY creates a slightly stronger mid-level jet over the Gulf Coast.

In summary, in the event case the environment is predisposed to create a mid-level jet due to the warm air mass transported over the Gulf States from the Mexican plateau. Late in the period, convection enhances the aerial coverage of the mid-level jet over the Gulf Coast. The convection and surface trough over the Gulf Coast are associated with the right entrance region of the jet. The thermally direct ageostrophic circulation about the jet maintains the trough and convection by removing mass from the

air column. In the non-event case, latent heating associated with a frontal boundary over MO, IL and KY enhances the mid-level jet north of the Gulf Coast so the ageostrophic circulation (ascent) does not enhance convection along the coast.

4. Surface convergence zone and squall line

Part 1 discussed the differences in the synoptic scale forcing between the cases. In the non-event case, there is a large anticyclone located over the Gulf creating flow up the mountains. In the event case, the warm Mexican airmass moves eastward down the lee side of the Sierra Madre Mountains creating a low-level trough (convergence zone).

a. Surface trough development and propagation.

The model output of the event case compares very well with the NWS analysis. At 1500 UTC 26 November 1988 the MASS simulation depicts strong surface confluence over the TX/LA border extending into AR (Fig. 16a). The model depicts a meso-trough associated with the confluence zone. Moist air is to the east of the confluence zone with dry air over central TX. The NWS surface analysis (Fig. 16b) has similar features. The wind pattern is very similar with a confluence zone over the TX/LA border. A surface trough is shown over eastern TX and a squall line over central AR. Also, the moist air is east of the confluence zone and the dry air is over central TX. Both the radar summary (Fig. 16c) and the simulated convective precipitation field (not shown) indicate that convection occurs in the same areas. The strongest simulated convective precipitation is over the TX/LA border and the convection on the radar summary has the highest cloud tops (~15 km) in that area. For the next 24 hours the model-simulated surface trough (confluence area) propagates across the Gulf Coast states. At the same time, the NWS

analysis modifies the squall line into a trough and by 1200 UTC 27 November 1988 the trough is depicted as a cold front (moving over GA and AL).

In the non-event case, the MASS-simulated environment (Fig. 17a) is almost identical to the NWS analysis (Fig. 17b). At the same relative time as the event case (0300 UTC 24 January 1990) there is a quasi-stationary front over the TX/OK border extending across AR, TN and KY. This front is moving very slowly to the south. Also, a weak surface frontal system (trough) is moving onshore over the Gulf Coast. The lower atmosphere is much drier than the event case with the only moist air over the Gulf Coast. The only area of significant convective precipitation is over the Gulf Coast at the TX/LA border, as depicted on both the radar summary (Fig. 17c) and the simulated precipitation field. At this time, there is upper-level convergence over the Gulf Coast, which may inhibit deep convection. In the non-event case, the maximum tops of the convective cells over the Gulf Coast are 6-7 km lower than that of the event case. The NWS analysis depicts the front over the coast as a trough over the next 24 hours then begins to redevelop by 1800 UTC 24 January 1990. The only area of convective precipitation is associated with this front/trough over the coast, which increases in coverage and intensity but it is always much less than the event case. The absence of upper-level support (no STJ and the mid- and PJ are well to the north) inhibits deep convection.

Comparing the NWS surface analysis and the surface observations indicate several distinctive differences between the event case and non-event case. In the event case, a surface confluence zone propagates across the Gulf Coast states, while in the non-

event, a weak inverted trough moves north over the Gulf states. These synoptic patterns create several mesoscale differences. The event case mid-level PGF is at least twice as strong as the non-event case. The event case flow is more rotational (surface vorticity is not shown) than in the non-event case, which directly relates to storm development.

b. Mid-level jet coupling with low-level forcing.

The mid-level jet (600 mb) is examined to determine if it is coupled to the low-level forcing. At 0600 UTC 26 November 1988 winds over eastern TX are 20 ms^{-1} and by 2100 UTC 26 November 1988 there is a 40 ms^{-1} jet across eastern TX and central LA. Over eastern TX and LA, the wind is highly subgeostrophic (cross-stream momentum pointing towards lower heights), which accelerates in response to the environment (jet streak entrance region). The accelerating wind field produces an area of mid-level divergence and ascent, which maintains both the convection and the surface trough. Figure 18 depicts the vertical environment through the mid-level jetogenesis area and over the surface trough (confluence area). The low-level convergence and mid- and upper-level divergence facilitate strong ascent up to the 350 mb level. The surface trough moves in conjunction with the mid-level jet and the upper-level divergence. Figures 19a-c depict the surface trough (confluence zone) and the 600 mb jet and Figs. 19d-f depict the surface trough (confluence zone) and the 250 mb divergence valid 1800 UTC 26, 0600 UTC 27 and 1800 UTC 27 November 1988, respectively. The surface trough (confluence zone) is located to the right of the entrance region of the 600 mb jet and to

the left of the upper-level divergence. At 1800 UTC (Fig. 19c), the trough developed into a frontal boundary so the trough covers a much broader area.

In the non-event case, the mid-level jet (600 mb) is associated with the quasi-stationary front over TX/OK border and over TN (not shown). The mid-level jet is not associated with the area of convection along the Gulf Coast. At 0300 UTC the maximum winds (35 ms^{-1}) are over southern AR and northern MS. Over the next 24 hours, there is little change to the jet location except the maximum wind speeds have moved farther east (over GA). Throughout this mid-period the mid-level jet is not over the Gulf Coast.

In summary, the event case mid-level jet is coupled to the surface trough over the Gulf Coast. Under this situation, the low-level air parcels enter the convection area and confluence zone, ascend rapidly, exit at a much higher level and they are greatly unbalanced with respect to the local environment. They accelerate in the mid-levels as evidenced by the wind barbs pointing toward the lower height field (subgeostrophy). This area of subgeostrophy creates mid-level divergence, which in turn helps maintain the low-level trough (confluence area). The non-event case is considerably different from the event case. The mid-level jet is associated with a frontal boundary over AR and TN, much farther to the north than the event case (not located over the Gulf Coast).

5. Potential Vorticity

Potential vorticity may increase locally either by transport or generation. The generation of PV, through diabatic processes, may be examined using Eq. 1. Gyakum et al. (1995) related the diabatic production of PV to rapid surface cyclogenesis. In this section, we will discuss the generation, maintenance and propagation of the low-level PV maximum for the event and non-event case.

During this period, approximately 48 hours, the PV maxima paths are investigated for both cases. Figure 20 depicts the 900 mb PV maxima every 12 hours. In the event case (Figs. 20a-d), the PV maximum starts over the TX coast (just west of Houston) and moves east. When the maximum reaches the Alabama Gulf coast it turns to the northeast and moves over the Carolina Piedmont at the time of the tornado. The non-event case (Fig. 20e-h) has several PV maxima originating near the TX/OK border and moving across central AR and TN. These PV maxima weaken over time. A final PV maximum develops over central MS (associated with convection) at 1200 UTC 25 January 1990 and tracks to the Appalachian Mountains. The movement and location of the PV maxima are significantly different between the two cases. First, the event case PV maximum is about 500 km farther south than the non-event case PV. Second, the event case PV maximum tracks south and east of the Appalachian Mountains while the non-event case PV maxima move along the northwest side of the mountains.

a. Downward transport of potential vorticity

For the non-event case, two low-pressure systems develop in the lee of the Rocky Mountains and move northeast from TX to IN. There are several low-level PV maxima associated with the frontal boundary that extends across northern TX, AR and TN and within the PJ entrance region. The PV is transported downward in the lee of the Rocky Mountains and associated with the PJ entrance region (Fig. 21a). The upper-level PV maximum is located in the cold air, north of the left entrance region of the PJ. The distribution of PV resembles a tropopause fold (Danielsen 1968). As the upper-level jet and surface front propagate eastward, there is a link between the upper-, mid- and low-level PV (Fig. 21b). A trajectory is constructed to show a parcel moving through the area of downward transport. Table 7 and Fig. 22 depicts the sinking motion of the air parcel. The PV distribution and parcel trajectory support the concept that the low-level PV originates and is maintained, in part, by the downward transport of stratospheric PV. The downward transport of PV is not linked to any low-level forcing thus there is not any rapid cyclogenesis.

In the event case, the PV maximum over the TX coast moves east across the Gulf, then northeast to the Carolina Piedmont. In this case, the PV is maintained in the low-levels and builds vertically. The cross section valid 1500 UTC 26 November 1988 (Fig. 23) extends from eastern OK, bisects the strong low-level PV in eastern TX, and ends over the Gulf (south of LA). The upper- and mid-level PV maximum is associated with the intense thermal gradient located to the left of the PJ. The upper-level PV is not

transported down to the low-levels. As the low-level PV maximum propagates along the Gulf Coast, the PV is maintained in the low-levels.

Figures 24a and b depict the 900 mb PV, sea level pressure and surface streamlines (confluence) for the event case at 1500 UTC 26 and 2100 UTC 27 November 1988, respectively. At 1500 UTC over TX and the western Gulf there exists an intense line of low-level PV associated with a surface trough (convection). Cross sections from southern TX across the Gulf Coast to the FL panhandle (not shown) indicate a boundary between airmasses; the potential temperature lines are tilted toward and concentrated near the surface. Also, the 900 mb PV maximum is separated from the mid- and upper-level PV. Figure 23 depicts a cross section perpendicular to the airmass boundary. The upper-level PV is not transported to the low-levels indicating that the upper-level PV is decoupled from the low-levels. By 2100 UTC 27 November 1988 the NWS analysis modifies the trough to a cold front over the Gulf States. A frontal boundary can be analyzed in the simulated data. The strongest PV is over the southern portion of the cold front (where the confluence zone was last analyzed) while the northern portion of frontal system does not have any associated low-level PV. The low-level PV maximum propagating along the Gulf Coast maintains its integrity.

The low-level PV maintenance is different between these two cases. In the event case, the low-level PV maximum is maintained in the low-levels. In the non-event case, the low-level PV originates and is maintained, in part, by continuous downward transport of PV associated with the PJ entrance region.

b. Possible energy sources maintaining the low-level potential vorticity

We examine other potential energy sources (diabatic heating, thermal and wind shear gradients) and their relationship to the low-level PV. These energy sources act to produce and/or maintain the PV via Term 3 in Eq. (1). Low-level PV maxima (> 1 PV unit) are associated with strong vertical and horizontal wind shear gradients, localized areas of strong potential temperature gradients, and confluence areas. In this section we switch to a Lagrangian frame of reference. The relative contribution of each term in the PV Eq. (1) is evaluated in a manor analogous to Kaplan and Karyampudi (1992) using parcel trajectory data with the exception of the gradient field which is calculated using a centered finite differencing scheme over the center trajectory point. Using trajectories, we examine the PV maximum at the beginning of this time period (over southeast LA at 0000 UTC 26 November 1988) and late in this time period (over central AL at 1000 UTC 27 November 1988).

The parcel over southeastern LA originates in the PV maximum and moves northeastward (Table 8) encountering higher environmental PV. Convective precipitation is present over LA for the first 3 hours of the trajectory generating a large amount of latent heating. The relative contribution of each term in the PV Eq. (1) is evaluated. Term one contributes 37% to the production of PV by the change in static stability associated with the latent heating or the surface sensible heating in a well-mixed layer. Term two contributes 22% to the change in PV resulting from horizontal gradients of

diabatic heating within regions of wind covariances (friction). Term three contributes 41% to the production of PV resulting from the tilting of the horizontal component of vorticity into the vertical through horizontal diabatic heating. In this case, the parcel experiences growing stretching and tilting as it ascends in conjunction with the surface trough and convection, which then generates PV.

We follow the PV maximum as it moves over central AL. The parcel enters the PV maximum at 0900 UTC. The parcel's PV increases from 0.2298 PV units to 13.33 PV units from 0800 to 0900 UTC (Table 9). Figure 25 depicts the parcel trajectory, PV maximum and latent heating associated with convection. By 0800 UTC 27 November 1988 the surface trough (confluence zone) is over central AL. The greatest PV increase occurs when the parcel moves through a latent heating maximum (>10 $°Ch^{-1}$) at 0900 UTC. Sensible heating has also been examined, but is negligible. The increase in the low-level PV is directly related to latent heating.

The non-event case has several PV maxima moving out of western OK, across TN and into VA. These maxima weaken as they propagate across the central part of the country. A final PV maximum develops over central MS and propagates over northern AL and into TN (Fig. 20h). Initially, this low-level PV maximum develops rapidly over 6 hours as it moves into central AL. This PV maximum appears to develop in conjunction with convection. A MASS simulation without latent heating release is completed to investigate this PV maximum. Figure 26 depicts the 900 mb PV distribution (without latent heating) over the southeast US. The PV maximum over AR

and MO is not altered in the simulation without latent heating supporting the concept that this PV maximum is maintained by downward transport of stratospheric PV. However, the PV maximum over LA and MS (simulation with latent heating) does not exist indicating that this PV maximum is completely dependent on convection.

In summary, in the non-event case there are numerous PV maxima originating in the lee of the Rocky Mountains and move eastward into VA. The upper-level PV maximum is located in the cold air, north of the left entrance region of the PJ. The distribution of PV resembles a tropopause fold. The PV distribution and upper-level sinking support the concept that the low-level PV originates and is maintained, in large part, by the downward transport of stratosphere PV. As the upper-level jet and weak surface front propagate eastward there is a link between the upper-, mid- and low-level PV. These low-level PV maxima are associated with a weak quasi-stationary front across northern TX, AR and TN and the PJ entrance region. A final PV maximum develops over central MS and moves northeastward to TN. This PV maximum develops from the latent heating associated with convection.

In the event case, the PV maximum over the TX coast (originates from central MX) moves eastward across the Gulf, then northeastward to the Carolina Piedmont. In this case, the PV is maintained in the low-levels and builds vertically. The PV maximum is associated with an area of surface confluence, surface trough and convection. As the low-level PV maximum propagates along the Gulf Coast it is maintained by low-level mechanisms. The upper-level PV is not transported down to the low-levels.

6. Concluding remarks

Observed data and model simulations highlight the differences between the event and non-event cases and the relationship between the upper-level jets and convection. In the event case, a STJ was located over the Gulf Coast region. The upper-level wind was subgeostrophic over the north TX coast, LA and MS indicating acceleration and divergence, which facilitated ascent and deep convection. In the non-event case, there was a strong PJ over northern TX extending northeast. The upper-level wind was supergeostrophic over the TX coast, LA, MS and AL indicating deceleration, convergence and sinking, which inhibited deep convection.

The mid-level jet differed dramatically for these cases. In the event case, a mid-level jet developed over TX and moved eastward across the southern states, from TX to GA. The jet developed rapidly over eastern TX in response to the increased PGF, which developed as the trough propagated eastward over the Midwestern states while the warm Mexican airmass maintained the heights over the Gulf Coast. The environment was predisposed to produce a midlevel jet due to the warm, low-level airmass that moved from the Mexican plateau to the Gulf Coast near the TX/LA border. The mid-level jet right entrance region was closely associated with the surface trough. The thermally direct ageostrophic circulation enhanced ascent over the surface trough, which helped maintain the trough and convection.

In the non-event case, there were two distinct mid-level jets covering two time periods. First, until approximately 0600 UTC 25 January 1990, there was a narrow mid-

level jet that extended across northern LA, MS, AL and TN. The jet was closely associated with the surface front and a narrow band of cold air advection and a strong height gradient. After 0600 UTC 25 January 1990 a strong mid-level jet developed over the Tennessee Valley Region, which was associated with a balanced, QG system.

Observed data and model simulations highlight the surface differences between the event and non-event cases. The event case had strong surface confluence, a meso-trough and strong convection which propagated across the Gulf Coast states. The upper-level divergence and the thermally direct circulation about the mid-level jet removed mass from the air column creating ascent, which helped to maintain the surface trough and convection. In the non-event case, there was a quasi-stationary front and mid-level jet over OK, AR, TN and KY. Also, there was a weak surface frontal system (trough) over the Gulf Coast. There was upper-level convergence over the Gulf Coast, which inhibited the development of deep convection.

There are striking differences between the origins and maintenance of the low-level PV between these two cases. In the non-event case, several PV maxima originated in the lee of the Rocky Mountains and moved eastward to VA. The PV distribution and the upper-level sinking support the concept that the low-level PV originated and is maintained, in large part, by the downward transport of stratospheric PV (tropopause fold). However, the downward transport of PV is not linked to any strong low-level forcing thus there is not any rapid cyclogenesis. Late in the period, another PV maximum developed in association with convection over central MS and it moved northeast to the

Appalachian Mountains. In the event case, the low-level PV maximum over the TX coast propagated eastward across the Gulf then northeast to the Carolina Piedmont. The PV maximum was associated with a surface trough, confluence and convection. As the low-level PV maximum propagated along the Gulf Coast, the PV was primarily maintained in the low-levels by tilting effects associated with diabatic heating.

In summary, the mid-period of the event case had a self-maintaining, low-level circulation that originated over Mexico, propagated across the Gulf Coast and moved over the Carolina Piedmont at the time of the tornado outbreak. This circulation moved across the Gulf Coast States as a coherent feature and was characterized by a surface trough, low-level PV maximum, mid-level jet, a warm Mexican airmass and upper-level divergence associated with the STJ. In the non-event case, these features were absent along the Gulf Coast states.

Acknowledgements. I would like to thank the Air Force Institute of Technology for the opportunity to pursue my advanced degree. The authors wish to thank Drs Robert Rozumalski and Kenneth Waight III of MESO Inc. for access to and help with the MASS model.

7. References

Daley, R., 1991: *Atmospheric Data Analysis*, Cambridge University Press, 457 pp.

Danielsen, E., 1968: Stratospheric-tropospheric exchange based on radioactivity, ozone, and potential vorticity. *J. Atmos. Sci.*, **25**, 502-518.

Egentowich, J. M., M. L. Kaplan, Y.-L. Lin and A. J. Riordan, 1999a: Mesoscale simulations of dynamical factors discriminating between a tornado outbreak and non-event over the southeast US part I: 84 - 48 hour precursors. Submitted to *Weather and Forecasting*.

Fawbush, E. J. and R. C. Miller, 1954: The types of airmasses in which North American tornadoes form. *Bull. Amer. Meteor. Soc.*, **35**, 154-165.

Gidel L. T., and M. A. Shapiro, 1979: The role of clear air turbulence in the production of potential vorticity in the vicinity of upper tropospheric jet stream-frontal systems. *J. Atmos. Sci.*, **36**, 2125-2138.

Gonski, R. F., B. P. Woods, and W. D. Korotky, 1989: The Raleigh tornado - 28 November 1988: An operational perspective. Preprints, *12th Conf. on Weather Analysis and Forecasting*, Monterey, CA Amer. Meteor. Soc., 173-178.

Gyakum J. R., Y-H Kuo, Z. Guo, and Y-R Guo, 1995: A case of rapid continental mesoscale cyclogenesis. Part II: Model and observational diagnosis. *Mon. Wea. Rev.*, **123**, 998-1024.

Kalnay, E., M. Kanamistu, R. Kistler, W. Collins, D. Deaven, L. Gandin, M. Iredell, S. Saha, G. White, J. Woollen, Y. Zhu, M. Chelliah, W. Ebisuzaki, W. Higgins, J. Janowiak, K. C. Mo, C. Ropelewski, J. Wang, A. Leetmaa, R. Reynolds, R. Jenne, and D. Joseph, 1996; The NMC/NCAR 40-year reanalysis project. *Bull. Amer. Meteor. Soc.*, **77**, No. 3, 437-471.

Kaplan, M. L., and D. A. Paine, 1977: The observed divergence of the horizontal velocity field and pressure gradient force at the mesoscale. It's implications for the parameterization of three-dimensional momentum transport in synoptic-scale numerical models. *Beitr. Phy. Atmos.*, **50**, 321-330.

Kaplan, M. L., V. M. Karyampudi, 1992: Meso-beta numerical simulation of terrain drag-induced along stream circulations. Part I: Midtropospheric frontogenesis. *Met. and Atm. Physics*, **49**, 133-156.

Kaplan, M. L., V. M. Karyampudi, 1992: Meso-beta numerical simulation of terrain drag-induced along stream circulations. Part II: Concentration of potential vorticity within dryline bulges. *Meteor. Atmos. Phys.*, **49**, 157-185.

Kaplan, M. L., J. W. Zack, V. C. Wong, and J. J. Tuccillo, 1982a: Initial results from a mesoscale atmospheric simulation system and comparisons with the AVE-SESAME I data set. *Mon. Wea. Rev.*, **110**, 1564-1590.

Kaplan, M. L., Y-L. Lin, D. W. Hamilton, and Rozumalski, R. A., 1997: The numerical simulation of an unbalanced jetlet and its role in the Palm Sunday 1994 tornado outbreak in Alabama and Georgia. *Mon. Wea. Rev.*, **126**, 2133-2165.

Keyser, D., and M. A. Shapiro, 1986: A review of the structure and dynamics of upper-level frontal zones. *Mon. Wea. Rev.*, **114**, 452-499.

Lanicci, J. M. and T. T. Warner, 1991a: A synoptic climatology of the elevated mixed-layer inversion over the southern Great Plains in Spring. Part 1: Structure, dynamics, and seasonal evolution. *Wea. & Forecasting*, **6**, 181-197.

Lanicci, J. M. and T. T. Warner, 1991b: A synoptic climatology of the elevated mixed-layer inversion over the southern Great Plains in Spring. Part 2: the life cycle of the lid. *Wea. & Forecasting*, **6**, 198-213.

Lanicci, J. M. and T. T. Warner, 1991c: A synoptic climatology of the elevated mixed-layer inversion over the southern Great Plains in Spring. Part 3: Relationship to severe-storms climatology. *Wea. & Forecasting*, **6**, 214-226.

Lin, Y.-L., R. D. Farley, and H. D. Orville, 1983: Bulk parameterization of the snow field in a cloud model, *J. Clim. Appl. Meteorol.*, **22**, 1065-1092.

Mahrt, L., and H. Pan, 1984: A two-layer model of soil hydrology. *Bound.-Layer Meteor.*, **29**, 1-20.

MESO, 1995: MASS Version 5.8 Reference Manual, MESO, Inc., Troy, NY, 119 pp.

NOAA, 1988: Storm data, **30, 11,** 72 pp.

Noilhan, J., and S. Planton, 1989: A simple parameterization of land surface processes for meteorological models. *Mon. Wea. Rev.*, **117**, 536-549.

Rozumalski, R. A., 1997: The role of jet streak regeneration forced by a deepening continental planetary boundary layer in the explosive surface cyclogenesis of 28

March 1984. Ph. D. Thesis., North Carolina State University, 360 pp. (Available from the corresponding author).

Uccellini L. W. and D. Johnson 1979: The coupling of upper and lower tropospheric jet streaks and implication for the development of severe convective storms. *Mon. Wea. Rev.*, **107**, 682-703.

Uccellini L. W., and P. J. Kocin, 1987: The interaction of jet streak circulations during heavy snow events along the East Coast of the United States. *Wea. & Forecasting*, **1**, 289-308.

Uccellini L. W., P. J. Kocin, R. A. Petersen, C. H. Wash and K. F. Brill, 1984: The President's day cyclone of 18-19 February 1979: Synoptic overview and analysis of the subtropical jet streak influencing the pre-cyclogenetic period. *Mon. Wea. Rev.*, **112**, 31-55.

Zang, D. L., and R. A. Anthes, 1982: A high resolution model of the planetary boundary layer-sensitivity tests and comparisons with SESAME-79 data. *J. Appl. Meteor.*, **21**, 1594-1609.

Zehnder, J. A., and D. Keyser, 1991: The influence or interior gradients of potential vorticity on rapid cyclogenesis. *Tellus*, **43A**, 198-212.

Table 1. Forward trajectory initiated at 1600 UTC 26 November 1988 and ending at 2000 UTC 26 November 1988. Trajectory data is derived from 24 km full physics MASS model run. The following abbreviations are defined: Latitude (LAT), Longitude (LON), Pressure (PRS), Total Wind (V_t), Divergence (DIV), and Omega (OMG).

Time UTC	LAT (°N)	LON (°W)	PRS (mb)	V_{total} (ms^{-1}) spd/dir	DIV ($x10^{-5}$ s^{-1})	OMG ($mcbrs^{-1}$)
26/1600	30.4	95.4	410	45.1/251	2.86	4.18
26/1700	30.9	93.8	416	45.2/247	4.59	-3.182
26/1800	31.5	92.2	395	45.4/245	10.9	-17.6
26/1900	32.2	90.6	381	46.5/243	3.25	-0.96
26/2000	32.8	99.6	387	45.4/244	-0.93	5.08

Table 2. Same as table 1 except trajectory initiated at 0400 UTC 24 January 1990 and ending at 0800 UTC 24 January 1990.

Time UTC	LAT (°N)	LON (°W)	PRS (mb)	V_{total} (ms^{-1}) spd/dir	DIV ($x10^{-5}$ s^{-1})	OMG ($mcbrs^{-1}$)
24/0400	30.4	94.5	412	34/253	-4.432	-1.357
24/0500	30.7	93.2	407	35/253	-4.191	-1.591
24/0600	31.0	92.0	400	35/253	-2.685	-1.069
24/0700	31.3	90.7	399	36/254	-2.178	-0.136
24/0800	31.6	89.4	393	36/255	-1.070	-1.877

Table 3. Forward trajectory initiated at 1200 UTC 26 November 1988, passing through the mid-level jetogenesis, and ending at 2100 UTC 26 November 1988. Trajectory data is derived from 24 km full physics MASS model run. The following abbreviations are defined: Latitude (LAT), Longitude (LON), Pressure (PRS), Coriolis force vector (CO), Pressure gradient force vector (PGF), Magnitude difference between PGF and CO (PGFCO), Total Wind (V_t), and Omega (OMG).

Time UTC	LAT (°N)	LON (°W)	PRS (mb)	CO 10^{-3} ms^{-2} spd/dir	PGF 10^{-3} ms^{-2} spd/dir	PGFCO 10^{-3} ms^{-2}	V_{total} (ms^{-1}) spd/dir	OMG mcbr s^{-1}
26/1200	27.5	98	671	1.7/320	1.8/140	0.1	25/230	0.25
26/1300	28.5	97	671	1.93/324	1.73/162	0.2	28/234	-2.47
26/1400	28.8	96	671	2.1/328	2.4/153	0.3	30/238	-.1
26/1500	29.1	95	666	2.23/328	2.39/166	0.16	31/238	-6.28
26/1600	29.6	94.2	653	2.41/325	3.36/166	0.95	33/235	-1.31
26/1700	30.3	93.2	634	2.68/323	3.81/155	1.13	36/233	-5.32
26/1800	31.1	92	595	2.83/321	4.54/189	1.71	37/231	-33.6
26/1900	31.8	91	571	2.92/320	3.3/143	0.38	37/230	-3.19
26/2000	32.6	89.8	568	3.01/318	3.54/151	0.53	38/228	0.035
26/2100	33.5	88.7	550	3.2/322	3.51/143	0.31	40/227	-15.66

Table 4. Same as Table 3 except trajectory is initiated at 0100 UTC 24 January 1990 and ending 0900 UTC 24 January 1990.

Time UTC	LAT (°N)	LON (°W)	PRS (mb)	CO 10^{-3} ms^{-2} spd/dir	PGF 10^{-3} ms^{-2} spd/dir	PGFCO 10^{-3} ms^{-2}	V_{total} (ms^{-1}) spd/dir	OMG mcbr s^{-1}
24/0100	29.1	95.4	614	1.2/332	1.3/165	0.1	17.4/242	0.124
24/0200	29.4	94.8	612	1.3/333	1.5/171	0.2	18.7/242	-0.926
24/0300	29.7	94.1	610	1.4/332	1.5149	0.1	20.4/242	-0.832
24/0400	30.0	93.4	606	1.6/333	1.4/190	-0.2	21.7/243	-1.026
24/0500	30.3	92.7	602	1.7/334	1.5/182	-0.2	22.6/244	-1.565
24/0600	30.6	91.9	594	1.7/335	1.9/175	0.2	23.4/245	-1.975
24/0700	31	91.1	587	1.8/335	1.9/168	0.1	23.8/245	-2.768
24/0800	31.3	90.3	572	1.8/335	1.7/162	-0.1	23.9/245	-4.847
24/0900	31.6	89.4	557	1.9/335	2.0/137	0.1	24.3/245	-10.23

Table 5. Same as Table 3 except the data is derived from 24 km MASS simulation without latent heating.

Time UTC	LAT (°N)	LON (°W)	PRS (mb)	CO 10^{-3} ms^{-2} spd/dir	PGF 10^{-3} ms^{-2} spd/dir	PGFCO 10^{-3} ms^{-2}	V_{total} (ms^{-1}) spd/dir	OMG mcbr s^{-1}
26/1300	27.3	97.3	637	1.6/319	1.7/187	0.1	23/229	0.457
26/1400	27.8	96.6	635	1.8/322	2.0/171	0.2	27/232	-3.842-
26/1500	28.4	95.7	620	2.1/232	2.1/183	0.0	29/232	-3.175
26/1600	29.0	94.8	613	2.3/324	2.3/177	0.0	33/234	-0.368
26/1700	29.6	93.8	609	2.5/325	2.3/148	-0.2	35/235	-3.645
26/1800	30.3	92.7	600	2.7/324	2.8/153	0.1	36/234	-0.786
26/1900	31.0	91.6	592	2.8/323	3.0/154	0.2	37/233	-3.377
26/2000	31.8	90.4	584	2.9/323	3.0/142	0.1	38/233	-2.153
26/2100	34.5	89.3	583	2.9/323	3.0/139	0.1	38/234	-0.479

Table 6. Same as Table 4 except the data is derived from 24 km MASS simulation without latent heating.

Time UTC	LAT (°N)	LON (°W)	PRS (mb)	CO 10^{-3} ms^{-2} spd/dir	PGF 10^{-3} ms^{-2} spd/dir	PGFCO 10^{-3} ms^{-2}	V_{total} (ms^{-1}) spd/dir	OMG mcbr s^{-1}
24/0100	29.4	96.3	610	1.4/339	1.3/160	0.1	19/249	-0.358
24/0200	29.6	95.6	609	1.4/343	1.6/158	0.2	20/253	0.482
24/0300	29.8	94.9	607	1.5/344	1.5/159	0.0	20/254	-1.358
24/0400	30.0	94.2	603	1.5/344	1.5171	0.0	20/254	-0.421
24/0500	30.1	93.4	602	1.5/344	1.5/172	0.0	20/254	0.076
24/0600	30.3	92.7	600	1.5/345	1.6/167	0.1	20/255	-1.426
24/0700	30.5	92	594	1.5/346	1.5/166	0.0	20256	-2.142
24/0800	30.6	91.3	587	1.5/345	1.4/135	-0.1	20/255	-1.333
24/0900	30.8	90.6	583	1.4/343	1.3/151	-0.1	19/253	-1.062

Table 7. Trajectory from 0100 UTC 24 January 1990 to 0500 UTC 24 January 1990. Trajectory was derived from hourly data of a 24 km MASS simulation. The following abbreviations are defined: Latitude (LAT), Longitude (LON), Pressure (PRS), Wind Speed & Direction (V_{total}), and Potential Vorticity (PV).

Time (UTC)	LAT (°N)	LON (°W)	PRS (mb)	OMG mcbr s^{-1}	V_{total} (ms^{-1}) spd/dir	PV (PV units)
0100	36.8	97.8	364	0.252	273/41.4	0.5
0200	37	94.5	372	11.39	272/41.1	0.66
0300	36.8	94.5	397	10.98	269/40.4	1.45
0400	36.8	92.9	428	6.02	268/40.1	0.74
0500	36.9	91.3	439	0.265	265/39.7	0.42

Table 8. Trajectory from 2200 UTC 26 November 1988 to 0300 UTC 27 November 1988. Trajectory was derived from hourly data of a 24 km MASS simulation. The following abbreviations are defined: Latitude (LAT), Longitude (LON), Pressure (PRS), Temperature (TMP), and Potential Vorticity (PV).

Time (UTC)	LAT (°N)	LON (°W)	PRS (mb)	TMP (°C)	PV (PV units)
26/2200	29.66	92.36	894.3	17.79	1.548
26/2300	29.37	91.71	895.2	17.42	1.470
27/0000	30.25	91.25	899.4	17.24	2.138
27/0100	30.58	90.72	905.4	17.41	2.074
27/0200	30.94	90.20	907.3	17.06	2.282
27/0300	31.35	89.69	905.5	16.42	2.353

Table 9. Trajectory from 0600 UTC 27 November 1988 to 1000 UTC 27 November 1988. Trajectory was derived from hourly data of a 24 km MASS simulation. The following abbreviations are defined: Latitude (LAT), Longitude (LON), Pressure (PRS), Temperature (TMP), and Potential Vorticity (PV).

Time (UTC)	LAT (°N)	LON (°W)	PRS (mb)	TMP (°C)	PV (PV units)
27/0600	31.29	88.01	944.9	19.16	0.06716
27/0700	31.79	87.62	939.9	18.78	0.1112
27/0800	32.29	87.20	939.7	18.78	0.2298
27/0900	32.76	86.75	902.8	15.22	13.33
27/1000	33.17	86.25	846.2	12.37	3.329

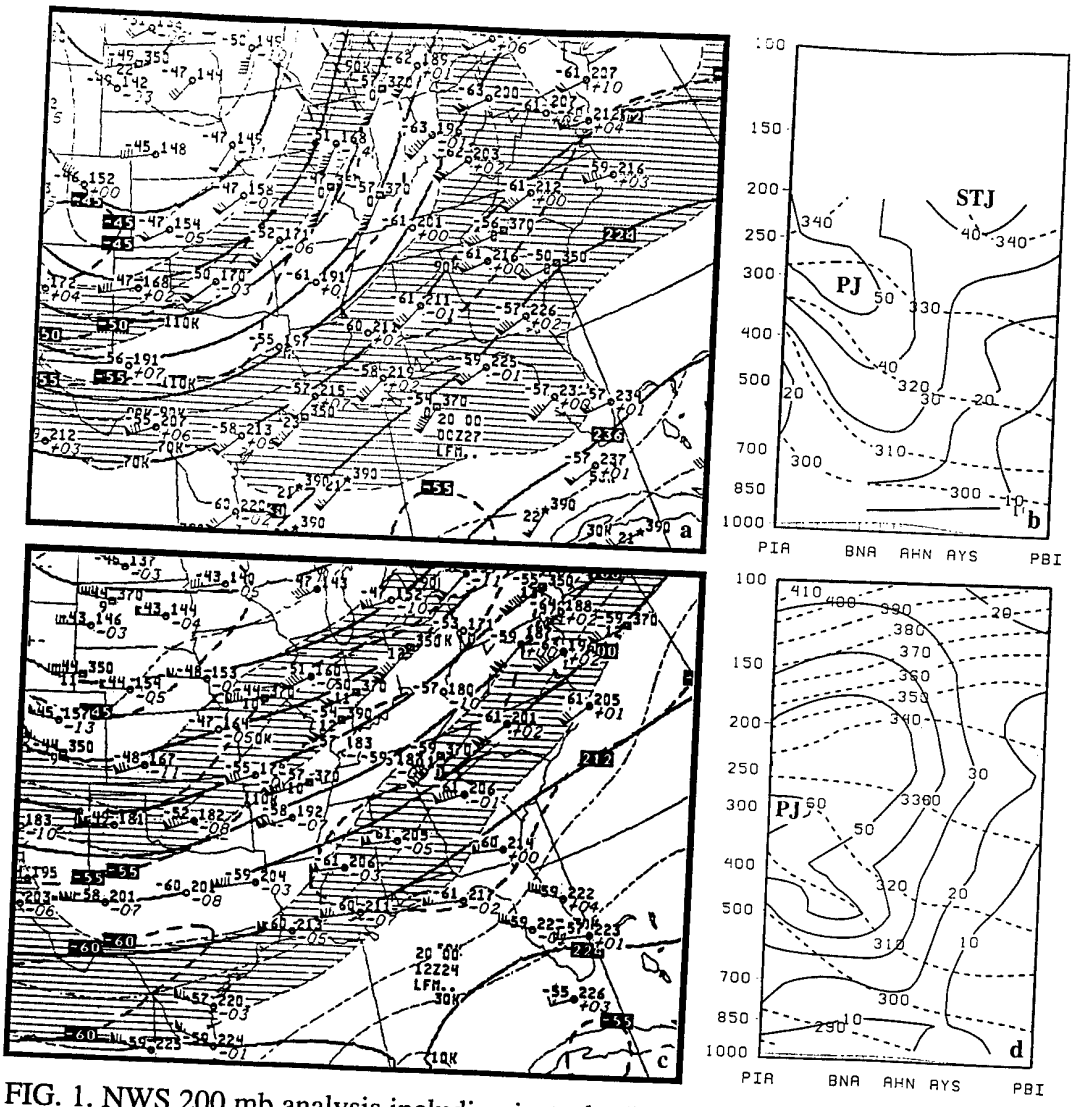

FIG. 1. NWS 200 mb analysis including isotachs (knots) and vectors, temperature (C) and height (dm) and observation derived cross section from Peoria, IL (PIA) to West Palm Beach, FL (PBI), isotachs (solid line, ms^{-1}) and θ (dashed line, K) valid at (a & b) 0000 UTC 27 November 1988 and (c & d) 1200 UTC 24 January 1990.

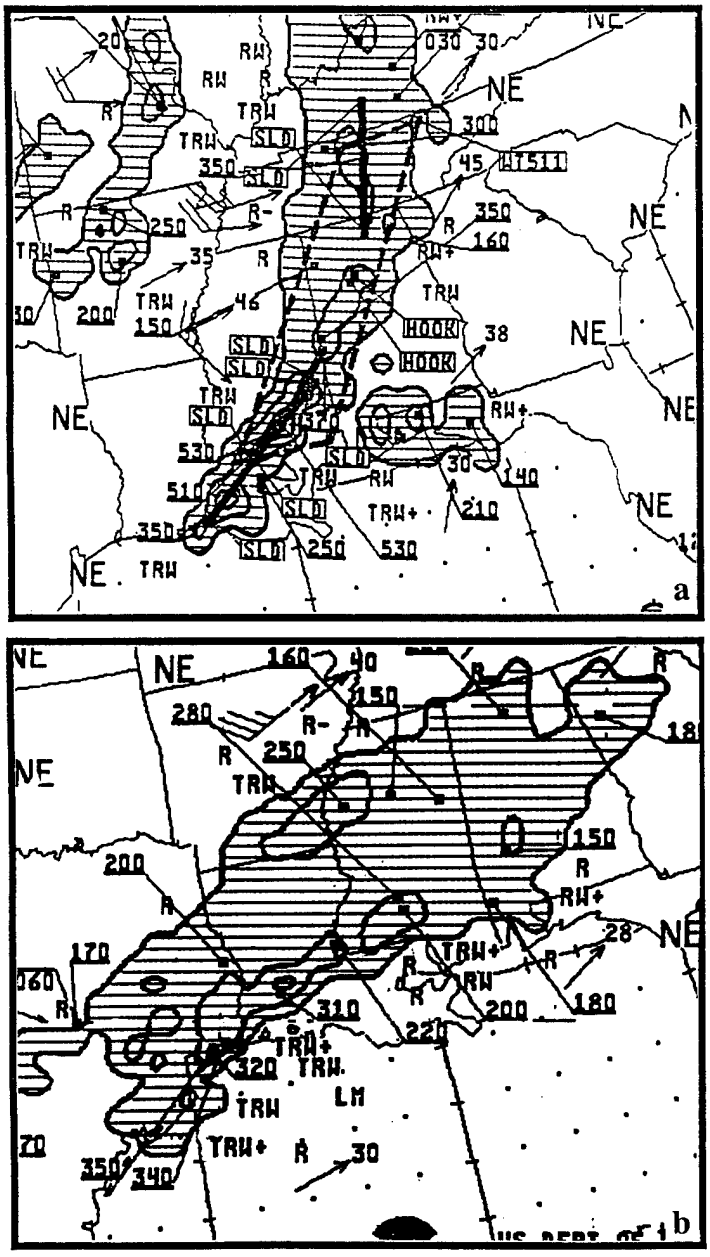

FIG. 2. NWS radar summaries valid at (a) 0035 UTC 27 November 1988 and (b) 1235 UTC 24 January 1990.

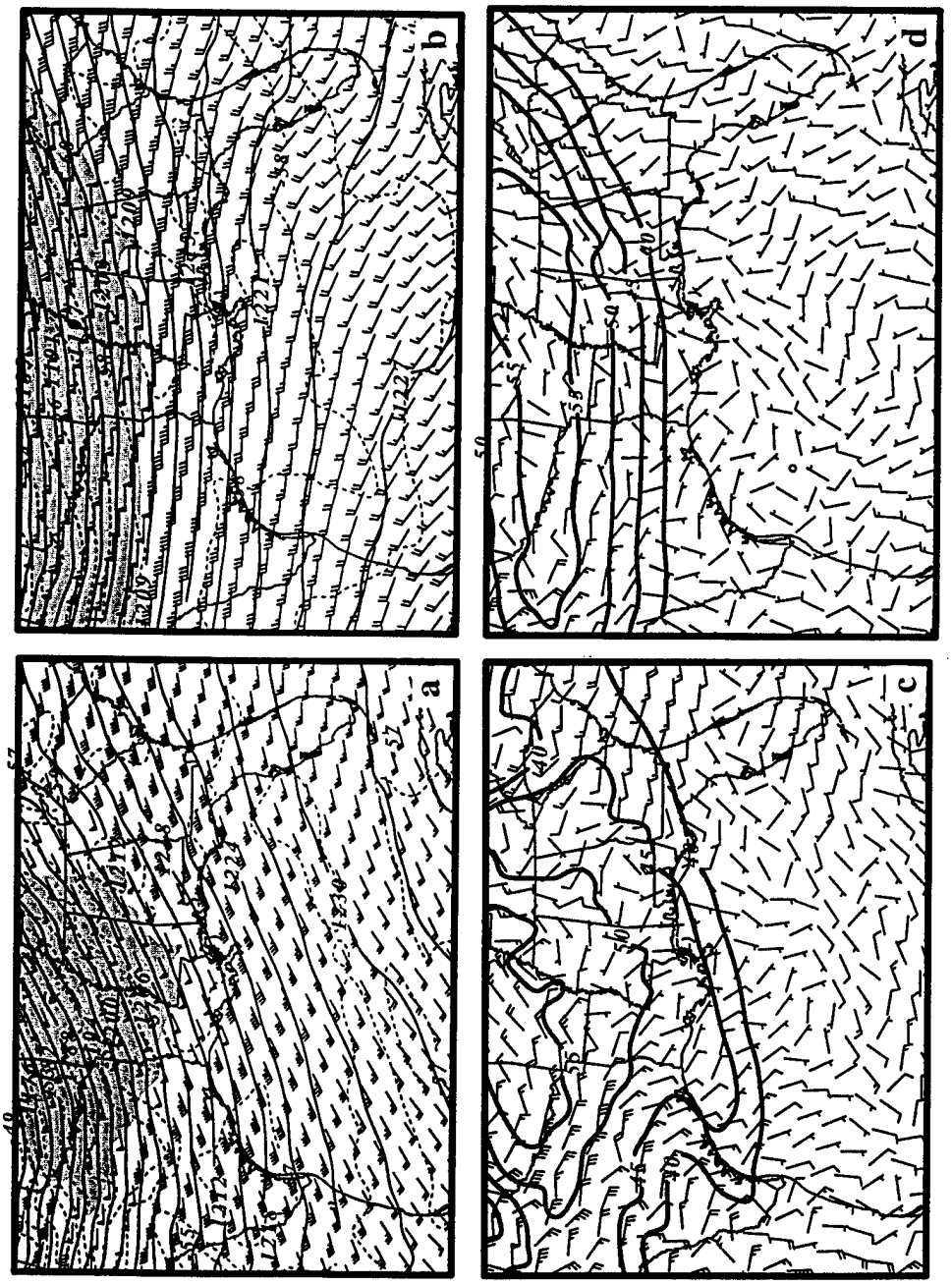

FIG. 3. MASS simulated, 24 km mesh, 200 mb (a) wind vectors and isotachs (shaded at intervals of 5 for speeds greater than 50), temperature (dashed lines, C), and height (solid lines, dm) and (c) isotachs (contoured at intervals of 5 for speeds greater than 40, ms^{-1}) and ageostrophic wind vectors valid at 0000 UTC 27 November 1988. (b) and (d) Are the same as (a) and (b) but valid at 1200 UTC 24 January 1990.

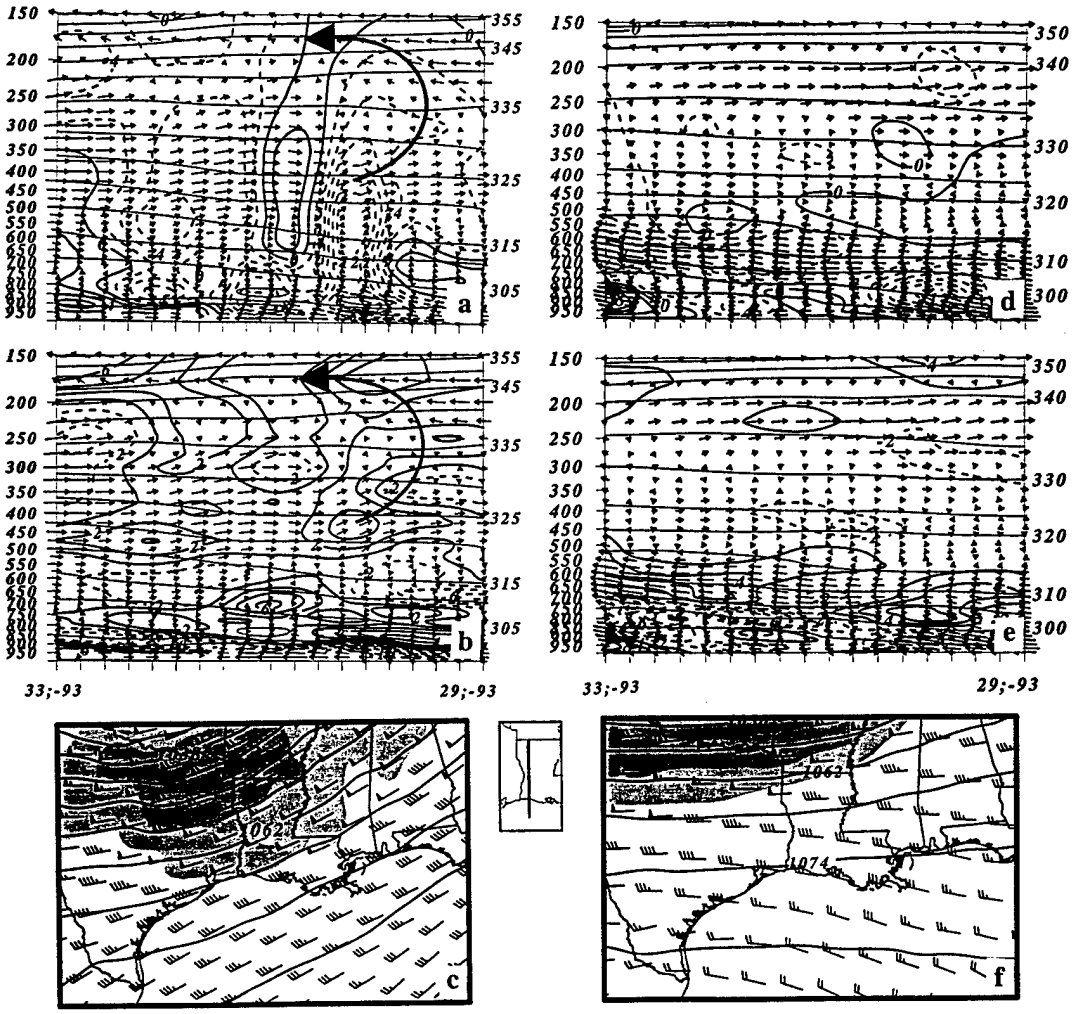

FIG. 4. MASS simulated, 24 km mesh, cross section extending from 33N, 93W to 29N, 93W. Thick arrows represent the structure of the transverse ageostrophic circulations. Including ageostrophic wind vectors, θ (thin solid lines, K), (a) vertical velocity (contoured every 2 μbs^{-1}, solid lines indicate descent and dashed lines indicate ascent) (b) divergence (contoured every $2x10^{-5}$ s^{-1}, solid lines positive values and dashed lines negative values) and (c) 250 mb wind isotach (shaded at intervals of 10 for speeds greater than 50), and vectors, and height (solid lines, dm) valid at 1500 UTC 26 November 1988. (d), (e) and (f) Are the same as (a), (b) and (c) but valid at 0300 UTC 24 January 1990.

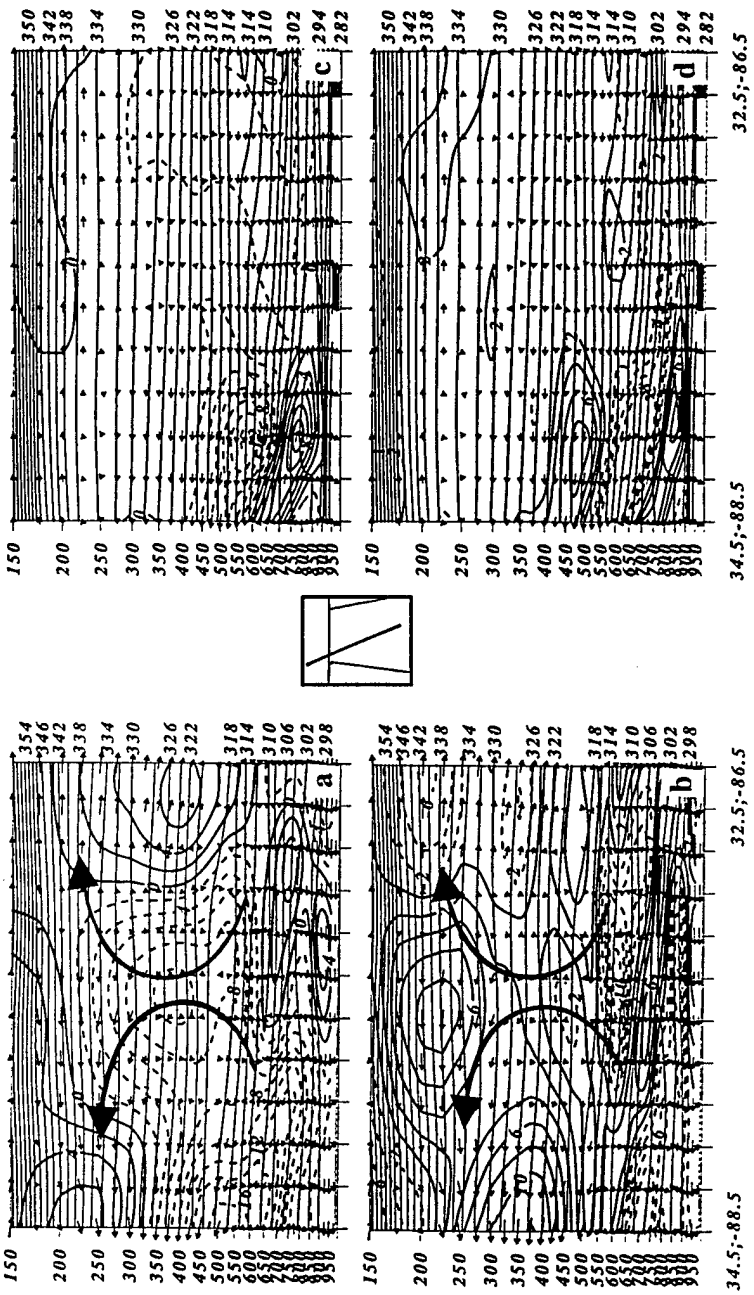

FIG. 5. MASS simulated, 24 km mesh, cross section extending from 34.5N, 88.5W to 32.5N, 86.5W. Thick arrows represent the structure of the transverse ageostrophic circulations. Including ageostrophic wind vectors, θ (thin solid lines, K), (a) vertical velocity (contoured every 2 μbs^{-1}, solid lines indicate descent and dashed lines indicate ascent) and (b) divergence (contoured every $2x10^{-5}$ s^{-1}, solid lines positive values and dashed lines negative values) valid at 0000 UTC 27 November 1988. (c) and (d) Are the same as (a) and (b) but valid at 1200 UTC 24 January 1990.

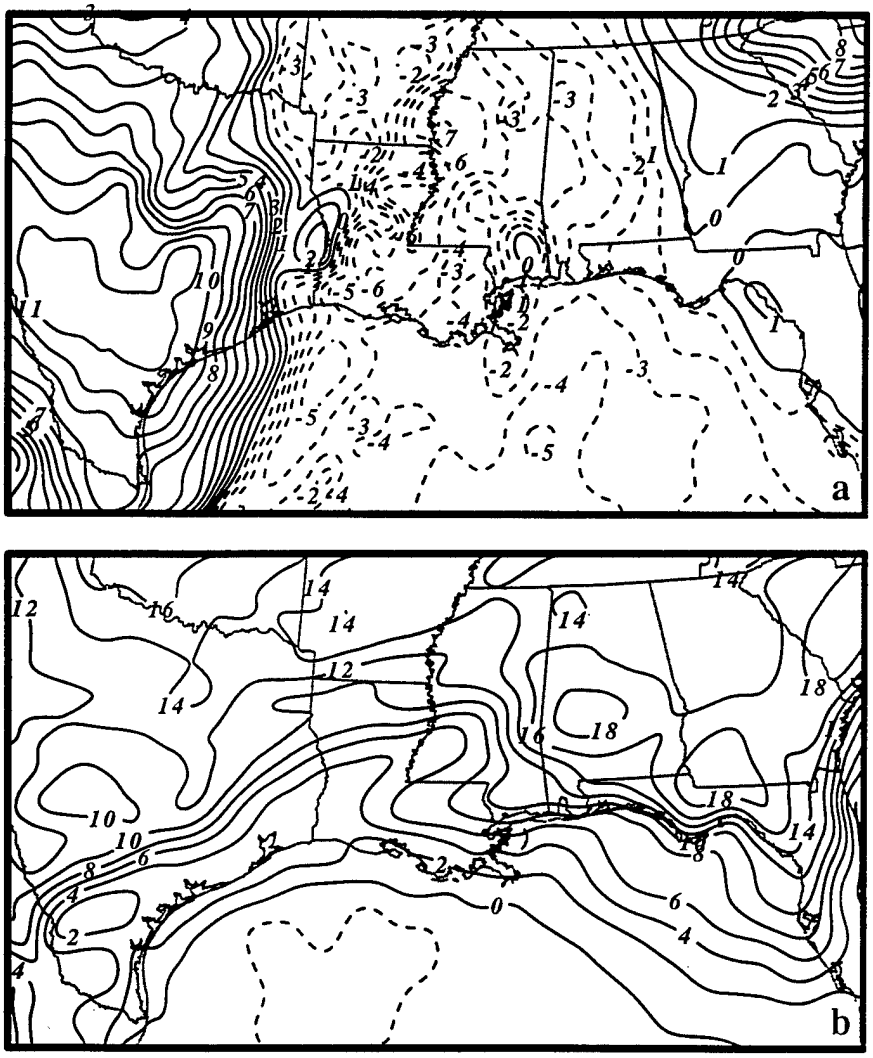

FIG. 6. MASS simulated, 24 km mesh, Lifted Index values (solid lines denote positive values and dashed lines denote negative values) valid at (a) 1800 UTC 26 November 1988 and (b) 0600 UTC 24 January 1990.

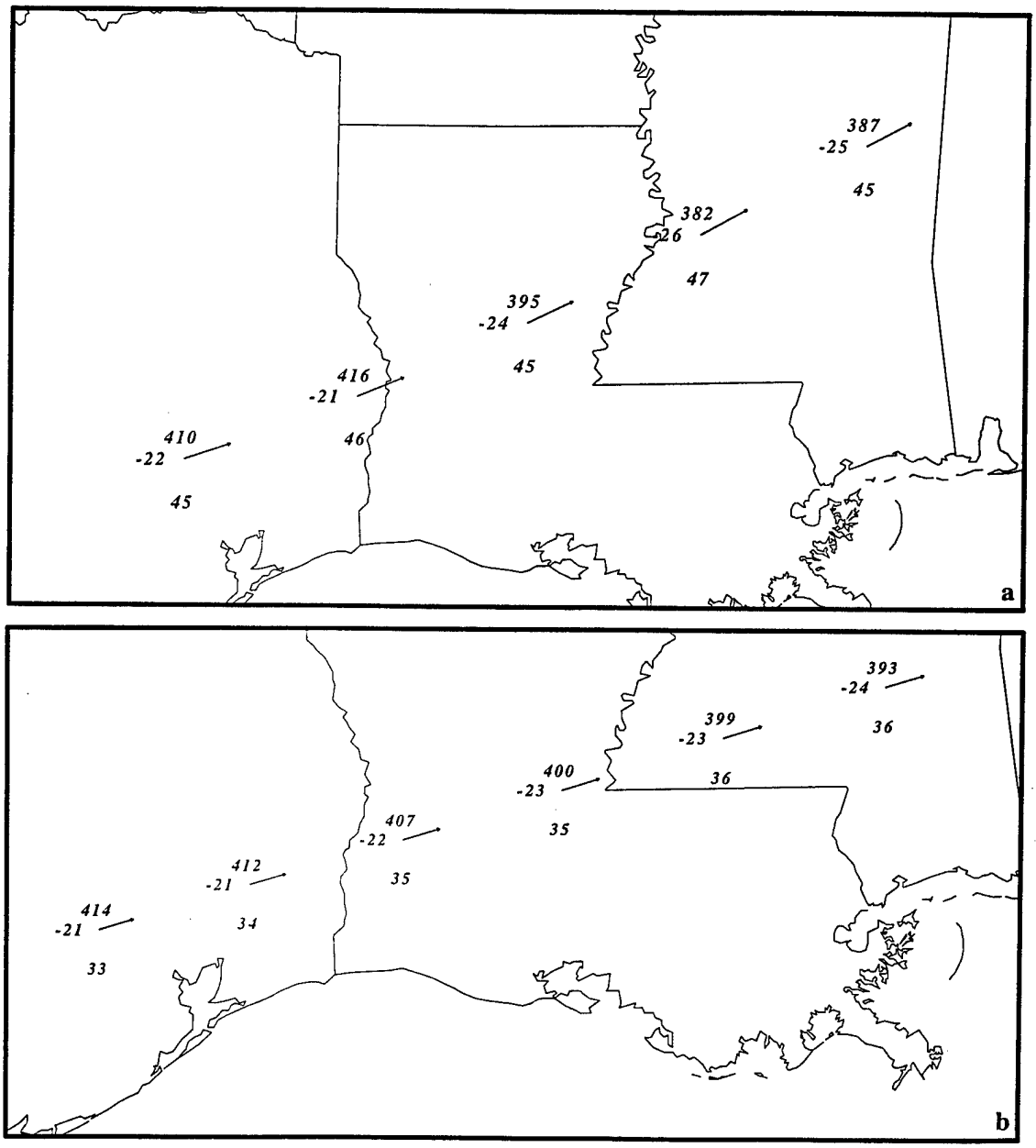

FIG. 7. Trajectories constructed from the 24 km MASS simulations. Station plots contain pressure (mb), temperature (C), and total wind speed (ms^{-1}). Displayed wind vectors depict total wind. (a) Parcels initialized at 1600 UTC and ended 2000 UTC 26 November 1988. (b) Parcels initialized at 0400 UTC and ended 0800 UTC 24 January 1990.

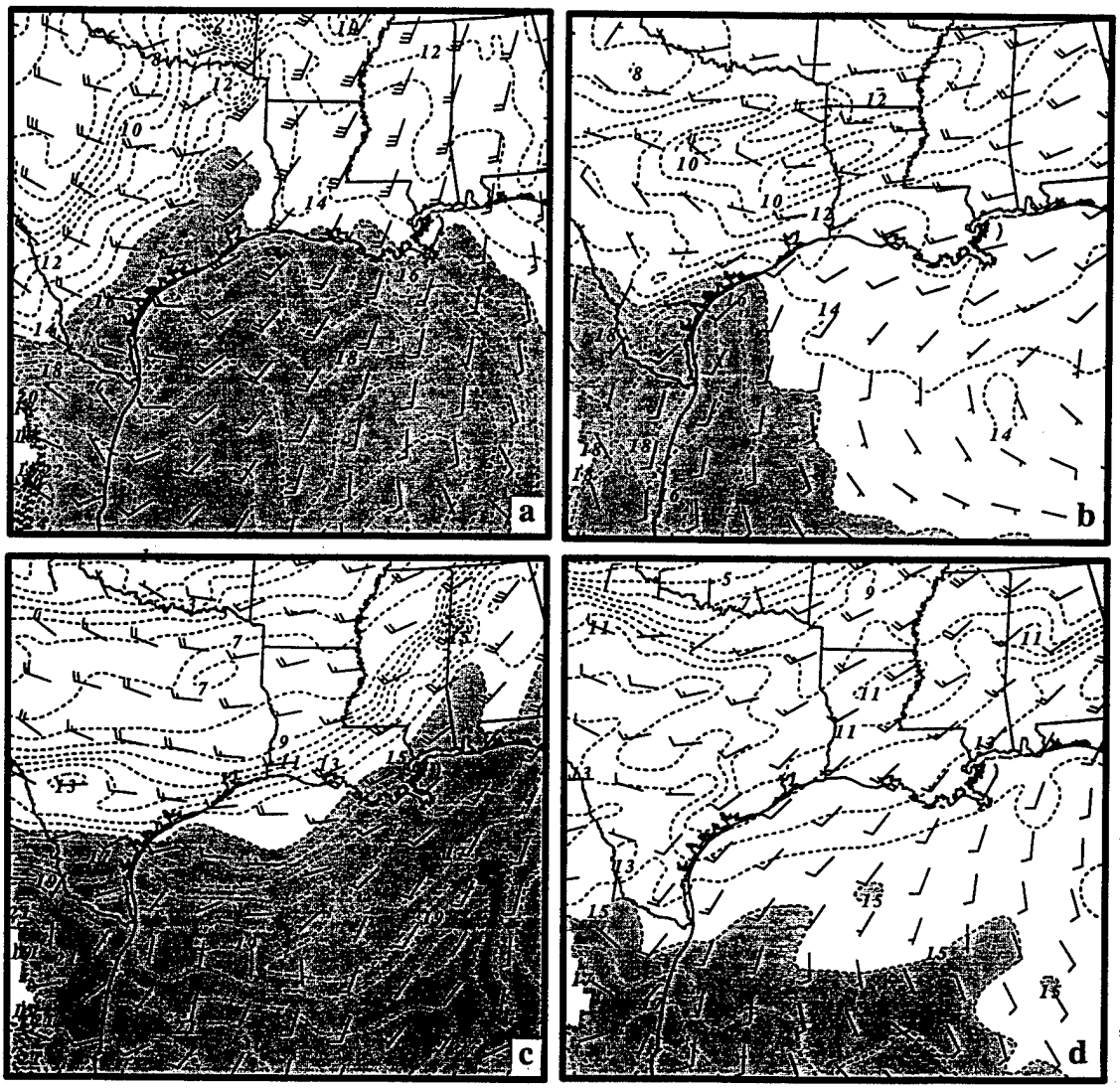

FIG. 8. MASS simulated, 24 km mesh, 850 mb wind vectors (ms^{-1}) and temperature (dashed lines, (C) and shaded greater than 15) valid at (a) 1200 UTC 26 November 1988, (b) 0000 UTC 24 January 1990, (c) 0600 UTC 27 November 1988 and (d) 0000 UTC 25 January 1990.

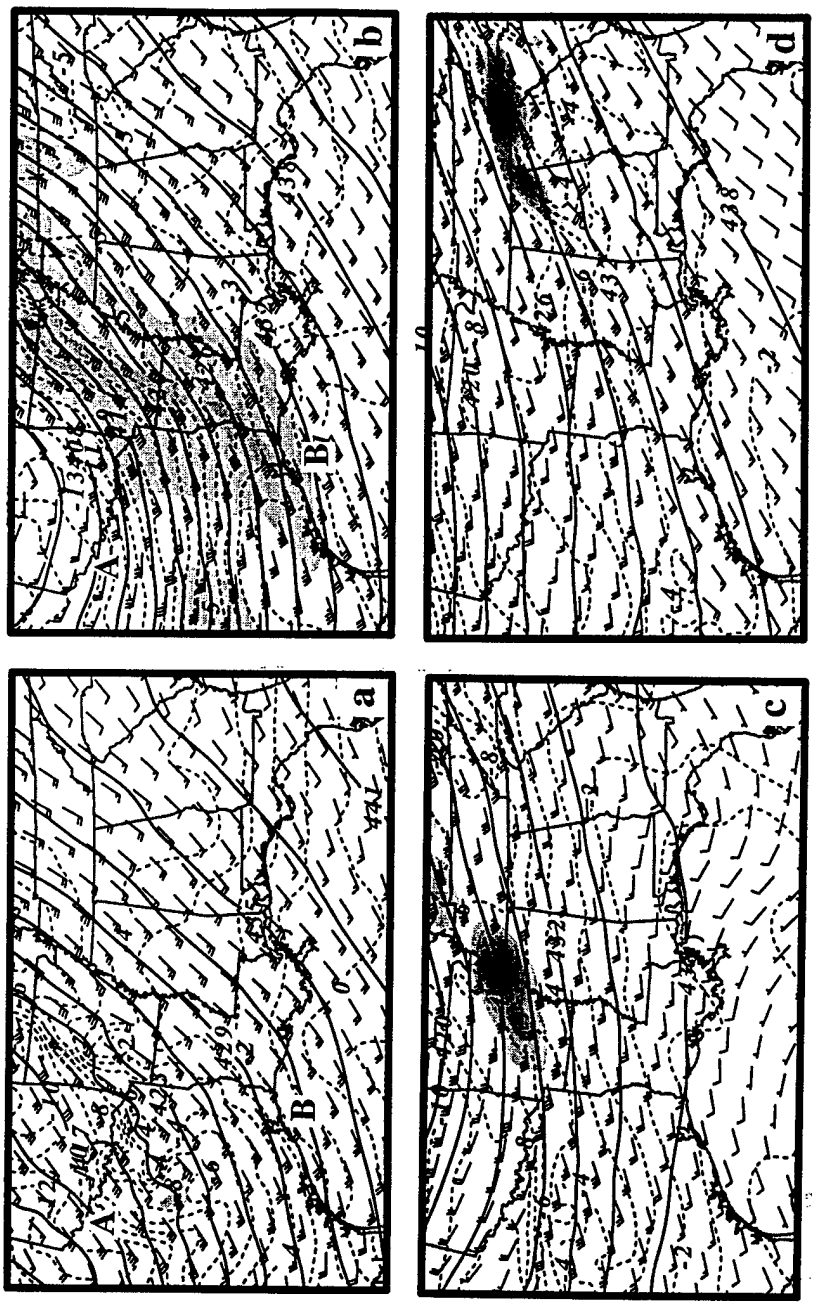

FIG. 9. MASS simulated, 24 km mesh, 600 mb, wind vectors and isotachs (shaded at intervals of 5 for speeds greater than 35), temperature (dashed lines, C), and height (solid lines, dm) valid at (a) 0900 UTC, (b) 1800 UTC 26 November 1988, (c) 21 UTC 23 and (d) 1800 UTC 24 January 1990. A denotes an area northwest of the jetogenesis area and B denotes an area southeast of the jetogenesis area.

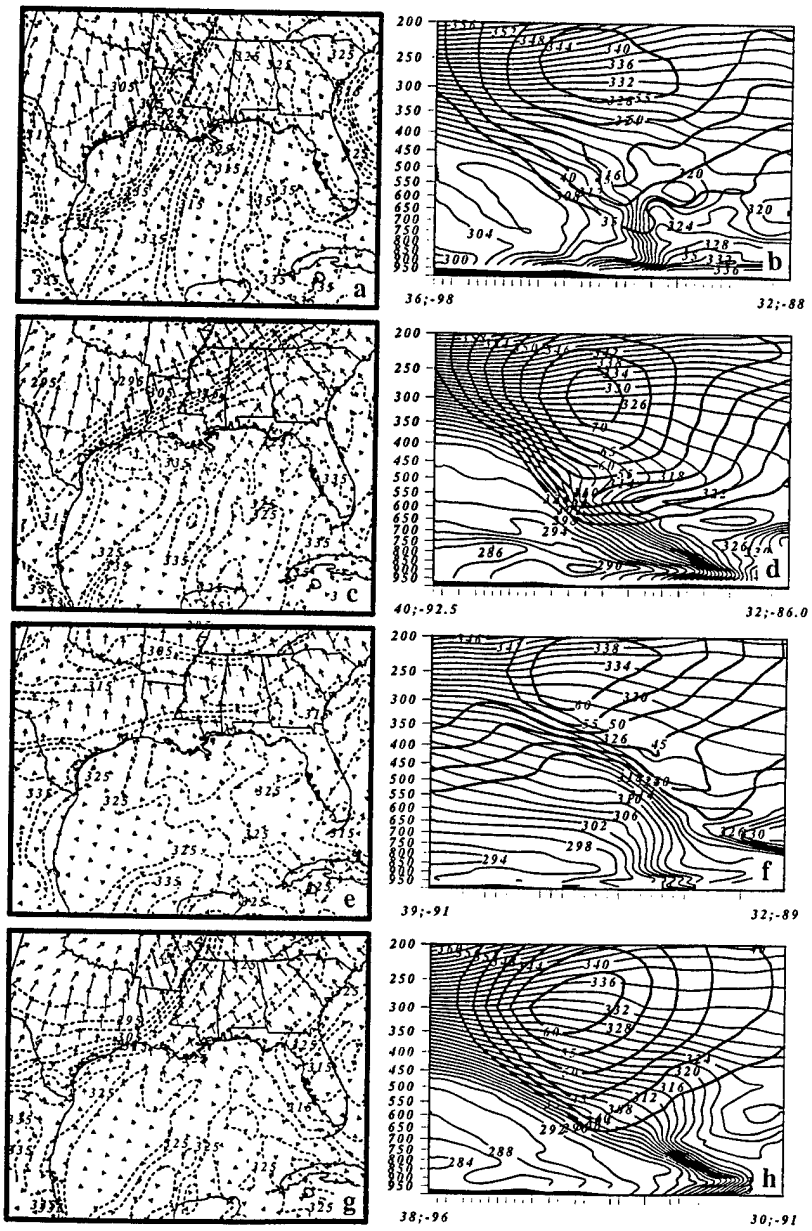

FIG. 10. MASS simulated, 24 km mesh, 600 mb, wind isotachs (shaded at intervals of 5 for speeds greater than 35 ms^{-1}), θ_e (dashed lines, K), and pressure gradient force vectors (ms^{-2}). Cross sections include θ_e (thin solid lines, K) and isotachs (thick solid lines, contoured at intervals of 5 for speeds greater than 35 ms^{-1}). Valid at (a) and (b) 1800 UTC 26, (c) and (d) 1800 UTC 27 November 1988, (e) and (f) 0900 UTC 24 and (g) and (h) 0900 UTC 25 January 1990.

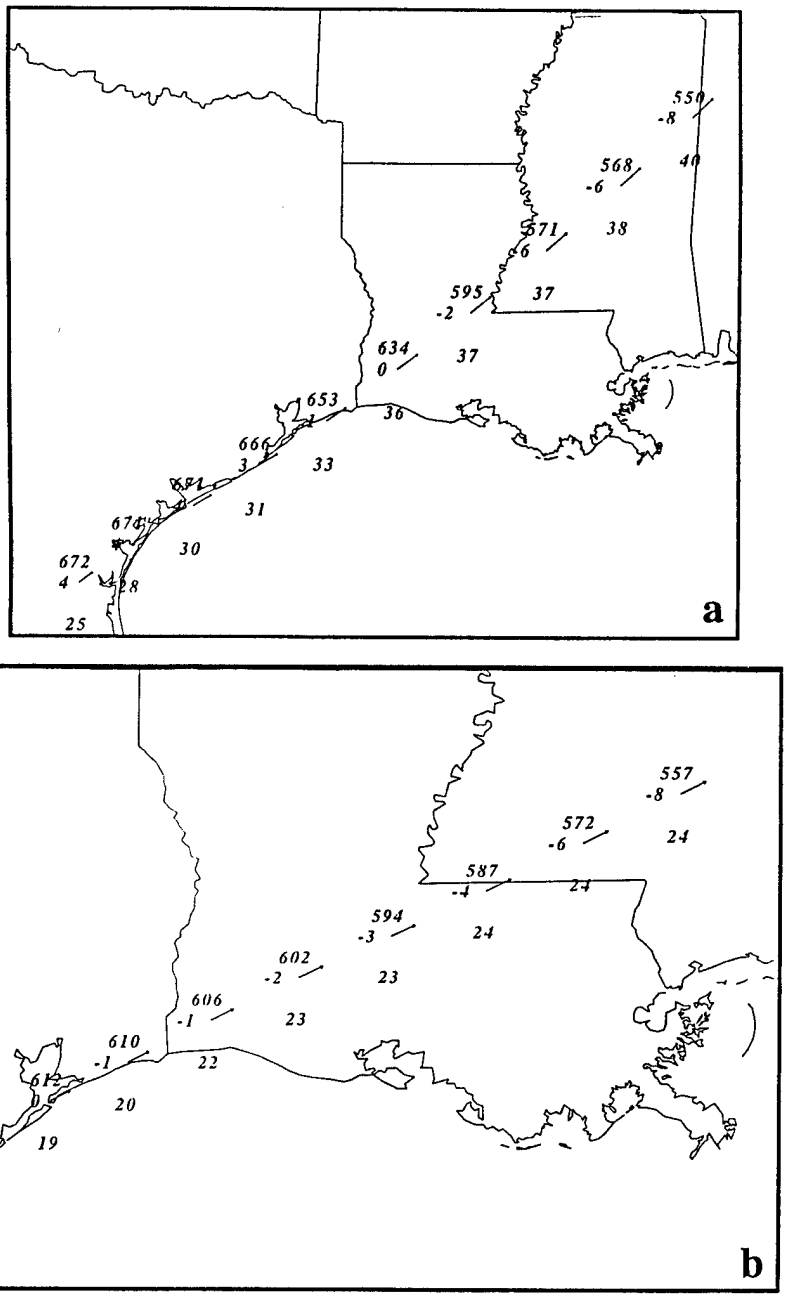

FIG. 11. Trajectories constructed from the 24 km MASS simulations. Station plots include pressure (mb), temperature (C), and total wind speed (ms^{-1}). Displayed wind vectors depict total wind. (a) Parcels initialized at 1200 UTC and ended at 2100 UTC 26 November 1988. (b) Parcels initialized at 0100 UTC and ended at 0900 UTC 24 January 1990.

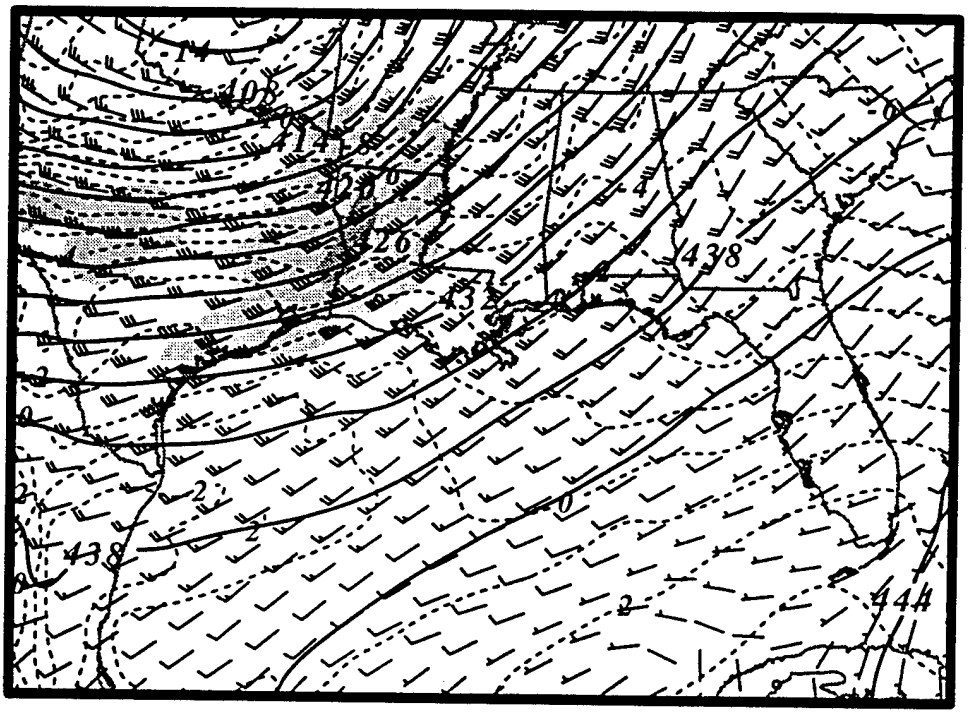

FIG. 12. MASS simulation without latent heating, 24 km mesh, 600 mb, wind vectors and isotachs (shaded at intervals of 5 for speeds greater than 35), temperature (dashed lines, C), and height (solid lines, dm) valid at 1800 UTC 26 November 1988.

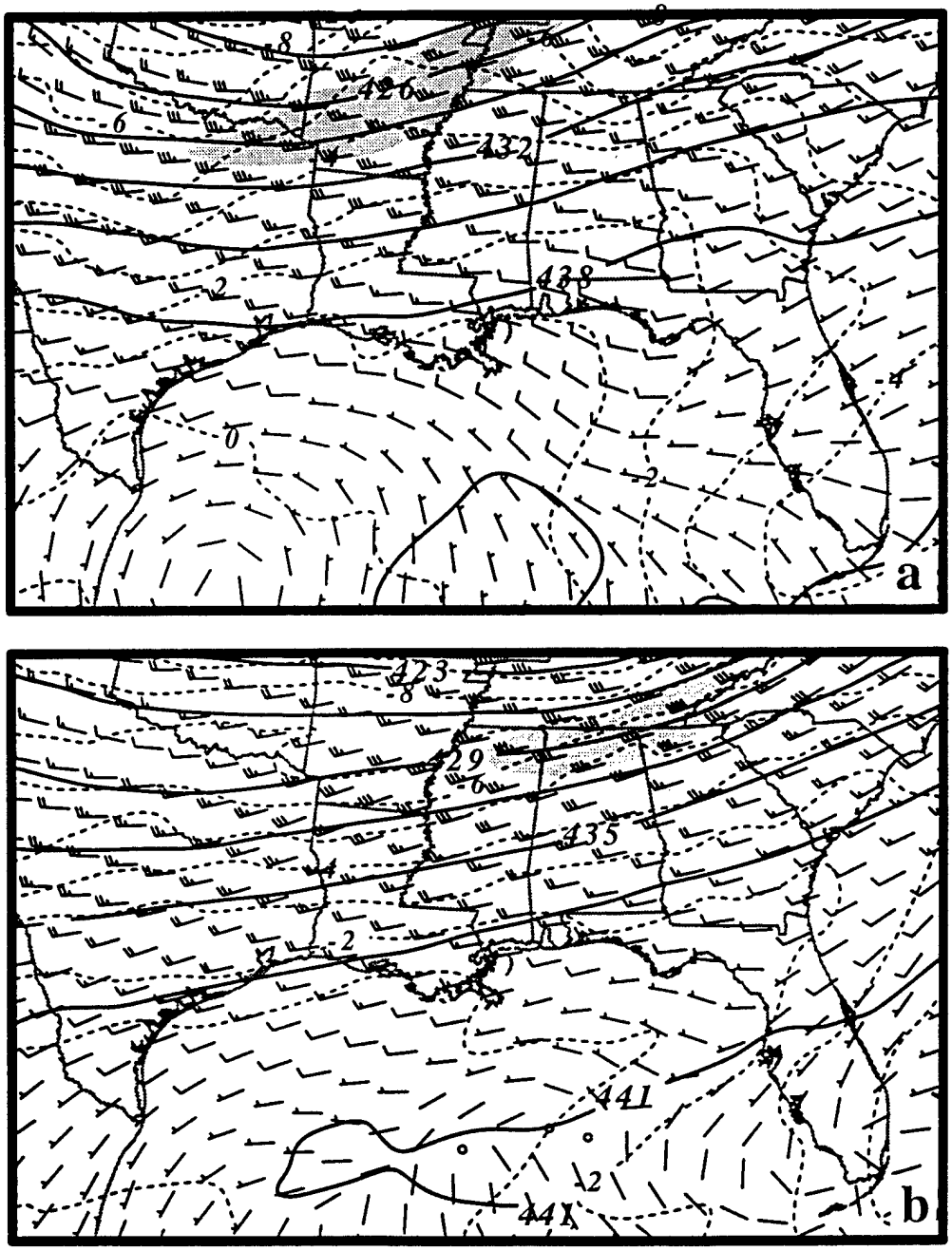

FIG. 13. MASS simulation without latent heating, 24 km mesh, 600 mb, wind vectors and isotachs (shaded at intervals of 5 for speeds greater than 35), temperature (dashed lines, C), and height (solid lines, dm) valid at (a) 0900 UTC 23 January 1990 and (b) 1800 UTC 23 January 1990.

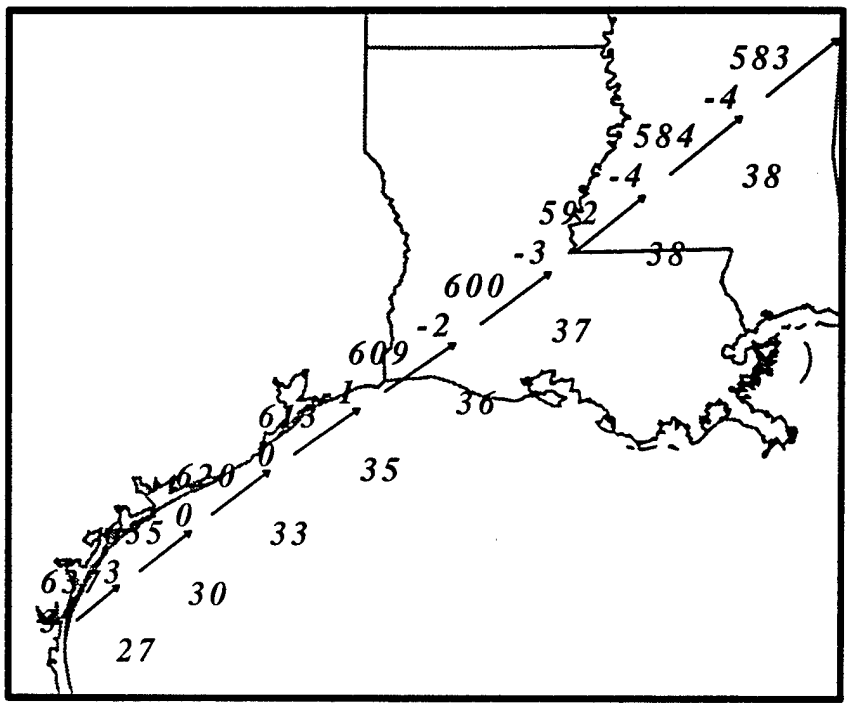

FIG. 14. Trajectory constructed from the 24 km MASS simulation without latent heating. Station plots contain pressure (mb), temperature (C), and total wind speed (ms^{-1}). Displayed wind vectors depict total wind. Parcels initialized at 1300 UTC and ended 2100 UTC 26 November 1988.

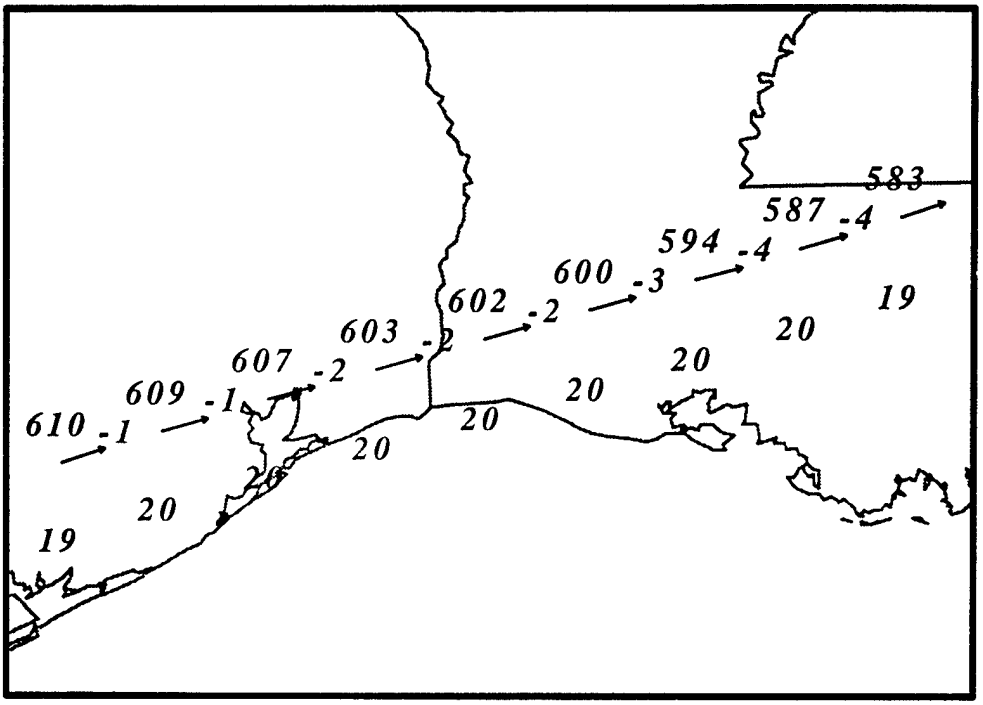

FIG. 15. Trajectory constructed from the 24 km MASS simulation without latent heating. Station plots contain pressure (mb), temperature (C), and total wind speed (ms^{-1}). Displayed wind vectors depict total wind. Parcels initialized at 0100 UTC and ended 0900 UTC 24 January 1990.

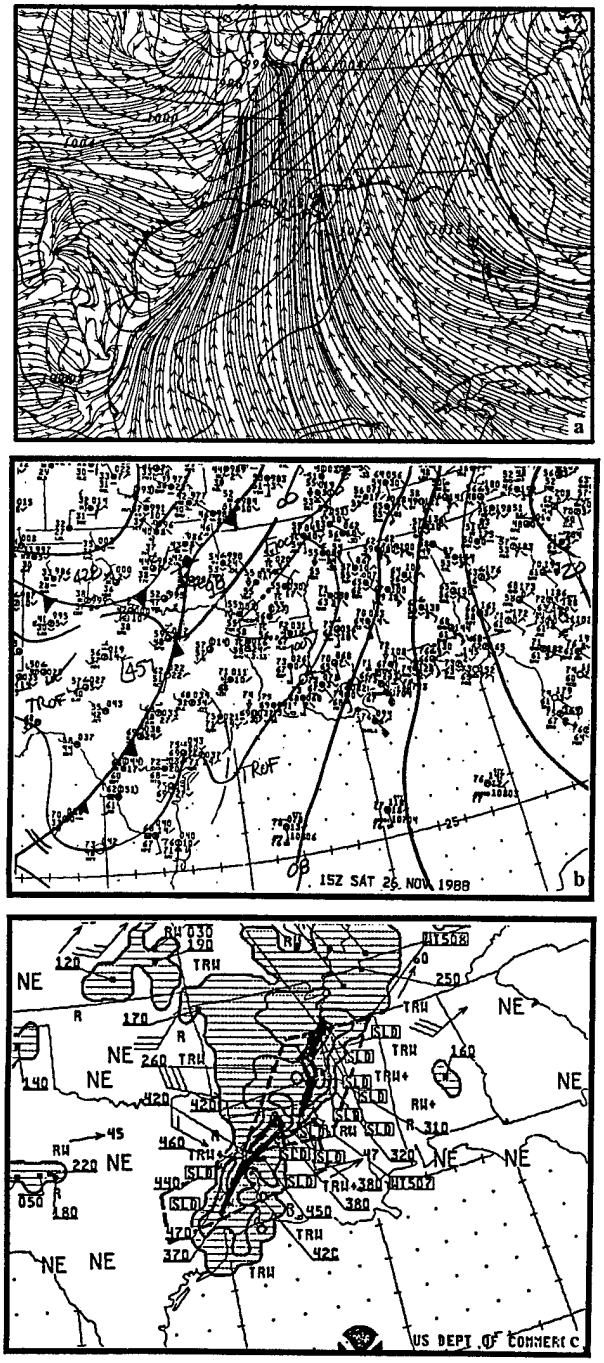

FIG. 16. (a) MASS simulated, 24 km mesh, surface depiction including surface streamlines, mean sea level pressure (solid lines, mb), (b) NWS surface analysis and (c) NWS radar summaries valid at 1500 UTC 26 November 1988.

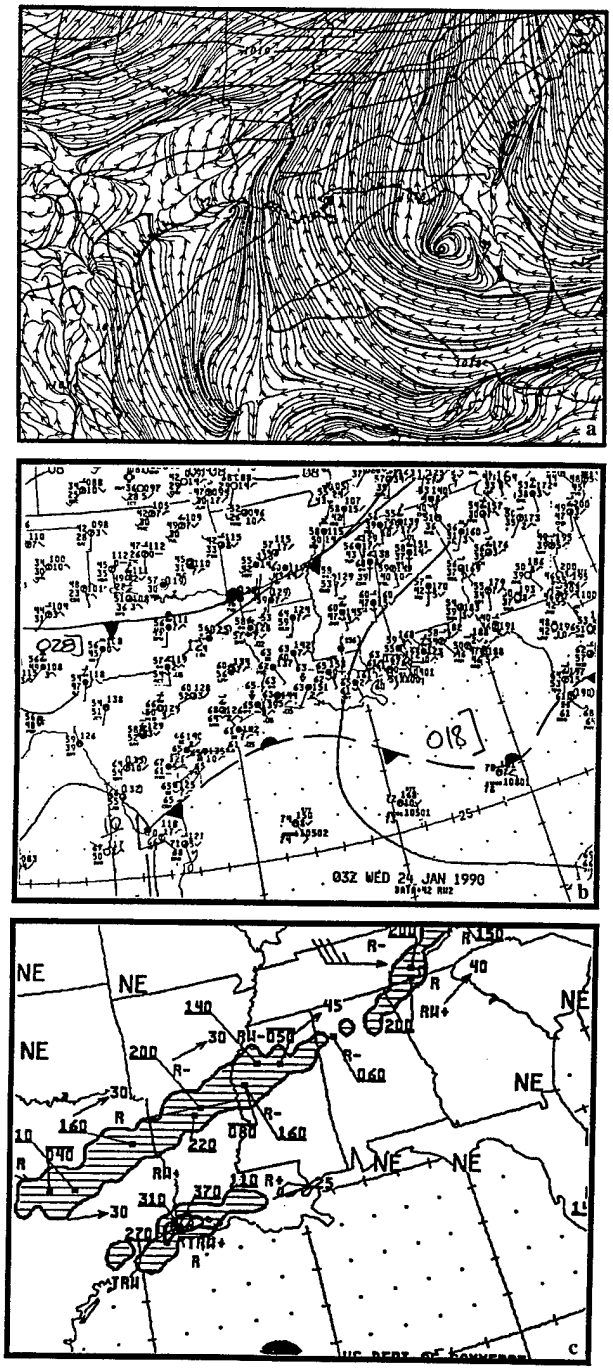

FIG. 17. (a) MASS simulated, 24 km mesh, surface depiction including surface streamlines, mean sea level pressure (solid lines, mb), (b) NWS surface analysis and (c) NWS radar summaries valid at 0300 UTC 24 January 1990.

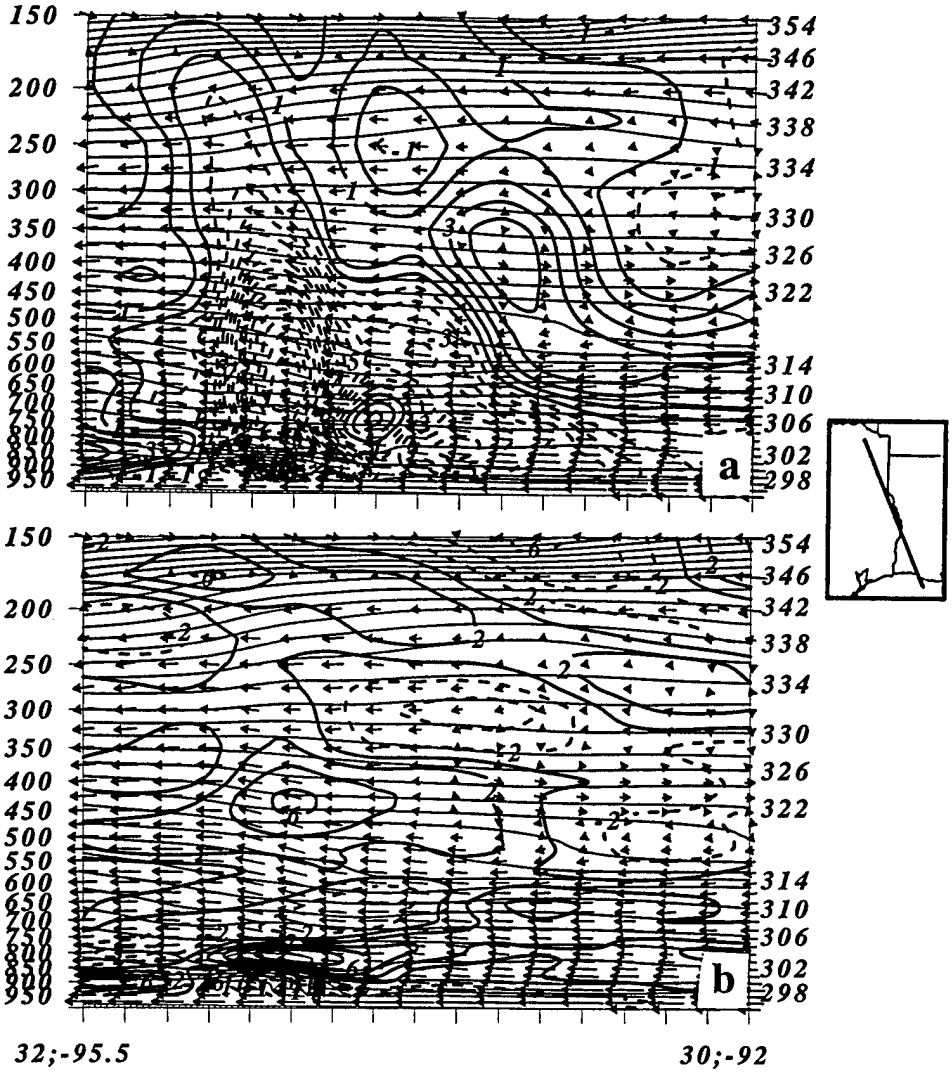

FIG. 18. MASS simulated, 24 km mesh, cross section extending from 32N, 95.5W to 30N, 92W valid at 1500 UTC 26 November 1988. Including ageostrophic wind vectors, θ (thin solid lines, K), (a) vertical velocity (contoured every 2 μbs^{-1}, solid lines indicate descent and dashed lines indicate ascent) and (b) divergence (contoured every $2x10^{-5}$ s^{-1}, solid lines positive values and dashed lines negative values).

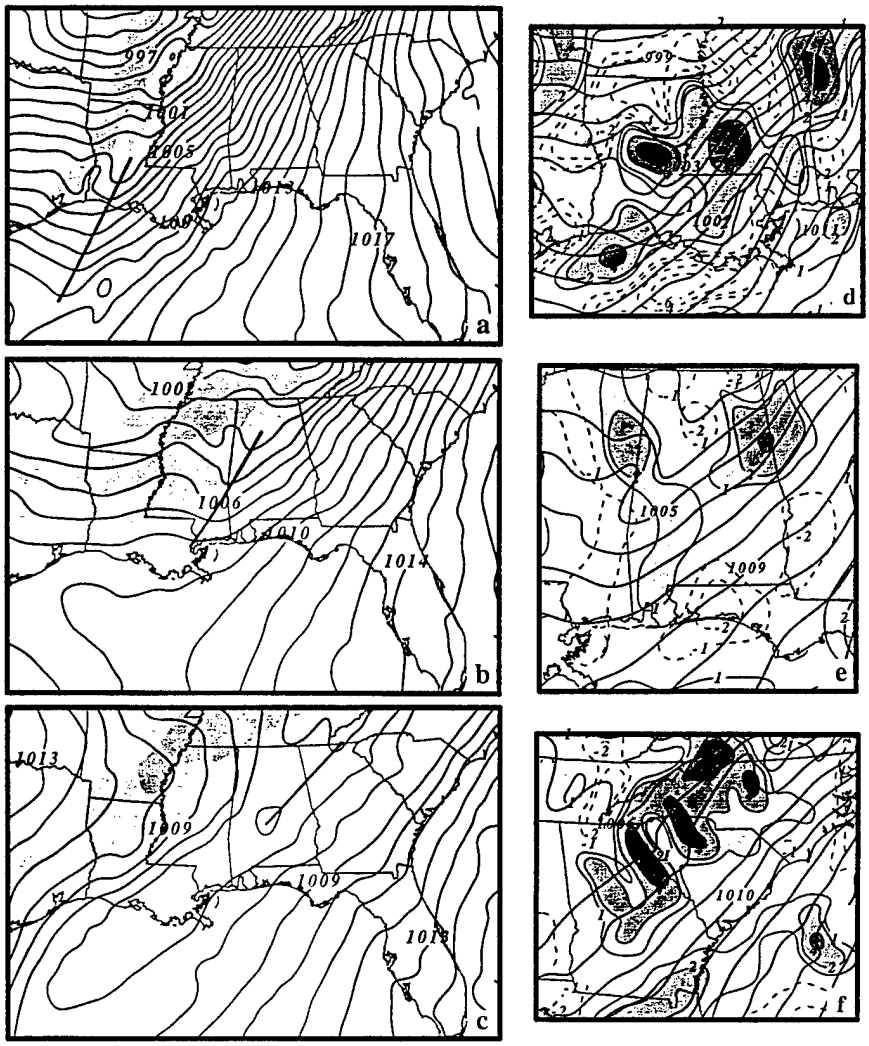

FIG. 19. MASS simulated, 24 km mesh, 600 mb, wind isotachs (shaded at intervals of 5 for speeds greater than 35 ms^{-1}), mean sea level pressure (solid lines, mb) and analyzed trough (solid line) valid at (a) 1800 UTC 26, (b) 0600 UTC 27 and (c) 1800 UTC 27 November 1988. Mean sea level pressure (thick solid lines, mb) and 250 mb divergence, contoured 1, 2, 4 & 6 (solid lines positive values and dashed lines negative values) and shaded greater than 1 ($x10^{-5}$ s^{-1}) valid at (d) 1800 UTC 26, (e) 0600 UTC 27 and (f) 1800 UTC 27 November 1988.

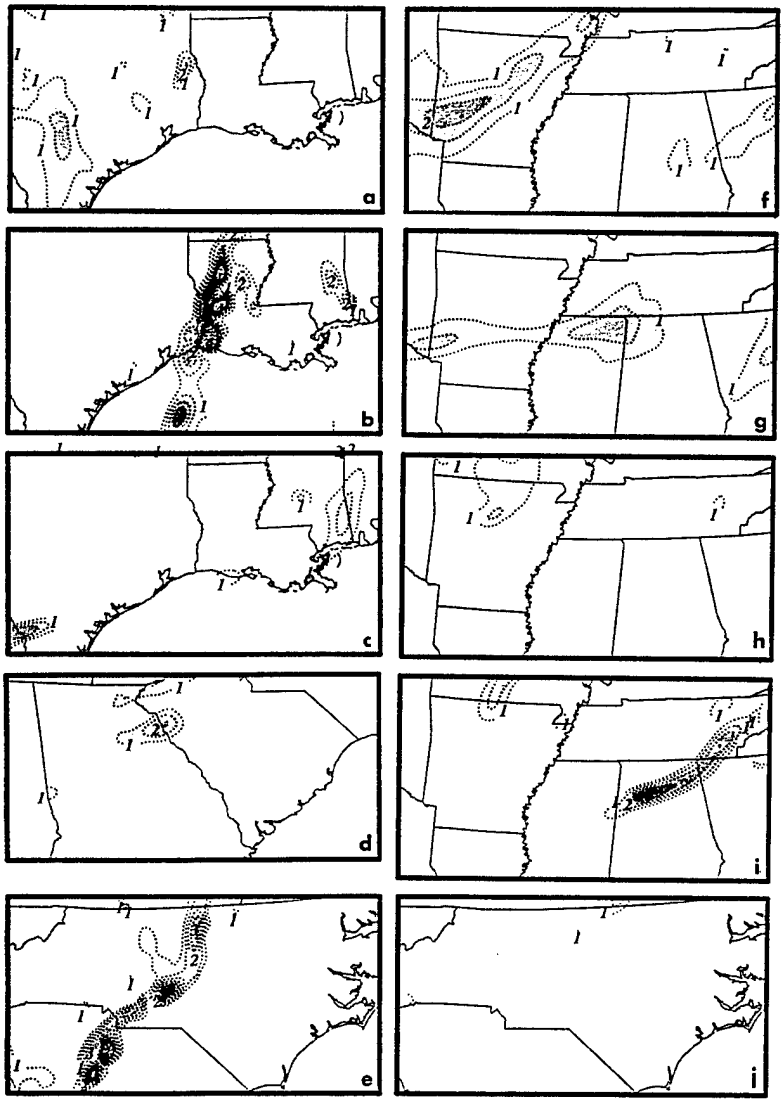

FIG. 20. MASS simulated, 24 km mesh PV (shaded greater than 1 PV unit by 0.5) valid at (a) 0600 UTC 26, (b) 1800 UTC 26, (c) 0600 UTC 27, (d) 1800 UTC 27, (e) 0600 UTC 28 November 1988, (f) 1800 UTC 23, (g) 0600 UTC 24, (h) 1800 UTC 24, (i) 0600 UTC 25 and (j) 0000 UTC 26 January 1990.

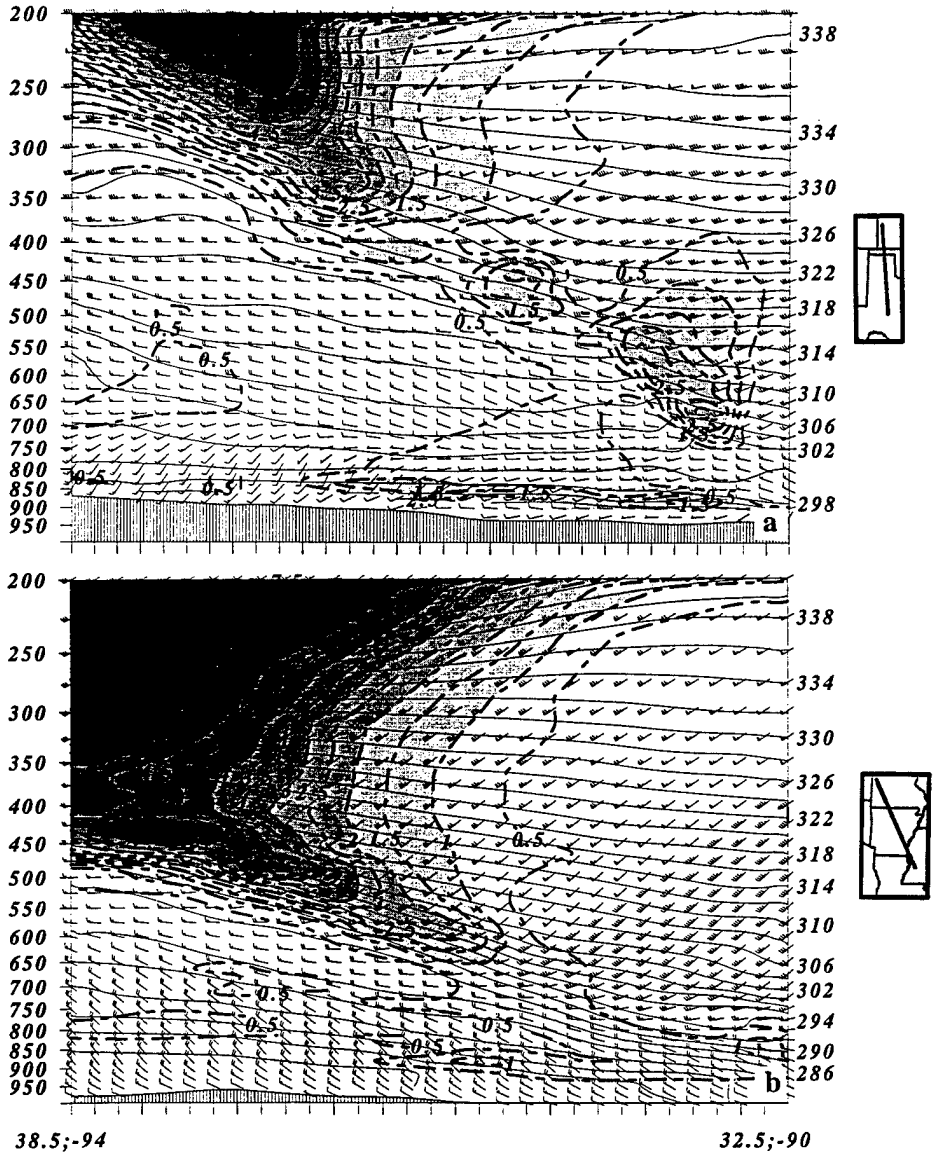

FIG. 21. MASS simulated, 24 km mesh, cross section including wind vectors (ms^{-1}), θ (solid lines, K), and PV (dashed lines, contoured greater than 0.5 and shaded greater than 1 PV units) (a) from 37N, 102.5W to 30.5N, 100W valid at 0300 UTC and (b) from 38.5N, 94W to 32.5N, 90W valid at 0600 UTC 24 January 1990.

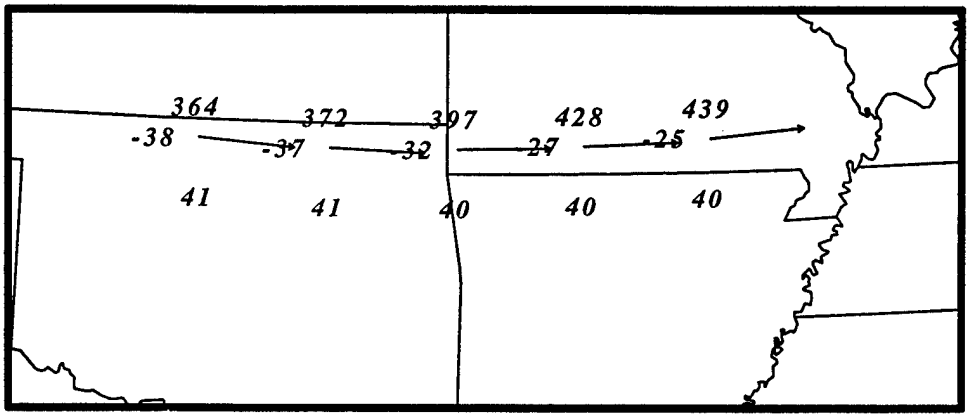

FIG. 22. Trajectory constructed from a 24 km MASS simulation. Station plots contain pressure (mb), temperature (C), and total wind speed (ms^{-1}). Displayed wind vectors depict total wind. Parcels initialized 0100 UTC and ended 0500 UTC 24 January 1990.

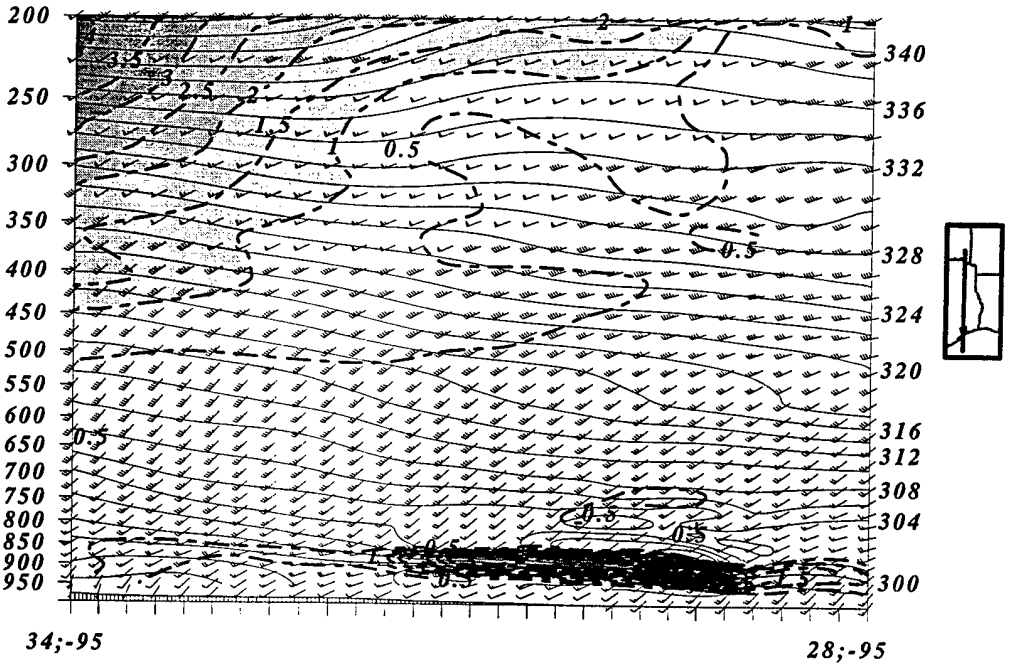

FIG. 23. MASS simulated, 24 km mesh, cross section including wind vectors (ms^{-1}), θ (solid lines, K), and PV (dashed lines, contoured greater than 0.5 and shaded greater than 1 PV units) from 34N, 95W to 28N, 95W valid at 1500 UTC 26 January 1988.

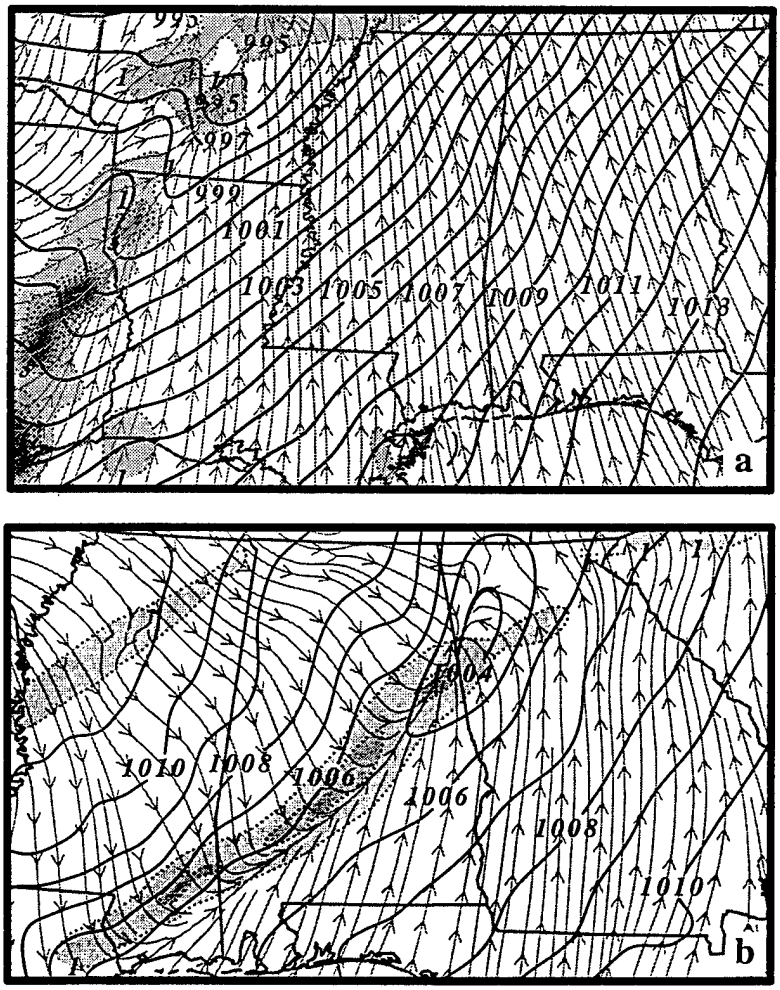

FIG. 24. MASS simulated, 24 km mesh, 900 mb PV (shaded greater than 1 by 0.5 PV units), sea level pressure (solid lines, mb) and surface streamlines valid at (a) 1500 UTC 26, and (b) 2100 UTC 27 November 1988.

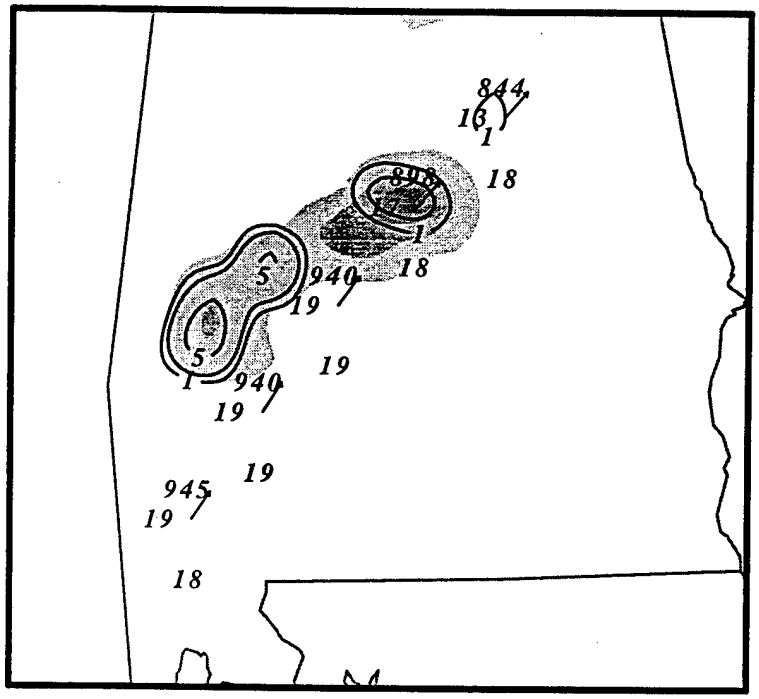

FIG. 25. Trajectory constructed from a 24 km MASS simulation initialized at 0600 UTC and ending at 1000 UTC 27 November 1988 plotted over convective latent heating (contoured at 1, 2, 5, 10, 15, 20 C h^{-1}) at 900 mb. Station plots contain pressure (mb), temperature (C), and total wind speed (ms^{-1}). Displayed wind vectors depict total wind.

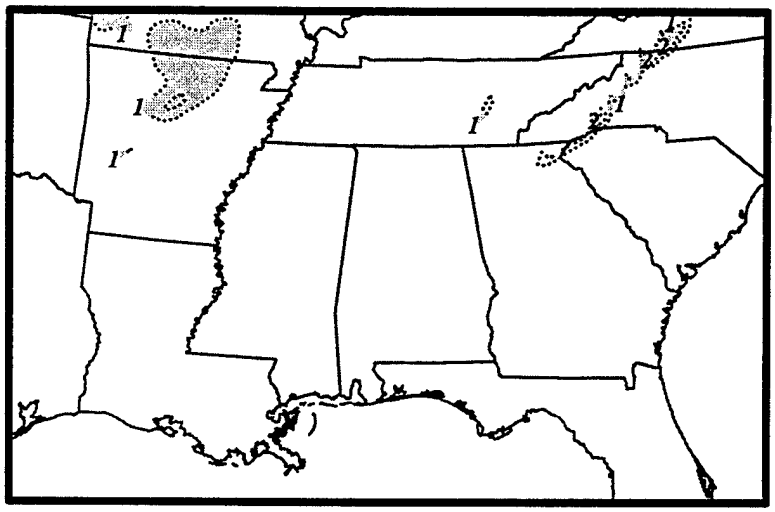

FIG. 26. MASS simulated, without latent heating, 24 km mesh, 900 mb level of PV (shaded greater than 1 by 0.5 PV units) valid at 1800 UTC 24 January 1990.

CHAPTER 4

MESOSCALE SIMULATIONS OF DYNAMICAL FACTORS DISCRIMINATING BETWEEN A TORNADO OUTBREAK AND NON-EVENT OVER THE SOUTHEAST US

PART III: 6 HOUR PRECURSORS

John M. Egentowich, Michael L. Kaplan, Yuh-Lang Lin* and Allen J. Riordan

(Submitted to Weather and Forecasting for publication)

**Corresponding author address*: Dr. Yuh-Lang Lin, Department of Marine, Earth and Atmospheric Sciences, North Carolina State University, Raleigh, NC 27695-8208.

E-mail: yl_lin@ncsu.edu

Abstract

Using observational analysis and mesoscale numerical simulations we investigate the subtropical jet (STJ) and the associated mass and momentum adjustments, development of a low-level jet (LLJ), and low-level potential vorticity (PV), 6 hours before the 1988 Raleigh (RDU) tornado outbreak. We also compare the environment to a synoptically similar event with severe weather forecasted but nothing developed over central NC.

In the event case there is a self-maintaining, low-level circulation, which was characterized by a surface trough, low-level PV maximum, mid-level jet and a warm Mexican airmass, that originated over Mexico, propagated across the Gulf Coast and moved over central NC at the time of the tornado. A meso-cyclone and low-level PV propagates over the Piedmont at the time of the RDU tornado outbreak. The low-level PV maximum is maintained by low-level forcing; specifically, tilting about a diabatic heat source (convection). In the non-event case, this feature is absent along the Gulf Coast states. In the event case, the polar jet right entrance region moves near the STJ left exit region which creates strong ascent and upper-level divergence over the Piedmont. The lifted index indicates the airmass over the Piedmont is unstable. We developed a Divergence Profile Buoyancy Index (DPBI) based on: upper-level divergence, airmass buoyancy and low-level tilting effects associated with shear and thermal gradients. We found DBPI values over 15 correspond to tornadic activity.

1. Introduction

The Raleigh, North Carolina tornado of 28 November 1988 was an extraordinary event that stimulated a great deal of interest from the weather forecasting and research communities. This tornado violated climatology as it occurred in the middle of the night in late November with an unusual F4 intensity and was part of a larger outbreak across NC and VA. It occurred in the vicinity of the polar jet (PJ) entrance region, instead of the exit region often proposed jet streak dynamical paradigms. Severe weather predictive indices based upon typical jet exit region dynamics were all sufficiently unremarkable to prevent the National Weather Service from issuing *any* severe weather watch or warning boxes prior to observations of severe weather (Gonski 1989). The inability of standard indices/dynamical paradigms to indicate at least modest tornadic potential for such an *extreme* climatologically anomalous event clearly shows limited scientific understanding of the mechanism of tornadic development.

Egentowich et al. (1999a) (hereafter Part I) compared the event (RDU tornado, 28 November 88) to the non-event (25 January 1990), and discussed the early synoptic situation (84-48 hours before hand), jet development, low-level PV development and warm air transport. The event and non-event cases were synoptically very similar for the 48 hours preceding the event case. Before the 48-hour point the synoptic situations were very different. Seventy-two hours before the event, a STJ streak over TX and MX with its thermally indirect ageostrophic circulation forced air down the eastern side of the Sierra Madre Mountains, warmed the air, and created a low-level trough and low-level jet

(LLJ) over the western Gulf of Mexico. The non-event case had a different synoptic pattern; the upper-level flow was very zonal over the US with a ridge over MX. The PJ developed over northern TX, OK and MO. The ridge prevented the STJ from developing or moving over the Gulf of Mexico. During the early period, no transport mechanism (LLJ) developed to move the hot air off the Mexican plateau over the Gulf.

In the event case, low-level PV was generated in the upper levels and transported downward in the lee of the Sierra Madre Mountains. The STJ exit region and its associated thermally indirect circulation transported the PV down to the midlevels (~500 mb) over the Mexican plateau. At the same time, a mountain-plains solenoid developed due to strong heating over the Mexican plateau creating convergence in the 500-600 mb layer increasing the thermal gradient (static stability), generating PV. A hydrostatic mountain wave transported the PV downward near the Mexican coast. The low-level PV moved northeastward along the Gulf Coast. In the non-event case, the STJ was absent, thus PV was not transported downward to the midlevels. The low-level flow over the western Gulf of Mexico transported moisture/clouds over the Mexican plateau, which minimized surface heating and inhibited the development of a deep, dry adiabatic layer. The easterly low-level flow also prevented the development of mountain waves.

Egentowich et al. (1999b) (hereafter Part II) compared the time period 48 to 6 hours before the event and the non-event. In the event case, a surface trough, low-level PV maximum, mid-level jet, a warm Mexican airmass and STJ exit region were co-located and moved across the Gulf Coast states as an entity. Initially, an STJ exit region

(with thermally indirect ageostrophic circulation) approached the Gulf Coast. This created upper-level divergence and ascent in the left exit region, which helped to maintain a low-level trough. The warm Mexican airmass was located over the Gulf Coast (southeast of the surface trough) and facilitated the development of a mid-level, northwestward directed pressure gradient force (PGF) creating a mid-level jet. The mid-level jet entrance region had an associated thermally direct ageostrophic circulation, which enhanced ascent over the low-level trough. These features created an environment favorable to deep convection. The PV maximum over the TX coast (originating from central MX) propagated eastward across the Gulf then northeast to the Carolina Piedmont at the time of the RDU tornado. The PV was maintained in the low-levels, built vertically, and was associated with an area of surface confluence, surface trough and convection. As the low-level PV maximum propagated along the Gulf Coast, the PV was primarily maintained in the low-levels by tilting effects. These features interacted to produce a self-sustaining feature that moved across the northern Gulf Coast of the United States and over central NC at the time of the tornado (some 48 hours later). In the non-event case, these features were absent along the Gulf Coast. There was no low-level warm Mexican airmass, a weaker mid-level jet, no low-level PV and no surface trough near the Gulf Coast. A PJ entrance region and small mid-level jet was over northern MS and AL -- well north of the Gulf Coast. During this period, the synoptic situations resembled each other but mesoscale differences existed.

Throughout the three part series of the papers, we compare the RDU tornado event to a synoptically similar non-event where severe weather was forecasted but none developed over central NC. The Raleigh NWS (Gonski, personal communication, 1998) expected severe weather to develop over central NC at 1800 UTC (designated as the onset of the non-event). The convective outlook and second day severe outlook were forecasting severe thunderstorms across the Piedmont, with possible isolated tornadoes over GA. In fact, at 1437 UTC, the National Severe Storms Forecast Center (Kansas City) issued a severe thunderstorm watch for central GA, SC and NC valid from 1400 to 2000 UTC. The window of the non-event ends when a front moves over central NC near 0000 UTC 26 January 1990. Since the actual time of the non-event is ambiguous, we will examine the non-event over a period of time starting at 1800 UTC 25 and ending 0000 UTC 26 January 1990.

In this paper, we will explore the relationship between the existence of the STJ and its effects on the lower-layer environment (associated mass and momentum adjustments, development of a LLJ, and low-level PV) the last 6 hours before the severe weather outbreak. We also will compare the environment to a synoptically similar non-event case. Our investigation of the pre-tornadic environment will concentrate on the mesoscale and how the self-sustaining feature (circulation) propagates over central NC at the time of the tornado outbreak. In section 2 we will briefly describe the mesoscale model used for the simulations. Section 3 deals with the development of the upper-level jet streaks. Section 4 focuses on the development and movement of the mid-level jet. In

section 5 we will investigate the transport of the low-level PV. Section 6 describes the low-level environment conducive to severe weather over the Carolina Piedmont. In section 7 we will propose and describe a new Divergence Profile Buoyancy Index (DPBI). Finally, in section 8 we will summarize and present our conclusions.

2. Model Summary

Due to the lack of high-resolution observational data, numerical simulations are employed to understand the environments prior to the event and non-event. The MASS model version 5.8 (MESO 1995) was employed for the simulations in this study. This MASS model is a modified version of the model originally developed by Kaplan *et al.* (1982). The numerical model specifics and experiments are summarized in Part I. For this study, we use a larger 24km grid (205x155x40) with both the 24km and 12km grids shifted to the northeast, centering NC in the simulation domain. Three-dimensional parcel trajectories used in this paper are derived from the Mesoscale Atmospheric Simulation System Trajectory software package (Rozumalski 1997).

3. Upper-level jet development

The PJ streak and STJ streak development over the 24 hour period before the event and non-event is described in detail in Kaplan et al. (1995). At 0000 UTC 28 November 1988, the NWS analysis (Fig. 1a) depicts the exit region of the STJ over the Carolina Piedmont. There is supergeostrophic flow over VA, NC and SC coastal region. At the same time, the PJ moves to the west of the Appalachian Mountains thus the PJ's right entrance region comes in close proximity to the STJ's left exit region. The associated transverse ageostrophic jet streak circulations are arranged so that a region of intense ascent develops between the jet streaks and over the Carolina Piedmont. At 1200 UTC 25 January 1990, the NWS analysis (Fig. 1b) depicts that a PJ extends from TX northeast to the north Atlantic Ocean, with supergeostrophic flow over the entire East Coast. There is no STJ over the eastern US; thus no jet streak phasing occurs. Figures 1c and d depict a cross section bisecting the jets. In the event case, two jet streaks are present, while only one is present in the non-event case.

a. Model simulated cross sections for event and non-event cases

Model generated cross sections depict the details of the jet streaks, which are perpendicular to the jet streaks and over the Carolina Piedmont extending from southern OH (39N, 83W) to the Atlantic Ocean, east of SC (33N, 75W). The first event case cross section is valid at 0100 UTC 28 November 1988 (Fig. 2a). At this time, the STJ streak does not even appear in the cross section, it is still located to the southwest. There is no

well-defined thermally direct ageostrophic circulation about the jet streak as the PJ entrance region begins to enter the cross section. The ageostrophic circulation extends all the way to the surface. There is strong organized ascent from the surface to the 300 mb level with a maximum value near the 700 mb level. The jet streaks are still to the west of the Appalachian Mountains so the upward vertical velocity is over the mountains.

At 0600 UTC 28 November 1988 the PJ streak entrance region is located to the west of RDU and the STJ streak exit region is located to the east of RDU. The 0600 UTC cross section (Fig. 2b) depicts ageostrophic motions and ascent over the Piedmont. The subtropical jet exit region is depicted as a wind velocity bulge that extends over the 200 mb level (A) with a strong southeastward-directed ageostrophic wind (near the 200 mb level). The PJ extends from 250 to 450 mb (B) with a strong northwestward-directed ageostrophic wind (200-250 mb level). Also, there is a strong thermally direct circulation about the mid-level jet (~ 600 mb). These ageostrophic circulations phase, which creates strong ascent over central NC.

The cross section of the non-event case valid at 1300 UTC 25 January 1990 is shown in Fig. 3a. The PJ streak core (maximum winds greater than 60 ms^{-1}) is located near the 250 mb level (C). The bulge on the south side of the PJ core (D) could represent a transient signal of the STJ streak. Also, there is an ill-defined ageostrophic circulation around the jet streak. There is an ascent maximum over the Appalachian Mountains associated with a mid-level jet. The PJ core is still located to the southwest of the cross

section so the entrance region and its associated thermally direct circulation is still to the southwest.

The second cross section is valid at 1800 UTC on 25 January 1990 (Fig. 3b), the expected time of severe weather. The PJ core (winds greater than 60 ms^{-1}) covers a larger area than that in the event case cross section and is located near the 300 mb level. There is a discernible thermally direct ageostrophic circulation around the upper-level jet streak. Also, the STJ streak is noticeably absent. The ascent maximum over the Appalachian Mountains has weakened. The mid-level jet is intensifying and being assimilated into the main body of the PJ. However, the ageostrophic circulation about the jet is very weak and so is the ascent over the Piedmont.

The third cross section valid at 0000 UTC 26 January 1990 (Fig 3c) depicts the atmosphere after the expected time of severe weather. The PJ core increases in strength with the maximum winds greater than 70 ms^{-1} and covers a larger area than the previous cross section. A thermally direct ageostrophic circulation is associated with the upper-level jet streak. The ascent maximum over the Piedmont has increases slightly. Therefore, 6 hours after the expected time of severe weather, there is weak ascending motion over the Carolina Piedmont.

b. Upper-level divergence

The model simulated ageostrophic circulations associated with the PJ entrance region and the STJ exit region transport mass away from the area between these two jets.

This creates upper-level divergence and the removal of mass in turn facilitates ascent and deep convection beneath it. We examine the removal of mass from the upper-levels by integrating the divergence over the 375 - 200 mb layer. At 0300 UTC 28 November 1988 (Fig. 4a), over eastern TN, western NC and western SC, there is a large area of weak upper-level divergence as the right entrance region of the PJ approaches the left exit region of the STJ. By 0600 UTC (Fig. 4b) the two jets have superimposed one another in such a way as to create very strong ascent over the central Carolina Piedmont (also depicted in the previous section). There is very strong upper-level divergence between the jet streaks, which dramatically intensifies the ascent and facilitates severe weather. Additionally, upper-level divergence is calculated at 0600 UTC (Fig. 4c) using data from a simulation with convection deactivated. As in the simulation with convection, there are upper-level divergence maxima over the Appalachian Mountains and over the central Piedmont. Convection enhances upper-level divergence; however, the juxtapositioning of the PJ and the STJ predisposes the environment to strong divergence over western and central NC. In the non-event case, only the PJ exists over the southeast US (no STJ exit region). Figures 5a-c depict the upper-level divergence at 1800 UTC 25, 2100 UTC 25 and 0000 UTC 26 January 1990, respectively, for the non-event case. Thus, the non-event case has upper-level divergence associated with the thermally direct circulation about the PJ entrance region. The upper-level divergence remains over the Appalachian Mountains because the PJ propagates to the northeast through this period.

In summary, the cross sections, upper-level divergence and backward trajectories (not shown) support the concept that the PJ, STJ and mid-level jet merge over the Piedmont in the event case. The juxtaposition of the thermally direct ageostrophic circulations (about the PJ and the mid-level jet) and the thermally indirect ageostrophic circulation (about the STJ) creates an area of very strong ascent, which in concert with strong upper-level divergence facilitates the development of deep convection and surface pressure falls.

4. Mid-level jet development

a. Mid-level jet development

In the event case, the simulated mid-level jet (centered near the 600 mb level, speed >35ms^{-1}) develops near the Carolina Piedmont. Figure 6 depicts the 600 mb PGF, wind field and the 850 mb equivalent potential temperature fields of the event case. After 0000 UTC 28 November 1988, a significant jetlet with a maximum wind speed of 50 ms^{-1} develops over central Georgia and western North Carolina. By 0600 UTC 28 November 1988, there is a jet streak which covers most of the region. In addition, the jetlet development corresponds well with the 850 mb thermal gradient and the tightest gradient is adjacent to the area of development. The warm air from MX (>330 K) at 850 mb elevates the heights to the southeast of the mid-level jet creating a mid-level PGF. The elevated heights are in the right exit region forcing the development of an unbalanced jetlet. As the air parcel accelerates in the exit region a thermally direct ageostrophic circulation develops as the atmosphere tries to balance itself. This forcing mechanism is continually regenerated as the surface frontogenesis and the low-level baroclinic zone develops, the warm MX air remains to the southeast and latent heating is generated as convection develops. The jetlet develops into a large mid-level jet over the ensuing few hours and moves between the PJ entrance region and the STJ exit region producing an area strong ascent.

For the non-event case, after 0000 UTC 25 January 1990, a mid-level jet develops with a balanced QG system west of the Carolina Piedmont (Fig. 7). The jet develops as a trough of low pressure develops over central US and this jet is closely associated with a strong height (pressure) gradient. It develops over eastern OK (extending to the northeast) and propagates northeastward. The right flank of the jet streak is over western Carolina from 1200 25 January to 0000 26 January. In contrast to the event case, the warm air from MX (>330 K) at 850 mb has not moved over the Carolina Piedmont. The strongest thermal gradient is over the Appalachian Mountains; thus the height gradient (PGF) and mid-level jet are located to the west of the Carolina Piedmont. The mid-level jet is much closer to a state of balance. The large-scale circulation associated with the PJ disrupts the ageostrophic circulation about the mid-level jet. Between 1800 UTC 25 (Fig. 3b) and 0000 UTC 26 January 1990 (Fig. 3c), there is descent in the low-levels and very weak ascent in the mid-levels over the Carolina Piedmont.

b. Three-dimensional trajectory analysis

Three-dimensional parcel trajectories are constructed to illustrate the mid-level jetogenesis. We examine the forced adjustments (accelerations) imposed upon the air parcels as they move through the mid-level jetogenesis region before the event and non-event. Figure 8 and Table 1 depicts the event case jetlet development (0000 UTC to 0400 UTC 28 November 1988). The parcel originates upstream of the mid-level jet and passes through the jetogenesis area. Table 1 depicts the parcel accelerations as it moves through

the jetlet, from 0000 to 0400 UTC. As the parcel moves into the jetlet exit region it deflects to the left, accelerates and ascends. The higher heights to the southeast produce a northwest-directed PGF that is consistently larger in magnitude than the opposing Coriolis force (Table 1) thus the parcels accelerate in the exit region. There is a net acceleration directed to the left of the flow creating the mid-level jetlet. The Lagrangian Rossby numbers are considerably larger than 0.5 indicating the flow is unbalanced (Table 1). Also, the nonlinear balance equation (NBE) totals are considerably larger than 10^{-8}, which again indicates unbalanced flow because of its exit region location (Kaplan and Paine, 1977). The parcel stays on the same pressure level as it moves through the jet streak until it moves into the exit region with a thermally direct ageostrophic circulation where it begins to ascend rapidly (from 584 mb to 490 mb in 1 hour). The vertical velocity (Table 1) confirms there is little ascent for the first few hours of the trajectory but in the last few hours there is tremendous ascent. The mid-level jet over the Carolinas is accelerating, unbalanced, and has a direct circulation in the exit region, in sharp contrast to the balanced jet dynamics (Uccellini and Johnson, 1979).

The non-event case jet development (1200 to 1600 UTC 25 January 1990) is depicted in Fig. 9a and Table 2. The parcel originates at the same position as the event case so the parcel again passes over western NC. In the entrance region, the PGF is directed to the northwest and it is consistently larger in magnitude than the opposing Coriolis force (Table 2) thus the parcel accelerates rapidly. As the parcel moves into the jetlet exit region it decelerates and deflects to the right into an area of convergence

(indicating indirect circulation). The Lagrangian Rossby numbers (Table 2) are less than 0.5, which indicates balanced flow. The vertical velocity, parcel speed, Rossby numbers and areas of divergence surrounding the jet all indicate balanced flow. The NBE totals are an order of magnitude lower than the event case (near $1x10^{-8}$) indicating balanced flow (Kaplan and Paine, 1977). The parcel ascends slowly as it moves through the jet streak then levels out as it moves into the jetlet exit region. The mid-level jet over the Carolina Piedmont is decelerating, balanced, and has a thermally indirect circulation in the exit region, very much consistent with the Uccellini and Johnson (1979) paradigm.

The non-event case jet development from 1800 to 2200 UTC 25 January 1990 (Fig. 9b) is also examined with nearly identical results as above (data not shown). The parcel originates at 600 mb over southern SC so the parcel passes over central NC at the expected time of severe weather. As the parcel moves through the jet it accelerates from 28 to 35 ms^{-1} and ends on the 606 mb level; the vertical velocity being essentially zero. The Lagrangian Rossby numbers average 0.1, again indicating balanced flow. The mid-level jet over the Carolina Piedmont is balanced, and there is weak mid-level descent over the Piedmont region.

c. Mid-level jet development and convection

We also examine the relationship between convection (release of latent heat) and jetlet development. As convection develops, the local environment warms due to the release of latent heat. In the event case, the unbalanced, accelerating, mid-level jetlet exit

region has a thermally direct circulation with ascent in the right exit region. Convection locally warms the area due to latent heating increasing the thermal gradient and the PGF, in-turn, accelerating the jet (Hamilton et al. 1998).

Figure 10 depicts the mid-level jetlet and accumulated convective precipitation (over 1/2 h) of the event case. The convection tends to develop toward the right exit region. At 0200 UTC 28 November 1988, convection is associated with the accelerating jetlet in the right exit region of the jetlet core (area shaded > 40 ms^{-1}) and an area of warm air is also associated with it. By 0600 UTC 28 November 1988, the jetlet develops into a large mid-level jet with a thermally direct circulation and has very strong ascent, an elongated area of convection and a relative temperature maximum in the right exit region of the jet.

Another MASS simulation with convection deactivated (no latent heat) is performed to examine the relationship to mid-level jet development. In the "no latent heat" simulation, the mid-level jet is present over GA, SC and NC at 0600 UTC 28 November 1988 (Fig. 11a); the simulation with latent heating is depicted in Fig. 11b. The mid-level jet over NC is similar between the simulations. Over the Piedmont, on average, the wind is 2 ms^{-1} less in the simulation without latent heating. Over the Appalachian Mountains, the wind is approximately 5 ms^{-1} less in the simulation without latent heating. The environment is predisposed (due to the warm Mexican air that has been transported over the Piedmont) to develop a strong mid-level jet. However, latent heating from convection significantly increases the magnitude of the mid-level jet.

Parcel trajectories are constructed for the "no latent heating" simulations. Figure 12 depicts a parcel trajectory derived from a MASS simulation suppressing the release of latent heat. Over western NC, the wind speed is ~5 ms^{-1} slower in the run without latent heating. The Lagrangian numbers (Table 3) are much less than 0.5, which indicates a balanced flow. While the environment is conducive to mid-level jet development, it appears the latent heat energy, in part, enhances the development of a mid-level unbalanced jetlet. The PGF is roughly twice as strong in the event case with latent heating. The dramatically stronger PGF (with latent heating) continues to accelerate the jet in what normally would be the exit region, which then creates an unbalanced jet with a thermally direct ageostrophic circulation. In addition, this ascent is over the warm air, which destabilizes the environment. As this jetlet develops and propagates eastward, the thermally direct ageostrophic circulation merges with an area of ascent between the PJ and the STJ creating an area of intense ascent over the Carolina Piedmont.

In the non-event case, the main area of convection generally occurs in the left exit region of the jet (not shown), which is opposite of the event case. The balanced jet exit region has an associated thermally indirect circulation, which creates ascent in the left exit region. At 1400 - 2100 UTC 25 January 1990, the jet continues to develop. At 1800 UTC 25 January 1990, there is no convection, which suggests weak dynamics about this jet (Fig. 13a). By 0000 UTC 26 January 1990, the right entrance region of the mid-level jet is over eastern TN, which creates ascent and an area of light convective precipitation over western NC (Fig. 13b). Another MASS simulation is performed with no convection

to examine the relationship to jetlet development. In the non-event "no latent heat" simulation, the mid-level jet develops farther to the west associated with the balanced QG system over the TN valley. While the convection areas are disconnected from the ageostrophic circulations about the jet, it appears that the latent heat release from convection does modify the mid-level jet (on a meso-α scale).

We compare the mid-level jets at the event time (0600 UTC 28 November 1988, Fig. 14) and non-event time (Fig. 13a - 1800 UTC 25 and Fig. 13b - 0000 UTC 26 January 1990) and found several differences. Comparing Fig. 14 to Fig 13a the right side of the jetlet is over central NC (event case) while in the non-event case the jetlet is moving into central VA. There is a line of convective precipitation along the right side of the jetlet and over central NC in the event case, while the non-event case does not have any convective precipitation near the jetlet or central NC. We also compare Fig. 14 to Fig 13b. The right side of the jet is over central NC in both the event and non-event case. The location of the convective precipitation relative to the jetlet is very different. In the event case, there is a line of convective precipitation along the right side of the jetlet and over central NC; in the non-event case, convective precipitation is much less intense and located beneath the mid-level jet over western NC.

In summary, this warm pool, i.e. air from MX and warmed by latent heating, help maintain the height gradient and the PGF. This, in turn, accelerates the jet in what normally would be the jet exit region and induces a thermally direct circulation. In the non-event case, the thermal gradient is much weaker and not as well organized.

5. Potential vorticity

Parts I and II detail the 3-day evolution of the low-level PV maximum. The PV maximum originated in the upper-levels over central MX is transported to the mid-levels by an ageostrophic circulation associated with a subtropical jet streak and down the Sierra Madre mountains by an ensemble of hydrostatic mountain waves. This PV is associated with a surface trough that develops in the lee of the Sierra Madre Mountains. This trough and its associated confluence zone move northeastward along the TX coast and then eastward over the Gulf Coast. The PV is primarily maintained by the tilting of the horizontal component of vorticity into the vertical through horizontally varying diabatic heating. This PV maximum intensifies and moves northeastward to RDU at the time of the tornado outbreak. The non-event case, in contrast, does not develop a surface trough (confluence zone) and associated low-level PV over the East Coast of TX and MX. Also, no surface trough or confluence zone propagates along the Gulf Coast. The only low-level PV is associated with a weak frontal boundary over AK and TN. The low-level PV is transported downward from the upper-levels in the lee of the Rocky Mountains (over western KS, OK and northern TX). Without any strong low-level forcing there is weak interaction of upper- and lower-level PV so there is no cyclogenesis (Zehnder and Keyser, 1991). Late in the evolution of the non-event case low-level PV develops (due to convection and not associated with a long lasting surface confluence zone) over AL and northern GA and propagates into the Appalachian Mountains.

For the last 6 hours, the evolutions of the PV maxima are investigated and are related to surface cyclogenesis for both cases. In the event case, Figs. 15a, b and c depict the surface pressure and PV over the 925 to 875 mb layer valid 0200, 0400 and 0600 UTC 28 November 1988. These figures highlight the relationship between low-level PV and surface cyclogenesis. The 900 mb PV maxima are located just to the west of the surface trough and are collocated with the areas of maximum trough deepening. At 0000 UTC there is a PV maximum (>5 PV units) over northeastern GA and by 0200 (Fig. 15a) the PV maximum propagates over western SC and is closely associated with a mesocyclone (<1002 mb). By 0400 UTC (Fig. 15b), the PV maximum is near Charlotte, NC (CLT) and is associated with the 1000.5 mb isobar. By 0600 UTC (Fig. 15c), the PV maximum (>4.5 PV units) moves over to central NC at the time of the tornado outbreak and is associated with a 995.5 mb isobar.

Figs. 16a, b, c and d depict the relationship between the surface pressure and PV over the 925 to 875 mb layer valid 1500, 1800, 2100 UTC 25 and 0000 UTC 26 January 1990 for the non-event case. At 1500 UTC (Fig. 16a), there are isolated PV maxima associated with the surface trough. By 1800 UTC (Fig. 16b), the low-level PV (>2 units) is still associated with the surface trough. However, most of the PV is over GA and far western NC. By 2100 UTC (Fig. 16c), the low-level PV maxima over GA is weakening considerably and the maximum over western NC is moving to the northeast. Finally, at 0000 UTC (Fig. 16d), the low-level PV maximum is moving over southern VA. The surface front over the Carolina Piedmont does not have any associated low-level PV.

We examine vertical cross sections which bisect the low-level PV maximum and the upper-level jet streaks. Figure 17a depicts θ_e and PV along the northwest to southeast cross sections centered over northern SC for 0400 UTC 28 November 1988. At 0600 UTC (Fig. 17b), the cross section is centered over RDU. These cross sections depict the strongest PV in the low-levels. Hourly cross sections (not shown) bisecting the low-level PV maximum indicate that the PV is a low-level feature. Just as in the preceding 48 hours, PV in the event case (over the Carolina Piedmont) is transported and/or generated in the low-levels.

The non-event cross section (Fig. 18a) valid 1800 UTC 25 January 1990 extends from IL, over the Piedmont to the Atlantic Ocean (east of Cape Hatteras). The non-event depicts the PV transport from the left flank of the PJ entrance region down to the low-levels west of the Carolina Piedmont. This supports the concept that PV is transported downward by a tropopause fold (Danielsen, 1968). At 2100 and 0000 UTC (Figs. 18b and c), the same cross section depicts downward transport of PV but the eastward extent of the PV only reaches the Appalachian Mountains. The low-level PV maxima over the Carolina Piedmont are not associated with the downward transport of PV. The low-level PV maxima over the Piedmont are weak, sporadic and associated with convection. There is no interaction between upper- and lower-level disturbances characterized by non-uniform PV which would result in a significant increase in relative vorticity at the surface (Zehnder and Keyser, 1991).

We also examine the relationship between convective precipitation (diabatic energy source) and PV generation. The 900 mb PV and the latent heating are generally associated with convective precipitation. The low-level PV maxima increase, in part, from latent heat energy associated with convection. At 0635 UTC, the radar summary (Fig. 19a) agrees well with the model simulated convective precipitation at 0600 UTC (Fig. 19b). Also, the low-level PV is associated with the diabatic convective heating rates (Fig. 19c).

The simulated 1800 UTC convective precipitation for the non-event case (Fig. 20b) agrees very well with the 1735 UTC radar summary (Fig. 20a). There is convective precipitation over the western NC and SC and central GA, a dry area over the Carolina Piedmont and more convection over eastern NC. The low-level PV (Fig. 20c) along the Appalachian Mountains is closely associated with the convective precipitation and latent heating. Also, at 2100 UTC 25 and 0000 UTC 26 January 1990 (not shown) there is the same relationship between low-level PV, convective precipitation and latent heating.

Potential vorticity can be increased locally either by transport or generation. The generation of PV, through diabatic processes, may be examined using the Lagrangian PV equation (Eq. 1) (Gidel and Shapiro 1979) and may be estimated by:

$$\frac{d}{dt}\left[-(\zeta_\theta+f)\frac{\partial\theta}{\partial p}\right]=\underbrace{-(\zeta_\theta+f)\frac{\partial}{\partial p}\left[\frac{d\theta}{dt}\right]}_{1}\underbrace{-\left(\frac{\partial\theta}{\partial p}\right)\hat{k}\nabla_\theta\times F}_{2}+\underbrace{\left(\frac{\partial\theta}{\partial p}\right)\hat{k}\bullet\nabla_\theta\left[\frac{d\theta}{dt}\right]\times\frac{\partial\vec{V}}{\partial\theta}}_{3}. \quad (1)$$

Term one relates to the production or destruction of PV to vertical gradients of diabatic heating with isentropic absolute vorticity. Term two represents the change in PV

resulting from horizontal gradients of diabatic heating within regions of horizontally varying frictional stresses. Term three represents the change in PV resulting from the tilting of the horizontal component of vorticity into the vertical through horizontally varying diabatic heating. The relative contribution of each term in the PV Eq. (1) is evaluated in a manor analogous to Kaplan and Karyampudi (1992) using parcel trajectory data with the exception of the gradient field. The gradient field is calculated using a centered finite differencing scheme over the center trajectory point.

Using trajectories, we examine the PV maximum over central NC at the time of the RDU tornado (0600 UTC 28 November 1988, Table 4). Figure 21a depicts the parcel trajectory and the latent heating due to convection at 0600 UTC. There is a maximum (>5 C h^{-1}) over central NC. The parcel's PV increases to 3.647 PV units as it passes through the latent heating associated with convection. The diabatic heating produces PV so we evaluated the relative contribution of each term in Eq. (1). Term one contributes 32% to the production of PV by the change in static stability. Term two contributes 19% to the change in PV resulting from horizontal gradients of diabatic heating within regions of friction. Term three contributes 49% to the production of PV resulting from the tilting of the horizontal component of vorticity into the vertical through horizontally varying diabatic heating.

We also examine the PV maximum over central NC at the expected time of the non-event (1800 UTC 25 January 1990, Table 5). Figure 21b depicts the parcel trajectory and the latent heating due to convection at 1200 UTC. There is no latent heating >1 C h^{-1}

over eastern GA or western NC and SC so the parcel's PV increases to only 0.471 (PV units) as it moves over the central NC. We evaluate the relative contribution of each term in the PV Eq. (1). Term one produces a small amount of anticyclonic PV while term two (friction) and term three (tilting) produce cyclonic PV. At 0000 UTC 26, the only area of low-level PV is well north or RDU (over central VA) so the data is not included.

We conclude that the PV maxima in the event case increase over central NC through the tilting term associated with diabatic forcing. In the non-event, there is little change in the low-level PV over central NC.

6. Low-level environment favorable for severe weather

We examine how unstable the low-level environment is over the Carolina Piedmont. First, we examine the lifted index (LI) (Bluestein, 1993). For the event case, at 0600 UTC 28 November 1988 the LI pattern (Fig. 22a) depicts large negative LI over the eastern Carolina Piedmont, which was associated with the warm Mexican airmass above the warm moist air from the Carolina coast, indicating strong potential for severe weather. On the other hand, the non-event case LI field (Fig. 22b) at 1800 UTC 25 January 1990 depicts positive LI values over the Piedmont, which indicates little chance for severe weather. By 0000 UTC 26 January 1990 (Fig. 22c), the LI over the Piedmont indicates a more stable airmass. *Note that at the time of the event and non-event, the forecasters did not have access to the high-resolution model data.* The RDU forecasters calculated the lifted index from the Greensboro, NC sounding, which yielded a value of 1 for the event case and 2 for the non-event case.

The mesoscale environment of the event case is much more conducive for severe weather outbreak compared with the non-event, is also reflected in the radar summaries at 0635 UTC 28 November 1988 (Fig. 19a) and 1735 UTC 25 January 1990 (Fig 20a). These figures reveal several striking differences. In the event case, a solid line of heavy thunderstorms is over central NC with maximum tops of nearly 15 km. There are additional thunderstorms over western NC and the NC coastal region. In the non-event case there are no thunderstorms over central or western NC. There are rainshowers over western NC with maximum tops of 6.5 km and thunderstorms over the NC coast with

maximum tops of 8.4 km. In summary, the event case has more clusters of cumulonimbus clouds with a much greater depth, which indicates a stronger convective instability and a better organization. Also, we compare the radar summaries at 0635 UTC 28 November 1988 (Fig. 19a) and 2335 UTC 25 January 1990 (not shown), which again highlight significant differences. In the event case, a solid line of heavy thunderstorms is over central North Carolina with maximum tops of nearly 15 km. In the non-event case, there are no thunderstorms over the Piedmont.

We also examine the mid-level jet streaks and the low-level total wind velocity shear they create. Figures 23a and b (event case) and Figs. 23c-f (non-event case) depict the magnitude of wind shear between the wind vectors (ms^{-1}) at 925 or 850 and 500 mb levels. Figure 23a and b is valid at 0600 UTC 28 November 88 (event case). Very strong shear (between 850 and 500 mb) propagates over central NC as the low-level easterly flow veers to west-south-west in the mid-level jet, in which the wind shear approaches 32 ms^{-1}. The shear of the 925 - 500 mb layer is even more dramatic, which approaches 40 ms^{-1}. The lower layer (850 to 700 mb layer) contains ~ 90 percent of the total shear. As the mid-level jet moved over central NC, the low-level vertical shear increased tremendously in a very short time period, which increases the possibility of severe weather. Figures 23c and d depict the non-event case at 1800 UTC on the 25 January 1990. The amount of vertical shear (over the 850 to 500 mb layer) over central NC is insignificant. At 1900 UTC (not shown) there is even less shear across the 850 to 500 mb level. The 925 to 500 mb layer at 1800 UTC 25 January 1990 has a larger shear quantity

but decreases dramatically by the following hour (not shown). By 0000 UTC 26 January 1990 (Figs. 23e and f) the low-level shear increases slightly. Also, most of the shear is near the mid-levels (over the 700 to 500 mb layer). In the non-event case, the weak vertical shear indicates less potential for severe weather over the Piedmont than in the event case.

Another way we examine wind shear is to examine the thermal wind in the low-levels. In the event case, there is a strong thermal wind (over the 900 to 500 layer) east of the 600 mb jet and the surface cold air advection over the western Piedmont. There is a second thermal wind maximum associated with the polar jet/front structure located over TN. In the non-event case, the strongest thermal wind is associated with the polar jet/front system located over the TN valley. Figures 24a-c depict the thermal wind over the 900 to 500 mb layer, the 600 mb jet and the surface temperature for both the event and Figs. 25a-d depict the non-event case. There is a remarkable difference in the thermal wind fields between these cases. In the event case, there is a strong thermal wind (30-35 ms^{-1}) on the leading edge of the 35 ms^{-1} isotach; while the non-event case has a thermal wind of only 5 ms^{-1} associated with the 35 ms^{-1} isotach. Also, this imbalance, i.e., where the thermal wind and total wind shear differ substantially, is out over the very warm surface air (>20 °C). In the non-event case, the strong thermal wind (30-35 ms^{-1}) is farther to the west, associated with the 40 ms^{-1} isotach, which is more representative of a QG balanced system. Also, the strong thermal wind is over moderately warm surface air

(~ 16 °C). We conclude that the event case is much more unstable in the lower levels and far more conducive to severe weather formation.

We also calculate the storm relative helicity (SRH) for numerous points over central NC. SRH is defined by as (e.g. Davies-Jones et al., 1990):

$$SRH = -\int_0^h \mathbf{k} \bullet (\mathbf{V} - \mathbf{c}) \times \frac{d\mathbf{V}}{dz} dz \qquad (1)$$

where V is the wind velocity, c is the storm relative motion and dV/dz is the wind shear vector over the layer. For our study, c is inferred from operational radar summaries. For the event case (0635 UTC summary), the storm was moving at 24 ms^{-1} from 225° and for the non-event case (1835 UTC summary) the storm was moving at 22 ms^{-1} from 215°. At 0600 UTC 28 November 1988 (event case), the maximum value over central NC is 560 m^2s^{-2}. At 1800 UTC 25 (non-event case), the value over central NC was ~240 m^2s^{-2}. By 0000 UTC 26 January 1990, the value over central NC increases to ~300m^2s^{-2}. The SRH indicates the potential for severe tornadoes for the event case, but not for the non-event case.

7. Divergence profile buoyancy index (DPBI)

The overall objective of this research is to develop a new way of forecasting severe weather. To this end, we incorporate all the features we found to be significant in our research for the event case study but not for the non-event case study. (1) both the PJ and the STJ are present over the southeast US over the entire 84 hour period. (2) the STJ exit region and the PJ entrance region juxtapose over the Carolina Piedmont, which creates extremely strong upper-level divergence over the Piedmont and induces upper-level stretching. (3) warm air moves from the Mexican plateau, across the Gulf coast states and over the Carolina Piedmont. (4) the warm MX airmass over the southeast US in conjunction with the cold air advection over the central US produces a strong PGF and creates a robust mid-level jet. (5) the strong low-level imbalance can be measured by strong low-level thermal wind which is out of phase with the mid-level jet and out ahead of surface cold air advection (front). (6) the mid-level jet right entrance region and its associated thermally direct ageostrophic circulation is associated with a surface trough, surface confluence and convection. All these features interact to maintain themselves as a coherent entity that moves across the Gulf Coast and over the Carolina Piedmont at the time of the tornado outbreak. (7) the movement of the low-level trough (confluence zone) can be traced by following the low-level PV. As the low-level PV propagates along the Gulf Coast and over the Piedmont, diabatic effects (associated with tilting effects) maintain it. We have incorporated all these features into the DPBI. This index utilizes integrated upper-level divergence, low-level development of a strong baroclinic

and shear zone and PV generation associated with low-level tilting effects incorporating shear and thermal gradient, Term 2 of Eq. (2), (Karyampudi et al. 1995).

$$\mathrm{PV} = \underbrace{-\frac{\partial\theta}{\partial p}(\zeta + f)}_{1} \underbrace{-\hat{k} \bullet \left[\frac{\partial V}{\partial p} \times \nabla\theta\right]}_{2} \tag{2}$$

Initially, a strong thermal gradient develops over the Piedmont as two baroclinic zones merge into one. Associated with this very strong boundary, is a very strong low-level wind shear. These two factors become extremely large in the low-levels along the baroclinic zone. As air parcels encounter this boundary, they are tilted, generate vorticity, and ascend rapidly. Thus, Term 2 (Eq. 4) is the key for the low-level initiation of severe weather. Also, the strong upper-level divergence (Term 1, Eq. 4) removes tremendous amounts of mass stretching the air column, generating more vorticity and maintaining the surface anomaly. Term 1 (Eq. 4) is calculated by adding the divergence at every 25 mb over the 375 to 200 mb layer. Term 2 (Eq. 4) wind shear is calculated over the 925-875 mb layer and thermal gradient is calculated on the 900 mb level. Finally, the buoyancy of the airmass is incorporated into the index by including the LI, shown below.

$$\mathrm{LI} = \mathrm{T}_{500} - \mathrm{T}_{\mathrm{Parcel}} \tag{3}$$

Where T_{500} is the 500 mb temperature (C) and $\mathrm{T}_{\mathrm{Parcel}}$ is the 500 mb temperature (C) of a lifted parcel with the average pressure, temperature and dewpoint of the layer in the lowest 100 mb above the surface. The DPBI is shown below.

$$\mathrm{DPBI} = \underbrace{\left(\sum_{375}^{200} \nabla \bullet \vec{\mathrm{V}}\right)}_{1} \cdot \underbrace{\left[-\hat{k} \bullet \left(\frac{\partial V}{\partial p} \times \nabla\theta\right)\right]}_{2} \cdot \underbrace{(-\mathrm{LI})}_{3} \tag{4}$$

Values over 15 correspond to tornadic activity. We expanded our investigation to encompass the previous 48 hours over the southeastern US. Figures 26a-f depict the DPBI for the event case and Figs. 27a-f depict the DPBI values for the non-event case. At 1200 UTC 26 November 1988 (Fig. 26a), the DPBI depicts large values (>15) over AR, TX and LA until 2200 UTC 26. Storm data (NOAA, 1988) indicates there were numerous F0, F1 and F2 intensity tornadoes over that area at that time. The last funnel cloud over that area (MS) was at 2120 UTC. At 2100 UTC the DPBI over MS is >15. The index decreased dramatically by 0000 UTC 27 November 1988 (Fig. 26b). After a period of time with low values (Figs. 26c-e) the values increase to over 15 at 0600 UTC 28 November 1988 over central NC. Over the entire 48 hour period of the non-event case, the maximum DPBI value is only 5. Storm data (NOAA, 1990) indicates there were no tornadoes over the southeast US for this time period. The DPBI predicts no severe weather over the Piedmont for the non-event (1800 UTC 25 to 0000 UTC 26 January 1990). Finally, the DPBI is being evaluated on a daily basis (Cram, personal communication, 1999).

8. Summary and conclusions

In the last six hours before the RDU tornado there was supergeostrophic upper-level flow over VA, NC and SC coastal region. At the same time, the PJ moved to the west of the Appalachian Mountains thus the PJ's right entrance region came in close proximity to the STJ's left exit region. The two associated transverse ageostrophic jet streak circulations were juxtaposed (phased) creating a region of intense ascent and strong upper-level divergence over the Carolina Piedmont. For the non-event case, a PJ extended from TX northeast to the North Atlantic Ocean. There was no STJ over the eastern US thus there could be no phasing of jet streaks as in the event case.

In the mid-levels of the event case, the warm Mexican air (>330 K) at 850 mb elevated the heights to the southeast of the mid-level jet. The elevated heights in the right exit region created a mid-level PGF and forced the continued development of the jet. The warm air also enabled the mid-level jet to be farther east than in a balanced QG system. As the jet accelerated it induced a thermally direct ageostrophic circulation. Thus, the ascent created by the ageostrophic circulation was over the warm MX air. This forcing mechanism was continually regenerated as the low-level baroclinic zone continued to develop and latent heating was generated by convection. By the time of the tornado outbreak, the mid-level jet had intensified greatly and moved between the PJ entrance region and the STJ exit region, which enhanced ascent. For the non-event case, a mid-level jet developed with the QG front/trough system over the Midwest US and propagated northeastward. In contrast to the event case, the warm air from MX (>330 K) at 850 mb

had not moved over the Carolina Piedmont. At the expected time of the non-event there was descent in the low-levels and very weak ascent in the mid-levels over the Piedmont.

The PV was examined for the last 6 hours for both the event and non-event. In the event case, the low-level PV maximum was closely related to the surface trough (across the Carolina Piedmont) and with the areas of maximum trough deepening. As the PV maximum approached RDU at the time of the tornado outbreak it was associated with a mesocyclone. The strongest PV was in the low-levels and the low-level PV maximum was disconnected from the upper-levels. Just as in the preceding 48 hours, the PV over the Carolina Piedmont was transported and/or generated in the low-levels. In the non-event, the low-level PV over NC and SC was very sporadic (generated in large part by diabatic effects associated with convection).

We also found a direct relationship between convective precipitation and low-level PV. Convection generates PV through diabatic heating; the low-level PV maxima increase, in large part, from latent heat energy associated with convection. One critical difference between these cases was that the event case had existing low-level PV maxima (traceable over the previous 72 hours) so convection was a maintainer rather than primary generator of PV. In the non-event case, convection was the primary generator of low-level PV over the Carolina Piedmont.

The mesoscale model-generated data indicated the potential for severe weather for the event case, which is something the forecasters did not have at that time. Simulation-produced LI, SRH, low-level shear and wind imbalance as measured by the thermal wind

were clearly different between the cases. All these indicators forecast the development of severe weather in the event case and not in the non-event case.

We developed a new divergence profile buoyancy index based on: large scale synoptic features (upper-level divergence); mesoscale features (low-level tilting effects which incorporate shear and thermal gradients); and the buoyancy of the airmass. We found values over 15 corresponded to tornadic activity over both the MO, AK, TX, LA and MS (early in the period) and over central NC (late in the period).

Overall, we found that low-level potential vorticity in the event case can be traced from RDU at the time of the tornado outbreak back to its origins (some 84 hours earlier). The low-level PV facilitated the tracking of a mesoscale surface trough that developed over the western Gulf of Mexico, propagated northeastward along the Gulf Coast States, developed (merged) into a surface cold front and moved over the Carolina Piedmont at the time of the tornado outbreak. *The STJ was crucial to this 3-day process. First, it transported stratospheric PV rich air to the south then downward to the mid-levels over the Mexican plateau. Second, its associated ageostrophic circulation created upper-level divergence (mass removal from the air column) that helped to maintain deep convection and the surface trough. Third, it phased with the PJ creating extreme upper-level divergence and ascent over the Carolina Piedmont.* At the same time, the warm low-level Mexican airmass propagated over the Gulf Coast States (southeast of the surface trough). The warm airmass was located to the southeast of the surface trough, and in conjunction with cold air advection to the northwest created an intense northwestward-

directed PGF and a mid-level jet. The mid-level jet entrance region had an associated thermally direct ageostrophic circulation, which enhanced ascent over the low-level trough. These features created an environment favorable to deep convection and the release of latent heat that helped to maintain the low-level trough (confluence zone) and PV as it propagated across the Gulf Coast. Additionally, the latent heating, associated with convection, helped create an unbalanced jet with a thermally direct circulation in the jet exit region. The direct circulation associated with the mid-level jet facilitated convection ahead of the surface (over the warm air). The latent heating from convection and surface sensible heating helped maintain the surface front. Cold air advection from the northwest further enhanced the strength of the front. As air parcels moved over this front, they encountered a very strong shear and thermal gradient, thus, they were tilted, generated vorticity and ascended rapidly.

Acknowledgements. I would like to thank the Air Force Institute of Technology for the opportunity to pursue my advanced degree. The authors wish to thank Drs Robert Rozumalski and Kenneth Waight III of MESO Inc. for access to and help with the MASS model.

9. References

Bluestein, H. B., 1993: Synoptic-Dynamic Meteorology in Midlatitudes, Volume II Observations and Theory of Weather Systems, Oxford University Press, 594 pp.

Davies-Jones, R., D. Burgess, and M. Foster, 1990: Test of helicity as a forecast parameter. *Preprints*, 16th Conf. Severe Local Storms, Kananaskis, Alberta, Amer. Meteor. Soc., 588-592.

Egentowich, J. M., M. L. Kaplan, Y.-L. Lin and A. J. Riordan, 1999a: Mesoscale simulations of dynamical factors discriminating between a tornado outbreak and non-event over the southeast US part I: 84 - 48 hour precursors. Submitted to *Weather and Forecasting*.

Egentowich, J. M., M. L. Kaplan, Y.-L. Lin and A. J. Riordan, 1999b: Mesoscale simulations of dynamical factors discriminating between a tornado outbreak and non-event over the southeast US part II: 48 - 6 hour precursors. Submitted to *Weather and Forecasting*.

Gidel L. T., and M. A. Shapiro, 1979: The role of clear air turbulence in the production of potential vorticity in the vicinity of upper tropospheric jet stream-frontal systems. *J. Atmos. Sci.*, **36**, 2125-2138.

Gonski, R. F., B. P. Woods, and W. D. Korotky, 1989: The Raleigh tornado - 28 November 1988: An operational perspective. Preprints, *12th Conf. on Weather Analysis and Forecasting*, Monterey, CA Amer. Meteor. Soc., 173-178.

Gyakum J. R., Y.-H. Kuo, Z. Guo, and Y-R Guo, 1995: A case of rapid continental mesoscale cyclogenesis. Part II: Model and observational diagnosis. *Mon. Wea. Rev.*, **123**, 998-1024.

Hamilton, D. W., Y. L. Lin, R. P. Weglarz, and Kaplan, M. L., 1998: Jetlet formation from diabatic forcing with applications to the 1994 Palm Sunday tornado outbreak. *Mon. Wea. Rev.*, **126**, 2061-2089.

Kaplan, M. L., and D. A. Paine, 1977: The observed divergence of the horizontal velocity field and pressure gradient force at the mesoscale. It's implications for the parameterization of three-dimensional momentum transport in synoptic-scale numerical models. *Beitr. Phy. Atmos.*, **50**, 321-330.

Kaplan, M. L., V. M. Karyampudi, 1992: Meso-beta numerical simulation of terrain drag-induced along stream circulations. Part I: Midtropospheric frontogenesis. *Meteor. Atmos. Phys.*, **49**, 133-156.

Kaplan, M. L., V. M. Karyampudi, 1992: Meso-beta numerical simulation of terrain drag-induced along stream circulations. Part II: Concentration of potential vorticity within dryline bulges. *Meteor. Atmos. Phys.*, **49**, 157-185.

Kaplan, M. L., J. W. Zack, V. C. Wong, and J. J. Tuccillo, 1982a: Initial results from a mesoscale atmospheric simulation system and comparisons with the AVE-SESAME I data set. *Mon. Wea. Rev.*, **110**, 1564-1590.

Kaplan, M. L., R. A. Rozumalski, R. P. Weglarz, Y. L. Lin, S Businger, and R. F. Gonski, 1995: Numerical simulation studies of the mesoscale environment conductive to the Raleigh tornado. *NOAA Tech. Memo ER-90*, 1-101.

Karyampudi, V. M., M. L. Kaplan, S. E. Koch, and R. J. Zamora, 1995. The influence of the Rocky Mountains on the 13-14 April 1986 severe weather outbreak. Part 1: Mesoscale lee cyclogenesis and its relationship to severe weather and dust storms. *Mon. Wea. Rev.*, **123**, 1394-1422.

Lin, Y.-L., and T.-A. Wang, 1996: Flow regimes and transient dynamics of two-dimensional stratified flow over an isolated mountain ridge. *J. Atmos. Sci.*, **53**, 139-158.

MESO, 1995: MASS Version 5.8 Reference Manual, MESO, Inc., Troy, NY, 119 pp.

NOAA, 1990: Storm data, **32, 01**, 66 pp.

NOAA, 1988: Storm data, **30, 11,** 72 pp.

Zehnder, J. A., and D. Keyser, 1991: The influence or interior gradients of potential vorticity on rapid cyclogenesis. *Tellus*, **43A**, 198-212.

Table 1. Forward trajectory initiated at 0000 UTC 28 November 1988 and ending at 0400 UTC 28 November 1988. Trajectory data is derived from 12 km full physics MASS model run. The following abbreviations are defined: Latitude (LAT), Longitude (LON), Pressure (PRS), Coriolis force vector (CO), Pressure gradient force vector (PGF), Lagrangian Rossby Number (Ro_L), Nonlinear balance form of the divergence equation (NBE), Total Wind (V_t), Omega (OMGA), and divergence computed on a theta surface (DIV).

Time (UTC)	LAT (°N)	LON (°W)	PRS (mb)	CO $x10^{-3}ms^{-2}$ speed/dir	PGF $x10^{-3}ms^{-2}$ speed/dir	NBE Total $x10^{-8}s^{-1}$	V_{total} (ms^{-1}) speed/dir	Ro_L	OMGA mcbr/s	Div $(x10^{-5})$
28/0000	33.5	84.5	600	3.04/319	2.34/129	-3.920	38.6/229	****	-1.075	-6.548
28/0030	33.91	83.93	592	3.14/319	3.48/141	3.405	38.6/228	0.736	-6.26	-0.999
28/0100	34.33	83.33	590	3.27/320	4.2/148	14.73	39.8/230	0.794	5.128	-2.201
28/0130	34.76	82.73	596	3.33/319	4.65/145	18.63	40.0/229	0.696	3.484	0.959
28/0200	35.19	82.13	598	3.41/317	9.57/127	12.32	40.6/227	0.714	-2.97	-2.418
28/0230	35.65	81.54	596	3.54/314	2.88/137	-27.63	41.6/224	1.754	-8.53	-6.504
28/0300	36.13	80.94	584	3.71/314	5.3/160	10.416	43.2/224	1.31	-26.04	-0.546
28/0330	36.64	80.32	544	4.16/314	4.29/173	15.82	47.7/224	2.567	-23.37	18.54
28/0400	37.19	76.69	490	4.30/313	4.08/143	-2.248	48.8/223	2.002	-26.43	10.73

Table 2. Same as Table 1 except trajectory is initiated at 1200 UTC 25 January 1990 and ending 1600 UTC 25 January 1990.

Time (UTC)	LAT (°N)	LON (°W)	PRS (mb)	CO $x10^{-3}ms^{-2}$ speed/dir	PGF $x10^{-3}ms^{-2}$ speed/dir	NBE Total $x10^{-8}s^{-1}$	V_{total} (ms^{-1}) speed/dir	Ro_L	OMGA mcbr/s	Div $(x10^{-5})$
25/1200	33.50	84.25	600	2.7/323	3.73/145	-9.886	33.6/233	***	-6.229	1.093
25/1230	33.84	83.73	584	2.76/322	2.44/137	1.465	34/231	0.117	-14.678	6.743
25/1300	34.20	83.2	560	2.88/319	4.5/192	1.431	35.1/229	0.291	-8.14	2.893
25/1330	34.57	82.67	550	2.99/320	3.43/158	4.435	36.1/230	0.089	-5.452	1.532
25/1400	34.95	82.11	547	3.07/321	3.27/150	-5.25	36.7/231	0.196	-3.654	3.168
25/1430	35.32	81.54	537	3.14/322	2.34/122	2.227	37.3/232	0.370	-4.803	1.442
25/1500	35.68	80.95	527	3.21/323	2.35/122	3.814	37.8/233	0.450	-2.701	1.762
25/1530	36.05	80.35	519	3.23/323	2.99/134	4.750	37.6/234	0.416	-1.178	-0.967
25/1600	36.40	79.75	518	3.19/324	2.88/138	3.903	36.9/236	0.364	-1.058	-2.067

Table 3. Forward trajectory initiated at 0000 UTC 28 November 1988, originating at the same location as previous parcel and ending at 0400 UTC 28 November 1988. Trajectory data is derived from 24 km MASS simulation without latent heating. The following abbreviations are defined: Latitude (LAT), Longitude (LON), Pressure (PRS), Temperature (TMP), Total Wind (V_t), Pressure gradient force vector (PGF), Coriolis force vector (COR) and Lagrangian Rossby Number (RO_L).

Time (UTC)	LAT (°N)	LON (°W)	PRS (mb)	TMP (°C)	V_{total} (ms^{-1}) speed/dir	PGF $x10^{-3}$ ms^{-1}	COR $x10^{-3}ms^{-2}$	Ro_L
28/0000	33.5	84.5	600	-4.04	32.3/228	2.92/149	2.6/319	****
28/0100	34.21	83.53	591	-5.14	34/228	2.63/151	2.79/318	0.455
28/0200	34.96	82.51	588	-5.38	35.3/228	4.63/154	2.95/318	0.256
28/0300	35.75	81.45	579	-6.72	37.1/228	2.63/143	3.16/318	0.266
28/0400	36.57	80.33	577	-6.79	38.3/228	3.73/128	3.32/318	0.084

Table 4. Trajectory initialized at 0400 UTC 28 November 1988, passed over RDU at 0600 UTC and ended at 0700 UTC 28 November 1988. Trajectory data are hourly and were derived from a 24 km MASS simulation. The following abbreviations are defined: Latitude (LAT), Longitude (LON), Pressure (PRS), Temperature (TMP) and Potential vorticity (PV).

Time (UTC)	LAT (°N)	LON (°W)	PRS (mb)	TMP (°C)	PV (PV units)
0400/28	35.0	79.6	951	19.98	1.302
0500/28	35.7	79.17	944	19.45	2.906
0600/28	36.3	78.7	898	14.70	3.647
0700/28	36.9	78.0	846	11.68	2.092

Table 5. Same as Table 4 except trajectory initiated at 1600 UTC 25 January 1990 and ended at 2000 UTC 25 January 1990.

Time (UTC)	LAT (°N)	LON (°W)	PRS (mb)	TMP (°C)	PV (PV units)
1600/25	34.3	79.9	903	15.82	0.014
1700/25	34.9	79.2	901	15.52	0.035
1800/25	36.5	78.5	900	15.43	0.122
1900/25	36.2	77.7	899	14.75	0.405
2000/25	36.8	77.0	907	14.96	0.471

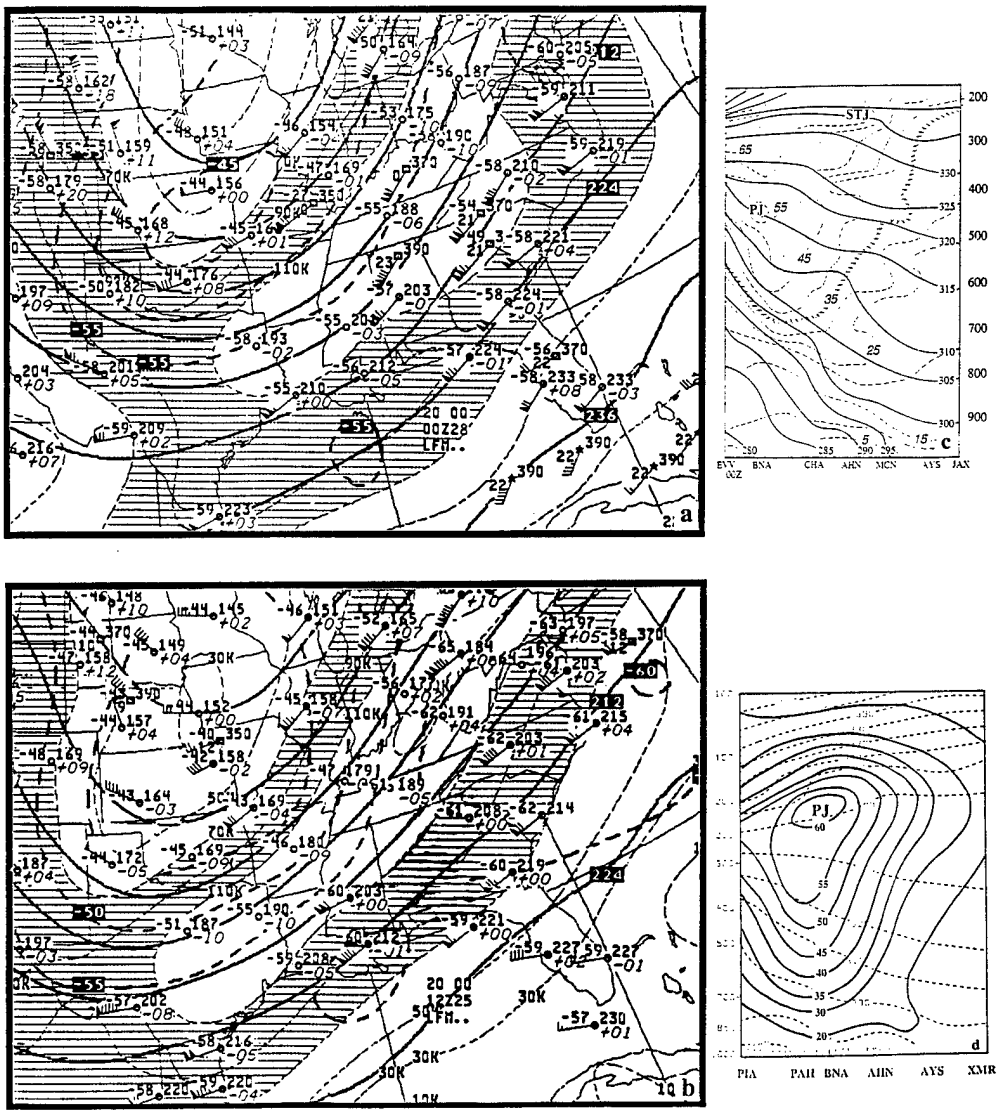

FIG. 1. (a) NWS 200 mb analysis of isotachs (knots) and vectors, temperature (C) and height (dm) and (c) observationally derived cross section from Evansville, IN (EVV) to Jacksonville, FL (JAX), isotachs (dashed line, ms^{-1}) and θ (solid line, K) valid at 0000 UTC 28 November 1988. (b) NWS 200 mb analysis of isotachs (knots) and vectors, temperature (C) and height (dm) and (d) observationally derived cross section from Peoria, IL (PIA) to Cape Kennedy, FL (XMR) isotachs (solid line, ms^{-1}) and θ (dashed line, K) valid at 1200 UTC 25 January 1990.

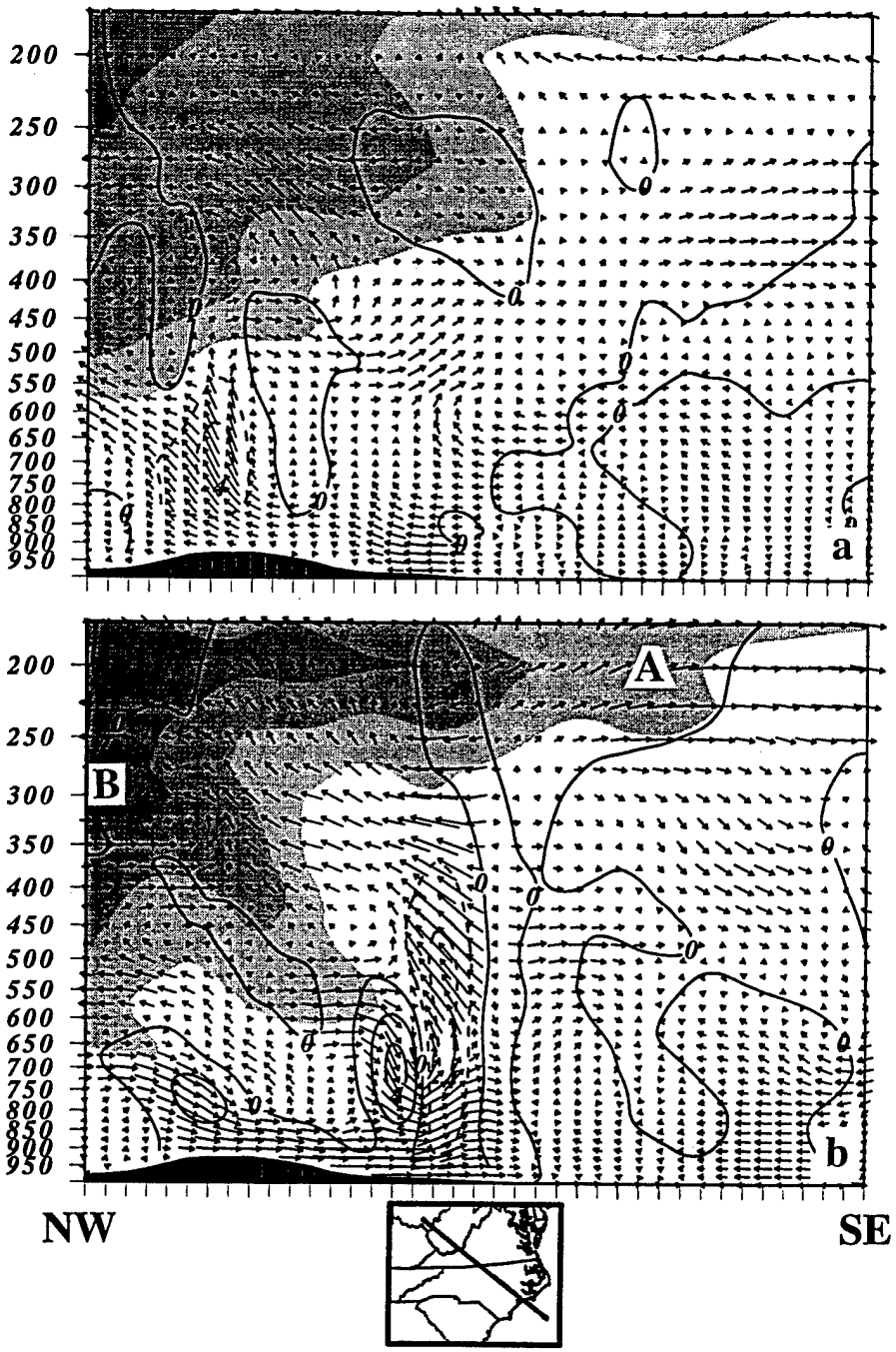

FIG. 2. MASS simulated, 24 km mesh, cross sections extending from (38N, 93W) to (33N, 75W). Including ageostrophic wind vectors, wind isotachs (shaded at intervals of 10 for speeds greater than 40), and vertical velocity (contoured every 20 μbs^{-1}, solid lines indicate descent and dashed lines indicate ascent) valid at (a) 0100 UTC and (b) 0600 UTC 28 November 1988. A denotes the STJ and B denotes the PJ.

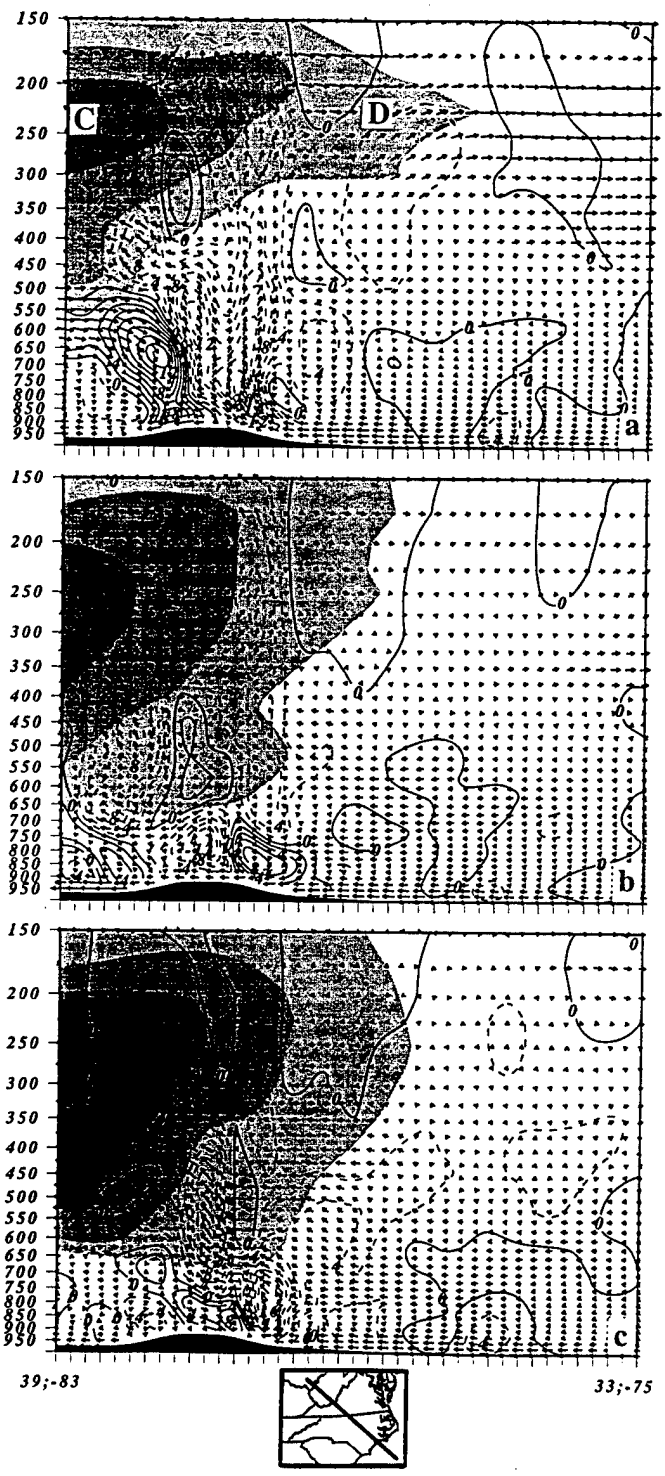

FIG. 3. MASS simulated, 24 km mesh, cross sections extending from (38N, 93W) to (33N, 75W). Including ageostrophic wind vectors, wind isotachs (shaded at intervals of 10 for speeds greater than 40 ms^{-1}), and vertical velocity (contoured every 20 μbs^{-1}, solid lines indicate descent & dashed lines indicate ascent) valid at (a) 1300 UTC 25, (b) 1800 UTC 25 and (c) 0000 UTC 26 January 1990. D denotes the STJ and C denotes the PJ.

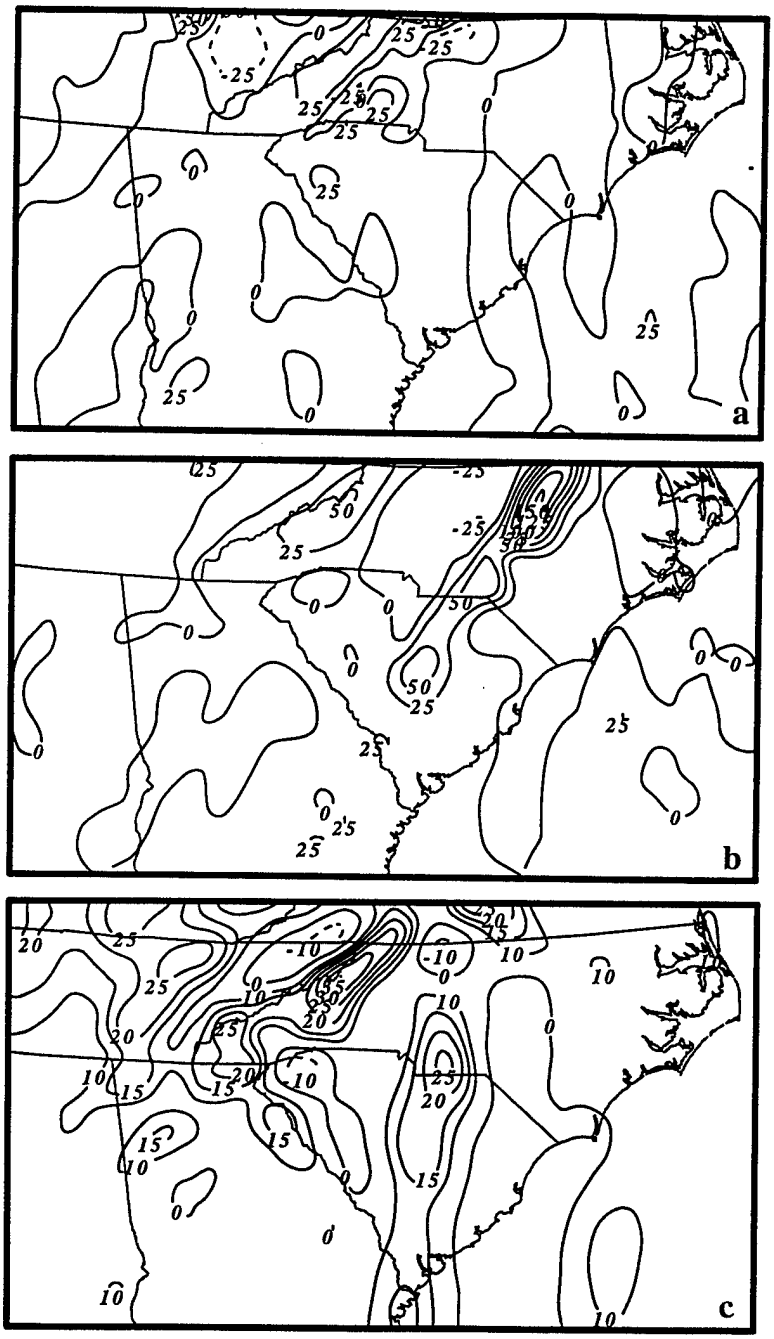

FIG. 4. MASS simulated, 12 km mesh, integrated divergence over the 375 to 200 mb layer (solid lines indicate divergence and dashed lines indicate convergence, $x10^{-5}s^{-1}$) valid at (a) 0300 UTC, (b) 0600 UTC and (c) MASS simulated divergence field at 0600 UTC 28 November 1988 with convection deactivated.

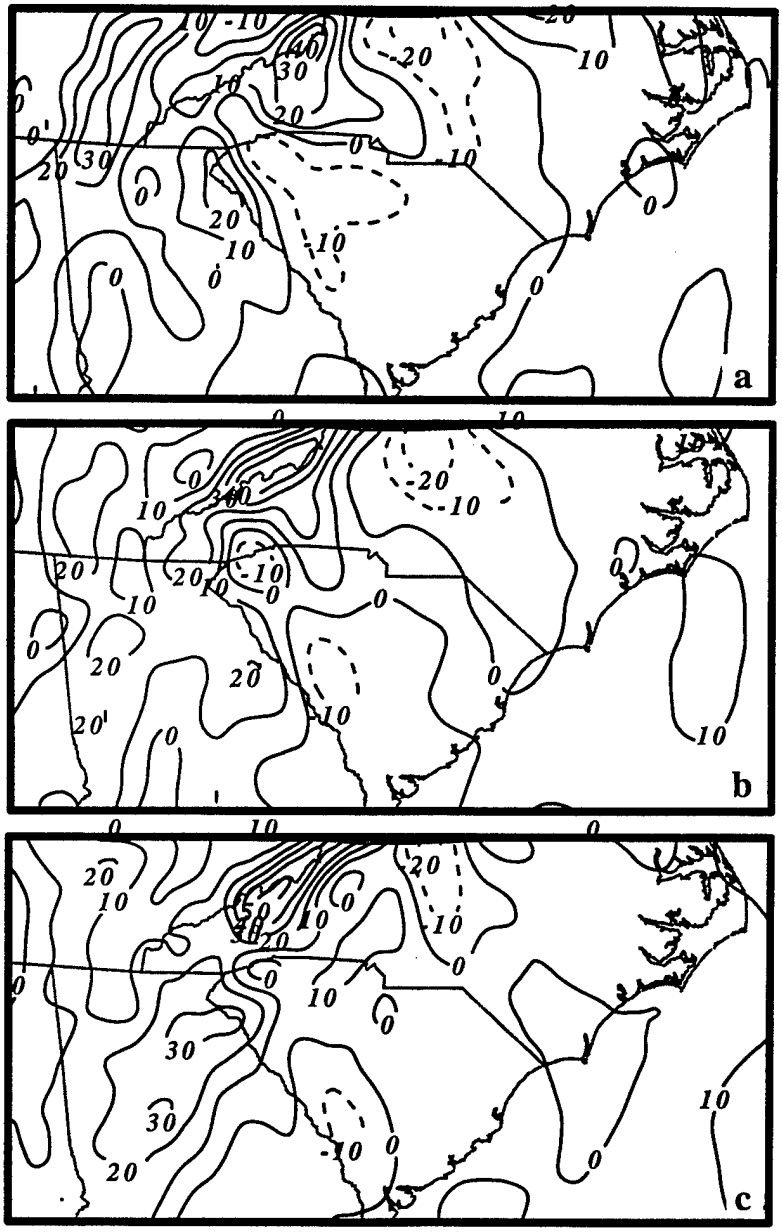

FIG. 5. MASS simulated, 12 km mesh, integrated divergence over the 375 to 200 mb layer (solid lines indicate divergence and dashed lines indicate convergence, $x10^{-5}s^{-1}$) valid at (a) 1800 UTC 25, (b) 2100 UTC 25 and (c) 0000 UTC26 January 1990.

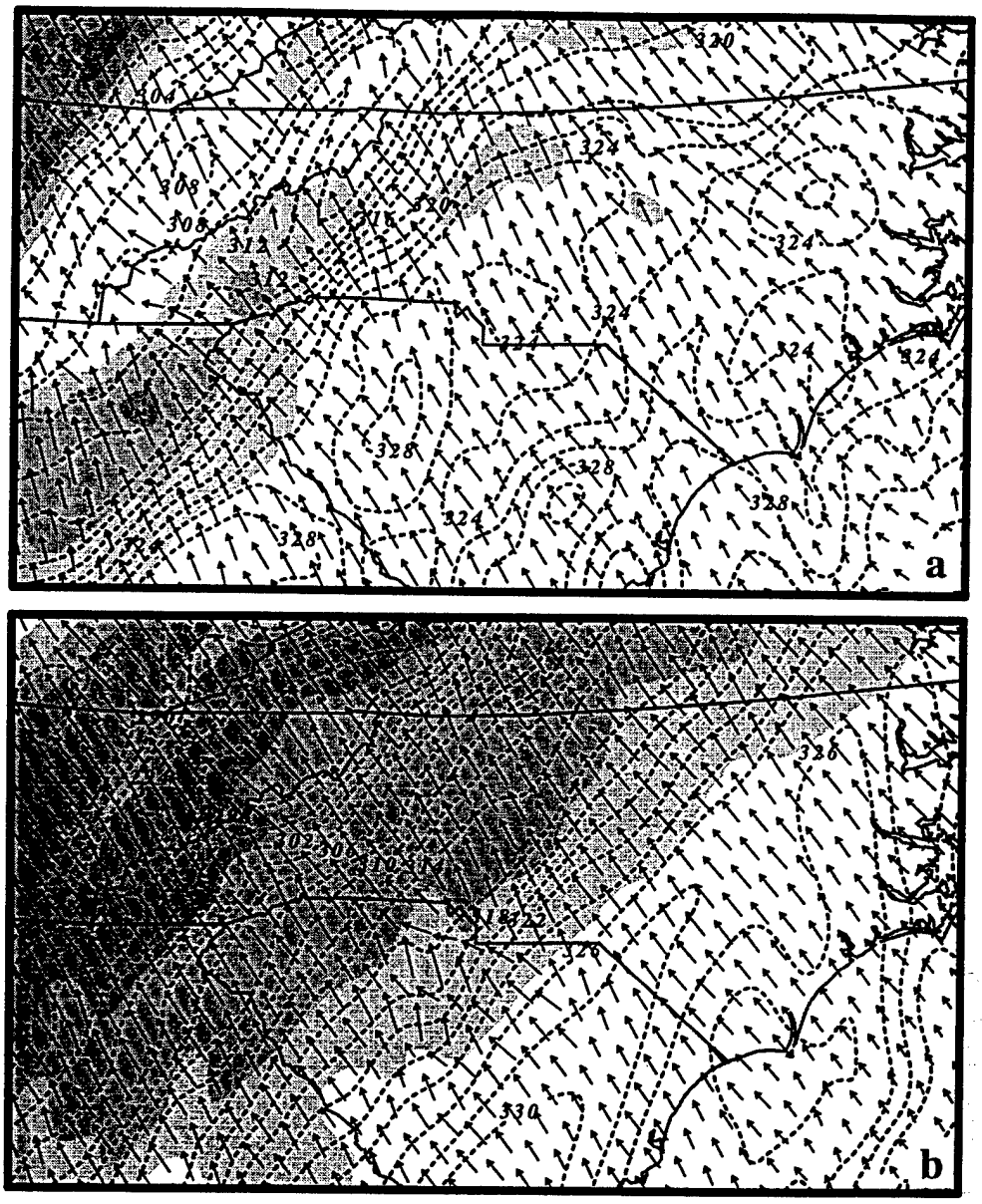

FIG. 6. MASS simulated, 12 km mesh, 600 mb, wind isotachs (shaded at intervals of 5 for speeds greater than 35 ms^{-1}), pressure gradient force vectors (ms^{-2}) and 850 mb θ_e (dashed lines, K) valid at (a) 0000 UTC and (b) 0600 UTC 28 November 1988.

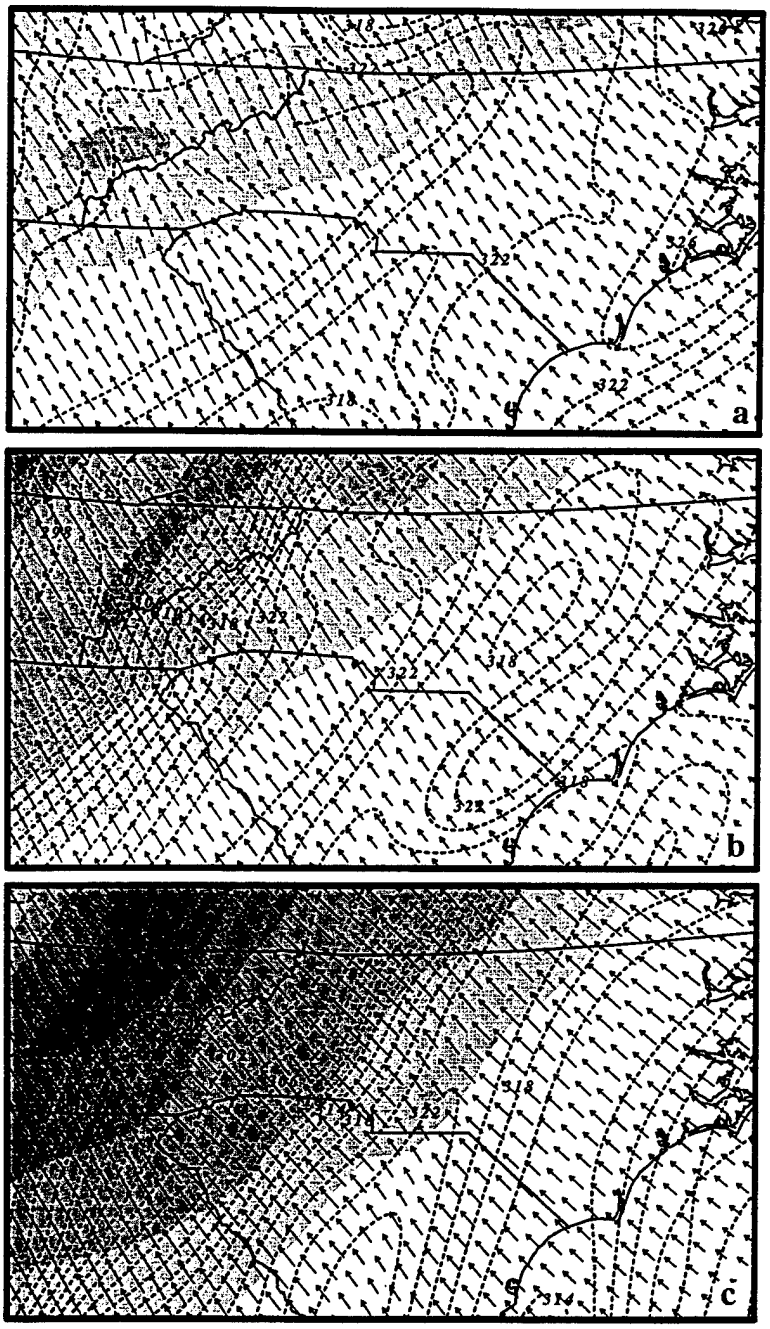

FIG. 7. MASS simulated, 12 km mesh, 600 mb, wind isotachs (shaded at intervals of 5 for speeds greater than 35 ms^{-1}), θ_e (dashed lines, K), and pressure gradient force vectors (ms^{-2}) valid at (a) 1200 UTC, (b) 1800 UTC 25 and (c) 0000 UTC 26 January 1990.

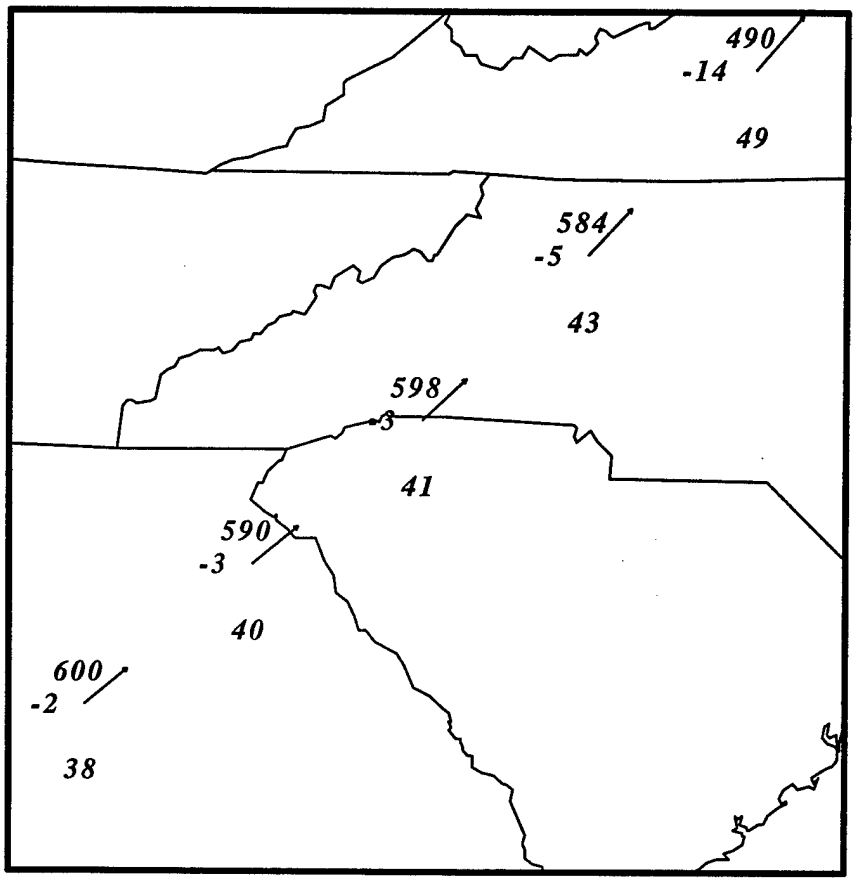

FIG. 8. Trajectory constructed from the 12 km MASS simulation initialized at 0000 UTC and ended at 0400 UTC 28 November 1988. Station plots contain pressure (mb), temperature (C), and total wind speed (ms^{-1}). Displayed wind vectors depict total wind.

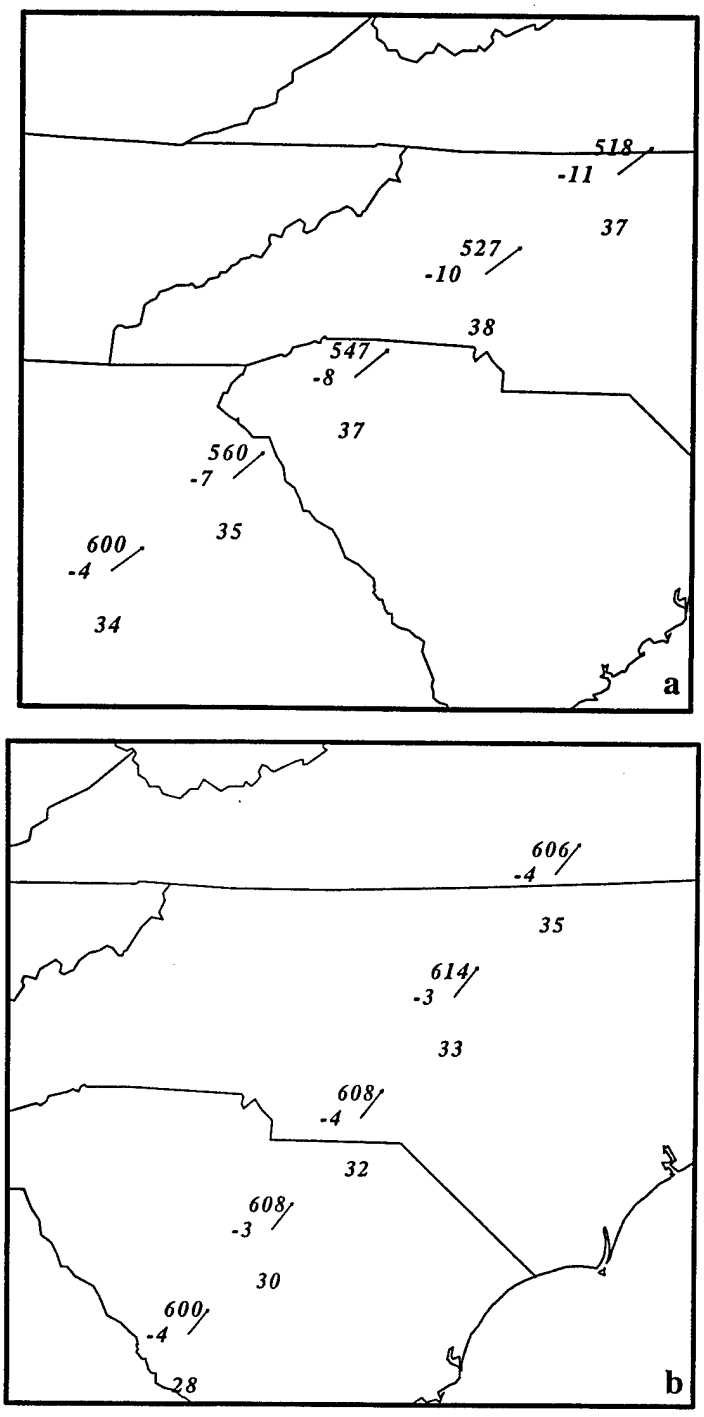

FIG. 9. Trajectories constructed from the 12 km MASS simulation. Station plots contain pressure (mb), temperature (C), and total wind speed (ms^{-1}). Displayed wind vectors depict total wind. Parcels initialized at (a) 1200 UTC and ended 1400 UTC 25 January 1990 and (b) 1800 UTC and ended 2200 UTC 25 January 1990.

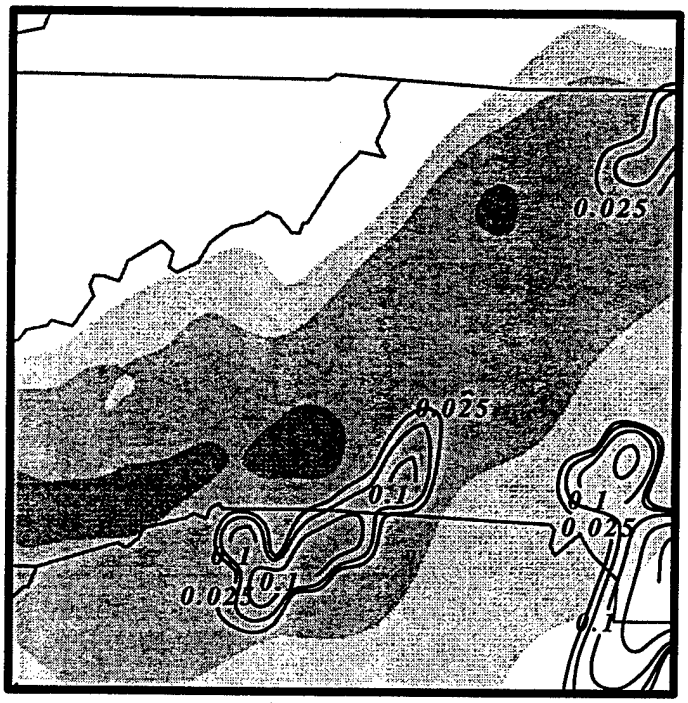

FIG. 10. MASS simulated, 12 km mesh, 600 mb, wind isotachs (shaded at intervals of 5 for speeds greater than 35 ms^{-1}) and convective precipitation (solid lines, contoured at 0.025, 0.05, 0.1 and 0.15, mm/0.5h) valid at 0200 UTC 26 November 1988.

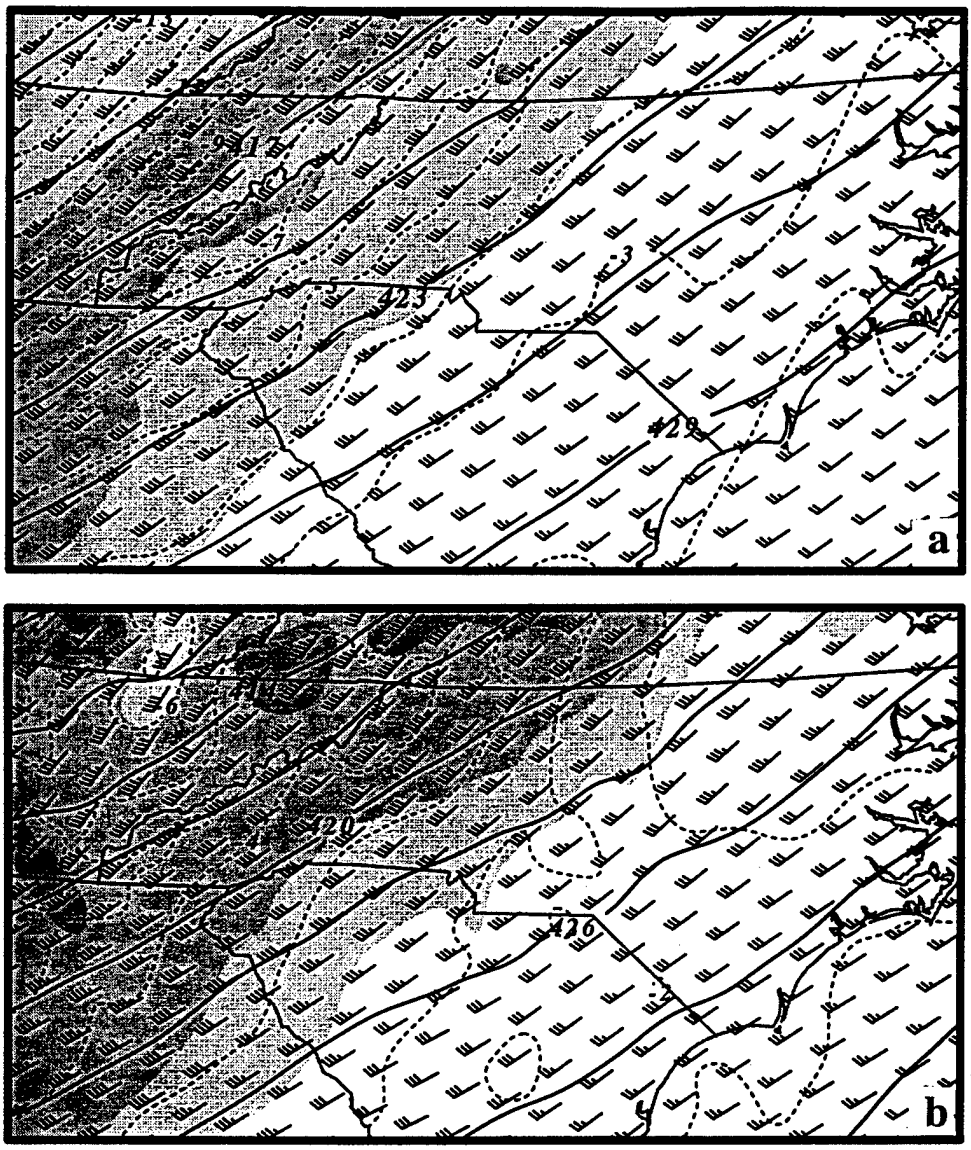

FIG. 11. MASS simulated, 12 km mesh, 600 mb, wind isotachs and vectors (shaded at intervals of 5 for speeds greater than 35 ms^{-1}), temperature (dashed lines, C), and height (solid lines, dm) valid at 0600 UTC 28 November 1988 (a) without latent heating and (b) with latent heating.

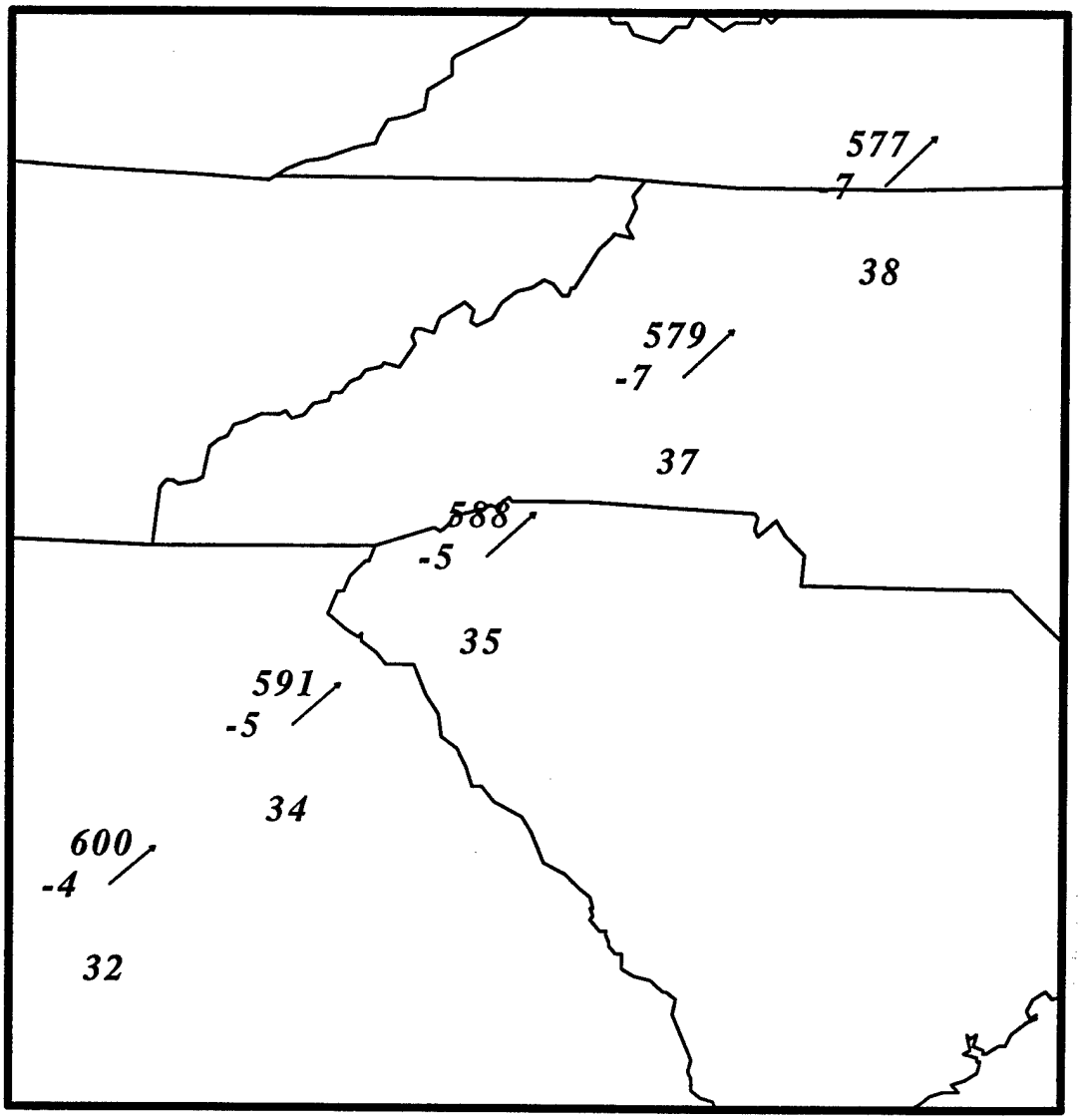

FIG. 12. Trajectory constructed from the 12 km MASS simulation without latent heating. Station plots contain pressure (mb), temperature (C), and total wind speed (ms^{-1}). Displayed wind vectors depict total wind. Parcels are initialized at 0000 UTC and ended 0400 UTC 28 November 1988.

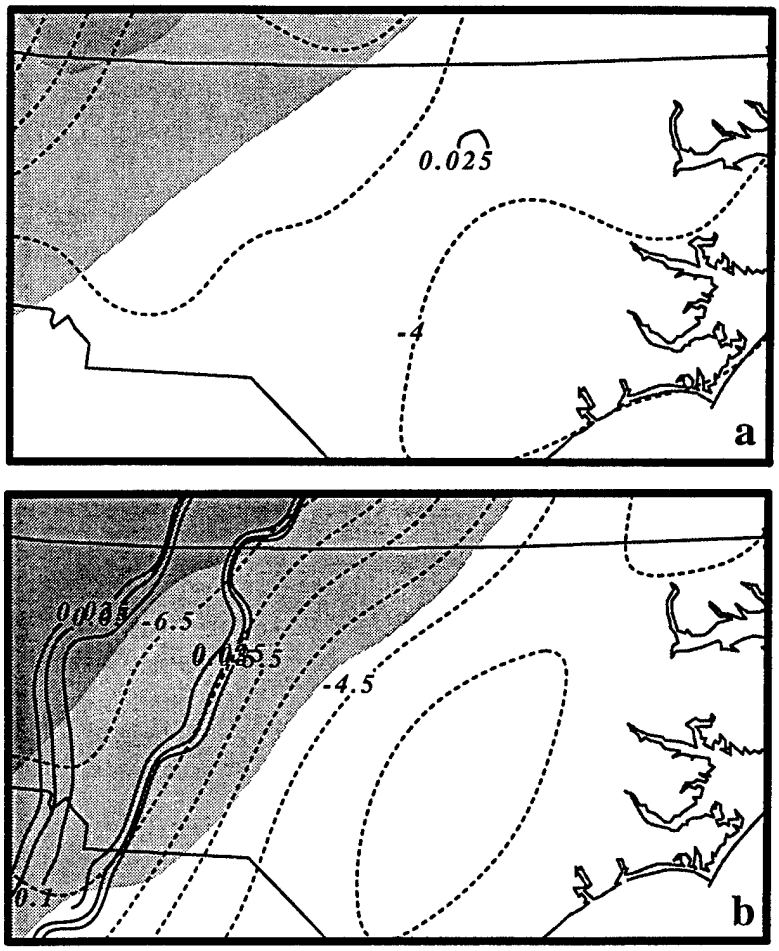

FIG. 13. MASS simulated, 12 km mesh, 600 mb, wind isotachs (shaded at intervals of 5 for speeds greater than 35 ms^{-1}), surface convective precipitation (solid lines, contoured 0.025, 0.05, and 0.1, mm/0.5h) and temperature (dashed lines, C) valid at (a) 1800 UTC 25 and (b) 0000 UTC 26 January 1990.

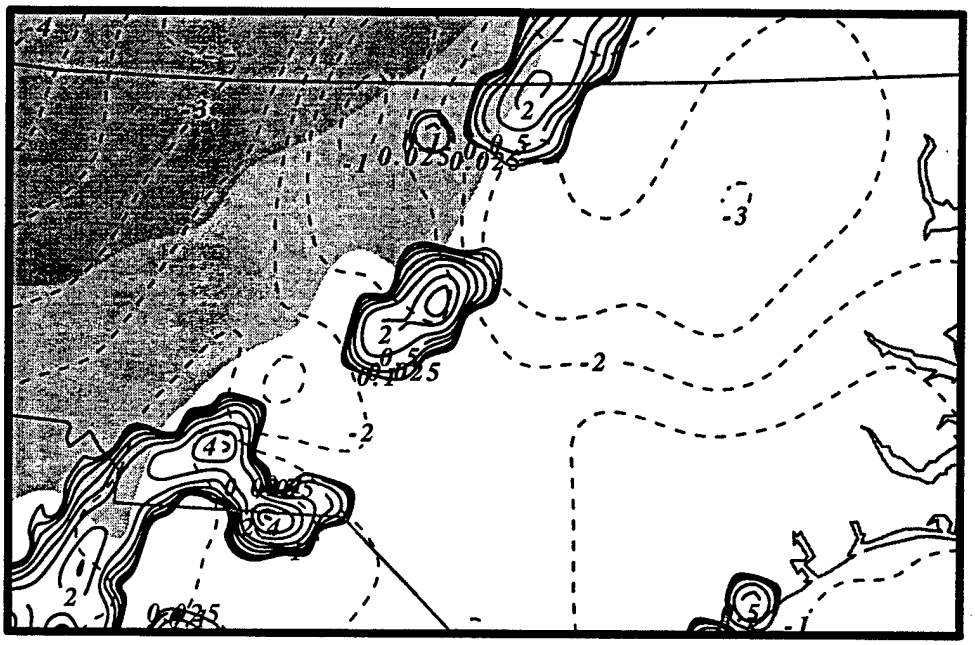

FIG. 14. MASS simulated, 12 km mesh, 600 mb, wind isotachs (shaded at intervals of 5 for speeds greater than 35 ms^{-1}), temperature (dashed lines, C), and surface convective precipitation (solid lines, contoured 0.01, 0.025, 0.05, 0.1, 0.2, 0.3 and 0.4, mm/0.5h) valid at 0600 UTC 28 November 1988.

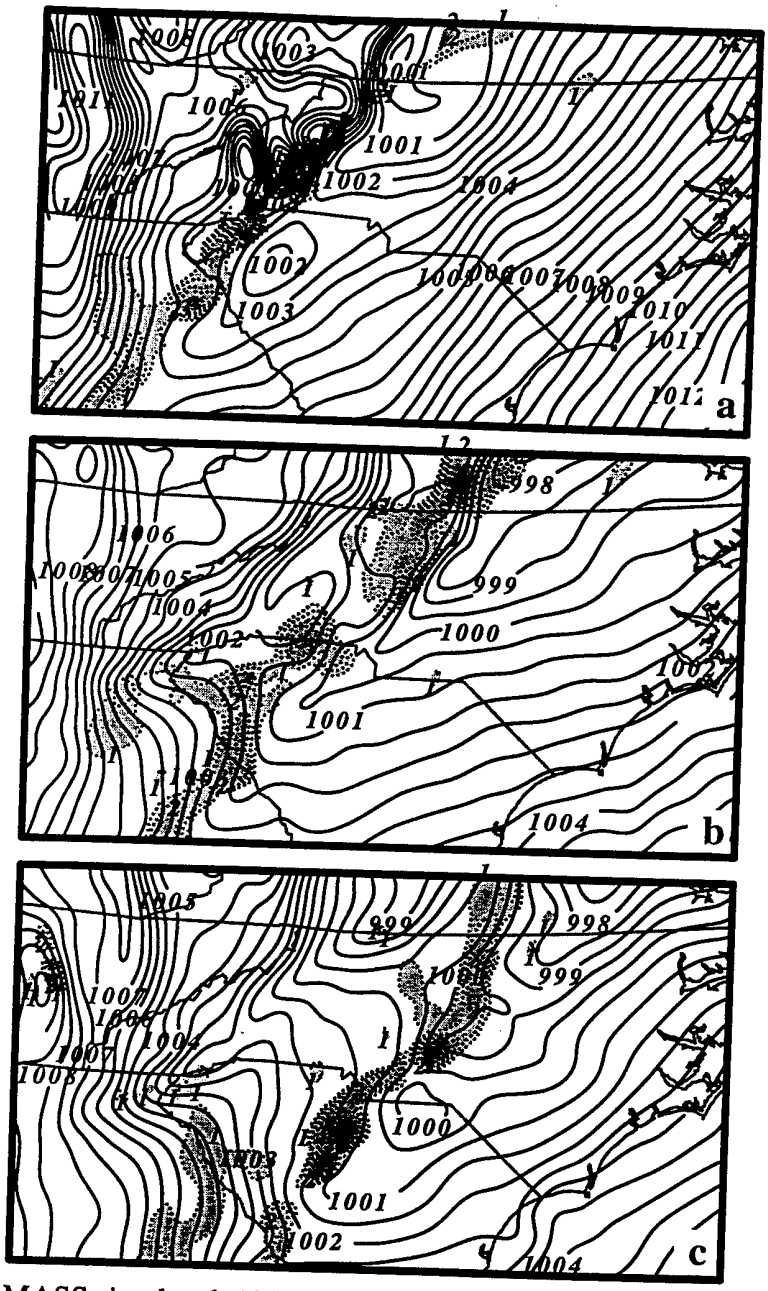

FIG. 15. MASS simulated, 12 km mesh, 900 mb PV (shaded greater than 1 by 0.5 PV units) and mean sea level pressure (solid lines, mb) valid at (a) 0200 UTC (b) 0400 UTC and (c) 0600 UTC 28 November 1988.

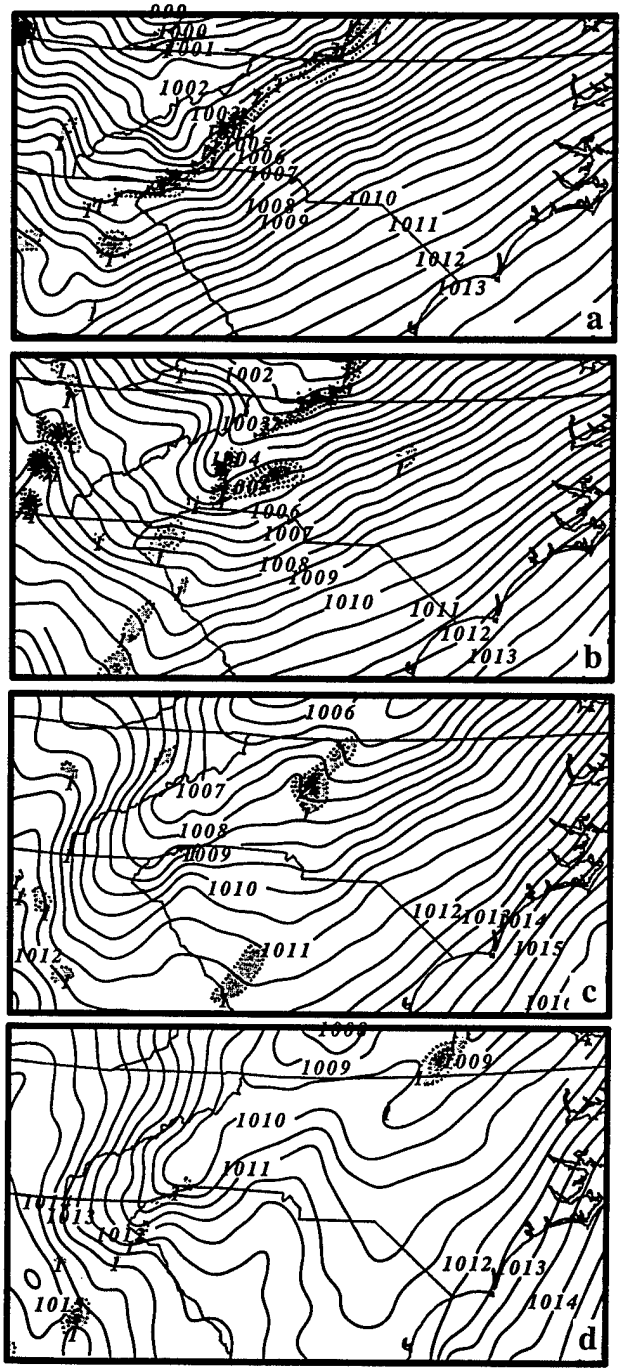

FIG. 16. MASS simulated, 12 km mesh, 900 mb PV (shaded greater than 1 by 0.5 PV units) and mean sea level pressure (solid lines, mb) valid at (a) 1500 UTC 25, (b) 1800 UTC 25, (c) 2100 UTC 25 and (d) 0000 UTC 26 January 1990.

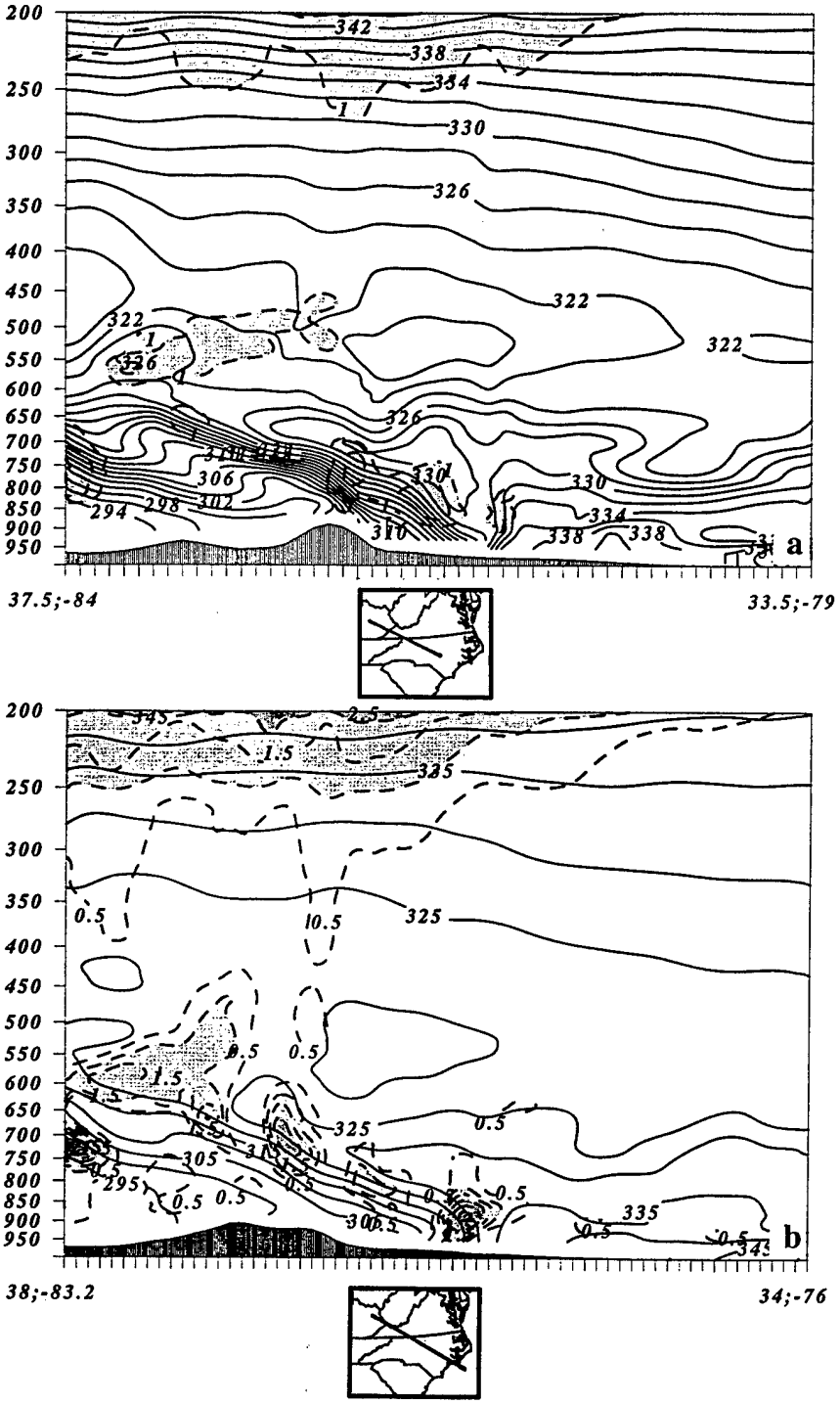

FIG. 17. MASS simulated, 12 km mesh, cross sections of θ_e (solid lines, K) and PV (contoured by 0.5 and shaded greater than 1 PV units) (a) from (37.5N, 84W) to (33.5N, 79W) valid at 0400 UTC 28 November 1988 and (b) from (38N, 83.2W) to (34N, 76W) valid at 0600 UTC 28 November 1988.

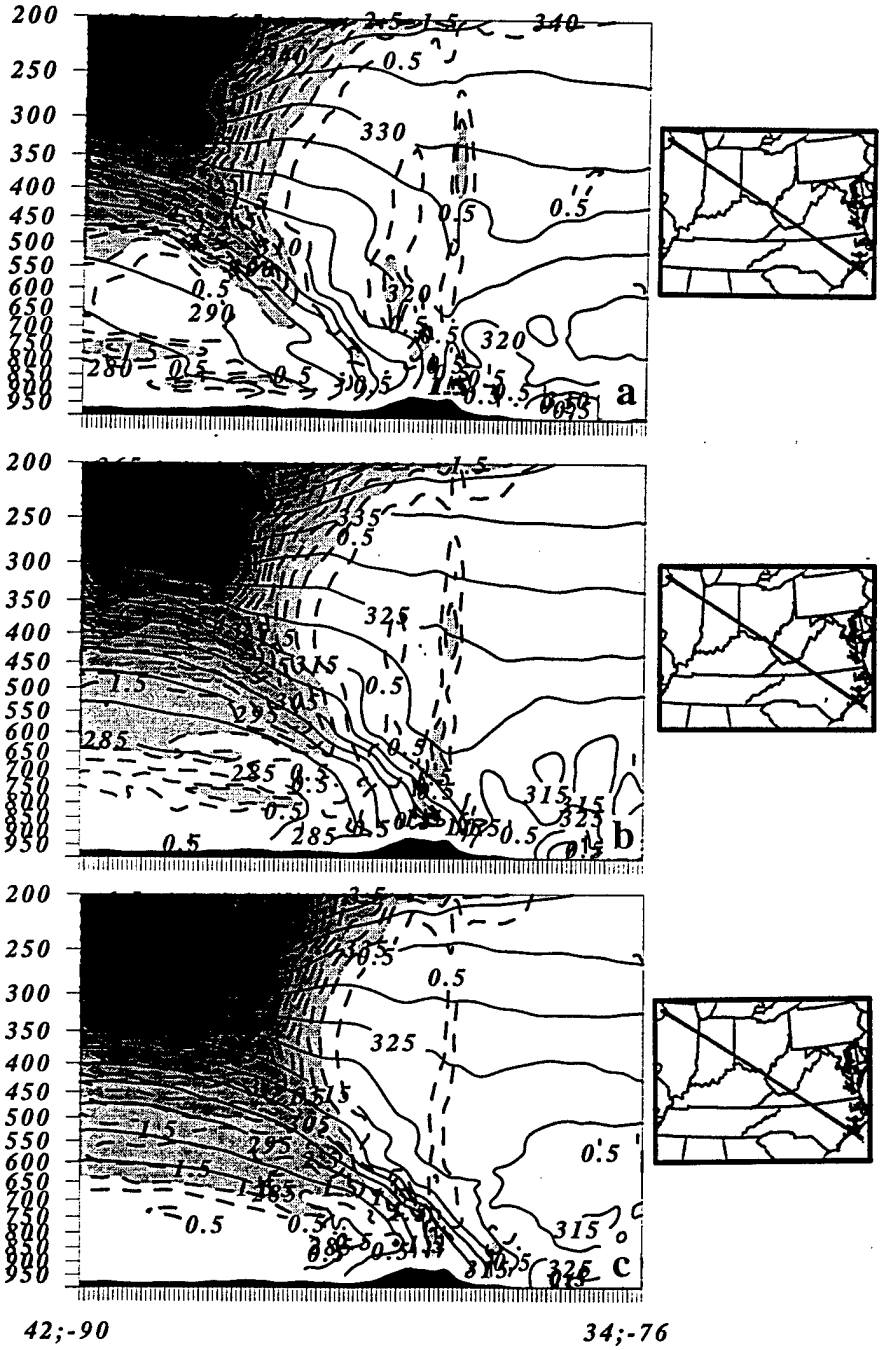

FIG. 18. MASS simulated, 12 km mesh, cross section from 42N, 90W to 34N, 76W. Including, θ_e (solid lines, K) and PV (contoured by 0.5 and shaded greater than 1 PV units) valid at (a) 1800 UTC 25, (b) 2100 UTC 25 and (c) 0000 UTC 26 January 1990.

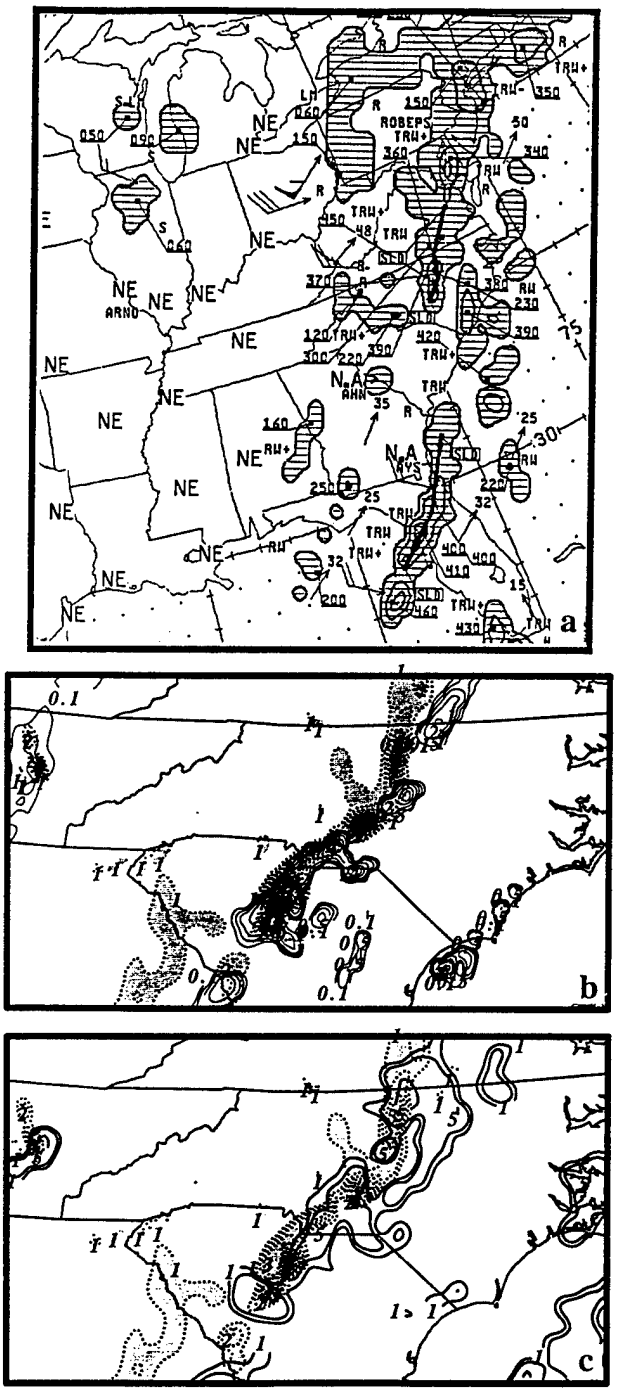

FIG. 19. (a) NWS radar summary for 0635 UTC 28 November 1988, (b) MASS simulated, 12 km mesh, 900 mb PV (contoured by 0.5 and shaded greater than 1 PV units) and surface convective precipitation (contoured 0.1, 0.5, 0.1, 0.2, 0.3, 0.4 and 0.5, mm/0.5h) and (c) 900 mb PV (contoured by 0.5 and shaded greater than 1 PV units) and latent heating (contoured at 1, 2 and 5 C h^{-1}) valid at 0600 UTC 28 November 1988.

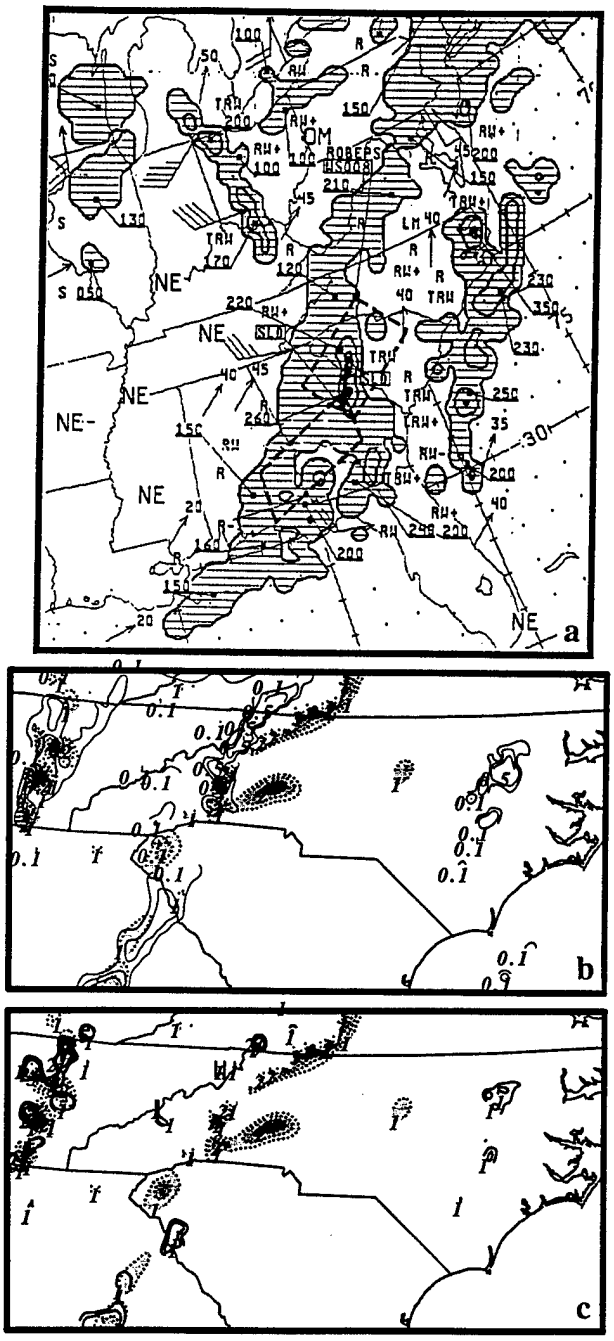

FIG. 20. (a) NWS radar summary for 1735 UTC 25 January 1990, (b) MASS simulated, 12 km mesh, 900 mb PV (contoured by 0.5 and shaded greater than 1 PV units) and surface convective precipitation (contoured 0.1, 0.5, 0.1, 0.2, 0.3, 0.4 and 0.5, mm/0.5h) and (c) 900 mb PV (contoured by 0.5 and shaded greater than 1 PV units) and latent heating (contoured at 1, 2 and 5 C h^{-1}) valid at 1800 UTC 25 January 1990.

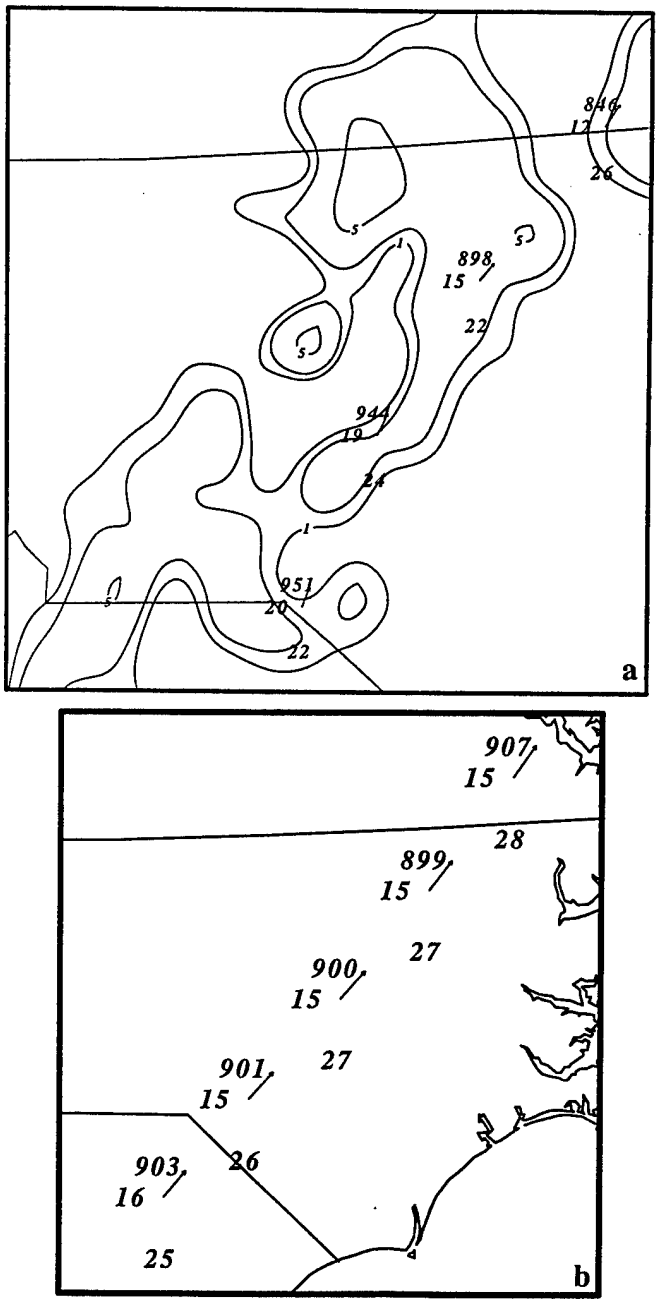

FIG. 21. MASS simulated, 12 km mesh, trajectory and 900 mb latent heating (contoured at 1, 2 and 5Ch^{-1}). Station plots contain pressure (mb), temperature (C), and total wind speed (ms^{-1}). Displayed wind vectors depict total wind (a) from 0400 to 0700 UTC 28 November 1988 and (b) from 1600 to 2000 UTC 25 January 1990.

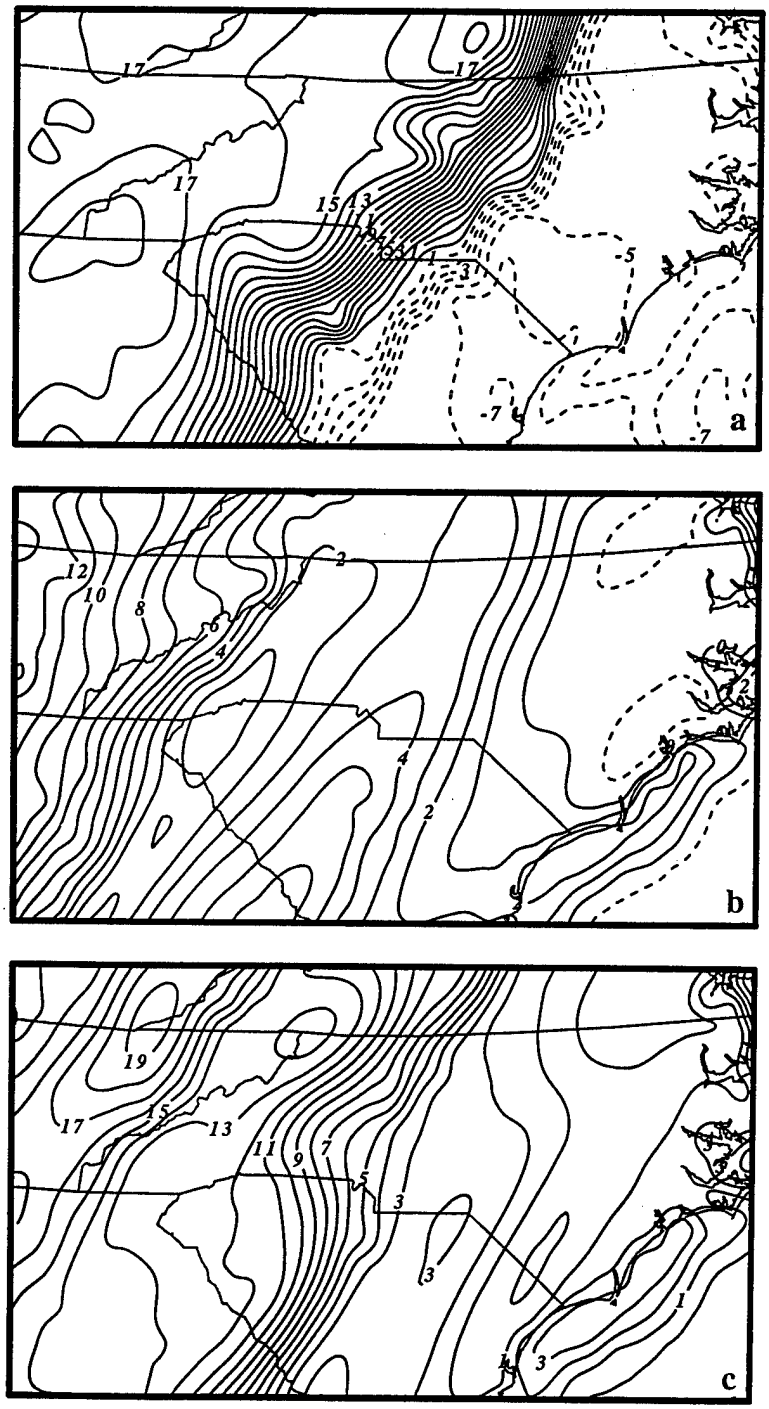

FIG. 22. MASS simulated, 12 km mesh, Lifted Index values (solid lines indicate positive values and dashed lines indicate negative values) valid at (a) 1800 UTC 28 November 1988, (b) 1800 UTC 25 and (c) 0000 UTC 26 January 1990.

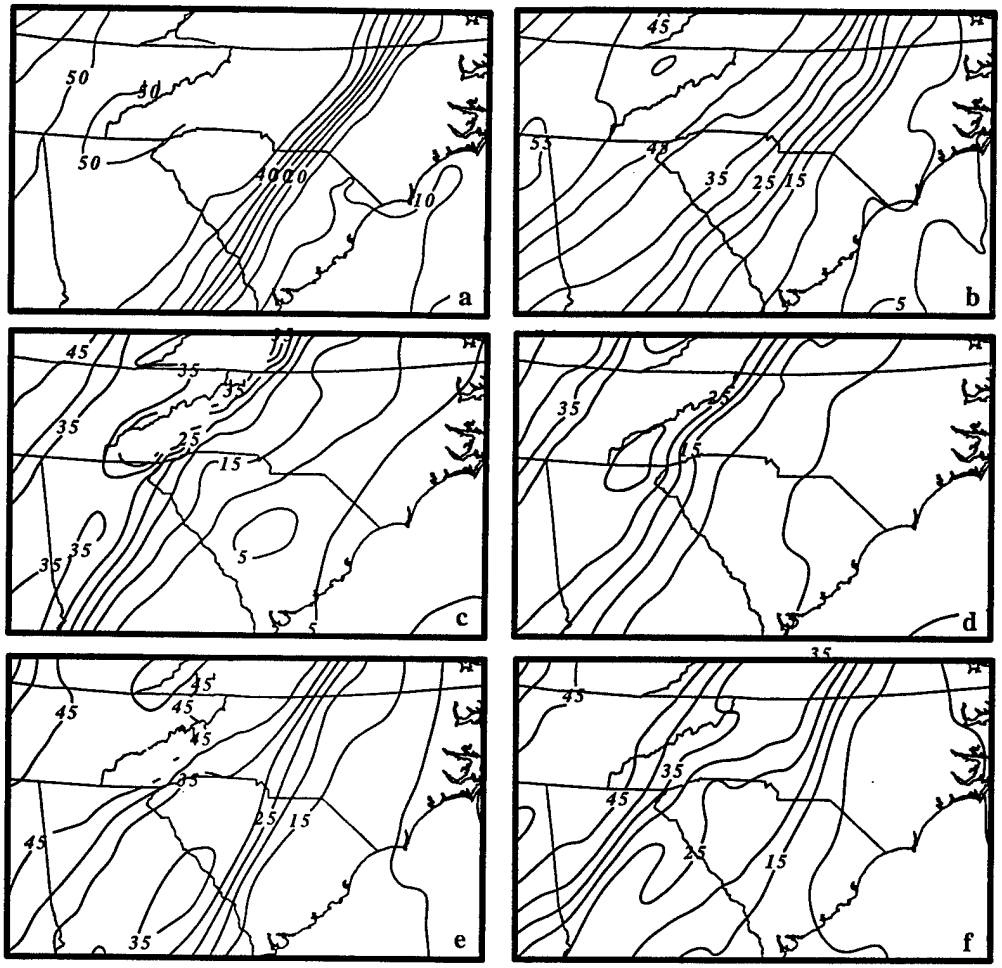

FIG. 23. MASS simulated, 12 km mesh, magnitude of the total wind velocity shear (solid lines, ms^{-1}) between the 925 mb and the 500 mb levels valid at (a) 0600 UTC 28 November 1988, (c) 1800 UTC 25 January 1990 and (e) 0000 UTC 26 January 1990; and between the 850 mb and the 500 mb levels valid at (b) 0600 UTC 28 November 1988, (d) 1800 UTC 25 January 1990 and (f) 0000 UTC 26 January 1990.

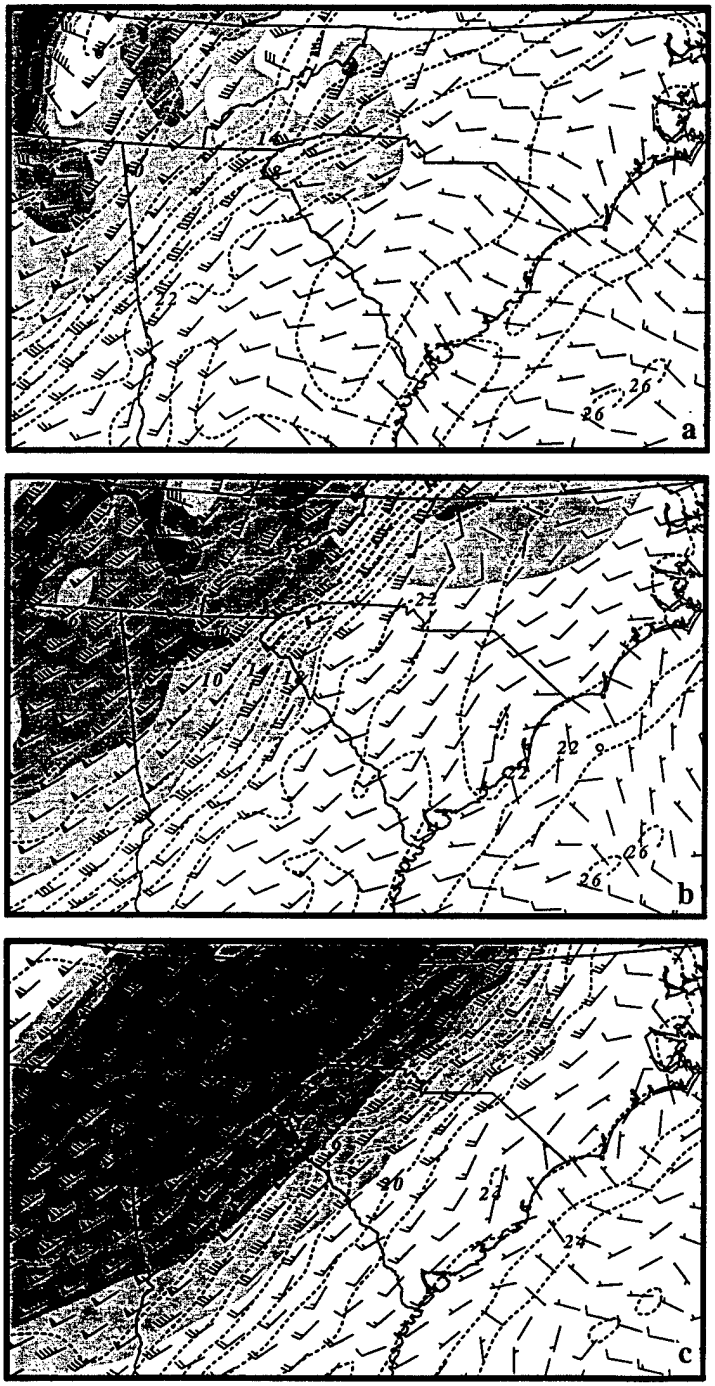

FIG. 24. MASS simulated, 12 km mesh, 600 mb wind isotachs (shaded at intervals of 5 for speeds greater than 35 ms^{-1}), surface temperature (dashed lines, C), thermal wind barbs over the 900 to 500 mb layer (ms^{-1}) valid at (a) 0000 UTC, (b) 0300 UTC and (c) 0600 UTC 28 November 1988.

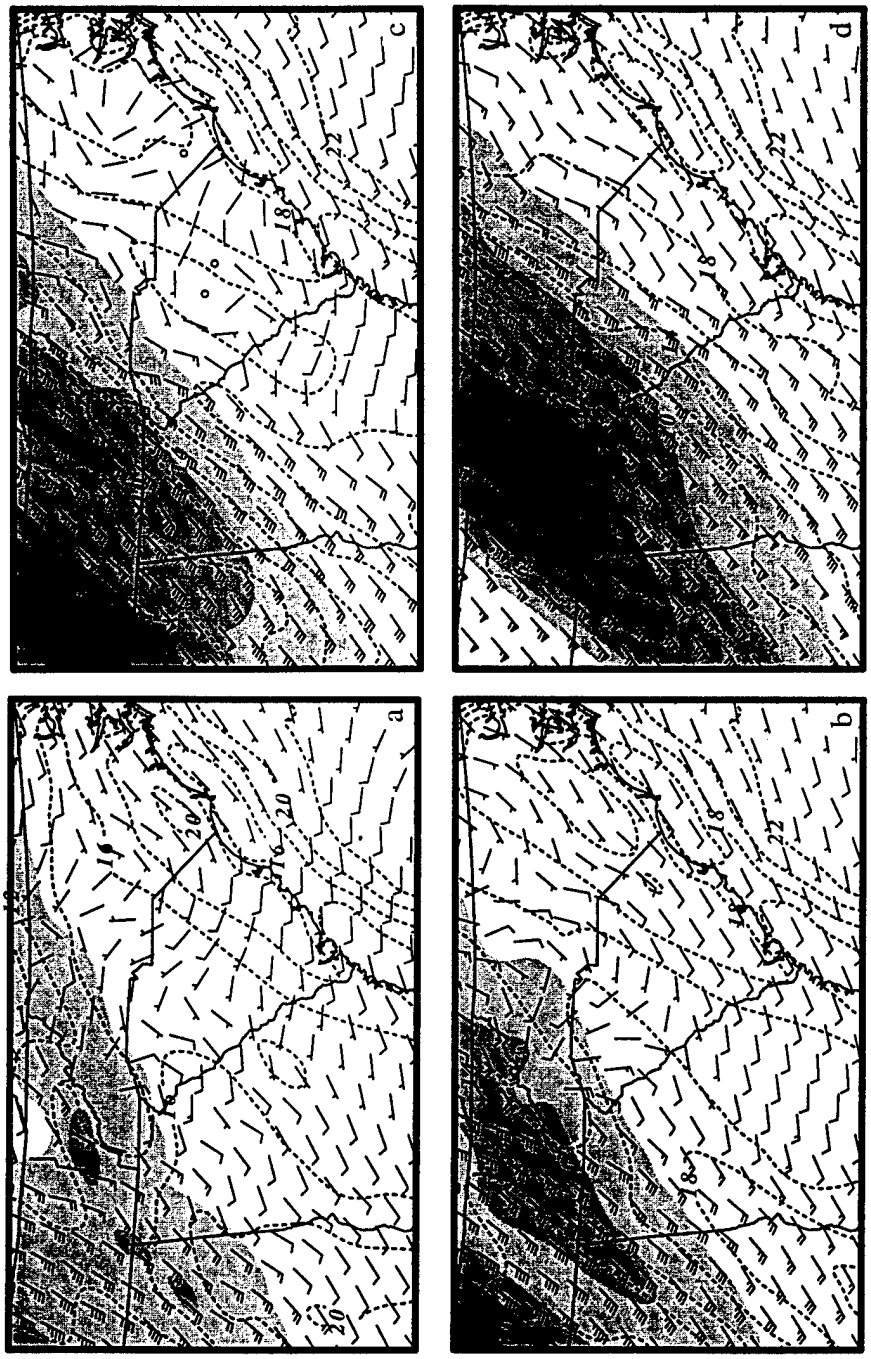

FIG. 25. MASS simulated, 12 km mesh, 600 mb wind isotachs (shaded at intervals of 5 for speeds greater than 35 ms^{-1}), surface temperature (dashed lines, C), thermal wind barbs over the 900 to 500 mb layer (ms^{-1}) valid at (a) 1200 UTC, (b) 1500 UTC, (c) 1800 UTC 25 and (d) 0000 UTC 26 January 1990.

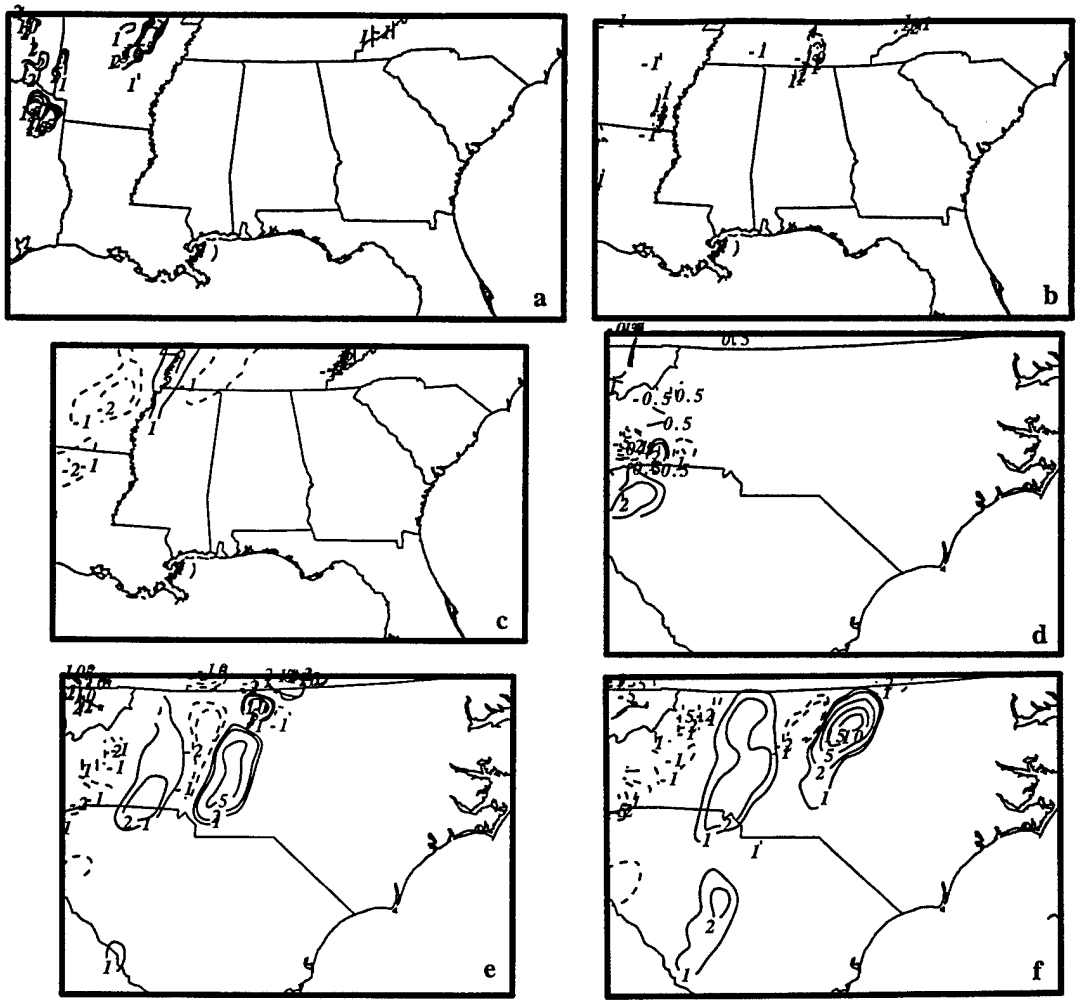

FIG. 26. MASS simulated, 24 km mesh, Divergence Profile Buoyancy Index. Solid lines indicate positive values and dashed lines indicate negative values (contoured -15, -10, -5, -2, -1, 1, 2, 5, 10, 15, 20) valid at (a) 1200 UTC 26, (b) 0000 UTC 27, (c) 1200 UTC 27, (d) 0000 UTC 28, (e) 0400 UTC 28, and (f) 0600 UTC 28 November 1988.

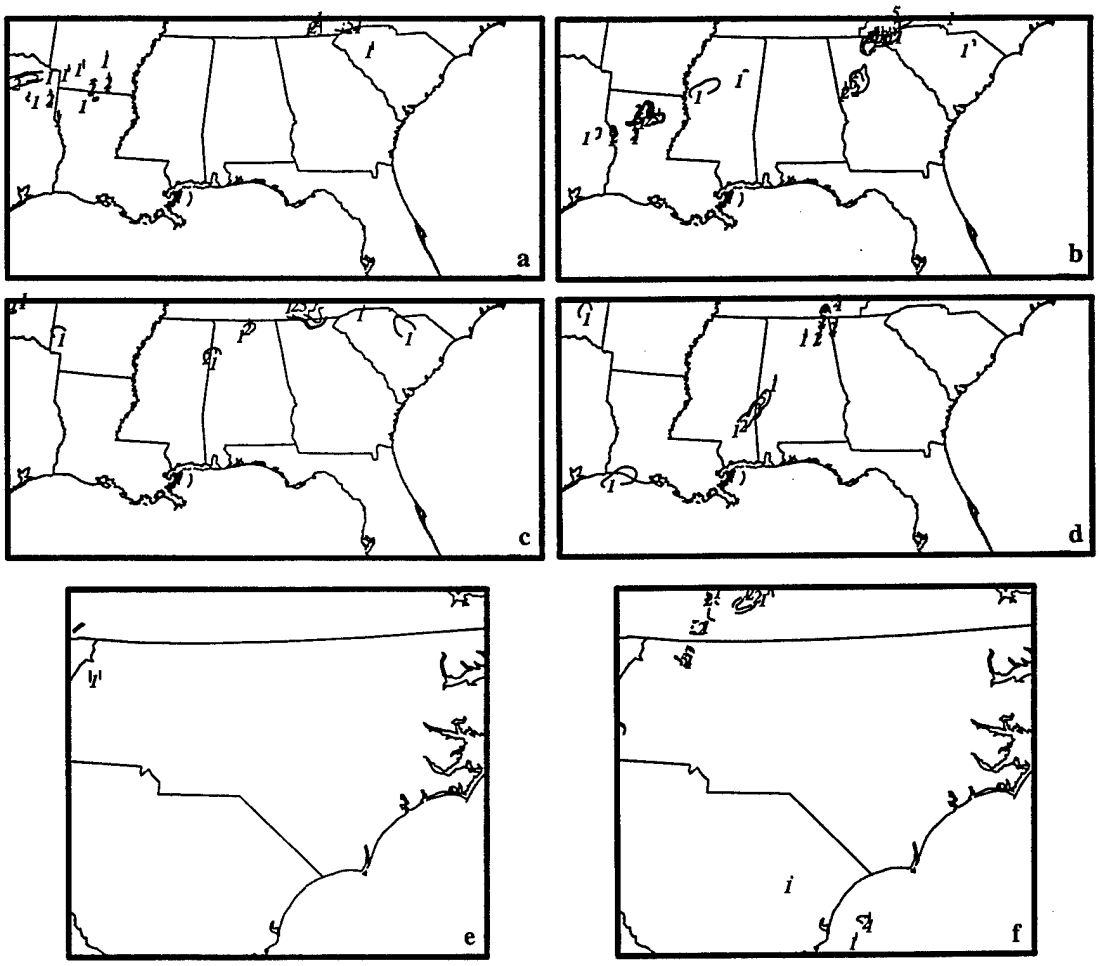

FIG. 27. MASS simulated, 24 km mesh, Divergence Profile Buoyancy Index. Solid lines indicate positive values and dashed lines indicate negative values (contoured -15, -10, -5, -2, -1, 1, 2, 5, 10, 15, 20) valid at (a) 0300 UTC 24, (b) 1500 UTC 24, (c) 0300 UTC 25, (d) 1500 UTC 25, (e) 1800 UTC 25, and (f) 0000 UTC 26 January 1990.

CHAPTER 5

SUMMARY AND CONCLUSIONS

Observational analysis and mesoscale numerical simulations were in agreement concerning key dynamical processes which occurred over MX and the Gulf of Mexico up to 72 hours prior to the 1988 Raleigh, NC, tornado outbreak (event case). Upper-level jetogenesis (STJ) created a transverse ageostrophic circulation, which forced air down the eastern side of the Sierra Madre Mountains creating adiabatic warming due to compressional heating. Along with this warm air, a low-level trough of low pressure forms over the western Gulf of Mexico. A LLJ developed over the western Gulf which began the process to transport warm low-level air to the southeast US.

Analysis of the non-event case implied a different synoptic pattern. Seventy-two hours before the expected event, the upper-level flow was very zonal over the US with a ridge over MX. The ridge prevented the development of a STJ over Mexico and the Gulf of Mexico. During the early period, no transport mechanism developed to move the hot, dry air off the Mexican plateau and over the Gulf of Mexico. So, there was one very important difference -- the air over the Gulf was much cooler than the event case (generally 4 to 6 C cooler).

The low-level PV of the event case was generated in the upper-levels, transported downward in the lee of the mountains to the lower-levels, then advected over central NC arriving 72 hours later at the time of a tornadic event. Initially, there were two jet streaks embedded within the STJ; the first streak (located over TX and the Gulf Coast States)

facilitated PV production and transported the PV southward. Then, the second STJ and its associated thermally indirect circulation transported the PV down to the mid-levels over the Mexican plateau. Also, there was substantial heating over the Mexican plateau producing a very deep and warm dry adiabatic layer over MX. A mountain-plains solenoid circulation developed over the Mexican plateau creating an area of strong vertical convergence in the 500-600 mb layer increasing the thermal gradient, producing low-level diabatic heating and generating PV (due to increasing static stability near diabatic heating). This midlevel PV maximum then moved eastward and an ensemble of hydrostatic mountain waves transported the PV downward near the Mexican coast. As the PV maximum moved downward, it increased due to strong static stability, tilting, vortex tube stretching, and frictional effects. The low-level PV then moved along the Gulf Coast and finally north along the East Coast to RDU at the time of the tornado outbreak. The low-level PV maximum was maintained and increased by a combination of low-level wind shear, latent heating, frictional effects and sensible heating.

In the earliest period, there was a dramatic difference between the event and non-event. The STJ was absent in the non-event case, thus PV was not transported downward to the midlevels. The low-level wind field over the western Gulf of Mexico was from the east, which advected clouds over the Mexican plateau minimizing surface heating and inhibiting a deep dry adiabatic layer. The easterly low-level flow prevented the development of mountain waves southwest of BRO inhibiting the downward transport of mid-level PV. In addition, the non-event case did not have a LLJ over the TX coast or

Gulf of Mexico to transport northward any low-level PV. There were two distinct differences in the low-level PV maxima between the cases. First, the PV maximum was a coherent and traceable entity over 72 hours in the event case. In the non-event case, the origin of the PV maximum was not readily apparent. Several PV maxima originated in the Rocky Mountains in western OK then tracked to the east into the Appalachian Mountains. Second, the event case PV maximum originated much farther to the south than that of the non-event case. It originated in the lee of the Sierra Madre Orientals then traveled across the southern states and finally propagated up the eastern part of SC and NC. In the non-event case, the PV maxima most likely originated over western OK and northern TX then they moved to the east and northeast from the Rocky Mountains to NC.

In the event case mid-period, a STJ was located over the Gulf Coast region. The winds over the north TX coast, LA and MS were subgeostrophic indicating accelerating flow and divergence, which facilitated ascent and deep convection. In the non-event case, there was a strong PJ over northern TX extending northeastward. Winds over the TX coast, LA, MS and AL were supergeostrophic indicating deceleration, convergence and sinking, which inhibited deep convection.

The mid-level jet was dramatically different between these cases. In the event case, a mid-level jet developed over TX and moved eastward across the southern states, from TX to GA. The jet developed rapidly over eastern TX in response to the increased PGF, which was created as the trough propagated eastward over the Midwestern states while the warm Mexican airmass maintained the heights over the Gulf Coast. The

environment was predisposed to produce a midlevel jet due to the warm, low-level airmass that moved from the Mexican plateau to the Gulf Coast near the TX/LA border. The mid-level jet right entrance region was closely associated with the surface trough. The thermally direct ageostrophic circulation enhanced ascent over the surface trough, which helped to maintain the trough and convection.

In the non-event case, there were two distinct mid-level jets covering two time periods. First, until approximately 0600 UTC 25 January 1990, there was a narrow mid-level jet extending across northern LA, MS, AL and TN. The jet was closely associated with the surface front and a narrow band of cold air advection and a strong height gradient. After 0600 UTC 25 January 1990 a strong mid-level jet developed over the Tennessee Valley Region, which was associated with a developing QG system.

Observed data and model simulations highlight the surface differences between the event and non-event cases. The event case had strong surface confluence, a meso-trough and strong convection. The surface trough, confluence area and intense convection propagated across the Gulf Coast states over the next 24 hours. The upper-level divergence and the thermally direct circulation about the mid-level jet removed mass from the air column creating ascent, which helped to maintain the surface trough and convection. In the non-event case, there was a QG balanced front and mid-level jet over OK, AR, TN and KY. Also, there was a weak surface frontal system (trough) over the Gulf Coast. There was upper-level convergence over the Gulf Coast, which inhibited the development of deep convection.

There are striking differences between the origins and maintenance of the low-level PV between these two cases. In the non-event case, several PV maxima originated in the lee of the Rocky Mountains and moved eastward to VA. The PV distribution and the upper-level sinking support the concept that the low-level PV originated and is maintained, in large part, by the downward transport of stratospheric PV (tropopause fold). Late in the period another PV maximum developed in association with convection over central MS and it moved northeast to the Appalachian Mountains. In the event case, the low-level PV maximum over the TX coast propagated eastward across the Gulf then northeast to the Carolina Piedmont. The PV maximum was associated with a surface trough, confluence and convection. As the low-level PV maximum propagated along the Gulf Coast, the PV was primarily maintained in the low-levels by tilting effects associated with diabatic heating.

In summary, the mid-period of the event case had a self-maintaining, low-level circulation that originated over Mexico, propagated across the Gulf Coast and moved over the Carolina Piedmont at the time of the tornado outbreak. This circulation moved across the Gulf Coast States as a coherent feature and was characterized by a surface trough, low-level PV maximum, mid-level jet, a warm Mexican airmass and upper-level divergence associated with the STJ. In the non-event case, these features were absent along the Gulf Coast states.

In the last six hours before the RDU tornado outbreak there was supergeostrophic upper-level flow over VA, NC and SC coastal region. At the same time, the PJ moved to

the west of the Appalachian Mountains thus the PJ's right entrance region came in close proximity to the STJ's left exit region. The two associated transverse ageostrophic jet streak circulations were juxtaposed (phased) creating a region of intense ascent and strong upper-level divergence between the jet streaks and over the Piedmont. For the non-event case, a PJ extended from TX northeast to the North Atlantic Ocean. There was no STJ over the eastern US thus there could be no phasing of jet streaks as in the event case.

In the mid-levels of the event case, the warm Mexican air (>330 K) at 850 mb elevated the heights to the southeast of the mid-level jet. The elevated heights in the right exit region created a mid-level PGF and forced the continued development of the jet. The warm air also enabled the mid-level jet to be farther east than in a balanced QG system. As the jet accelerated it induced a thermally direct ageostrophic circulation. Thus, the ascent created by the ageostrophic circulation was over the warm MX air. This forcing mechanism was continually regenerated as surface frontogenesis and the low-level baroclinic zone continued to develop and latent heating was generated as convection developed. By the time of the severe weather at RDU, the jet had intensified greatly and moved between the PJ entrance region and the STJ exit region, producing strong ascent. For the non-event case, a mid-level jet developed with the QG balanced system west of the Carolina Piedmont. The jet developed as a trough of low pressure developed over the Midwest US and propagated northeastward. In contrast to the event case, the warm air from MX (>330 K) at 850 mb had not moved over the Carolina Piedmont. At the

expected time of the non-event there was descent in the low-levels and very weak ascent in the mid-levels over the Piedmont.

Potential vorticity was examined for the last 6 hours for both the event and non-event. In the event case, the low-level PV maximum was closely related to the surface trough (across the Carolina Piedmont) and with the areas of maximum trough deepening. As the PV maximum approached RDU at the time of the tornado outbreak it was associated with a mesocyclone. The strongest PV was in the low-levels and the low-level PV maximum was disconnected from the upper-levels. Just as in the preceding 48 hours, the PV over the Carolina Piedmont was transported and/or generated in the low-levels. In the non-event, the low-level PV over NC and SC was very sporadic (generated in large part by diabatic effects associated with convection).

We also found a direct relationship between convective precipitation and low-level PV. Convection generates PV through diabatic heating; the low-level PV maxima increase, in part, from latent heat energy associated with convection. One critical difference between these cases is that the event case had existing low-level PV maxima so convection was a maintainer rather than primary generator of PV. In the non-event case, convection was the primary generator of low-level PV where there was not any before the convection developed.

The mesoscale model-generated data indicated the potential for severe weather for the event case, which is something the forecasters did not have at that time. Simulation-produced LI, SRH, low-level shear and wind imbalance as measured by the total wind

shear - thermal wind were clearly different between the cases. All these indicators forecast the development of severe weather in the event case and not in the non-event case.

We developed a new divergence profile buoyancy index (DPBI) based on: large scale synoptic features (upper-level divergence); mesoscale features (low-level tilting effects which incorporate shear and thermal gradients); and the buoyancy of the airmass. We found values over 15 corresponded to tornadic activity over both the MO, AK, TX, LA and MS (early in the period) and over central NC (late in the period).

Overall, we found that low-level potential vorticity in the event case can be traced from RDU at the time of the tornado outbreak back to its origins (some 84 hours earlier). The low-level PV facilitated the tracking of a mesoscale surface trough that developed over the western Gulf of Mexico, propagated northeastward along the Gulf Coast States, developed (merged) into a surface cold front and moved over the Carolina Piedmont at the time of the tornado outbreak. *The STJ was crucial to this 3-day process. First, it transported stratospheric PV rich air to the south then downward to the mid-levels over the Mexican plateau. Second, its associated ageostrophic circulation created upper-level divergence (mass removal from the air column) that helped to maintain deep convection and the surface trough. Third, it phased with the PJ creating extreme upper-level divergence and ascent over the Carolina Piedmont.* At the same time, a warm low-level Mexican airmass was transported over the Gulf Coast States (southeast of the surface trough). The warm air was located to the southeast of the surface trough, and in

conjunction with cold air advection to the northwest created an intense northwestward-directed PGF and a mid-level jet. The mid-level jet entrance region had an associated thermally direct ageostrophic circulation, which enhanced ascent over the low-level trough. These features created an environment favorable to deep convection and the release of latent heat that helped to maintain the low-level trough (confluence zone) and PV as it propagated across the Gulf Coast. Additionally, the latent heating, associated with convection, helped create an unbalanced jet with a thermally direct circulation in the jet exit region. The direct circulation associated with the mid-level jet facilitated convection ahead of the surface (over the warm air). The latent heating from convection and surface sensible heating maintained the surface front. Cold air advection from the northwest further enhanced the strength of the front. As air parcels moved over this front, they encountered a very strong shear and thermal gradient, thus, they were tilted, generated vorticity and ascended rapidly.